# Dynamic Imaging of Hepatitis C Virus RNA Localisation and Traffic During Viral Replication

Guillaume Nicolas Fiches

Engineer in Biotechnology and Biochemistry

(National Institute of Applied Sciences, Lyon, France)

Department of Molecular and Cellular Biology

School of Biological Sciences

The University of Adelaide


A dissertation submitted to The University of Adelaide

in candidature for the degree of

Doctor of Philosophy in the Faculty of Science

March 2015

# Table of Content

# List of Figures

**Chapter 4**

**Chapter 5**

**Chapter 6**

# List of Movies

**Table Number**

**Chapter 4**



**Chapter 5**

Dear reader,

Please find on this DVD the movies relevant to my thesis. If you are experiencing any problems to play the files, please try installing the free multimedia player VLC, available for either windows (http://www.videolan.org/vlc/download-windows.html) and Mac OS (http://www.videolan.org/vlc/download-macosx.html) or contact Associate Professor Michael Beard (Michael.beard@adelaide.edu.au).

Thanks you for your time.

Best regards,

Guillaume Fiches

# List of Tables

# Abstract

Much of our understanding of the HCV life cycle and host-viral interactions has evolved from the visualisation of fixed images of infected cells. However, the recent development of live cell imaging techniques now allows viral life cycles to be visualised in live cell cultures. We have tagged the NS5A protein of the infectious Jc1 chimera (J6/JFH-1) with fluorescent tags and shown that NS5A segregates into two distinct populations: one relatively static and one highly motile, although the role and composition of these structures is not well understood. To investigate HCV RNA dynamics throughout the viral life cycle and examine whether either or both sub-classes of NS5A-positive structures are enriched with HCV RNA we developed a system to simultaneously track HCV RNA and NS5A in living cells.

MS2 bacteriophage RNA stem loop sequences (6x /8x /12x /24x repeats) were inserted into the 3'UTR of the Jc1/5A-TCM virus (Jc1/5A-TCM+3'UTR:MS2) to allow indirect tracking of HCV RNA in Huh-7.5 cells via MS2.Coat-mCherry fusion protein that interacts specifically with MS2 stem loops. Jc1/5A-TCM+3'UTR:MS2 viruses replicated to significantly lower levels than the parent Jc1 as assessed by immunofluorescence analysis. However, long-term culture resulted in emergence of more efficient viral replication, with PCR and sequence analysis indicating at least partial retention of MS2 stem loops at 8 days post electroporation of HCV RNA. To further characterize and overcome the replication handicap induced by the insertion of the MS2 stem loop sequences we also generated Huh-7.5 cells that harbour the HCV subgenomic replicon featuring these MS2 stem loops insertions. Deep sequencing

analysis was conducted to identify emerging adaptive mutations. However none was found to be particularly predominant.

Most importantly, redistribution of the mCherry tagged-MS2 coat protein from a homogenous cytoplasmic distribution to a more punctate localisation was observed in the context of the full-length viral cultures indicating specific binding to HCV RNA. Using this approach we have simultaneously visualised HCV RNA (MS2.coat-mCherry) and NS5A traffic (FlAsH) in real-time during HCV replication. Both HCV RNA-positive small motile and larger static structures were enriched with NS5A. In contrast, a subset of the trafficking NS5A-positive structures was devoid of HCV RNA. We also investigated viral RNA traffic with respect to lipid droplets (LDs) and show that two sub-types of static HCV RNA-positive structures existed: one was closely juxtaposed to LDs while the second sub-class was localised away from LDs. Moreover the system enabled visualization of putative RNA delivery at the LD surface with examples of motile HCV RNA-enriched structures dynamically interacting with LDs. Finally performing co-imaging of HCV NS5A and Rab18, an NS5A-interacting host factor located at the LD surface, we were able to illustrate the often transient nature of NS5A interaction with the LD and putative sampling of the LD that may precede interaction with core and initiation of assembly steps of the viral life cycle. These studies reveal new insights into the dynamics of HCV RNA traffic and the interactions at play in the context of the HCV life cycle.

# Declaration

I certify that this work contains no material which has been accepted for the award of any other degree or diploma in my name, in any university or other tertiary institution and, to the best of my knowledge and belief, contains no material previously published or written by another person, except where due reference has been made in the text. In addition, I certify that no part of this work will, in the future, be used in a submission in my name, for any other degree or diploma in any university or other tertiary institution without the prior approval of the University of Adelaide and where applicable, any partner institution responsible for the joint-award of this degree.

I give consent to this copy of my thesis when deposited in the University Library, being made available for loan and photocopying, subject to the provisions of the Copyright Act 1968.

The author acknowledges that copyright of published works contained within this thesis resides with the copyright holder(s) of those works.

I also give permission for the digital version of my thesis to be made available on the web, via the University's digital research repository, the Library Search and also through web search engines, unless permission has been granted by the University to restrict access for a period of time

Guillaume Nicolas Fiches

March 2015

# Acknowledgements

I first would like to thank my supervisor Associate Professor Michael R. Beard to give me the opportunity to conduct my PhD in his laboratory and for the continued mentoring and support he provided me throughout the years.

I also would like to sincerely thank my co-supervisor Dr Nicholas Eyre for his excellent teaching, encouragements and technical assistance during these years.

I would like to extend my sincere gratitude to all the other members past and present of the Hepatitis C Virus research laboratory and especially Dr Amanda Aloia and Dr Kylie Van Der Hoek for their assistance and friendship.

I would also like to thank Dr Fabio Luciani and Dr Brigit Betz-Stablein (UNSW, Sydney) for their assistance in interpretating the deep sequencing data.

I would also like to thank The University of Adelaide for providing me with an ASI scholarship enabling me to conduct my PhD here in Adelaide.

Finally I would like to thank my family and especially my parents Marie-Christine and Bernard and my brother Anthony for their continued encouragements and support from afar. I would also like to thank my grand-pa Georges for his encouragements but who sadly passed away during the last year of my studies.

# Presentations Arising From PhD

## *International:*

**20th International Symposium on Hepatitis C and related Viruses, Melbourne – October 2013**: Dynamic imaging of HCV Viral RNA traffic and localisation *(Oral presentation)*

**19th International Symposium on Hepatitis C and related Viruses, Venice - October (2012).** Dynamic imaging of HCV Viral RNA traffic and localisation *(Poster presentation)*

## *National:*

**The Australian Society for Microbiology Annual Scientific Meeting, Adelaide, July 2013**: Dynamic imaging of HCV Viral RNA traffic and localisation *(Oral presentation)*

**Australian Centre for HIV and Hepatitis Virology Research Workshop, Adelaide - June 2012**: Dynamics of HCV Viral RNA traffic and localisation *(Oral presentation)*

**Australian Centre for HIV and Hepatitis Virology Research Workshop, Maroochydore - June 2011**: The influence of Hepatitis C Virus genotype on NS5A protein localisation and traffic *(Oral presentation)*

# Publication Arising During PhD

### *Directly related to thesis:*

**Fiches, G.N**., Eyre, N.S., Aloia, A., Van Der Hoek, K., Betz-Stablein, B., Luciani, F., Chopra, A., Beard. M.R., 2015. Dynamic imaging of HCV RNA traffic in living cells. *(In preparation).*

Eyre, N.S., **Fiches, G.N**., Aloia, A.L., Helbig, K.J., McCartney, E.M., McErlean, C.S., Li, K., Aggarwal, A., Turville, S.G., Beard, M.R., 2014. Dynamic imaging of the hepatitis C virus NS5A protein during a productive infection. Journal of virology 88, 3636-3652.

### *Unrelated to thesis:*

Helbig, K.J., Carr, J.M., Calvert, J.K., Wati, S., Clarke, J.N., Eyre, N.S., Narayana, S.K., **Fiches, G.N**., McCartney, E.M., Beard, M.R., 2013. Viperin is induced following dengue virus type-2 (DENV-2) infection and has anti-viral actions requiring the C-terminal end of viperin. PLoS neglected tropical diseases 7, e2178.

Helbig, K.J., Eyre, N.S., Yip, E., Narayana, S., Li, K., **Fiches, G.**, McCartney, E.M., Jangra, R.K., Lemon, S.M., Beard, M.R., 2011. The antiviral protein viperin inhibits hepatitis C virus replication via interaction with nonstructural protein 5A. Hepatology 54, 1506-1517.

# Awards Received During PhD

**2013** 20th International Symposium on Hepatitis C and related Viruses, Melbourne, student Travel grant – 450$

**2013** The Australian Society for Microbiology Annual Scientific Meeting, Adelaide, Bursary Award – 250$

**2012** Australian Centre for HIV and Hepatitis Virology Research Workshop, Adelaide, Robert Dixon award – 500$

# Abbreviations Used

| | |
|---|---|
| A | adenosine |
| aa | amino acids |
| AP2M1 | clathrin adaptor protein complex 2, µ1 sub-unit |
| ApoE | apolipoprotein E |
| ATP | adenosine triphosphate |
| BFP | blue fluorescent protein |
| bp | base pair |
| BrUTP | 5-bromouridine 5’-triphosphate |
| BSA | bovine serum albumin |
| °C | degrees Celsius |
| C | cytosine |
| cDNA | complimentary deoxyribosenucleic acid |
| CHC | chronic hepatitis C |
| cLD | cytoplasmic lipid droplet |
| CLDN | claudin |
| CMV | cytomegalovirus |
| cPLA | cytosolic phospholipase A2 |
| $C_T$ | threshold cycle |
| DAPI | 4’, 6-Diamidino-2-pheylinodole |
| $dH_2O$ | deionised water |
| DAA | direct acting antiviral |
| DGAT1 | diacylglycerol O-acyltransferase 1 |

| | |
|---|---|
| DMEM | Dulbecco’s Modified Eagle Medium |
| DMSO | dimethyl sulfoxide |
| DMV | double-membrane vesicle |
| DNA | deoxyribosenucleic acid |
| dNTP | deoxyribosenucleotide triphosphate |
| ds | double stranded |
| dsRNA | double stranded RNA |
| DTT | dithiothreitol |
| EASL | European Association for the Study of the Liver |
| ECMV | encephalomyocarditis virus |
| EDTA | ethylene diamine tetra acetic acid |
| ER | endoplasmic reticulum |
| FACS | fluorescence-activated cell sorting |
| FCS | foetal calf serum |
| FDA | Food and Drug Administration |
| ffu | focus forming units |
| FISH | fluorescent *in situ* hybridization |
| FITC | fluorescein isothiocyanate |
| g | grams |
| g | G-force |
| G | guanosine |
| GAG | glycosaminoglycan |
| GFP | green fluorescent protein |
| HBV | hepatitis B virus |
| HCC | hepatocellular carcinoma |

| | |
|---|---|
| HCV | hepatitis C virus |
| HCVcc | cell-culture propagated hepatitis C virus |
| HEPES | 4-(2-hydroxyethyl)-1-piperazineethanesulfonic acid |
| HIV | human immunodeficiency virus |
| HRP | horse radish peroxidase |
| HuH | human hepatoma |
| h-VAPA | human vesicle-associated membrane protein-associated protein A |
| h-VAPB | human vesicle-associated membrane protein-associated protein B |
| HVR1 | hyper variable region 1 |
| IFN-α | interferon alpha |
| Ig | Immunoglobulin |
| IRES | internal ribosome entry site |
| ISH | *in situ* hybridization |
| IV | intravenous |
| kb | kilobase |
| kDa | kilo Dalton |
| L-Agar | LB + agar |
| LB | Luria Bertani broth |
| LD | lipid droplet |
| LDL | low density lipoproteins |
| LDLR | low density lipoprotein receptor |
| LRA | long-range annealing |
| Luc | luciferase |
| LVP | lipoviral particle |
| µg | micrograms |

| | |
|---|---|
| μL | microlitres |
| μM | micromolar |
| mA | milliamps |
| mg | milligrams |
| mL | millilitres |
| mM | millimolar |
| MCL | monoclonal cell line |
| MCP | MS2 bacteriophage coat protein |
| MCS | multiple cloning site |
| min | minute |
| miR-122 | micro RNA 122 |
| MLV | murine leukemia virus |
| MMV | multi-membrane vesicle |
| MOI | multiplicity of infection |
| mRNA | messenger RNA |
| MW | membranous webs |
| MW | molecular weight |
| NANBH | non-A, non-B hepatitis |
| NCR | non coding region |
| ng | nanograms |
| nM | nanomolar |
| NPC1L1 | Niemann-Pick C1 like 1 |
| NS | non-structural |
| NTR | non translated region |
| nts | nucleotides |

| | |
|---|---|
| OCLN | occludin |
| OD | optical density |
| ORF | open reading frame |
| PAGE | polyacrylamide gel electrophoresis |
| PBS | phosphate buffered saline |
| PCL | polyclonal cell line |
| PCR | polymerase chain reaction |
| PEG | pegylated |
| PI4KIIIα | phosphatidylinositol 4-kinase III alpha |
| PI4P | phosphatidylinositol 4-phosphate |
| RBV | Ribavirin |
| RC | replication complex |
| RdRp | RNA-dependent RNA polymerase |
| RNA | ribonucleic acid |
| rpm | revolutions per minute |
| RT | room temperature |
| RT-PCR | reverse transcriptase polymerase chain reaction |
| sd | standard deviation |
| SDS | sodium dodecyl sulphate |
| sec | second(s) |
| SL | stem loop |
| SMV | single-membrane vesicle |
| SNR | signal-to-noise ratio |
| SOC | super optimal broth with catabolite repression |
| SRB1 | scavenger receptor class B1 |

| | |
|---|---|
| ss | single stranded |
| SV40 | simian virus 40 |
| T | thymidine |
| TAE | tris, acetic acid, EDTA (TAE) buffer |
| TBEV | tick-borne encephalitis virus |
| tk | thymidine kinase |
| Tris | tris(hydroxymethyl)aminomethane |
| U | unit(s) |
| UTR | untranslated region |
| UV | ultraviolet |
| V | volt(s) |
| VLDL | very low density lipoprotein |
| v:v | volume per volume |
| w:v | weight per volume |
| WHO | World Health Organization |
| WT | wild-type |

# Materials Providers

| | |
|---|---|
| Abcam | Cambridge, UK |
| Addgene | Massachusetts, USA |
| Amersham Pharmacia Biotech | Amersham, UK |
| Amresco | Ohio, USA |
| Applied Biosystem | Massachusetts, USA |
| Beckman Coulter | Miami, FL, USA |
| Bioline | Sydney, Australia |
| BioVision | San Francisco Bay, USA |
| Brand | Wertheim, Germany |
| BioRad Laboratories | California, USA |
| Clontech | California, USA |
| Corning | New York, USA |
| English and Scientific Conslting Kft. | Szirak, Hungary |
| Eppendorf | Hamburg, Germany |
| Geneworks | Adelaide, Australia |
| Genscript | New Jersey, USA |
| GraphPad | California, USA |
| Life Technologies | California, USA |
| Macherey Nagel | Düren, Germany |
| Merck | County Cork, Ireland |
| Nalge Nunc International | New York, USA |
| Nikon | Tokyo, Japan |

| | |
|---|---|
| New England Biolabs | Massachussets, USA |
| Okolab | Pozzuoli, Italy |
| Olympus | Tokyo, Japan |
| Promega | Wisconsin, USA |
| QIAgen | Limburg, Netherlands |
| Roche | Indiana, USA |
| Santa Cruz Biotechnology | Texas, USA |
| Sigma Aldrich | Missouri, USA |
| Stratagene | California, USA |
| Thermo Scientific | Massachusetts, USA |
| UVP | California, USA |

# Chapter 1

# Introduction

## 1.1 Hepatitis C virus a major worldwide health concern

### 1.1.1 Discovery

Chronic infection with the Hepatitis C Virus (HCV) is one of the major causes of severe liver disease worldwide. Until its identification in 1989 (Choo et al., 1989), the virus remained elusive and was referred as non-A, non-B hepatitis (NANBH) (Feinstone et al., 1975). Although, known to be a lipid-enveloped pathogen (Bradley et al., 1983; Feinstone et al., 1983) inducing liver diseases in both humans and chimpanzees, NANBH was first hypothesised to be a virus due to its size (Bradley, 1985; He et al., 1987) and transmissibility. The causative agent of NANBH could not be cultivated in cell culture and it was the emergence of bio-molecular techniques in the 1980's that finally helped in isolating the first cDNA clone of NANBH using an immunoscreening approach of cDNA libraries isolated from NANBH infected chimpanzee serum (Choo et al., 1989). HCV was the first virus to be isolated using a pure molecular approach.

### 1.1.2 Epidemiology

Today, hepatitis C virus infection remains a major public health concern despite its identification and the screening available which reduced spread of the virus. HCV is estimated to infect 2 to 3% of the worldwide population (Figure 1.1 (Lavanchy, 2008)) and approximately 230,000 people in Australia alone (1.7% of the population) (Gower et al., 2014). According to the World Health Organization (WHO) between 350 000 and 500 000 people die each year from HCV related liver disease.

In fact, 80% of infected individuals will develop a chronic infection which, over the course of 20 to 30 years, can result in liver disease ranging from fibrosis to hepato-cellular carcinoma (Poynard et al., 1997; Seeff et al., 1992) (Figure 1.2). The inflammatory response induced by chronic HCV infection is hypothesised to be responsible for the slow degeneration of the liver and emergence of the serious medical complications observed (Guidotti and Chisari, 2006) (Figure 1.3). Moreover chronic liver diseases induced by HCV infection generate a massive public health burden both in terms of treatments and care of patients who require regular medical follow-up.

### 1.1.3 Treatment

Until recently, the standard of care for treatment of chronic hepatitis C was a combination of pegylated Interferon-alpha (PEG-IFN-α) and Ribavirin (RBV) that has limited therapeutic efficacy (effective in only approximately 50-80% of patients depending on genotypes (Le Guillou-Guillemette et al., 2007)). Besides being expensive, this combination therapy could induce severe side effects (flu like illness, fatigue and anæmia). Consequently, the development of more efficient anti-HCV drugs has been a major focus of the field. In particular, development of direct acting antivirals

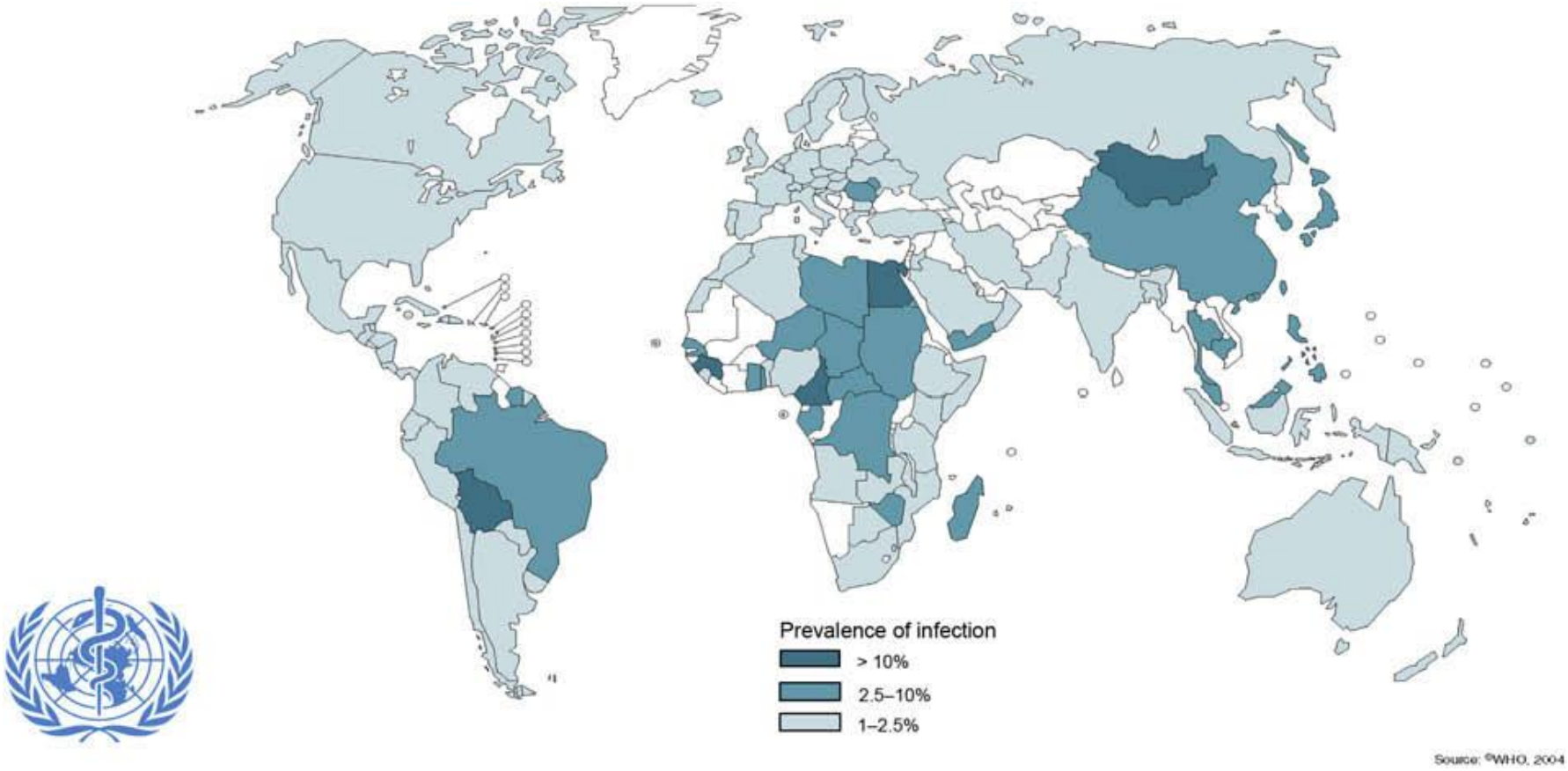


**Figure 1.1: Worldwide prevalence of HCV infection in 2008**
Taken from (Lavanchy, 2008)

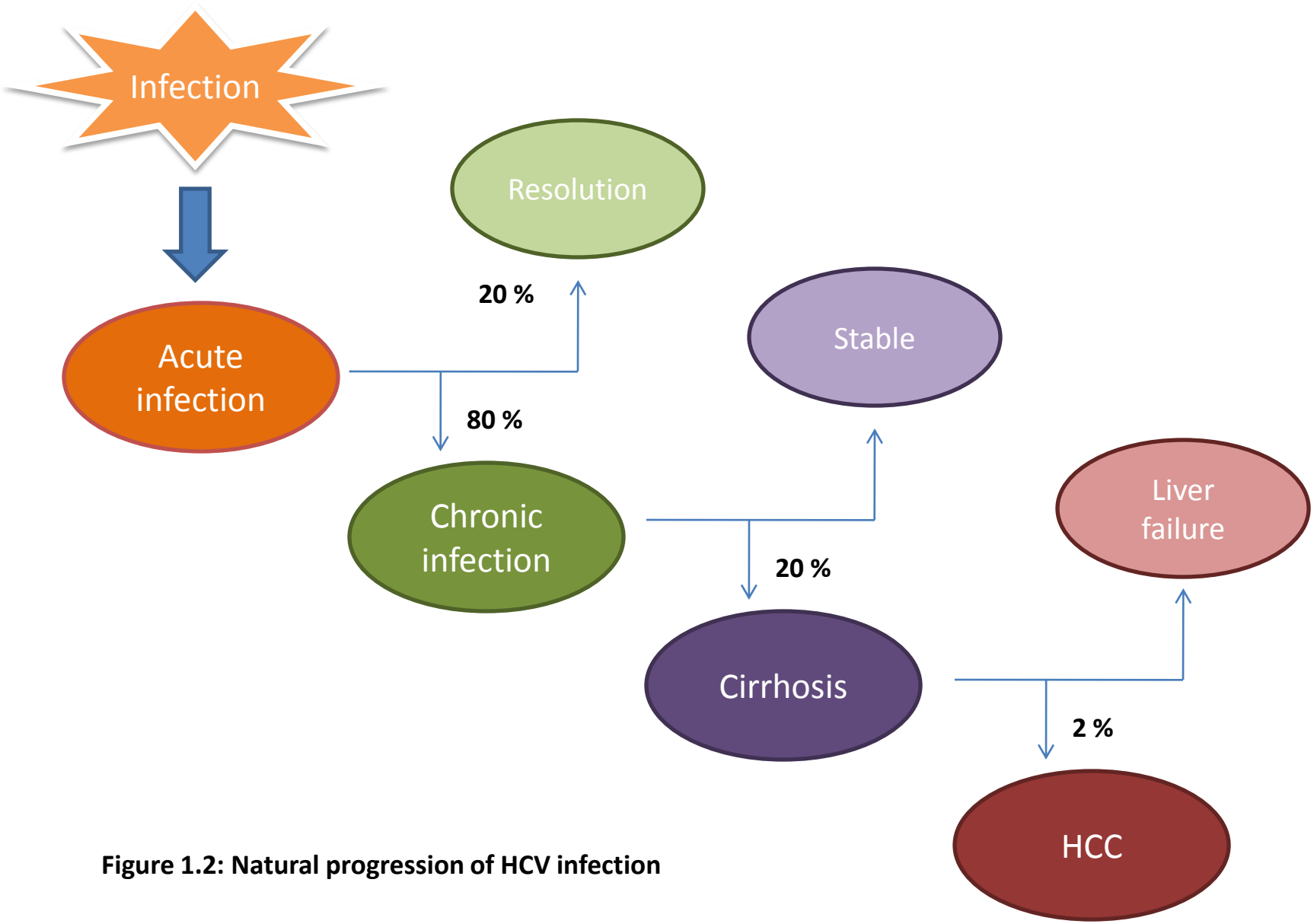


**Figure 1.2: Natural progression of HCV infection**

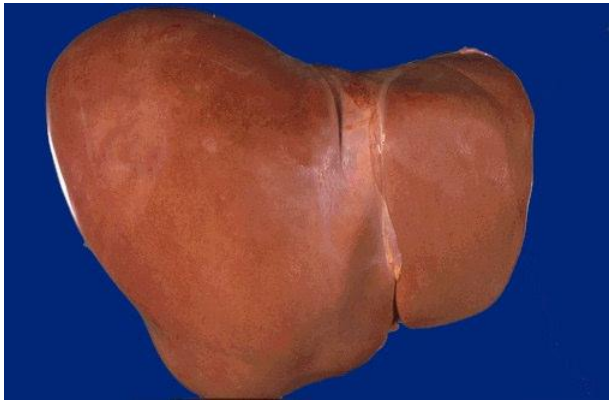

*Normal liver*

*Cirrhotic liver*


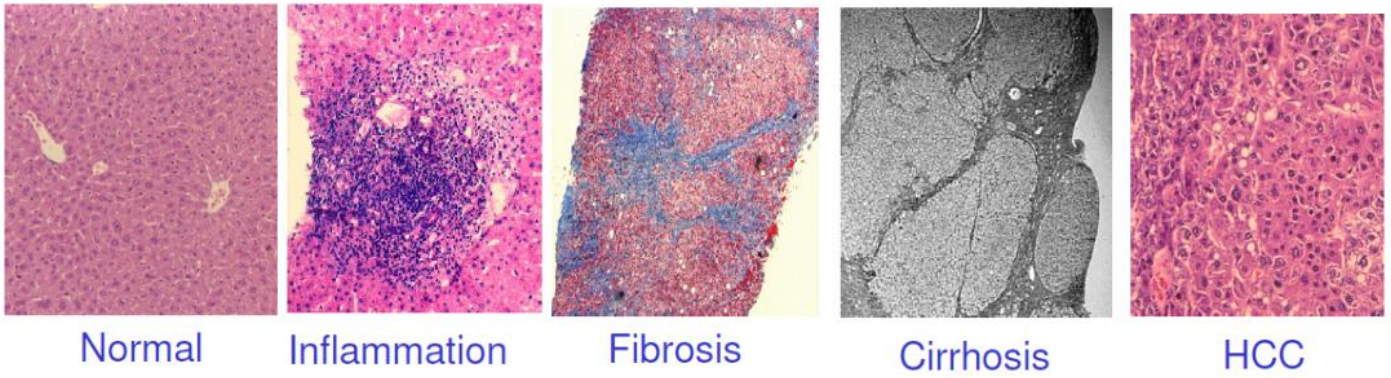


**Figure 1.3: Liver degeneration associated with HCV chronic infection**

(DAAs) that specifically target viral proteins to block precise steps of the viral life cycle offers hope for greatly improved treatment of HCV infection (Gao et al., 2010; Jensen, 2011; Targett-Adams et al., 2011).

In the past decade there has been remarkable progress in DAA development; from initial *in vitro* development to clinical testing and approval by regulatory bodies. Boceprevir (Merck) and Telaprevir (Vertex Pharmaceuticals / Johnson-Johnson), two inhibitors of the NS3-4A viral protease (see Section 1.2), were first approved by the US Food and Drug Administration (FDA) in 2011 and are prescribed in the context of treatment of genotype 1 HCV infection treatment. More recently in 2013 a new set of DAAs were approved by the FDA for treatment of HCV including an NS5B inhibitor (Sofosbuvir – Gilead Sciences) and second generation NS3-4A protease inhibitor with improved properties (Simeprevir – Johnson-Johnson). Nowadays, several other DAAs targeting all of the viral proteins are in various stages of development or clinical trials (Chukkapalli and Randall, 2014). For instance, NS5A inhibitors Ledipasvir (Gilead Sciences) and Daclatasvir (Bristol-Myers Squibb) have been approved in DAA combination therapies with Sofosbuvir. Furthermore new therapeutic targets are now emerging such as other viral proteins (NS4B) or host factors necessary for HCV life cycle such as Cyclophilin A (Alisporivir – Debiopharm and Novartis) and miRNA-122 with Miravirsen (Santaris Pharma) (reviewed in (Eyre et al., 2014b)).

Nevertheless, HCV displays a high replication activity with an estimated half-life of 2-5 hours associated with the production and clearance of $10^{10}$ to $10^{12}$ virions in infected individuals (Herrmann et al., 2000; Neumann et al., 1998). Together with the poor fidelity and the lack of proof-reading activity of its RNA-dependant-RNA polymerase (namely the NS5B viral protein), HCV has the proven ability to rapidly mutate and evade the action of first generation DAAs (Halfon and Locarnini, 2011; Pawlotsky,

2011). Therefore, the emergence of drug-resistant HCV genomes is likely to impact upon the success of these therapies, and, for the foreseeable future, DAAs will be used in combination with IFN α / RBV, RBV (for instance Sofosbuvir will be used in combination with RBV for genotype 2 and 3) and/or other DAAs to minimize the impact of emergence of resistance mutations according to the European Association for the Study of the Liver (EASL) recommendations on treatment of Hepatitis C 2014.

Although these new drugs show great efficacy even towards populations defined as hard to treat such as poor responders to IFN α/RBV, cirrhotic patients and HBV and/or HIV co-infected individuals, their accessibility will strongly be limited due to their very high cost. Thereafter, more research is needed towards development of drugs that are accessible to larger populations, including those of developing countries. In addition, despite the landscape change concerning treatment of hepatitis C virus infection, little progress has been made towards the development of a preventive vaccine.

### 1.1.4 HCV transmission

HCV is a blood borne virus mainly transmitted through blood transfer or blood products. Before the start of widespread blood screening for HCV in 1992, most infection resulted from contaminated blood transfusions and contaminated organ transplants. However, since this change in blood screening has been initiated, this type of transmission has greatly been reduced and is even considered eradicated in developed countries, although this type of transmission remains in the developing world where the access to a systemic screening of blood donation is not possible. Transmission of the virus today is often associated with but not restricted to intravenous (IV) drug use and needle sharing. Other occurrences of HCV transmission

are mostly linked to non-sterile medical and dental practices or cosmetic practices involving needles such as tattooing and body piercing. Finally vertical transmission from an infected mother giving birth to her child has also been reported due to the exposure of the baby to infected fluids, although it is thought that this mode of transmission is uncommon.

## 1.2 HCV biology

### 1.2.1 HCV genome

HCV is a single-stranded positive sense RNA virus. It is classified as a *Hepacivirus* of the *Flaviviridae* family amongst other significant human pathogens such as Tick-Borne Encephalitis Virus (TBEV), West Nile Virus and Dengue Virus. The HCV genome is approximately 9600 nucleotides in length and consists of a single open reading frame flanked by two untranslated regions (5'UTR and 3'UTR) (Figure 1.4). Both the 5'UTR and 3'UTR contain untranslated elements of critical importance for the viral life cycle. For instance the internal ribosome entry site (IRES) controlling the translation of the open reading frame into a single polyprotein is located in the 5'UTR. Moreover both untranslated regions of HCV genome contain multiple secondary structures such as stem loops which enable specific spatial organisation of the viral RNA due to internal long range interactions. Together with the seed sequence for miRNA-122 they are thought to greatly influence HCV replication (discussed in more details in Section 1.2.5).

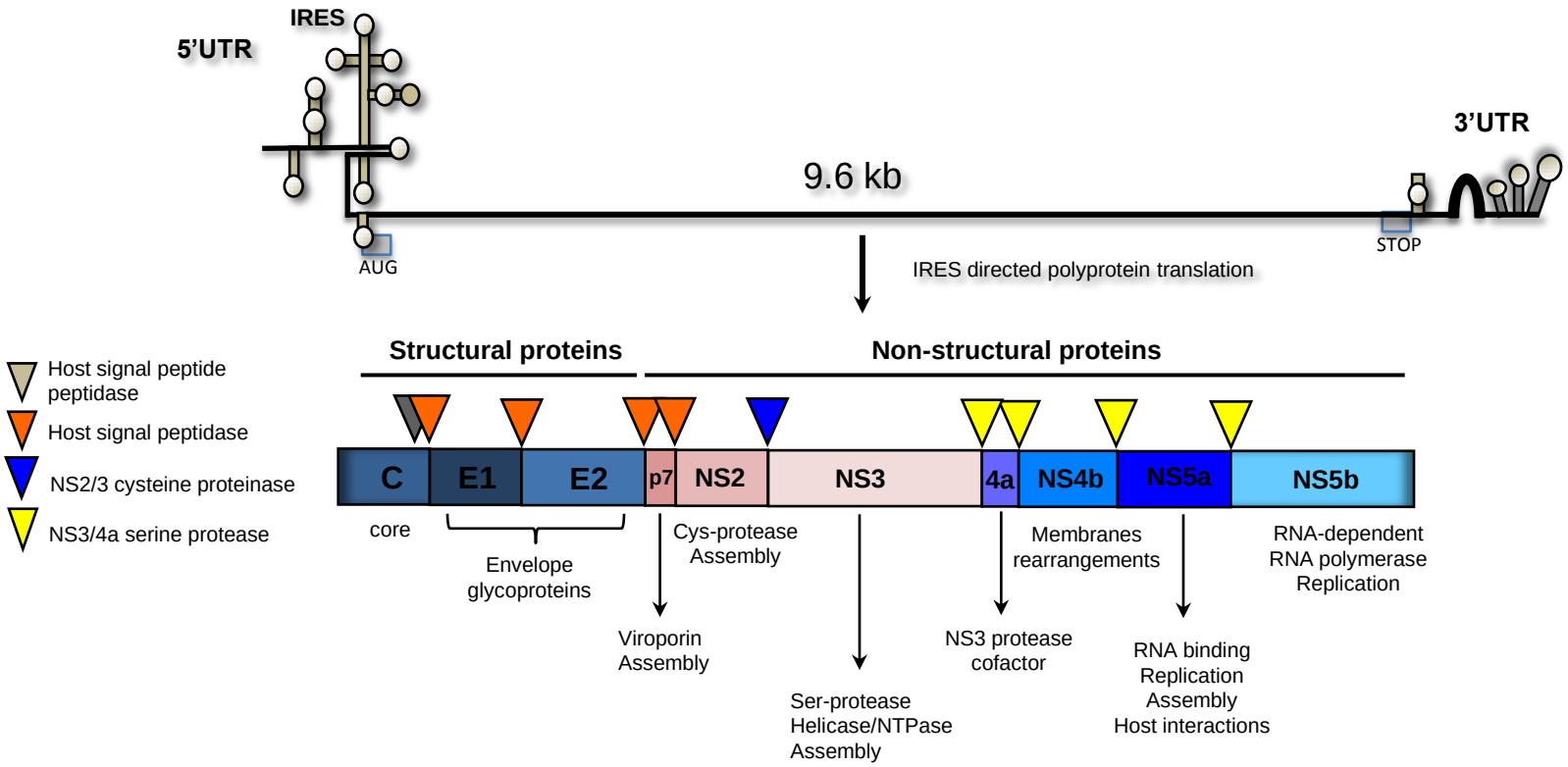


**Figure 1.4: Schematic representation of HCV genome organization.**
Adapted from (Eyre et al., 2014b)

The HCV open reading frame is translated into one polyprotein (about 3010 aa long) which is co- and post-translationally cleaved into 10 viral proteins: 3 structural proteins (Core, E1 and E2), the peptide p7 and 6 non-structural (NS) proteins (NS2, NS3, NS4A, NS4B, NS5A and NS5B). The 3 structural proteins are critical components of the viral particle and thus are involved in virion assembly and viral entry. On the other hand, non-structural proteins together with a long list of host factors enable viral genome translation, replication and particle assembly as well as taking part in the cellular membrane reorganisation to form structures known as membranous webs (See Figure 1.4 for a short summary of each viral protein's role in the life cycle).

### 1.2.2 HCV genotypes

Since HCV was first isolated in 1989 (Choo et al., 1989), seven major HCV genotypes (genotypes 1 to 7) and numerous subtypes each present in several isolates, have been characterised in the literature (Smith et al., 2014). These different genotypes display significant genetic variability which can influence HCV biology, viral pathogenicity and their sensitivity to treatments and immune responses (e.g. drug therapy and/or neutralizing antibodies).

As presented in Figure 1.5, different HCV genotypes display unique geographical prevalences. Genotype 1 (and especially subtypes 1a and 1b) is the predominant genotype in Western countries, although together with genotypes 2 and 3 they are present worldwide. On the other hand genotypes 4, 5 and 6 are more endemic to specific regions (respectively Middle East to central Africa, South Africa and Asia).

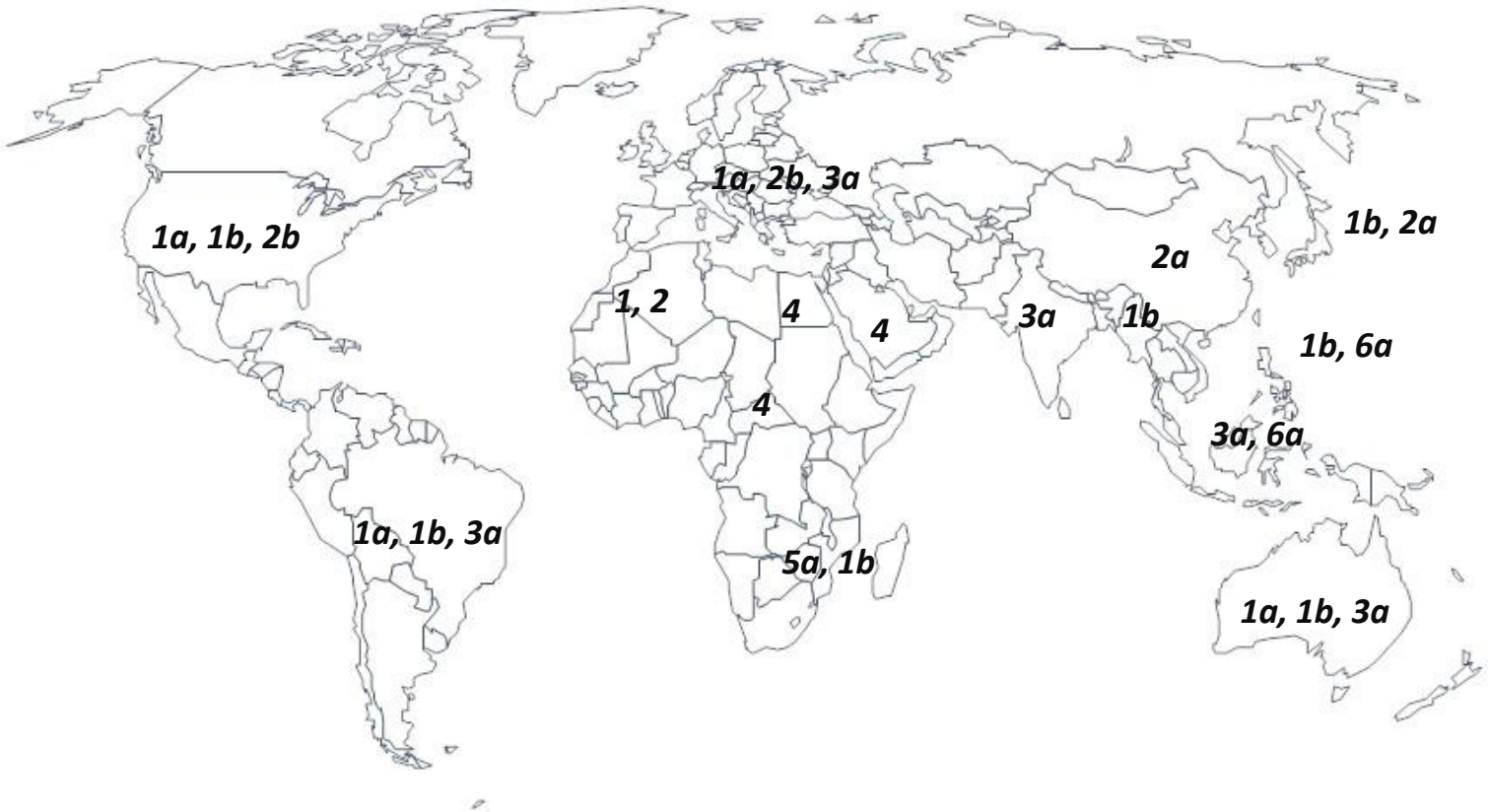


**Figure 1.5: Worldwide distribution of the HCV genotypes**
Prepared using data from Gower and al., 2014

### 1.2.3 HCV viral particles

HCV particles are 40 to 80 nm in diameter and transit through the blood stream in association with serum lipoproteins (Thomssen et al., 1992). The tight association between HCV virions and serum lipoproteins has given rise to the description of HCV viral particles as “lipoviral particles” (LVP). This association is critical for HCV as it facilitates viral entry into hepatocytes and escape from neutralizing antibodies. However, HCV-lipoprotein association is not specifically restricted to one class of lipoprotein (Merz et al., 2011). It has been hypothesised that HCV particles interact transiently with lipoproteins or are associated with lipoproteins and share a common envelope.

### 1.2.4 HCV entry

According to the current model (Figure 1.6 (McCartney et al., 2011)), HCV particle entry unravels as a temporally and spatially coordinated sequence. The first step of virus entry consists of attachment of the circulating HCV LVP to the cell surface of the hepatocytes. HCV LVP attachment is enhanced by a low affinity interaction between Apolipoprotein E (ApoE), a protein of LVP, and the low-density lipoprotein receptor (LDLR) (Agnello et al., 1999; Owen et al., 2009) and glycosaminoglycans (GAG) (Germi et al., 2002) located at the hepatocyte surface. Following this initial HCV LVP attachment to the hepatocytes, scavenger receptor class B type I (SR-BI) binds to the hypervariable region 1 (HVR1) of the virus glycoprotein E2 (Dao Thi et al., 2012; Scarselli et al., 2002). The binding is thought to induce a conformational change in E2, leading to the exposure of an epitope (Bankwitz et al., 2010) that has a high binding affinity for the CD81 plasma membrane receptor (Petracca et al., 2000). Subsequently, HCV E2 binding to CD81 induces a cascade of activation of signal transduction

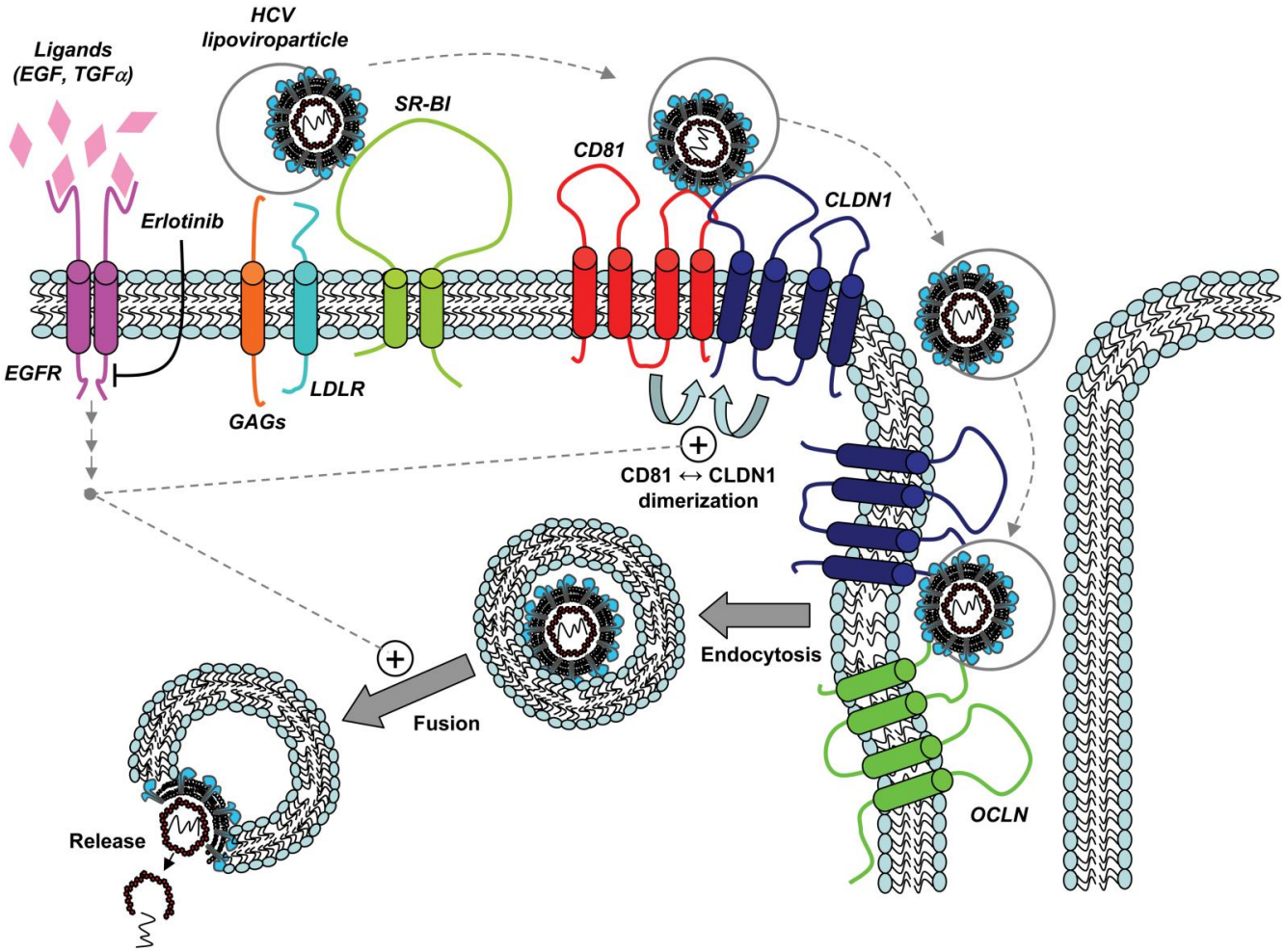


**Figure 1.6: Schematic representation of HCV entry**
Reproduced from McCartney et al., 2011.

resulting in an increase of the lateral mobility of the CD81-E2 complex towards the tight junction zone (Brazzoli et al., 2008), where claudin 1 (CLDN1) and occludin (OCLN) are concentrated.

Interaction between CLDN1 and the CD81-bound HCV LVP may trigger the second step of HCV entry, which is clathrin-mediated endocytosis (Farquhar et al., 2012) and results in internalisation of the viral particle. Although OCLN is necessary at this stage, its precise role is not yet understood (Ploss et al., 2009; Sourisseau et al., 2013). Finally, the cholesterol transporter Nieman-Pick C1-like 1 (NPC1L1) has recently been identified as a necessary co-factor for HCV entry at the post-binding step (Sainz et al., 2012), although its precise role remains unknown. Finally, more recently the transferrin 1 receptor has been described as an essential HCV entry factor (Martin and Uprichard, 2013), although the precise mechanism is not well understood.

The internalised HCV particle is then transported along actin stress fibres towards the Rab5A coated early endosome (Coller et al., 2009; Farquhar et al., 2012). Acidification of the endosome later induces fusion of the virus envelope and the endosomal membrane through the viral glycoproteins presumably primed by E2-CD81 interaction (Sharma et al., 2011). Membrane fusion results in disassembly of the nucleocapsid and release of the viral genome into the cytosol where it is readily translated to yield viral proteins to enable initiation of viral replication (Niepmann, 2013).

### 1.2.5 Viral translation

Translation of the HCV genome is cap-independent and is initiated by the internal ribosome entry site (IRES) located in the 5' end of the untranslated region (5' UTR) of the viral RNA (Brown et al., 1992; Tsukiyama-Kohara et al., 1992; Wang et al., 1993). Particularly, the 5'UTR stem loops II, IIIa/b/c and IIId/e/f, IV and part of the core coding sequence form secondary structures enabling binding of the small ribosomal 40s subunit (Spahn et al., 2001; Wang et al., 1995). The eukaryotic initiation factors (eIF) 3, eIF2 and eIF5 also contribute to the formation of the HCV genome translation complex. Additionally, a growing list of host factors have been identified as IRES trans-acting factors of HCV genome translation, for example La protein (Ali et al., 2000; Ali and Siddiqui, 1997) and NSAP1 (Kim et al., 2004; Park et al., 2011) which bind to the viral RNA or the ribosomal subunit 40S, respectively.

Recent research has identified micro-RNA122 (miR122) as an important factor in the regulation of HCV genome translation and a determining element in the hepatocyte specific cell tropism of HCV as it is specifically expressed at high levels in hepatocytes (Chang et al., 2004; Landgraf et al., 2007). Since miR122 was first described as an enhancer of HCV propagation (Jopling et al., 2005), multiple modes of action have been determined at different stages of the life cycle. MiR122 stimulates HCV RNA translation by enhancing interaction between HCV RNA and the small ribosomal 40s subunit through two binding sites in the 5'UTR (upstream of the IRES) (Henke et al., 2008). Moreover, miR122 has been shown to release constraint on the HCV IRES when binding to two sequences contained within the 5'UTR (Diaz-Toledano et al., 2009). Indeed, a long-range annealing (LRA) motif within the 5'UTR tends to lock HCV RNA in a closed conformation, blocking the functional role of the IRES (Honda et al., 1999; Kim et al., 2003). However when binding to the seed sequences within the

5’UTR, miR122 competes with these LRA motifs and enables a switch towards an open secondary structure where the IRES is available and thus enhances HCV RNA translation (Diaz-Toledano et al., 2009). Finally, miR122 physically stabilizes HCV RNA through binding to its seed sequences within the 5’UTR as an Ago2 RNA-protein complex. Furthermore, this interaction protects the viral RNA from 5’ exonuclease degradation and thus promotes HCV RNA accumulation (Shimakami et al., 2012a; Shimakami et al., 2012b).

As mentioned earlier, due to its involvement in HCV translation and its liver specificity, miR122 represent a good therapeutic target. Recently development of the molecule Miravirsen (Santaris Pharma), a locked nucleic acid (LNA)-modified oligonucleotide that bind miRNA-122, has shown encouraging results supporting targeting of miR122 in treatment of HCV infection (Baek et al., 2014).

### 1.2.6 Viral replication

HCV genome replication is a pivotal step of the virus life cycle, although the specific mechanisms involved are still not precisely understood. Following translation events and polyprotein processing, the viral non-structural proteins NS3 to NS5B are targeted to the endoplasmic reticulum (ER) where they associate to form the HCV RNA replication machinery, termed “replication complexes” (RC). Vesicular membrane reorganisation (see Figure 1.7 A) has been observed in both replicon-harbouring cells (Ferraris et al., 2010; Gosert et al., 2003; Romero-Brey et al., 2012) as well as infected hepatocytes (Shimizu, 1992). These alterations termed “membranous webs” (MW) represent an accumulation of single, double and multi membrane vesicles (respectively SMV, DMV or MMV) (see Figure 1.7 B (Paul et al., 2014)) and are a key feature of

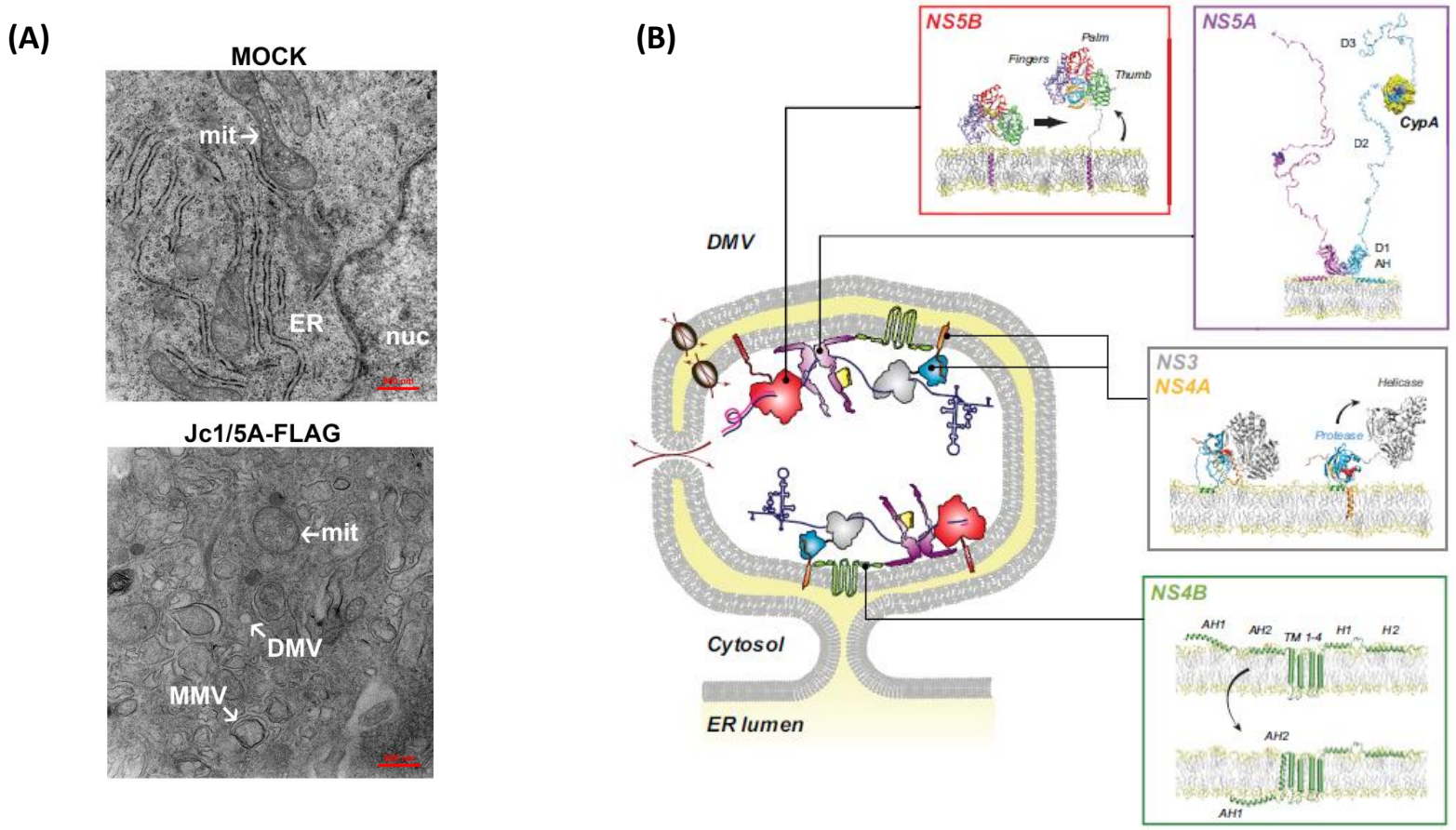


**Figure 1.7: HCV replication**

**(A)** Electron microscopy showing HCV-induced membrane rearrangements including double membrane vesicles (Unpublished data, provided by N. Eyre [The University of Adelaide]). **(B)** Schematic representation of the current model for the double membrane vesicles and the 3D representation of the non-structural proteins involved - Taken from (Paul et al., 2014).

HCV RNA replication. Indeed many positive-stranded RNA viruses induce the formation of membranous web-like structures that harbour viral replication.

The membranous vesicles are hypothesised to concentrate and protect HCV replication complexes. It is thought that the membranous structures predominantly originate from the ER (Egger et al., 2002; El-Hage and Luo, 2003; Gosert et al., 2003; Miyanari et al., 2003; Romero-Brey et al., 2012). Although it was originally thought that formation of the membranous web was solely NS4B dependent (Egger et al., 2002), recent studies have shown NS3/4A and NS5B could solely induce formation of SMVs while NS5A expression induces formation of DMVs and MMVs (Romero-Brey et al., 2012). Taken together, it is now believed that NS4B strongly drives formation of the membranous web in concert with NS5A, NS3/4A and NS5B. Furthermore oligomerisation of NS4B has been shown to play an important role in RNA replication, probably acting as a scaffold for membranous web biogenesis (Gouttenoire et al., 2010; Paul et al., 2011; Yu et al., 2006).

A large number of host factors have also been described as playing essential roles in membranous web morphogenesis. For example, recruitment of phosphatidylinositol 4-kinase III alpha (PI4KIIIα) by NS5A towards replication complexes induces an up-regulation of PI4KIIIα lipid kinase activity and thus an increase in phosphatidylinositol 4-phosphate (PI4P) levels within the replication complexes (Berger et al., 2009; Berger et al., 2011; Reiss et al., 2011). Moreover, PI4KIIIα has been shown to play a critical role in membranous web morphogenesis directly or through one of its downstream products, as knock-down of PI4KIIIα results in abnormal membranous web morphology (Reiss et al., 2011).

At the core of replication complexes is NS5B; a single-subunit RNA dependent RNA polymerase (RdRp) that mediates synthesis of both positive and negative strands of the viral RNA (Behrens et al., 1996; Lohmann et al., 1997). It is composed of a catalytic site within the N-terminus and a membrane anchor at the C-terminus joined through a short linker sequence. Furthermore, initiation of RNA synthesis requires interaction of NS5B with the viral helicase NS3 and NS5A (Binder et al., 2007), although the precise functional roles of NS3 and NS5A are not resolved yet. In addition to its activity as a protease with co-factor NS4A, NS3 is an NTPase / helicase and is hypothesised to be involved in replication through management of the viral RNA complex secondary structures such as the stem loops in the untranslated regions.

NS5A is a phosphoprotein without any known enzymatic activity and is critically involved in both replication of viral RNA and assembly of new virions. It is composed of 3 distinct domains (Tellinghuisen et al., 2004): domains 1 (D1) and 2 (D2) have been shown to be linked with HCV RNA replication, whereas domain 3 (D3) is critical for virion assembly (Appel et al., 2008; Kim et al., 2011; Tellinghuisen et al., 2008a; Tellinghuisen et al., 2008b). In addition, D2 and D3 are largely dispensable for RNA replication (Appel et al., 2005; Blight et al., 2000). Furthermore, D1 enables dimerisation of NS5A and consequent formation of a potential RNA binding groove (Tellinghuisen et al., 2005). NS5A contains multiple phosphorylation sites, however only two stable states of phosphorylation are commonly found in the cell: one termed as hypo-phosphorylated (p56) and the other one as hyper-phosphorylated (p58) (Tanji et al., 1995; Tellinghuisen et al., 2004). The cascade of phosphorylation shifting the balance between one or the other state may represent a molecular switch between NS5A involvement in HCV RNA synthesis (through p56) and virion assembly (through

p58) (Appel et al., 2005; Evans et al., 2004; Lemay et al., 2013; Neddermann et al., 2004; Pietschmann et al., 2009; Ross-Thriepland and Harris, 2014).

Various host factors have been reported as interacting partners with replication complex components that are necessary for viral RNA synthesis. For instance, the human vesicle-associated membrane protein-associated protein subtypes A and B (hVAP-A and hVAP-B) have both been found to interact with NS5B and NS5A and be essential for RNA replication (Evans et al., 2004; Gao et al., 2004; Hamamoto et al., 2005). Interestingly, hVAP-A appears to preferentially bind to the hypo-phosphorylated (p56) NS5A and not the hyper-phosphorylated form (p58) (Evans et al., 2004) and thus represents the only known host factor whose interaction is dependent on specific NS5A phophorylation state.

### 1.2.7 Viral assembly and release

The HCV core protein is synthesised at the ER membrane where it matures and homodimerizes (Boulant et al., 2005). With the support from cytosolic phospholipase A2 (cPLA2) (or downstream signalling pathways) (Menzel et al., 2012) and diacylglycerol O-acetyltransferase 1 (DGAT1) (Herker et al., 2010), core then rapidly migrates towards the surface of Lipid droplets (LDs) (Barba et al., 1997; Counihan et al., 2011), where it accumulates.

Upon appropriate NS5A phosphorylation (Appel et al., 2008; Kim et al., 2011; Masaki et al., 2008; Tellinghuisen et al., 2008a), it is hypothesised that core recruits NS5A associated with viral RNA and/or complete replication complexes to the cLD surface where they interact (Masaki et al., 2008; Miyanari et al., 2007; Pietschmann et al.,

2009; Tellinghuisen et al., 2008a). This interaction represents an essential step of viral particle assembly (Appel et al., 2008; Masaki et al., 2008; Miyanari et al., 2007), however the details of this process are not well understood.

Core is then thought to be slowly retrieved from the cLD surface towards the closely located ER surface where the assembly of immature virions is hypothesised to take place. This relocation is fundamental and depends on numerous factors: host factors such as AP2M1 (clathrin adaptor protein complex 2, μ1 sub-unit) (Neveu et al., 2012) and viral proteins: interaction between NS2 and p7 is required for assembly (Jirasko et al., 2010; Popescu et al., 2011) and enables NS2 to further interact with NS3/4A complex triggering core relocation (Counihan et al., 2011). Moreover, the NS3/4A complex plays a critical role in assembly through NS3 helicase activity as detrimental mutations severely handicap assembly of new virions (Jirasko et al., 2010; Jones et al., 2011; Ma et al., 2008; Phan et al., 2009). NS3 helicase could possibly be involved in RNA packaging into the forming capsid.

Meanwhile, viral glycoproteins E1 and E2 are synthesised and translocated into the ER membrane in premature forms (Dubuisson et al., 1994; Duvet et al., 1998; Rouille et al., 2006) where E1 and E2 hetero-dimerize (Op De Beeck et al., 2000; Yi et al., 1997). Both viral glycoproteins then fold in a slow and interdependent process (Brazzoli et al., 2005; Michalak et al., 1997; Patel et al., 2001).

Numerous gaps remain in our understanding of the processes involved at these steps of virion assembly, however it is believed that all of these events happen in a spatially and temporally coordinated manner towards encapsidation of viral RNA into budding immature virions (Figure 1.8 (Paul et al., 2014)). Although this remains controversial, virion biogenesis may be partially coordinated through the ESCRT (endosomal-sorting

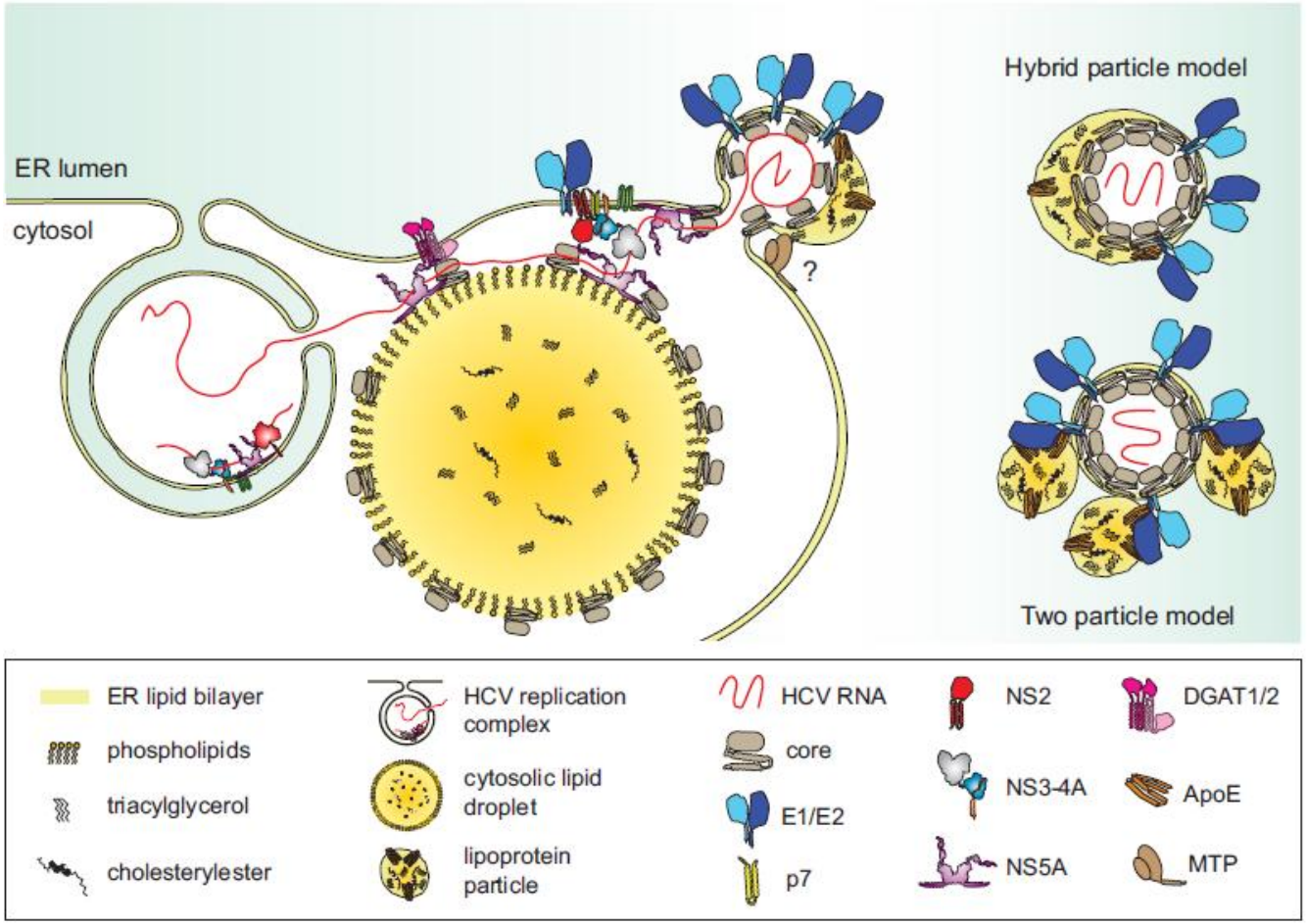


**Figure 1.8: Model of HCV particles biogenesis**
Reproduced from Paul et al., 2014

complex required for transport) pathway (Ariumi et al., 2011; Corless et al., 2010; Tamai et al., 2012).

The buoyant densities of immature virions and released viral particles differ strongly (Gastaminza et al., 2008; Gastaminza et al., 2006) and this suggests that viral release involve lipidations characteristic of the VLDL maturation and secretion pathway. In addition, the complex post-translational modifications of the viral glycoprotein E1-E2 complexes present on the surface of infectious HCVcc in comparison to those of immature virions (Vieyres et al., 2010) strongly suggests that particles undergo maturation through the Golgi apparatus before being released. The viral non-structural protein p7 has been shown to play a critical role in the release of infectious viral particles. Multiple lines of evidence indicate that p7 acts as a viroporin, such that its ion-channel activity equilibrates pH and buffers the different intracellular compartments involved in the secretion pathway, thus protecting viral particles from degradation during release (Clarke et al., 2006; Griffin et al., 2003; Luik et al., 2009; OuYang et al., 2013; Wozniak et al., 2010).

## 1.3 HCV model systems

Since 1989 and the original identification of hepatitis C virus by Choo and colleagues (Choo et al., 1989), HCV research has been hampered by the lack of accurate research models to study virus-host interactions in cell culture. Historically, chimpanzees were the only animal model and helped in the initial description of the virus. However the use of chimpanzees for research raises obvious technical and ethical challenges and development of cell culture research models was a major focus of the field. In the following years, research progressed in a step-wise manner dictated by three major breakthroughs each progressing further towards the possible study of the full viral life cycle. First the development of the subgenomic replicon system, enabling autonomous replication of HCV RNA and expression of viral non-structural proteins (Lohmann et al., 1999), succeeded in opening new ways of investigating HCV RNA replication and translation (Figure 1.9 A (Tellinghuisen et al., 2007)). Secondly a retroviral based system to generate HCV pseudo-particles (HCVpp) (Bartosch et al., 2003; Hsu et al., 2003) and mimic HCV entry constituted a new critical tool to increase our understanding of this evasive pathogen (Figure 1.9 B (Tellinghuisen et al., 2007)). Finally, a research model enabling the full viral life cycle to be studied in cell culture and generating infectious virions (HCVcc) was described in 2005 (Lindenbach et al., 2005; Wakita et al., 2005; Zhong et al., 2005) (Figure 1.9 C (Tellinghuisen et al., 2007)).

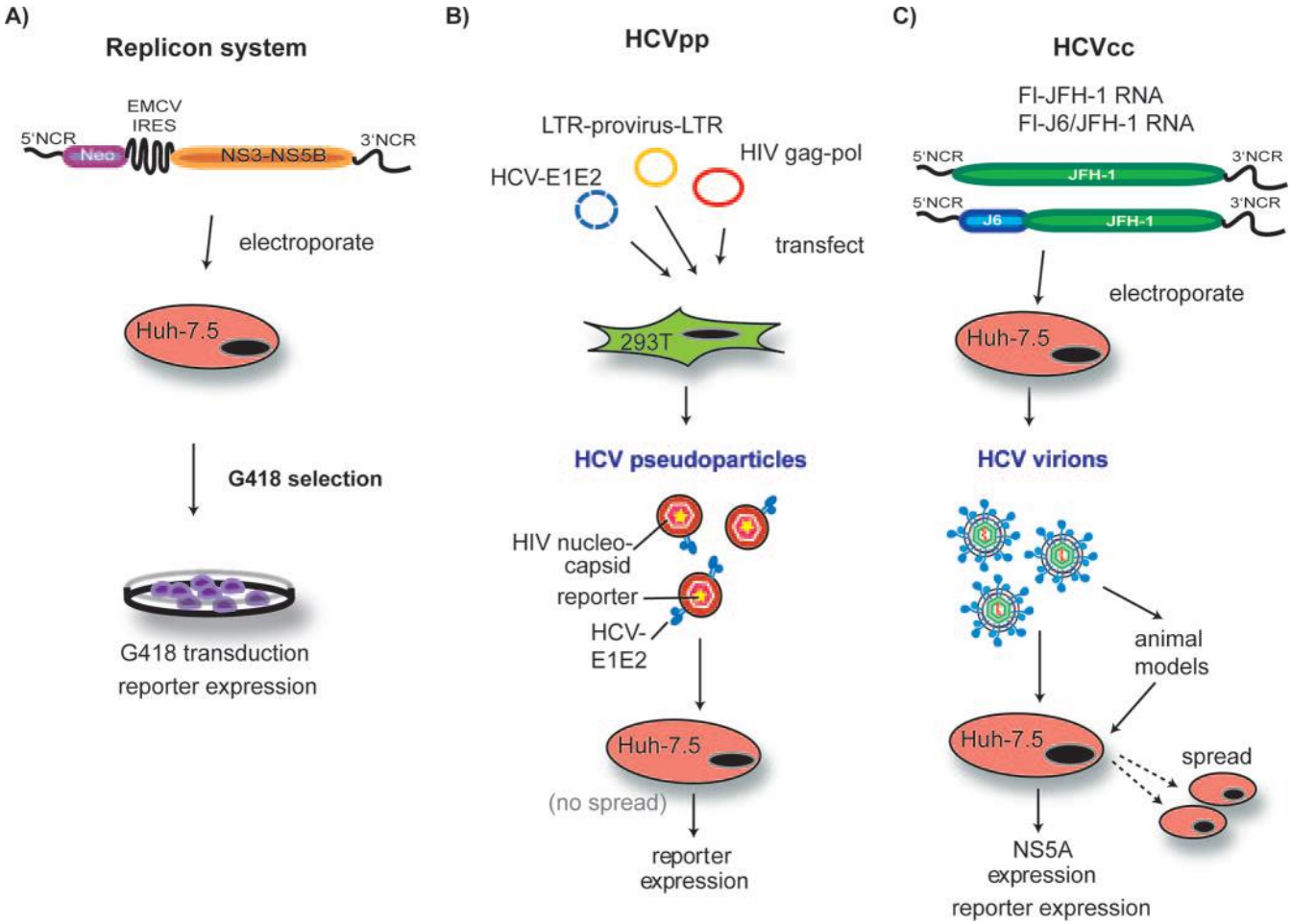


**Figure 1.9: Schematic representation of the different HCV research models**
Reproduced from Tellinghuisen et al., 2007.

### 1.3.1 HCV replicon system

The study of viral replication through the development of a subgenomic replicon was the first step towards understanding the HCV life cycle (Lohmann et al., 1999). Inspired from the studies of other positive strand RNA viruses such as West Nile virus (Kunjin virus) (Khromykh and Westaway, 1997; Mittelholzer et al., 1997), the system is based on the autonomous replication of part of a genotype 1b (Con1 isolate) HCV genome within a permissive cell line (Huh-7 – human hepatoma cell line). The construct was bicistronic and included two internal ribosomal entry sites (IRES). The first IRES was from HCV and controlled expression of an antibiotic (Neomycin) resistance gene while the second was of encephalomyocarditis virus (EMCV) and controlled expression of HCV non-structural proteins [NS3 to NS5B]. Viral replication associated to a resistance gene together with the high error rate of the NS5B RNA dependent RNA polymerase enabled selection of cell lines harbouring high levels of HCV RNA replication and determination of “replication enhancing mutations” (REM) within the coding sequence of the virus.

Improved replication was also achieved through the selection and usage of Huh-7 derived cell lines named Huh-7.5, Huh-7.5.1 and Huh-7 Lunet (Blight et al., 2002; Friebe et al., 2005; Zhong et al., 2005) which were selected through their ability to support replication of HCV subgenomic replicons and then cured of the virus by interferon therapy. Subsequent use of these cell lines showed higher levels of replication and today they remain widely used by the HCV research community.

### 1.3.2 Retroviral pseudo-particles

The second major development in understanding the HCV life cycle involved the development of a system enabling investigation of HCV entry and early stages of the infection (Bartosch et al., 2003; Hsu et al., 2003). This system is based on 2 or 3 expression vectors enabling production of retroviral particles in 293T cells mimicking HCV virus particles by incorporating the E1-E2 functional complex onto retroviral cores that contain a retroviral reporter genome. This system involves simultaneous transfection of 293T cells with vectors for the HCV glycoproteins (E1, E2), the human immunodeficiency virus (HIV) or murine leukemia virus (MLV) gag-pol proteins and the reporter retroviral genome, followed by collection of the HCV pseudo-particles (HCVpp) which are subsequently used to investigate viral entry. Moreover the reporter gene enables sensitive quantification of productive virus entry events.

### 1.3.3 Infectious HCV genomes

Finally the last major improvement in terms of research models was initiated in 2001 with the publication of the consensus sequence from a genotype 2a HCV genome isolated from a patient with fulminant hepatitis termed JFH-1 (Kato et al., 2001). The subgenomic replicon derived from JFH-1 was found to replicate at much higher levels (Kato et al., 2003) than other previously described HCV subgenomic replicons and did not require replication enhancing mutations which often impair the late stages of the HCV life cycle. Thereafter, in 2005, three groups (Lindenbach et al., 2005; Wakita et al., 2005; Zhong et al., 2005) reported the generation of full-length infectious HCV genomes based on JFH-1 which were able to undergo the full viral life cycle in cell culture. This model opened up the investigation of all stages of the viral life cycle,

including the production of infectious viral particles in both cell culture and animal models (Lindenbach et al., 2006).

## 1.4 Live imaging of viral life cycles

### 1.4.1 Introduction

Much of our understanding of viral life cycles, including that of HCV, has been based on observation of static images of fixed cells and biochemical analysis of replication. Cell fixation preserves the cell for downstream analysis, but it is also a potentially damaging process which may lead to artefacts that do not accurately reflect the appearance and localisation of proteins and structures in living cells. For instance fragile structures within the cells such as LDs can be readily disrupted by fixation (DiDonato and Brasaemle, 2003). Furthermore, observation of static images does not provide information about the intracellular dynamics of virus-host interactions which arise as a critical factor for the study of the HCV life cycle.

In contrast, live imaging of single cells through genetically encoded fluorescent proteins has emerged as a powerful technique to reveal intricate dynamics in protein expression, localisation and traffic at the sub-cellular level. Moreover, application of this technique in the context of active viral replication and expression of viral proteins has the potential to reveal new details about aspects of viral life cycles and virus-host interactions. For example, it has previously been shown that attachment, entry and intracellular transport of individual virions can be characterised by live cell imaging

(Brandenburg and Zhuang, 2007; Jouvenet et al., 2008; Jouvenet et al., 2009). Similar techniques based on the fusion of HCV core or NS5A viral proteins with a fluorescent protein (such as GFP or a tetracysteine motif (TCM) which can specifically be labelled (Hoffmann et al., 2010)) have been reported both in the context of a subgenomic HCV replicon (Moradpour et al., 2004; Wolk et al., 2008) and live infectious virus (Coller et al., 2012; Counihan et al., 2011; Eyre et al., 2014a).

### 1.4.2 HCV NS5A live imaging

Due to its unique and enigmatic role at the centre of the HCV life cycle, the viral NS5A protein has gathered significant attention from the HCV research field, including studies involving the use of live cell imaging. In 2004, Moradpour and colleagues developed the first *in vitro* replicon based HCV research model enabling imaging of NS5A viral protein in real time (Moradpour et al., 2004). Insertion of a green fluorescent protein (GFP) reporter within a newly identified site of tolerance in the NS5A coding sequence enabled visualisation of NS5A viral protein localisation and traffic within a single cell. Using the same system, further analysis of NS5A traffic and localisation revealed for the first time that NS5A existed as two types of structures in live cells: one described as relatively large and static, often located in the periphery of the nucleus and a second described as small or discrete and often highly motile trafficking sporadically throughout the cytoplasm at velocities in the order of 1 μm / s (Wolk et al., 2008). Furthermore, in this study, Wolk and colleagues determined that the saltatory movement observed for the small NS5A-positive structures was microtubule- (MT-) dependent as the use of Nocodazole, which depolymerises MTs (Dohner and Sodeik, 2005), significantly arrested their movement. Finally, fluorescence recovery after photobleaching (FRAP) experiments revealed that the

internal organisation of the large structures was rather static as there was no observable short-term reorganisation or recovery following photobleaching of part of these structures. Nevertheless, this initial work was limited to tagging NS5A in the context of a HCV subgenomic replicon not containing any of the viral structural proteins. Furthermore the replication enhancing mutation carried in NS5A by this particular replicon could influence the localisation and traffic of NS5A particularly with respect to its role at the intersection between replication and assembly as mentioned in Section 1.3.1. Consequently the relevance of this imaging was limited when considering the role(s) of NS5A in infectious virus production.

Interestingly, similar observations of putative replication complex traffic have been reported for mouse hepatitis coronavirus (MHV) non-structural protein 2 (nsp2) (Hagemeijer et al., 2010). Coronaviruses (CoVs) are enveloped positive-stranded RNA viruses which induce reorganisation of the endoplasmic reticulum (ER) membrane towards the formation of single or double membranes vesicles harbouring replication-transcription complexes (RTCs) in a manner similar to other plus-strand RNA viruses such as HCV (Mackenzie, 2005; Miller and Krijnse-Locker, 2008; Salonen et al., 2005). The traffic and behaviour of MHV nsp2 reported (Hagemeijer et al., 2010) is very similar to the observations made by Wolk and colleagues concerning HCV NS5A (Wolk et al., 2008) as nsp2 is described to primarily appear in 2 different structures. MHV nsp2 small and motile structures present a saltatory and MT-dependent movement with mean velocity calculated at 1.3 μm / s while the second larger structures remain static within the cell cytoplasm. However, in contrast to HCV, MHV replication and virus production were not impaired by Nocodazole treatment (Hagemeijer et al., 2010) meaning that this MT-dependent movement was not essential to the MHV life cycle.

Studies conducted in our laboratory expanded on the work of Wolk and colleagues (Wolk et al., 2008) and involved generation of infectious HCV Jc1-derived chimeras that enable live cell imaging of fluorescently labelled NS5A in the context of a productive HCV infection (Eyre et al., 2014a). Carrying an insertion of an optimised tetracysteine motif (TCM) (Hoffmann et al., 2010) within the Domain III of NS5A coding sequence (Schaller et al., 2007), the construct designated as Jc1/5A-TCM replicates and produces infectious virions at comparable efficiencies to parent Jc1 (Eyre et al., 2014a). More importantly, the TCM could be specifically labelled with membrane permeant biarsenical fluorescent dyes known as FlAsH-EDT (green) and ReAsH-EDT (Red). TCM labelling enabled NS5A real-time visualisation in living cells during a productive infection with minimal impact on virion production. Furthermore it enabled us to confirm the observations on NS5A types of structures throughout the whole viral life cycle. In addition this study showed that both NS5A structures were also enriched with host factors characteristic of RCs such as VAP-A and Rab5A. Finally pulse-chase imaging experiments enabled distinction between older and younger pools of NS5A-positive structures and showed that both pools were comprised of different relatively static and highly motile foci.

The NS5A protein is a well described marker of the HCV replication complex (described in Section 1.1.8) as well as being crucial for HCV RNA delivery and new virion assembly. As such NS5A is a crucial protein in numerous aspects of the HCV life cycle. However it is unclear from previous live cell imaging studies whether one or both pools of NS5A (static vs motile) represent replication complexes and/or sites of delivery of HCV RNA. If indeed these NS5A complexes are replication complexes or involved in delivery of HCV genomes then they should harbour HCV RNA. Therefore, development of a model system to track HCV RNA in real time together with NS5A

would greatly contribute towards improving our understanding of the HCV life cycle dynamics and potentially enhance development of new therapeutic strategies against Hepatitis C virus.

### 1.4.3 MS2 bacteriophage based system for live RNA imaging

Techniques that enable in vivo live imaging of mRNA can provide tremendous amounts of information about intracellular mRNA localisation, traffic and biogenesis within the cell. Pioneers in the field, Robert Singer and co-workers, first demonstrated visualization of mRNA traffic within yeast in 1998 using the MS2 bacteriophage system (Bertrand et al., 1998). Figure 1.10 presents a schematic of the model and of the elements involved for a greater clarity. The RNA live imaging system is based on two elements of the MS2 bacteriophage: the first element involves expression of a fusion protein between the MS2 Bacteriophage coat protein and a fluorescent protein (e.g. green fluorescent protein [GFP] or mCherry) within the experimental model (e.g. mammalian or yeast cell). The second element is an expression system where the mRNA of interest is engineered to carry an array of MS2 Bacteriophage stem loops (up to 24) in a variable untranslated region. Theoretically, when the mRNA is expressed, the high affinity between the MS2 bacteriophage coat protein and the MS2 bacteriophage stem loops should redistribute the fluorescently labelled MS2 coat protein to the site of the tagged mRNA.

Since it was first described in yeast (Bertrand et al., 1998), this technique has successfully been used to reveal new insights in mRNA biology and the visualization of viral RNA. Indeed, by engineering an MS2 bacteriophage stem loop array within the untranslated region of viral genomes, this technique has been applied to visualize

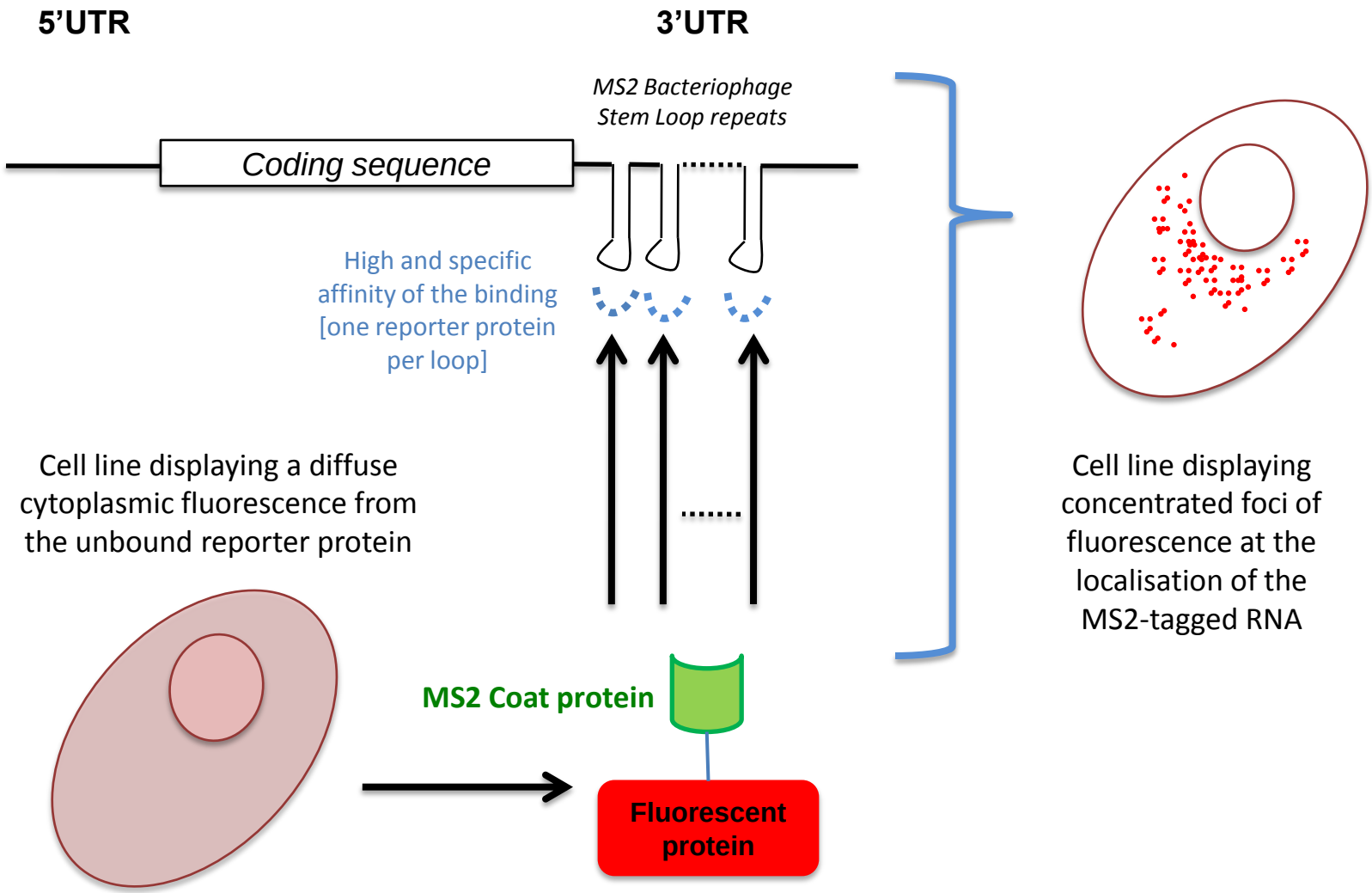


**Figure 1.10: Schematic representation of the MS2 bacteriophage stem loop system for RNA tagging**

murine leukaemia virus (MLV) RNA traffic (Basyuk et al., 2003), the human immunodeficiency virus type 1 (HIV-1) transcription cycle (Boireau et al., 2007; Maiuri et al., 2011) and HIV-1 mRNA biogenesis (Jouvenet et al., 2008). More recently this approach has enabled visualization of tick-borne encephalitis virus (TBEV) (an HCV-related Flavivirus) viral RNA localisation (Albornoz et al., 2014; Miorin et al., 2008; Miorin et al., 2013).

Like HCV, TBEV is a single-stranded, positive strand RNA virus of the *Flaviviridae* family. Although part of different genera of the *Flaviviridae* family, these two viruses are phylogenetically relatively close and are both known to reorganise the intracellular environment of the infected cell into single and double membrane vesicles to anchor their replication machinery. TBEV RNA localisation was visualized using an MS2 stem loop-tagged subgenomic replicon permissive for insertion within its 3'UTR (Miorin et al., 2008). In contrast with previous work involving cellular messenger RNAs, in the case of positive strand RNA viruses, replication occurs via a negative strand RNA as template (usually referred to as replication intermediate [RI]). The presence of the complementary sequence of the MS2 stem loops within this negative strand RNA does not yield the same secondary structure and therefore does not relocate the MS2 bacteriophage coat protein in the context of a tagged-TBEV replicon (Miorin et al., 2008). Subsequent work using this system in combination with electron microscopy enabled further characterisation of the TBEV replication sites and RNA traffic (Miorin et al., 2013). As TBEV and HCV are relatively close phylogenetically, the results provided by the TBEV RNA studies were promising towards a possible translation of the method to the study of HCV RNA traffic and localisation.

As stated previously, transition from HCV RNA replication to particle assembly is poorly understood primarily because of the dynamic nature of the process and the

multitude of host and viral proteins which contribute. Furthermore, dynamic events leading to or driving HCV RNA traffic remain unclear. Study and tracking of the viral RNA itself during infection of living cells would help to bridge gaps in our understanding of the intersections between HCV RNA replication and virus particle assembly pathways. Therefore, live imaging appears to be an ideal approach to study dynamic and functional interactions during replication and assembly of viral particles.

## 1.5 Hypothesis and Aims

The aims of this thesis converge towards the study and understanding of the HCV life cycle and especially the localisation and traffic of HCV RNA during viral replication and its interactions with replication complex components. Initial aims focus on the development of a full-length HCV chimera enabling visualization of HCV RNA in living cells for the first time. Furthermore we aimed to characterise the viral RNA localisation and traffic in living infected cells. In the later aims we investigated the relationships between HCV RNA, NS5A and the lipid droplets in living cells harbouring active viral replication to better understand the transition between HCV replication and viral assembly.

**Hypothesis** – We hypothesise that HCV RNA traffics throughout the cytoplasm in association with NS5A and that this represents a crucial delivery mechanism whereby HCV RNA is delivered to sites of virion assembly.

**Aims:**

(1) Construct and characterize a HCV infectious genome that contains the insertion of MS2 stem loop to enable visualization of HCV RNA in living cells.

(2) Investigate and characterise the localisation and traffic of tagged-HCV RNA in real-time during HCV replication.

(3) Study HCV RNA and NS5A localisation and traffic in the context of transition from viral replication to assembly and illustrate their underlying interaction with lipid droplets.

# Chapter 2

# Materials and Methods

## 2.1 General Molecular Biology Methods

### 2.1.1 Synthetic oligonucleotides

Synthetic oligonuleotides were purchased from GeneWorks and were received lyophilised. Oligonucleotide master stocks were produced by resuspending to a concentration of 100 µM in MilliQ water accordingly to:

Volume of water (µL) = (number of nmoles x 10)

Further dilution in water to 20 µM and 9.6 µM was performed to prepare user stocks. All oligonucleotides were stored at-20°C.

### 2.1.2 Bacterial transformation

The *E.coli* α-Select Chemically Competent Cells (Bioline$^{TM}$) were used for bacterial transformation. Aliquots of cells were thawed on ice and 50 µL were placed in a pre-chilled microcentrifuge tube. Approximately 5ng of plasmid DNA or 5 µL of ligation product (see Section 2.1.7) was added to the cell suspension and the tube was gently agitated before being incubated on ice for 30 mins. Then the mixture was heat shocked at 42°C for 45 seconds and returned to ice for 2 mins. The preparation was then diluted

with 950 µL of SOC Medium (see Appendix I) and incubated at 37°C for 1 hour under vigorous shaking. Cells were centrifuged down to a pellet on a table-top centrifuge at 6000g for 10 mins, supernatant discarded and pellets resuspended in 80 µL of 0.85 % saline solution. The solution was then spread on L-Agar plates containing the appropriate antibiotics and incubated overnight at 37°C.

### 2.1.3 Mini-preparation (small scale) of plasmid DNA

One single transformed bacterial colony was used to inoculate a 10 mL LB culture containing appropriate antibiotics. The broth culture was then incubated at 37°C under vigorous shaking overnight (around 16 hrs). Centrifugation of 8 mL of the culture was performed at 6000g for 10 mins and supernatant was discarded. Plasmid DNA extraction was performed using a QIAprep® Spin Miniprep Kit (QIAGEN™) and a table-top microcentrifuge as per manufacturer's instructions.

### 2.1.4 Maxi-preparation (large scale) of plasmid DNA

One single transformed bacterial colony was used to inoculate a 3 mL LB culture containing appropriate antibiotics. The solution was then incubated at 37°C under vigorous shaking for 6 hrs for culturing and a fraction (200 µL) was transferred to a 200 mL solution of LB containing the appropriate antibiotic. This culture was then placed at 37°C under vigorous shaking overnight (around 16 hrs). Bacterial cultures were then centrifuged in 500 mL Oak Ridge tubes at 6000g for 15 mins (4°C) using an Avanti™ J-25I Beckman Coulter centrifuge (JA10 rotor). Plasmid DNA extraction was performed using a NucleoBond® Xtra Maxi kit (Macherey-Nagel™) as per manufacturer's instructions.

### 2.1.5 Restriction endonuclease digestion

Restriction enzymes were purchased from New England Biolabs® Inc (NEB) and used to perform restriction endonuclease digestions. Enzymes specifications (activity, optimal buffer and temperature) and DNA quantity were considered for the preparation of the reactions accordingly to the NEB Technical Reference. The Double Digest feature of the NEB website (*https://www.neb.com/tools-and-resources/interactive-tools/double-digest-finder*) was used to determine the optimal buffer when performing double digestions.

### 2.1.6 Agarose gel electrophoresis

Agarose gels (1-2% w/v) were prepared by dissolving Low EEO Agarose (AppliChem) in 1x TAE buffer (see Appendix I). Gels were cast in a BioRad® Sub-Cell GT Mini tank. DNA samples were mixed with 6x EZVision one, DNA dye and Buffer (Amresco®) and loaded into wells of the agarose gel. Electrophoresis was performed at 100V. DNA band visualization was performed using a UV Transilluminator (BioDoc-It™ Imaging System, UVP).

### 2.1.7 DNA Ligation

DNA ligation was performed using the Quick Ligation™ Kit from New England Biolabs®. A 3-fold molar excess of digested insert DNA was mixed with approximatively 50ng of similarly digested expression vector. This volume was then adjusted to 10µL with $dH_2O$. 10µL of Quick Ligation Reaction Buffer (2x) was then added. Finally 1µL of Quick T4 DNA Ligase was added. The reaction was then

thoroughly mixed and incubated at 25°C for 5 mins before being processed. Bacterial transformations were subsequently performed with 5µL of DNA ligation product.

### 2.1.8 Gel purification

After electrophoresis, the band corresponding to the DNA of interest was cut out of the gel (with minimum exposure to UV light) and processed with the MinElute® Gel Extraction Kit (Qiagen®) as per manufacturer's instruction. Purified DNA samples were then stored at -20°C until further use.

### 2.1.9 DNA sequencing

DNA sequencing (Sanger sequencing) was performed by the Australian Genome Research Facility (AGRF, Australia) using Big Dye Terminator chemistry version 3.1 (Applied Biosystems). Samples were submitted according to the sample submission guidelines of the service provider: DNA samples (approximately 1 µg) were mixed with 1 µL of oligonucleotide (9.6 µM) and volumes were adjusted to 13 µL with $dH_2O$. Sequencing results were analysed using both FinchTV software (version 1.4.0) (Geospiza, Perkin Elmer®) and the Basic Local Alignment Search Tool (BLAST) from the National Centre for Biotechnology Information (NCBI) website (*http://blast.ncbi.nlm.nih.gov/Blast.cgi?PROGRAM=blastn&PAGE_TYPE=BlastSearch&LINK_LOC=blasthome*).

### 2.1.10 Extraction of total RNA

Total cellular RNA was extracted with TRIzol® Reagent (Life technologies$^{TM}$) as per manufacturer's instructions. Cells grown in monolayers (in 6 well tray) were directly lysed by adding 1 ml of TRIzol® Reagent per well, and passing the lysate through the pipette tip several times. Chloroform (0.2mL per 1mL of TRIzol® Reagent) was added to each sample, and samples were then mixed vigorously for 15 sec and centrifuged at 12,000g and 4°C for 15 mins. The upper aqueous phase was transferred to fresh pre-chilled microcentrifuge tubes and 0.5 mL of isopropanol was added to each tube. Samples were once again mixed vigorously for 15 sec and centrifuged at 12,000g and 4°C for 10 mins. Supernatants were then removed and 1 ml of 75% ethanol in $dH_2O$ was added to wash the pellet. Samples were thoroughly mixed centrifuged at 7,500g and 4°C for 10 mins. Finally after discarding supernatant, the pellet was air-dried for 5 mins and resuspended in RNAse free $dH_2O$ (Life Technologies).

### 2.1.11 Nucleic acid quantification

The UV spectrophotometer Nanophotometer® (IMPLEN) was used to measure the absorbance of DNA or RNA solutions and thus to assess their concentration. Samples were considered of acceptable purity when the ratio $OD_{260nm}/OD_{280nm}$ was above 1.80 for DNA and above 2.0 for RNA.

### 2.1.12 cDNA preparation

#### *2.1.12.1 M-MLV Reverse Transcriptase RNAse H*

M-MLV Reverse Transcriptase RNAse H minus, point mutant (Promega) was used to prepare cDNA from purified RNA. 1 µg of RNA was mixed with 1µg of random hexamer primers (GeneWorks) and $dH_2O$ to reach a volume of 14 µL. Samples were incubated at 72°C for 5 mins, before being incubated at 4°C for a further 5 mins and a mixture of 3.25 µL of dH2O, 5 µL of 5x M-MLV RT 5X Reaction Buffer, 0.5 µmol of dNTP mix (Promega), 200 unit of M-MLV RT (H–) Point Mutant and 40 unit of rRNAsin® RNAse Inhibitor (Promega) was added. Once being thoroughly mixed samples were incubated at 42°C for 50 mins. Finally samples were diluted to 100 µL in $dH_2O$ and stored at -20 °C.

#### *2.1.12.2 SuperScript III Reverse Transcriptase*

Preparation of cDNA in the context of future deep sequencing analysis was performed using approximately 350-600 ng of extracted RNA (see Section 2.1.10) using SuperScript® III Reverse Transcriptase (Life Technologies) with the NS5Bend_R primer (see Appendix V) following manufacturer's protocol.

### 2.1.13 Polymerase Chain Reaction (PCR)

PCR were performed using an S1000™ Thermal Cycler (BioRad®). Several different DNA polymerase enzymes were employed to perform PCR depending on the usage: AmpliTaq Gold® DNA polymerase (Invitrogen, Life Technologies) was mainly used to perform bacterial colony screening before plasmid DNA preparation and after cloning as per manufacturer's instructions, Deep $Vent_R$™ DNA polymerase (New England Biolabs® Inc.) was used to amplify the MS2 bacteriophage stem loops repeats (see Section 2.1.14), the iProof™ High Fidelity DNA Polymerase (Bio-Rad) was employed (as per manufacturer's instructions) when a higher fidelity PCR was required (for cloning for example), the Platinium Taq® DNA Polymerase High Fidelity (Life Technologies) was used to generate A overhang during the amplification and allow direct ligation in pGEM-t Easy vector and finally the SequalPrep Long PCR kit (Life Technologies) was used for preparation of the deep sequencing samples (see Section 2.1.15). AmpliTaq Gold®, iProof™ High Fidelity and Platinium Taq® High Fidelity DNA Polymerases were used following manufacturer's recommendation adapting the annealing temperature to the temperature associated to the primers and choosing an appropriate elongation time for the expected product (1 min / 1 kb).

### 2.1.14 MS2 stem loop amplification using Deep $Vent_R$™ DNA polymerase

Amplification of the segment carrying the MS2 bacteriophage stem loop insertion was performed using Deep $Vent_R$™ DNA polymerase (New England Biolabs® Inc.). Mastermixes were prepared for each reaction by mixing 35.5 µL of $dH_2O$, 5 µL of 10x reaction buffer (provided in the kit), 1 µL of $MgSO_4$ (provided in the kit), 0.5 µL of Deep $Vent_R$™ DNA polymerase (provided in the kit), 1 µL of dNTPs, 1 µL of JFH1-9258FP HighTm (20 µM) and 1 µL of JFH1-9651RP HighTm (20 µM) (see Appendix

V for primer description). For each reaction 45 µL of mastermix was then mixed with 5 µL of cDNA (prepared as in Section 2.1.12) or 5-10 ng of plasmid DNA in solution. Reaction cycles were performed as follow: denaturation at 95°C for 4 mins, 30 cycles of 95°C for 30 sec and 72°C for 2 mins, and a final step at 72°C for 7 mins. Finally DNA bands were visualized after agarose electrophoresis (see Section 2.1.6).

### 2.1.15 PCR products for deep sequencing analysis

After cDNA preparation using SuperScript® III Reverse Transcriptase (Life Technologies), a 6kb long PCR product was generated using SequalPrep Long PCR kit (Life Technologies) to be sent to the Murdoch Institute for Immunology and Infectious Diseases (Perth, Australia) for 454 Sequencing.

For each reaction a mastermix was prepared by mixing 14.7 µL of $dH_2O$, 2 µL of 10x reaction buffer (provided in the kit), 0.4 µL of DMSO (provided in the kit), 1 µL of enhancer A (provided in the kit), 0.4 µL of SequalPrep Long DNA polymerase (provided in the kit), 0.5 µL of Forward Primer [KL_NS3P_F] (20 µM) and 0.5 µL of Reverse Primer [KL-NS5Bc_R] (20 µM) (see Appendix V for primer description). Then 19.5 µL of mastermix was then added to 0.5 µL of cDNA (100 ng/µL). Reaction cycles were performed as follow: a first step at 94°C for 2 mins, 10 cycles of [94°C for 10 sec, 51°C for 30 sec and 68°C for 6 mins 25 sec], 20 cycles of [94°C for 10 sec, 51°C for 30 sec and 68°C for 6 mins 45 sec] and a final step at 72°C for 5 mins. Finally DNA bands were purified (see Section 2.1.8) after agarose electrophoresis (see Section 2.1.6), resuspended in 10 µL of TE buffer (see Appendix II) and sent for downstream analysis.

Sequencing data were analysed by Dr Fabio Luciani and Brigid Betz-Stablein (School of Medical Sciences, UNSW, Sydney, Australia).

### 2.1.16 Real-Time Quantitative PCR

The comparative $C_T$ method was used to determine relative levels of HCV RNA. Real-time quantification was performed using SYBR® Green PCR Master Mix (Applied Biosystems). Samples were processed in duplicate where 5 µL of cDNA was mixed with 10 µL of SYBR® Green PCR Master Mix and the adequate primers (300 nmol of HCVF and HCVR primers for quantification of HCV RNA levels (see Appendix V)). All samples were also processed for the quantification of the RPLPO housekeeping gene in parallel to normalize input cDNA levels (36B4-F and 36B4-R primers – description in Appendix V). An ABI StepOne Plus Real-Time PCR System (Applied Biosystems) coupled with the ABI PRISM 7000 SDS Software was used to control the reaction sequence as follows: denaturation at 95°C for 10 mins, 40 cycles of 95°C for 15 sec and 60°C for 1 minute. A final step of for melting curve analysis was performed with a step at 95°C for 15 sec and at 60°C for 1 minute, then followed by increasing the temperature by 0.5°C increment up to 95°C. Data were analysed using the Step one™ v2.2 software.

### 2.1.17 Extraction of cellular proteins

Protein extracts were prepared by lysis of near-confluent cell monolayers in 35 mm dishes with an IGEPAL (NP40)-based lysis buffer (1% IGEPAL [IGEPAL® CA-630; Sigma Aldrich], 150 mM NaCl, 50 mM TRIS (pH = 8.0) containing Protease Inhibitor Cocktail (Sigma Aldrich)) (see Appendix I) and incubated on ice for 30 mins. Extracts were then homogenised using a 29-gauge syringe (10 passes), and centrifuged in a table-top microcentrifuge at 4°C and 10000g for 5 mins. Supernatants cleared from nuclear debris were then used for further analysis or stored at -20°C.

### 2.1.18 SDS-PAGE and protein transfer

Proteins were boiled with 1x Laemmli sample buffer (see Appendix I) for 5 mins and then loaded on a separating gel (Mini Protean 4-15% Precast Gels) alongside 7.5 µg Precision Plus Protein® Standards – Kaleidoscope (BioRad). SDS PAGE was performed for up to 2 hours (depending on protein size) using Running Buffer (see Appendix I). Gels were then equilibrated in cold Transfer Buffer (see Appendix I) for up to 20 mins.

Nitrocellulose Blotting Membrane (Amershan ™ Hybond ECL) and filter papers were soaked in cold Transfer Buffer before assembling the Western Blot Transfer Apparatus (BioRad) as per manufacturer's instruction. Proteins were then transferred onto the Nitrocellulose Blotting Membrane (Amershan ™ Hybond ECL) overnight at 4°C and 25 Volts.

### 2.1.19 Western blotting

After blocking the membranes (1hr) using 5% skim milk or 5% BSA (in TBS-T (see Appendix I)) depending on primary antibody (see Appendix II), membranes were rinse twice with TBS-T and finally incubated with the appropriately diluted primary antibody (see Appendix II) overnight at 4°C. Thereafter, membranes were washed 3-5 times with TBS-T for at least 5 mins per wash under gentle agitation to limit non-specific antibody binding. Finally membranes were then incubated with the appropriate horseradish peroxidase- (HRP-)conjugated secondary antibody (see Appendix II) (diluted in 1% skim milk or 1% BSA in TBS-T) for 1 hour with gentle agitation.

After extensive washing (as above), ECL Super Signal® West Femto Maximum Sensitivity Substrate (Thermo Scientific) was used to detect the presence of antibody-labelled proteins on the membranes as per manufacturer's protocol. A Chemi Doc$^{TM}$ MP Imaging System (BioRad) was used to reveal and record the protein bands with appropriate exposure time depending of the signal intensity.

### 2.1.20 Immunoprecipitation of protein-RNA complexes

The protocol of immunoprecipitation of mRNA-protein complexes was based on previously described protocols (Peritz et al., 2006; Zielinski et al., 2006) and used to investigate MS2.Coat-mCherry binding to MS2 stem loop-tagged viral RNA. To investigate other interactions, antibody and primer combinations were altered accordingly.

All steps from sample collection to cDNA preparation were performed in RNAse free conditions, keeping samples on ice or at 4°C at all times. Total protein extracts were collected from 10 cm cell culture dishes using 1 mL of cold polysome lysis buffer (NP-

40 based lysis buffer containing RNAse inhibitors (see Appendix I)). Extracts were then homogenised through a 26-gauge syringe, and cellular debris were cleared by centrifugation (4°C/ 1000g/ 5 mins). 20 μL of Protein A/G-Plus Agarose Beads (Santa Cruz Biotechnology®) per sample were pre-cleared by washing in polysome lysis buffer (1 ml of buffer per 100 μL of beads) and resuspending the beads to their original volume with polysome lysis buffer. Lysates were then incubated with 20 μL of pre-cleared agarose beads (4°C/ light mixing/ 1hr) to limit non-specific antibody association. Finally, after clearing the samples from these beads by centrifugation (4°C/ 1000g/ 5 mins), lysates were then incubated with anti-mCherry antibody (BioVision) (used at 2 μg/ 1mL of sample) (4°C/ gentle mixing / overnight ≈16hrs). 30 μL of agarose beads per sample were pre-cleared (as above). Precipitation of the anti-mCherry antibody and the associated protein was achieved by addition of 30 μL of pre-cleared agarose beads (4°C/ gentle mixing/ 4hr). After centrifugation (4°C/ 1000g/ 5 mins) supernatants were discarded and beads were subsequently washed up to 10 times with ice cold polysome lysis buffer to minimize non-specific binding. Washed beads were then directly resuspended in Trizol (Life technologies, invitrogen) and RNA extraction was performed as previously described (see Section 2.1.10). Finally, cDNA was prepared using SuperScript® III Reverse Transcriptase (Life Technologies) as described in Section 2.1.15, followed by amplification of the HCV genome over the region encoding the non-structural viral proteins (NS2 to NS5B fragment - 6kb long) using SequalPrep Long PCR kit (Life Technologies) and the two primers used previously (see Section 2.1.15 and Appendix V) to visualize presence of bound near-full-length HCV RNA at the time of extraction.

### 2.1.21 *Renilla* Luciferase Assays

Near-confluent cell monolayers (24-well trays) were washed once with 1x PBS. Cells were then lysed with 75 µL of 1x *Renilla* Luciferase Assay Lysis Buffer (Promega) (diluted in $dH_2O$) per well for 24-well trays (100 µL per 12-well trays). Plates were either sealed with parafilm and stored at -20°C or used immediately for *Renilla* Luciferase Assay.

Lysates were homogenised and 20 µL of each sample was transferred to wells of a 96-well luminometer plate. *Renilla* Luciferase Assay Reagent was prepared by diluting 100x Reagent in Assay Buffer down to 1x (total volume was calculated as follows: 50 µL per sample + 500 µL for instrument priming). *Renilla* Luciferase assays were performed using a Glomax Luminometer from Promega according to manufacturer's instructions. Finally data were analysed using GraphPad Prism 6 software.

### 2.1.22 Small insertions using oligo-duplexes

An oligo-duplex strategy was used to perform small insertions at specific restriction sites of a backbone vector. The backbone vector was first digested using the appropriate restriction enzyme(s) and treated with Antarctic Phosphatase (New England Biolabs) according to manufacturer's instructions to avoid self-religation.

Two oligonucleotides complementary over the coding sequence of interest (to be inserted) and flanked by overhangs that are complementary to that of the appropriately digested vector and terminated with a 5'-phosphate were commercially synthesised by GeneWorks. The two oligonucleotides were prepared at a concentration of 20 µM, then 5 µL of each were mixed with 5 µL of NEB Buffer 2 and 35 µL of $dH_2O$, incubated at 95°C for 4 mins followed by a final incubation at 70°C for 10 mins. To complete

annealing of the oligonucleotides, the sample remained in the PCR machine to slowly cool-down until it reached room temperature (> 3 hours). Once annealed the oligo-duplex was used immediately for ligation. Finally using the method detailed previously (see Section 2.1.7), the oligo-duplex was ligated into the backbone and the resulting plasmid was transformed into competent cells (see Section 2.1.2) for subsequent screening.

## 2.2 Tissue Culture Techniques

### 2.2.1 Tissue Culture Medium

Dulbecco's Modified Eagle Medium (DMEM) (containing 4.5g/L of D-Glucose, 25mM HEPES) (Gibco®, Life technologies™ - Ref 12430-054 for further details) was used to maintain cell culture. Standard DMEM was supplemented with 10% foetal calf serum (FCS – BOVOGEN Biologicals) and antibiotics: Penicillin (Invitrogen; 100 U/ml) and Streptomycin (Invitrogen; 100µg/ml).

Other antibiotics were added as appropriate for selection and maintenance of stable cell lines: Blasticidin HCL (Invitrogen) (used at 3 µg / ml), Puromycin (Sigma-Aldrich) (used at 3 µg / ml) or Geneticin (G418) (used at 800 µg / ml).

### 2.2.2 Cell maintenance

Corning tissue culture labwares were used for maintenance of the cells: 0.2µm vented tissue culture flasks (25 $cm^2$, 75 $cm^2$ and 175 $cm^2$), tissue culture dishes (3.5$cm^2$, 6$cm^2$ and 10$cm^2$) and tissue culture trays (6, 12, 24, 48 and 96-well tray). Cells were maintained at 37°C under 5% $CO_2$ concentration in a humidified Panasonic $CO_2$ incubator (Panasonic Healthcare CO., Ltd).

Cells were passaged before reaching complete confluency. For this, culture medium was removed, the cell monolayer was then washed once with 1x PBS and a small volume of Trypsin-EDTA was added. Cells were returned to the $CO_2$ incubator at 37°C for 5 mins, before detachment and resuspension in fresh culture medium. Cells were counted using a Neubauer Haemocytometer (Brand) with Trypan Blue (see Section 2.2.3). Finally a fraction of the cell suspension was used to seed a fresh flask according to the needs.

### 2.2.3 Trypan blue exclusion

Cell counts were performed using a Neubauer Haemocytometer (Brand) and Trypan Blue Stain solution (prepared by the Tissue Culture Service Unit from cell culture tested Trypan Blue [Sigma-Aldrich]). For this, cell suspensions were diluted with an equal volume of Trypan Blue Stain and loaded into the haemocytometer chamber. Cell concentrations were then calculated as per manufacturer's instructions:

$$\text{Cell concentration} = 2\ (\text{Trypan Blue dilution factor}) \times \text{cell count per grid} \times 10^4 \quad (\text{cells/mL})$$

### 2.2.4 Cryopreservation of cells

Cells in suspension were centrifuged at 232g for 8 mins, supernatant was discarded and cells were resuspended in standard culture medium to a concentration between $5x10^6$ to $1x10^7$ cells per ml. An equal volume of Freezing Mix (50% DMEM, 30% FCS and 20% Dimethylsulfoxyde [DMSO]) was then added drop-wise to the cell suspension. After being gently mixed, cells were aliquoted (≈ 1 mL /vial) in sterile cryopreservation tubes (CryoTube™ vials, NUNC™). Tubes were transferred to a freezing chamber (Nalgene®) containing fresh isopropanol to achieve a cooling of -1°C / minute and store in an -80°C freezer overnight. Finally vials were transferred to a liquid nitrogen based cryopreservation system to constitute the master stock, while a user stock was kept in the -80°C freezer for short-term usage.

### 2.2.5 Resuscitation of frozen cells

Cryopreservation tubes containing frozen cell lines were taken out of storage and kept on dry ice. Aliquots were thawed quickly using a 37°C waterbath and gently transferred to a T25$cm^2$ or T75$cm^2$ tissue culture flask containing standard tissue culture medium (pre-warmed to 37°C). Cells were returned to culture in the $CO_2$ incubator overnight. The next day, tissue culture medium was replaced with fresh medium containing relevant antibiotics if necessary.

### 2.2.6 Transient transfection

Transient transfection of cells with expression plasmids in order to achieve over-expression was performed using FuGENE 6 Transfection Reagent (Promega). One day before transfection cells were seeded in order to reach 50-70% confluency on the following day. FuGENE 6 Transfection Reagent was used as per manufacturer's instruction. Briefly, transfection mixtures were prepared by mixing 100 µL of Opti-MEM® media (Life Technologies) with 2 µL of FuGENE 6 reagent and then adding and mixing 2 µg of DNA (for each transfection per well of a 6-well tray). If transfecting multiple expression plasmids at once, equal quantities of each plasmid were added to reach a total of 2 µg. After a 15 minute–incubation, the transfection mixture was added drop-wise to the cells with a gentle swirl. Cells were then returned to culture and assays were performed 24-72 hours post-transfection.

### 2.2.8 Generation of stable cell lines

Stable over-expressing cell lines were produced using two different methods: either using direct transfection of an expression vector containing a selectable marker or using an intermediate lentiviral particle to transduce the gene of interest using the pLenti6/V5 Directional TOPO® system (Life Technologies) and lentiviral packaging plasmids for production of lentiviral particles (see below).

#### *2.2.8.1 Direct transfection*

Cells were transfected using the protocol detailed previously (see Section 2.2.6). Three days post-transfection, an antibiotic specific for the selectable marker carried by the expression vector was added to the culture media (see Section 2.2.1 for concentration). Treatment of non transfected cells was used as a negative control. The cell line was considered as stable after the negative control cells were all dead (generally 2-3 weeks depending on the antibiotics applied).

#### *2.2.8.2 Lentiviral particles production*

The first step to establish a stable cell line using this technique was to produce the lentiviral particles by transfection of 293T cells using FuGENE 6 (Promega) (see Chapter 2.2.6) and an equal amount of the proviral expression plasmid, psPAX2 (a packaging vector (Addgene plasmid # 12260)) and pMD2.G (an envelope vector (Addgene plasmid # 12259)) (Didier Trono [Laboratory of Virology and Genetics, Ecole Polytechnique Fédérale de Lausanne, Switzerland]). Cells were returned to culture overnight and the supernatants were changed the following day. Finally supernatants containing lentiviral particles were collected at day 2 and 3 after transfection, filtered using a 0.45 µm syringe filter, aliquoted and frozen at -80°C.

The second step was the infection of the naïve cell lines with the lentivirus-containing supernatants. Aliquots were taken out of -80°C storage facility and kept on dry ice, then thawed quickly using a 37°C waterbath, gently resuspended and diluted 10-fold in complete media containing 8 µg / mL of Polybrene (Millipore). The supernatant of the naïve target cell monolayer was removed, the lentiviral solution was added and the cells were returned to normal culture conditions. The following day, the supernatant

was replaced with fresh media and antibiotic selection was started 3 days post-infection (Blasticidin for pLenti6/V5 Directional TOPO® derivatives and puromycin for pTRIPz derivatives) (see Section 2.2.1 for concentration) Treatment of non-infected cells was used as a negative control. The cell line was considered as stable after the negative control cells were all dead.

### 2.2.9 FACS

#### *2.2.9.1 Flow cytometry*

Fluorescence Activated Cell Sorting (FACS) was performed using a Beckman Coulter® MoFlo Astrios High Speed Cell Sorter coupled with the Summit Software version 6.2 (Beckman Coulter, Miami, FL, USA) enclosed within a Baker SterilGuard BSL class II biosafety cabinet.

#### *2.2.9.2 Sorting buffer*

The sorting buffer was composed of Dulbecco's Modified Eagle Medium without phenol red (DMEM (no phenol red)) (Gibco®, Life technologies™) supplemented with 2% FCS and 1% Penicillin/Streptomycin.

#### *2.2.9.3 Cell preparation and sorting*

Cell monolayers were rinsed once with 1x PBS and harvested using trypsin-EDTA. Cells were resuspended in complete media and centrifuged (220 g for 6 mins) and washed with sorting buffer. Finally cells were resuspended to a concentration of approximately $2.5x10^6$ cells / mL (approximately 1x T175 $cm^2$ flask in 4-5 mL).

Cell suspensions were then flow-sorted at the Detmold Family Trust Cell Imaging Centre (Hanson Institute, SA Pathology, Adelaide) using an Astrios flow cytometer (see Section 2.2.9.1). Normal culture media (see Section 2.2.1) was used as collection buffer. Sorted cell suspensions were then used to seed appropriately sized labware depending on the number of cells collected ($2x10^5$ cells in each well of a 6-well tray or $7x10^5$ cells in T25 $cm^2$ flask). Supernatants were replaced with fresh media the next day and antibiotic treatment was resumed 2 days post-sorting as required.

### 2.2.10 Colony formation efficiency assay

Huh 7.5 cells were electroporated with the subgenomic replicon(s) of interest and in parallel both a positive control (WT or parent) and a negative control (replication-defective "GND') replicon (see Section 2.4.2.1). Adequate volumes of the electroporated cell suspensions were used to seed 10 cm dishes or 6-well trayes and returned to culture. Three days post-electroporation, the supernatants were changed and the media was replaced with culture media containing the appropriate antibiotic to select only cells harbouring replication of the replicon.

Once all the cells belonging to the negative control sample had died (with the duration depending on the antibiotic used), cells were prepared for colony formation efficiency assay as previously described (Aloia et al., 2014). In brief, cell monolayers were washed twice with PBS, fixed with an acetone:methanol (1:1) solution (5-10 mins at 4°C) and stained using an adequate volume of crystal violet solution (2 mg / mL in $dH_2O$) for 5 mins at room temperature. Cell monolayers were then washed 3 times with PBS and number of colonies (and hence the replication efficiency of the replicons) was assessed for each sample.

## 2.3 Cell lines

### 2.3.1 Huh-7.5

The Huh-7.5 cell line is a cell line that is particularly permissive to HCV infection (Blight et al., 2002) as it is defective for RIG-I signalling (Sumpter et al., 2005). Huh-7.5 cell line is derived from a Huh-7 (Nakabayashi et al., 1982) (human hepatocellular carcinoma) cell line which used to harbour replication of an HCV subgenomic replicon but has been cured after IFN-α treatment. These cells were kindly provided by Charles Rice (Rockefeller University, New York, USA).

### 2.3.2 Huh-7.5 + MS2.Coat-mCherry

This Huh-7.5 derived cell line is a polyclonal cell line stably expressing the fusion protein between MS2 bacteriophage coat protein and the mCherry fluorescent protein. The cell line was maintained under the selective pressure of Blasticidin antibiotic after transduction of the MS2.Coat-mCherry gene by lentiviral particles. The two cell lines which were selected by FACS-sorting for specific levels of fluorescence ("low" and "medium" see Chapter 4.5.1) were maintained under the same conditions as the parent cell line.

### 2.3.3 Huh-7.5 expressing NLS-MS2.Coat-mCherry

This Huh-7.5 derived cell line is a polyclonal cell line stably expressing the fusion protein between MS2 bacteriophage coat protein and the mCherry fluorescent protein containing a nuclear localisation signal upstream of the MS2 coat protein. The cell line

was enriched for expression of MS2.Coat-mCherry by FACS-sorting and maintained under the selective pressure of Blasticidin antibiotic after transduction of the MS2.Coat-mCherry gene by lentiviral particles.

### 2.3.4 Huh-7.5 expressing Rab18-GFP

This Huh-7.5 derived cell line is a polyclonal cell line stably expressing the fusion protein between Rab18 protein and the green fluorescence protein (GFP). The cell line was enriched for expression of GFP by FACS-sorting and maintained under the selective pressure of Geneticin (G418) antibiotic after direct transfection of pEGFP-Rab18 (Ozeki et al., 2005) which was kindly supplied by T. Fujimoto (Department of Anatomy and Molecular Cell Biology, Graduate School of Medicine, Nagoya University, Nagoya, Japan).

### 2.3.6 HCV subgenomic replicon cell lines SGR/5A-TCM+3'UTR:MS2

Huh-7.5 + SGR/5A-TCM+3'UTR: 24xMS2, Huh-7.5 + SGR/5A-TCM+3'UTR: 12xMS2, Huh-7.5 + SGR/5A-TCM+3'UTR: 8xMS2, Huh-7.5 + SGR/5A-TCM+3'UTR: 6xMS2 and Huh-7.5 + SGR/5A-TCM are Huh-7.5 cell lines stably harbouring autonomous replication of the designated HCV subgenomic replicons. All the replicons were designed using the same principles and the cell lines were maintained under the selective pressure of Blasticidin antibiotic after initial RNA transfection with DMRIE-C (see Section 2.4.4). In most instances monoclonal derivatives were generated using 'cloning rings' expanded and maintained as appropriate (See Chapter 3.2.2).

## 2.4 HCVcc Infectious System

### 2.4.1 *In vitro* RNA transcription

Viral RNA was synthesised using a T7 High Yield RNA Synthesis Kit (New England Biolabs® Inc) as per manufacturer's instruction. In more detail, plasmid DNA was linearised using the appropriate restriction enzyme (see Section 2.1.5 for details). The RNA synthesis mastermix was prepared in a pre-chilled flat-cap PCR tube by adding kit reagents (2 µL of ATP, 2 µL of CTP, 2 µL of GTP, 2 µL of UTP, 2 µL of 10x Reaction Buffer, 2 µL of T7 RNA Polymerase Enzyme per reaction) to 1 µg of linearised plasmid DNA in a total volume of 20 µL (adjust to 20 µL by adding RNAse free water). After thoroughly mixing the reactions, tubes were incubated at 37°C for 3 hours. After incubation, 1 µL (2 Units) of TURBO DNAse$^{TM}$ (Ambion®) was added, reactions were then mixed and returned to 37°C for 15 mins. Reactions were then transferred to new pre-chilled RNAse free table-top microcentrifuge tubes (RNAse-Free 1.5 mL Microfuge Tubes (Ambion®)) and RNA was isolated using the RNA extraction protocol detailed previously (see Section 2.1.10). Finally RNA concentrations were measured using a UV spectrophotometer Nanophotometer® (IMPLEN) as described in Section 2.1.11.

### 2.4.2 HCV RNA transfection

#### *2.4.2.1 Electroporation*

Electroporation enables initiation of a semi-synchronous replication cycle in cells on a large scale. Cells were cultured according to the amount needed (approximately $4x10^6$ cells per electroporation). Cells were harvested using Trypsin-EDTA (see Section 2.2.2), washed in Opti-MEM® media (Life Technologies) twice to remove any traces of Trypsin, antibiotics and FCS. Finally cells were resuspended to a concentration of $1x10^7$ cells / mL in Opti-MEM® media.

0.4 mL of cell suspensions were aliquoted per Gene Pulser® cuvette and 10 μg of RNA was added. Electroporation was performed using a Gene Pulser Xcell™ (Biorad) by single pulse using the following settings (0.27 kV, 100 Ohms and 960 μF). Cell suspensions were then diluted in 20 mL of fresh culture media (without selecting antibiotics) and plated as needed. Experiments were performed 24 – 72 hours after transfection. Selecting antibiotics were used 3 days post-transfection.

#### *2.4.2.2 DMRIE-C transfection*

Viral RNA transfection was also performed using the DMRIE-C Transfection Reagent (Life Technologies). Cells were seeded into 6-well trays the day before transfection to reach 70% confluency at the time of transfection (typically seed at $2x10^5$ cells / dish the day before). Transfection mixtures were prepared by adding 7 μL of DMRIE-C Transfection Reagent to 1 mL of Opti-MEM® media (Life Technologies), mixing gently and then adding 5 μg of viral RNA per transfection reaction. Mixtures were then gently mixed and added to cell monolayers following washing with PBS. Plates were

then given a gentle swirl and returned to culture at 37°C. 4 hours later, supernatants were replaced with fresh culture media (without selecting antibiotics). Experiments were performed 24 – 72 hours after transfection. Selecting antibiotics were added 3 days post-transfection, where appropriate.

### 2.4.3 Titration of infectious virus – Focus Forming Assay (FFA)

Focus forming assays were performed to assess the viral titre of virus-containing culture supernatant. Naïve Huh-7.5 cells were seeded into 96-well plates at $2x10^4$ cells / well the day before the FFA. Virus-containing culture supernatants were serially diluted (1 in 10) in fresh culture media down to 1 in 10000. Naïve cultured cell supernatants were replaced with 40 µL of viral inocculum (in duplicate for each concentration), incubated for 3 hours, washed once with PBS and cells were then returned to culture in 150 µL of normal culture medium / well for 3 days. Finally cell monolayers were fixed using ice-cold acetone:methanol (1:1, v:v) (see Section 2.5.2.1) and immunolabelled (see Section 2.5.3) using anti-HCV human serum (prepared as previously described in (Eyre et al., 2009)). HCV-positive foci were visualized using fluorescence microscopy (see Section 2.5.7) and counted. Viral titres were calculated as follows:

**Titre** (focus forming units [ffu/mL]) = **Number of Foci** x **Dilution Factor** x **25**

### 2.4.4 Generation of stable cell lines harbouring autonomous HCV subgenomic replicon replication

To generate stable Huh-7.5 cell lines harbouring HCV subgenomic replicon replication, we used *in vitro* transcribed subgenomic replicon RNA (see Section 2.4.1) that we transfected into naïve Huh-7.5 cells using DMRIE-C transfection (see Section 2.4.2.2). Three days post-transfection, cells were harvested, resuspended and serially diluted into 1/10 and 1/100 dilutions to seed 10 cm culture dishes. Furthermore antibiotic selection was applied (Blasticidin for the subgenomic replicon carrying MS2 stem loop insertion developed in Chapter 3) (see Section 2.2.1).

After death of negative control cells (non-transfected) maintained under antibiotic selection and individual colonies of Huh-7.5 cell harbouring HCV subgenomic replicaton emerged, colonies were isolated using cloning rings, resuspended, and seeded into 96-well trays. Clones were then expanded until they reached the stage of populating a T75-T175 $cm^2$ flask. At that stage, cell lines were tested for HCV antigen positivity by fluorescence microscopy (see Section 2.5.3) and a frozen stock was prepared (see Section 2.2.4).

## 2.5 Fluorescence Microscopy

### 2.5.1 Coverslip preparation

Coverslips were used for high-resolution imaging. Coverslips were first sterilized then placed in 24 well tissue culture trays. Then coverslips were coated with gelatin by adding 0.5 mL of 0.2% gelatin in 1xPBS solution for 1 hour. Coverslips were then washed once with 1xPBS before being used.

### 2.5.2 Fixation

Depending on the subsequent immunofluorescence labelling, cell monolayers were either fixed a solution of Acetone:Methanol (1:1, v:v) or a 4% solution of paraformaldehyde in 1x PBS.

#### *2.5.2.1 Acetone:Methanol*

Acetone:methanol (1:1, v:v) fixation solution was prepared by mixing equal volumes of HPLC purified grade Acetone (Ajax Finechem Pty Ltd) and analysis grade methanol (Merck). Solutions were stored at-20°C and always used ice-cold.

For fixation cell monolayers were first washed once with PBS, PBS was then discarded and ice-cold acetone:methanol was added carefully onto the cells. Cells were incubated with fixative at 4°C for up to 10 mins. Fixation solution was then discarded, and cells were washed twice with PBS. Fixed cells were kept in PBS at 4°C before staining.

#### *2.5.2.2 4% paraformaldehyde solution*

Paraformaldehyde solution (4%) was prepared by dissolving 2g of paraformaldehyde (reagent grade, crystalline; Sigma-Aldrich®) in approximately 40 mL of $dH_2O$ under heating and stirring (up to 60°C). Once the paraformaldehyde was dissolved, 2.5 mL of 20x PBS was added. Finally $dH_2O$ was added to obtain a final volume of 50 mL of 4% paraformaldehyde in 1x PBS. The solution was filtered through an Acrodisc® 25 mm Syringe Filter with 0.22 µm Supor® Membrane (PALL Life sciences) before use. The fixative solution was stored at 4°C for up to 3 weeks.

For fixation with 4% paraformaldehyde solution, cell monolayers were washed once with PBS before addition of fixative solution and incubation for 15 mins at 4°C. Cells were then washed twice with PBS and stored in PBS at 4°C. Permeabilisation of the fixed cells was performed before immunolabelling using 0.05% IGEPAL (IGEPAL® CA-630 (Sigma-Aldrich,)) solution in PBS for 25 mins. Permeabilisation solution was then discarded, and cells were washed twice with 1xPBS. Samples were stored in PBS at 4°C prior to labelling by indirect immunofluorescence.

### 2.5.3 Immunofluorescence labelling

After being fixed (and permeabilised if needed), cells were then processed for immunofluorescence labelling. A blocking step was first performed for 1 hour using a 5% BSA solution in PBS. This solution was obtained by dissolving 2.5 g of BSA lyophilized powder (albumine from bovine serum; Sigma® Life Science) in 50 mL of PBS. Cells were then washed twice with PBS. Primary antibody solutions were prepared by diluting the antibody stock down to the correct concentration (see Appendix II) in 1% BSA in PBS and were applied to the cells for 45 mins (up to 1 hour) at room temperature. Cells were then washed twice with PBS solution. Secondary antibody solutions were prepared by diluting fluorescent anti-Ig antibody stock to the correct concentration (see Appendix II) in 1% BSA in PBS and were applied to the cells for 45 mins at room temperature and protected from light. BODIPY 493/503 staining was often performed at the same time (see Section 2.5.4). Optional DAPI nuclear staining was performed last (see Section 2.5.5). Finally cells were washed three times with PBS. Samples were stored at 4°C or mounted on glass microscope slides (see Section 2.5.6) and then observed with a fluorescent microscope (see Section 2.5.7).

### 2.5.4 BODIPY® 493/503: lipid droplet staining

A stock solution of BODIPY® 493/503 (1 mg/mL) was prepared by dissolving 5 mg of BODIPY 493/503® (4,4-difluoro-1,3,5,7,8-pentamethyl-4-bora-3a,4a-diaza-s-indacene; Molecular Probes – Life Technologies) in 5ml of ethanol. Working solutions were prepared by dilution to 5 µg / mL (1/200 dilution) in 1% BSA in PBS and were added to the cells for 45 mins (this staining was often performed at the same time as secondary antibody labelling) while keeping the cells protected from the light. Cells

were then washed three times with PBS solution and stored at 4°C prior to fluorescence microscopy visualization.

### 2.5.5 DAPI nuclear staining

After immunofluorescent staining, DAPI nuclear staining was often performed. The 4', 6-Diamidino-2-pheylinodole (Sigma-Aldrich) stock solution (1 mg / mL) was diluted to 1 µg/mL in $dH_2O$ and added to the cells for 5 to 10 mins. Cells were then washed three times with PBS solution. Preparations were stored at 4°C prior to fluorescence microscopy visualization.

### 2.5.6 Slide mounting

To visualize the immunolabelled cell preparation by fluorescence microscopy, coverslips were mounted onto glass microscope slides using the SlowFade® Antifade Kit (Invitrogen™, Life Technologies). A drop of Antifade reagent in Glycerol/PBS was placed on the microscope slide (Antifade reagent in PBS was used instead after BODIPY staining). Cell monolayers were washed once with the equilibrium buffer then placed face down towards the mounting media onto the slide. After letting the excess mounting media dry, coverslips were sealed using clear nail polish.

### 2.5.7 Microscope specification

A Nikon TiE inverted fluorescence microscope was used to perform wide-field fluorescence microscopy. The microscope was equipped with the following:

- a Plan Apochromat x60 NA 1.4 oil immersion lens and a Plan Fluor x10 NA 0.3 objective lens (Nikon),
- an Intensilight C-HGFIE precentered fiber illuminator mercury light source (Nikon) for illumination,
- BrightLine® single-band filter set (Semrock) - DAPI-5060C-NTE-ZERO, FITC-3540C-NTE-ZERO, and TxRed-4040C-NTE-ZERO,
- Monochrome 12-bit cooled charged-coupled camera (DS-Qi1, Nikon) – maximum resolution of 1280x1024.

Plan Apochromat x60 NA 1.4 oil immersion lens was used in conjunction with Immersol$^{TM}$ 518F (Zeiss) immersion oil for fluorescence microscopy.

Acquisition of the fluorescence images/movies was performed without binning or gain. Moreover for processing and analysis of the fluorescent images the auto-scaling function of the LUTs was used and coupled with the removal of the background fluorescence using a region of interest located within a region devoid of cells.

### 2.5.8 Deconvolution

Deconvolution was performed using the NIS-A Blind Deconvolution WF module of NIS-Element Advanced Research v 3.22.14 software (Nikon). This processing was generally performed on z-stacks comprising 60 to 80 images taking into consideration a medium background and a limited number of iterations (10). The other parameters

associated with the microscope and the sample, such as numerical aperture, refractive index, calibration, wavelength and z-step were directly accessed from the file metadata.

## 2.6 Live cell microscopy

### 2.6.1 Glassware

Live cell imaging was performed using gelatin-coated 35 mm cover (0.17 - 0.19 mm thick) glass bottom dishes (MatTek Corporation, USA). Dishes were seeded to be approximately 80% confluent at the time of imaging.

### 2.6.2 Tetracysteine tag labelling using FlAsH or ReAsH biarsenical dyes

The proteins tagged with a tetracysteine motif were labelled using the FlAsH or ReAsH biarsenical dyes according to a protocol adapted from (Hoffmann et al., 2010) with minor modifications. The biarsenical dyes FlAsH and ReAsH were synthesised by Christopher S. P. McErlean (School of Chemistry, The University of Sydney, Sydney, New South Wales, Australia) and provided by Stuart Turville (Kirby Institute UNSW, Immunovirology and Pathogenesis Program, Darlinghurst, New South Wales, Australia).

#### *2.6.2.1 HBSS[Glucose] solution*

HBSS[Glucose] was prepared by mixing 504 µL of a 20% (1.11 M) Glucose solution (TSU, The University of Adelaide) per 100 mL of commercial Hanks' Balanced Salt Solution (HBSS) (Gibco, Life Technologies) to a final concentration of 5.6mM of Glucose. Finally HBSS[Glucose] solution pH was measured using a TPS-901-pHmeter (TPS) and adjusted to pH = 7.3 – 7.4 by adding small volume of 2M NaOH (TSU, The University of Adelaide).

#### *2.6.2.2 Preparation of the staining solution*

The first step in preparing the FlAsH staining solution was to prepare a 1 mM FlAsH (light-sensitive reagents, avoid exposition to light) solution by mixing 10 mM of FlAsH stock solution with 90 µL of dimethyl sulfoxide (DMSO). Then 2.1 µL of 1,2-Ethanedithiol (EDT) (Fluka® Analytical, Sigma-Aldrich) was mixed to 1 mL of DMSO to prepare a 25 mM EDT solution. Then we mixed 6 µL of 1 mM FlAsH solution with 6 µL of the 25 mM EDT solution and incubated the mixure at room temperature for 5 – 10 minutes. Finally the last step is the dilution of the 12 µL-mixture into 6 mL of HBSS[Glucose]. FlAsH staining solution was then mixed thoroughly and incubated at room temperature for 5 mins before use.

#### *2.6.2.3 Preparation of the washing solution*

First 12.5 µL of 2,3-Dimercapto-1-propanol (BMP) (Sigma-Aldrich) was mixed to 87.5 µL of DMSO. After mixing thoroughly we then added the mixture to 2.4 mL of HBSS[Glucose] to form a 50 mM BMP solution. Finally 400 µL of the 50 mM solution was added to 7 mL of HBSS[Glucose] to finish preparing the 2.8 mM washing solution.

#### *2.6.2.4 FlAsH Staining*

FlAsH staining was performed in the 35mm glass bottom dishes. Cell monolayers were washed twice with 2 mL of HBSS[Glucose] and 1 mL of HBSS[Glucose] was finally added to each dish. 1 mL of staining solution (see Section 2.6.2.2) was then added to each dish and cells were incubated at 37°C for 30 mins. After the incubation the cell monolayers were washed again twice with 2 mL of HBSS[Glucose] before adding 1.5 mL of washing solution (see Section 2.6.2.3) to each dish. Dishes were returned to culture at 37°C for 10 mins. The washing solution was then discarded, replaced with 1.5 mL of fresh washing solution and dishes were returned to culture at 37°C for 10 mins. This step was repeated another time, before washing the cell monolayer twice with 2 mL HBSS[Glucose] and finally replacing it with 1.5 mL of Dulbecco's Modified Eagle Medium without phenol red (DMEM (no phenol red)) (Gibco®, Life technologies™) supplemented with 10% FCS (BOVOGEN Biologicals). The dishes were then returned to culture or imaged immediately.

ReAsH staining was performed similarly.

### 2.6.3 Lipid Droplet labelling using BODIPY 493/503 staining for live cell imaging

Stock solution of BODIPY 493/503 (1 mg / mL) (see Section 2.5.5) were diluted to 5µg/mL (1/200 dilution) in DMEM (no phenol red) (Gibco, Life Technologies) supplemented with 10% FCS (BOVOGEN Biologicals). BODIPY staining solution was then added to the cell monolayer (1 mL / 35mm glass bottom dish) and the dishes were returned to culture for 40 mins. Finally the cell monolayers were washed three times with fresh DMEM (no phenol red) supplemented with 10% FCS before being returned to culture or imaged immediately.

### 2.6.4 Labelling of SNAP-tagged NS5A using SNAP-Cell® TMR-STAR

Cell monolayers were labelled at 48 hours post-infection using the SNAP-Cell® TMR-Star substrate according to manufacturer's instructions with minor modifications. Briefly the 0.6 mM stock solution of SNAP-tag substrate in DMSO was diluted 1 in 400 in normal tissue culture media and cell culture supernatants were replaced with 1mL of SNAP-tag staining solution and incubated at 37°C for 15 mins. Cells were then rinsed three times, and incubated with normal tissue culture media at 37°C for 30 mins. To remove the unbound substrate, the media was replaced with fresh tissue culture media without phenol red. Cells were returned to normal culture conditions for approximately one hour before imaging.

### 2.6.5 Live cell imaging

A heated microscope stage insert (Okolab) was used to maintain cells at 37°C on the Nikon TiE inverted fluorescence microscope (described in Section 2.5.7). Only the Plan Apochromat x60 objective lens was used for the movies and associated figures presented in this thesis. Dishes were observed for approximately 1 hour maximum at a time and were otherwise maintained under normal culture conditions.

### 2.6.6 Movie formatting

To produce the movie presented, frames were generally recorded every 3 sec (except when detailed otherwise) and assembled using NIS-Elements software. If the movie presents two differently labelled components, frames were sequentially acquired and merged before being assembled. A time stamp is displayed on the different movies to indicate the real time lapse.

Image processing and analysis was performed as previously described in Section 2.5.7. The .avi files were generated with a playback speed of 5 frames / sec (approximately 15x the actual speed) without using any type of compression.

# Chapter 3

# An *in vitro* Cell Culture Model to Study HCV RNA in Live Cells

## 3.1 Introduction

A keystone for the replication of all positive strand RNA viruses is the characteristic formation of membrane-associated replication complexes to support viral RNA replication (reviewed in (Miller and Krijnse-Locker, 2008). HCV induces alterations of the endoplasmic reticulum into single, double and multi membranes vesicles termed the membranous web which harbour all necessary components (both viral and host) of the replication complex and are thought to be the site of HCV RNA replication. A significant amount of research has been conducted with the aim to understand virus-host interactions that govern HCV RNA replication and the dynamics involved (protein interaction, localisation) with the hope of not only answering basic research questions but ultimately to develop novel therapeutic strategies to combat HCV.

The development of the HCV sub-genomic replicon (Lohmann et al., 1999) and the full-length infectious HCV (Lindenbach et al., 2005; Wakita et al., 2005; Zhong et al., 2005) in vitro cell culture models have represented landmarks in HCV research and allow us to study all facets of the HCV life cycle. As an example and pertinent to this

thesis is the work of Moradpour and colleagues who developed an *in vitro* replicon based HCV research model enabling imaging of the NS5A viral protein in real time (Moradpour et al., 2004). Following identification of a site tolerating insertion within the NS5A sequence, they inserted a green fluorescent protein (GFP) reporter enabling visualisation of NS5A viral protein localisation and traffic within a single cell. Subsequent work revealed that NS5A is enriched in two types of structures in living cells: one being relatively large and static and a second being small and highly motile (Eyre et al., 2014a; Wolk et al., 2008). The initial work from Moradpour and colleagues and Wolk et al were limited to tagging NS5A in the context of a HCV replicon that did not contain the structural proteins (Moradpour et al., 2004; Wolk et al., 2008), however these observations were later confirmed by our laboratory in the context of an infectious HCV (Jc1) cell culture system with NS5A tagged with either a TCM tag or GFP (Eyre et al., 2014a). The NS5A protein is a well described marker of HCV replication complex however, it is unclear from previous live imaging studies if both pools of NS5A represent replication complexes and/or sites of delivery of HCV RNA for packaging. If indeed these NS5A complexes are active replication complexes or involved in delivery of HCV genomes then they should harbour HCV RNA. Thus the aim of this chapter was to develop a model system to track HCV RNA in real–time with the ultimate aim to further our understanding of the HCV life-cycle.

This chapter describes the development of the MS2 bacteriophage system to track HCV RNA in real time (see Figure 1.10). Using this system we inserted a large array of MS2 bacteriophage RNA stem loop repeat regions into the 3' UTR of the HCV genome to enable HCV RNA live imaging during viral replication. The MS2 stem loops were inserted into both the infectious Jc1 HCV cell culture (HCVcc) culture model and the HCV subgenomic replicon model. Both models were generated by using a site of

tolerance within the 3' untranslated region (3' UTR) of the HCV genome to insert a reporter sequence (MS2 bacteriophage stem loops). As mentioned previously in Chapter 1, this approach has been successfully applied to tick borne encephalitis virus (TBEV) (a closely related flavivirus) to investigate TBEV RNA localisation (Miorin et al., 2008; Miorin et al., 2013). However consequences of such modification of the HCV genome are unknown.

### 3.1.1 Generation of a HCV (Jc1)-based cell culture model carrying MS2 stem loop cassettes

Based on previous studies done with insertion of MS2 stem loops into the 3'UTR of the flavivirus, TBEV (Miorin et al., 2008), we investigated inserting the MS2 bacteriophage stem loop reporter sequence within an untranslated region of the HCV genome. The 5' untranslated region (5' UTR) of HCV genome is of critical importance for viral replication and translation of viral proteins and hence may not tolerate insertions or deletions. However, on the other hand, one of the three defined regions of the HCV 3'UTR (schematic representation in Figure 3.1), defined as the 3'UTR variable region, has previously been shown to be non essential for viral RNA replication in sub-genomic replicons (Friebe and Bartenschlager, 2002; Yi and Lemon, 2003). Although, it was expected to impact upon replication, we hypothesised that inserting the MS2 stem loops reporter at the start of this short region would give us the best outcome regarding viral fitness.

To engineer HCV genomes carrying an array of MS2 stem loops, we modified an established HCV genome used in live imaging studies in which the NS5A protein was tagged with a tetracysteine motif (TCM) in the background of the cell culture infections

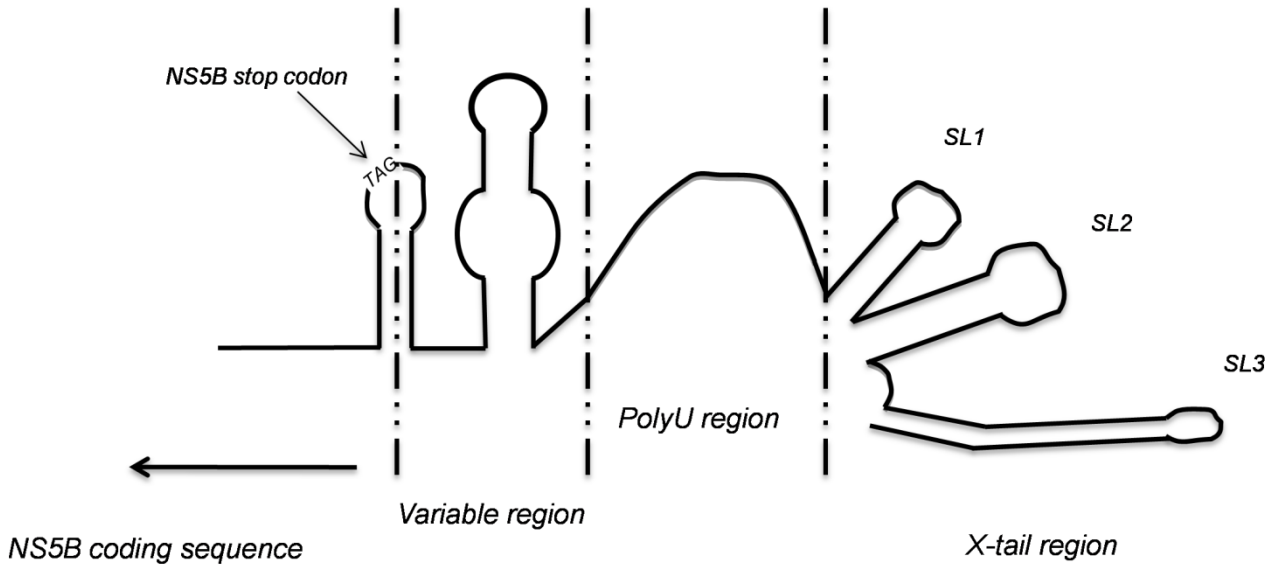


**Figure 3.1: Schematic representation of HCV positive strand 3'UTR.**
The HCV 3' untranslated region is composed of a series of complex secondary structures divided in 3 distinct regions: the variable region, the Poly-U tract and the X-region containing three stem loops (namely SL1, SL2 and SL3).

clone Jc1. This HCV genome termed Jc1/5A-TCM has been extensively used in our laboratory to visualise HCV NS5A traffic in real-time (Eyre et al., 2014a). We first performed site directed mutagenesis to insert two restriction sites (*EcoRI* and *BglII*) immediately following the NS5B stop codon (cf. Table 3.1 and Figure 3.2). We named this cloning intermediate Jc1/5A-TCM+3'UTR*(*EcoRI*/*BglII*).

Using the introduced restriction sites (*EcoRI* and *BglII*), we then inserted MS2 stem loops arrays of different sizes (24, 12, 8 and 6 repeats) to generate the constructs: Jc1/5A-TCM+3'UTR:MS2x24 /x12 /x8 /x6 (cf. Figure 3.3 for schematic representation). For insertion of the 24x MS2 stem loops we used the plasmid pTRIP-MS2x24 (deltaU3) (Boireau et al., 2007) that was kindly supplied by S. Boireau (IGMM, Montpellier, France) in which the stem-loops were removed by *EcoRI* and *BglII* digest (see Appendix VII for complete sequence) and directly sub-cloned into the plasmid Jc1/5A-TCM+3'UTR*(*EcoRI*/*BglII*). Introduction of the smaller arrays of stem loops was achieved by commercially synthesising (Genscript, Piscataway, NJ, USA - see Appendix VII for complete sequences) the stem loop regions flanked by *EcoRI* and *BglII* and subsequent cloning into Jc1/5A-TCM+3'UTR*(*EcoRI*/*BglII*).

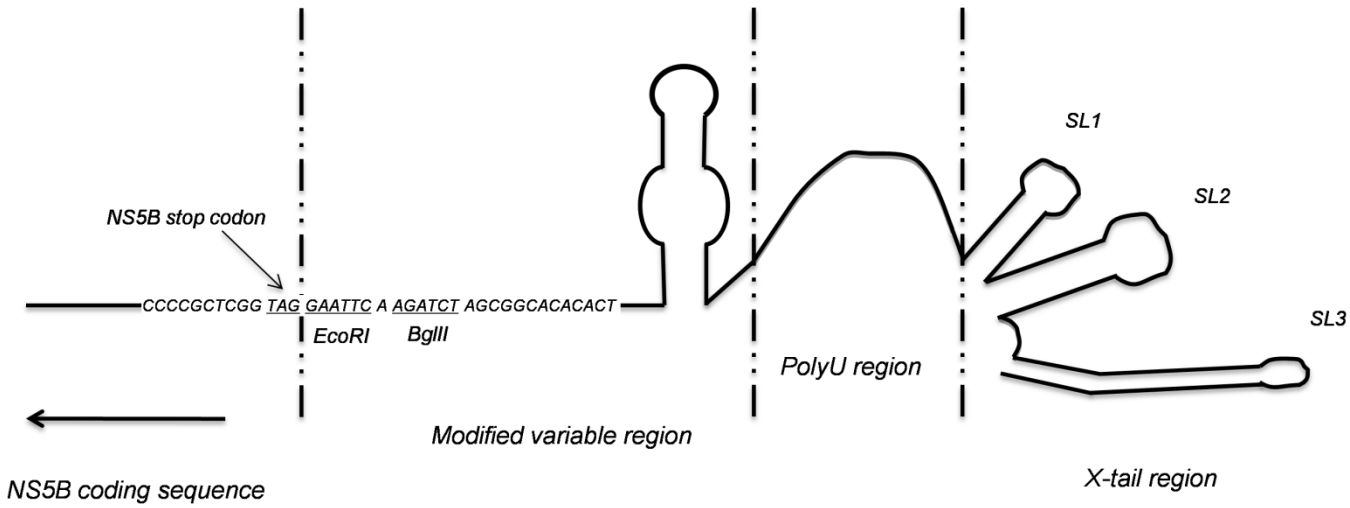


**Figure 3.2: Schematic representation of JC1/5A-TCM+3'UTR*(EcoRI/BglII) positive strand 3'UTR.**

We performed site directed mutagenesis to insert two restriction sites (*EcoRI* and *BglII*) immediately following the NS5B stop codon. We named this cloning intermediate Jc1/5A-TCM+3'UTR*(*EcoRI*/*BglII*).

| Primer name | Primer sequence (5’ to 3’) | Length | Tm |
|---|---|---|---|
| MFP.Eco.MS2.loop.INS | 5’- ccccg ctcgg tagga attca agatc tagcg gcaca cact -3’ | 39 nts | 80.08°C |
| MRP.Eco.MS2.loop.INS (antisense) | 5’- agtgt gtgcc gctag atctt gaatt cctac cgagc gggg -3’ | 39 nts | 80.08°C |

**Table 3.1: Primers used to generate Jc1/5ATCM+3’UTR* (EcoRI/BglII).** These primers were used to perform site-directed mutagenesis Jc1/5A-TCM and enabled insertion of both EcoRI and BglII restriction sites immediately following NS5B stop codon. Both primers were designed with the Stratagene online website and their primer design tool.

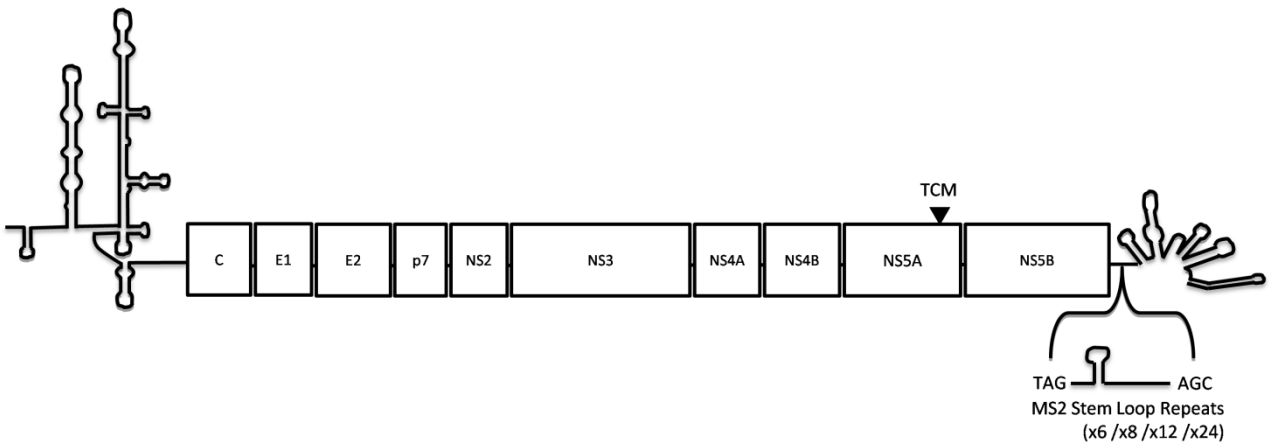


**Figure 3.3: Schematic representation of the Jc1/5A-TCM+3'UTR:MS2 constructs.** These constructs are based on the HCV Jc1 research model and carry 2 specific elements: a tetracysteine motif (TCM) within NS5A sequence and a sequence of MS2 bacteriophage stem loop repeats (6x /8x /12x /24x) in the 3'UTR.

### 3.1.2 Generation of a replicon based research model

We reasoned that the development of a subgenomic replicon containing the MS2 stem loops may also be useful to study HCV RNA traffic and hence we developed a replicon based system as well. From the full-length MS2 HCV genomes we then generated monocistronic subgenomic replicons named SGR.5A-TCM+3'UTR:MS2x24 /x12 /x8 /x6 (cf. Figure 3.4 for schematic representation). To do so, we replaced part of the coding sequence from our full-length MS2 HCV genomes (part of Core-E1-E2-p7-NS2) with the sequence used in the published cloning of SGRm-JFH1BlaRL (Zhou et al., 2011). In that study, Zhou and colleagues replaced the coding sequence from Core to NS2 of a JFH1 subclone with a combination of foreign proteins including a Blasticidin resistance gene (Blasticidin S Deaminase - Bla) fused to a *Renilla* Luciferase reporter gene (R.Luc), then the foot and mouse disease virus (FMDV) 2A autoprotease peptide and an ubiquitin (Ub) gene to control the cleavage of NS3 and induce correct processing of the rest of the viral proteins in the context of a monocistronic subgenomic JFH1 replicon. By using *AgeI* and *AvrII* restriction sites localised within the original coding sequence of JFH1 and thus present in our JFH1-derived HCV MS2 genomes and SGRm-JFH1BlaRL, we substituted the same Core to NS2 coding sequence with the Bla-R.Luc-FMDV 2A-Ub cassette. However, the Bla and R.Luc genes were initially fused using a *MluI* restriction site which was interfering with our strategy using a *MluI* site localised within the plasmids after the 3'UTR to linearize them for T7 RNA preparation. Therefore site directed mutagenesis was performed to generate a single nucleotide substitution to remove the *MluI* restriction site located between the Bla and R.Luc coding sequences without generating an amino acid change. The substitution performed was G>C at position 775 using the primers specified in Table 3.2.

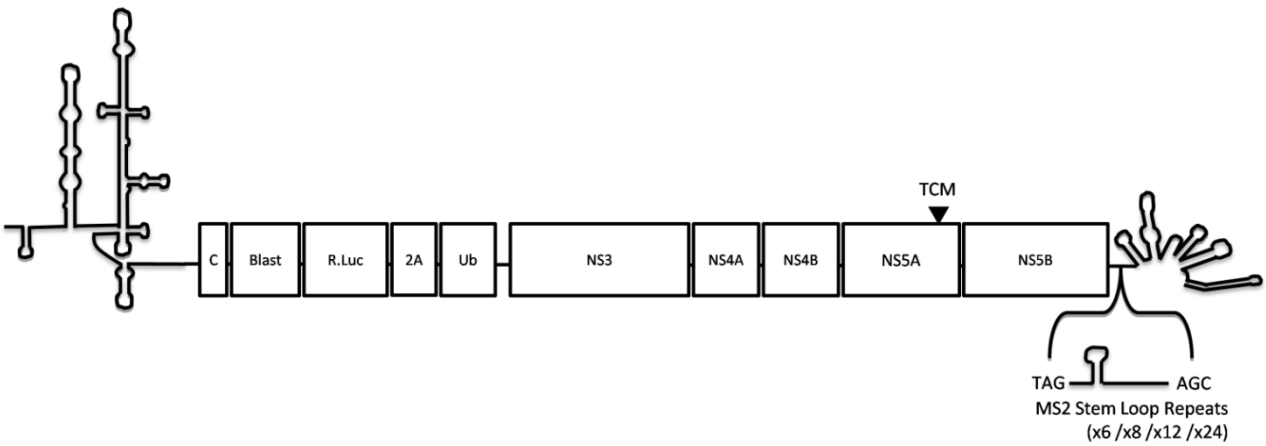


**Figure 3.4: Schematic representation of SGR/5A-TCM+3'UTR:MS2 constructs**
These constructs are based on the HCV sub-genomic research model SGRm-JFH1BlaRL (Zhou et al., 2011) starting with the 5'UTR and part of Core viral protein, then a Renilla Luciferase gene fused to a Blasticidin resistance gene, the foot and mouse disease virus (FMDV) 2 A autoprotease, an Ubiquitin (Ub) gene and the HCV JFH-1 non structural proteins (NS3 to NS5B) and 3'UTR. Furthermore the constructs carry 2 specific elements: a tetracysteine motif (TCM) within NS5A sequence and a sequence of MS2 bacteriophage stem loop repeats (6x /8x /12x /24x) in the 3'UTR.

| Primer name | Primer sequence (5’ to 3’) | Length |
|---|---|---|
| FP.Mut.KL.SGR.g775c | 5’- gtgtgggagggcacccgtatgacttcgaaa -3’ | 30 nts |
| RP.Mut.KL.SGR.g775c (antisense) | 5’- tttcgaagtcatacgggtgccctcccacac -3’ | 30 nts |

**Table 3.2: 775 (G>C) site-directed mutagenesis primer.**
Primers used to perform site directed mutagenesis to remove the MluI restriction site located between the Bla and R.Luc genes in SGR/5A-TCM+MS2:3’UTR. Using these primers enabled a single nucleotide substitution (G>C at position 775) without amino acid change.

Using both replicon and full-length HCV cell culture research models, we sought to characterise the impact of these insertions on the fitness of the virus and visualise the HCV RNA in the context of active HCV RNA replication.

## 3.2 Subgenomic replicon cell culture models

### 3.2.1 Insertion of stem loop arrays within the 3'UTR does not abolish replication

Initial experiments were performed to investigate the impact of the MS2 bacteriophage stem loops inserted within the 3'UTR on HCV replication. Furthermore, with 4 different sizes of MS2 stem loop arrays inserted (24, 12, 8 and 6 repeats respectively) we expected to determine the optimal number of stem loops that would represent the best compromise between replication fitness and strength of the MS2 coat binding signal observed (proportional to the number of loops). To evaluate the relative levels of replication between the different HCV genomes, we electroporated *in vitro* transcribed replicon RNA into Huh-7.5 cells and monitored luciferase activity at various time points post-electroporation. To account for differences in electroporation efficiency data were normalised to Luciferase output at 3 hour time points. In Figure 3.5, the four replicon based constructs carrying MS2 stem loop insertions were compared to a replication-defective negative control (GDD > GND mutation in the NS5B RdRp) (Krieger et al., 2001) and the parent replicon without stem loop insertions. Although relative luciferase activities were relatively unchanged between 24 and 48 hour time-points for replicons containing MS2 stem loops, we observed a significant increase at 72hrs. However while the replication capacity of these HCV genomes is considerably less than that of the parent HCV genome (SGR/5A-TCM) there is clear replication in

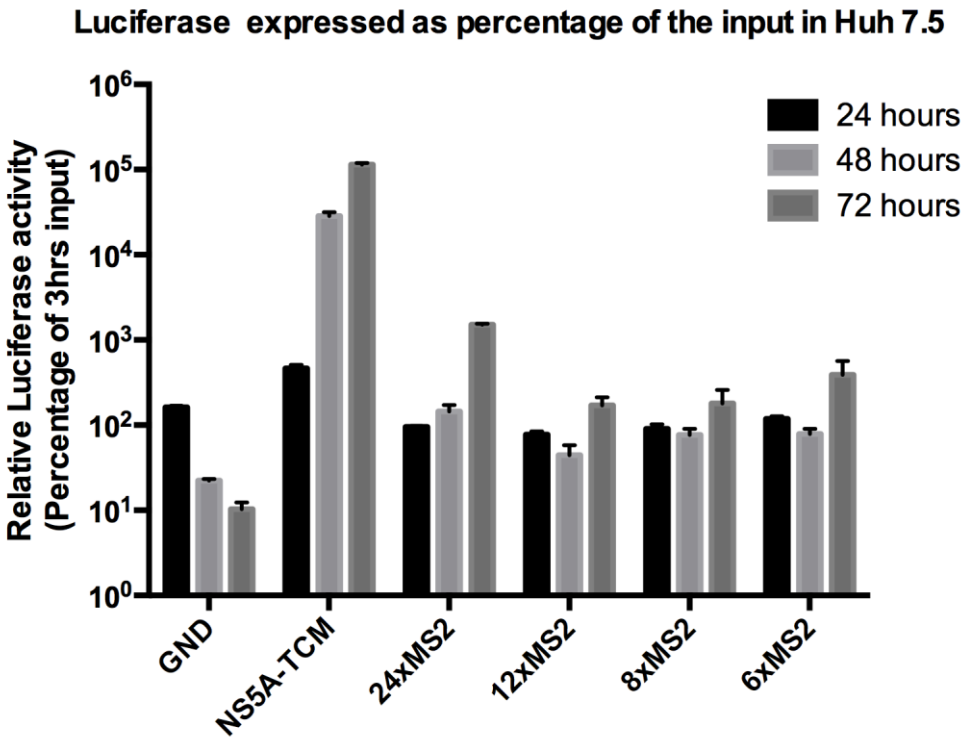


**Figure 3.5: Insertion of MS2 bacteriophage stem loops impairs but does not abolish replication.**

Renilla Luciferase assay comparing the sub-genomic replicons carrying MS2 stem loops sequence (6 /8 /12 /24 repeats) to the unmodified parent SGR.5A-TCM and a replication defective mutant (GND mutation in NS5B) negative control. Data show luciferase activity of the different constructs at 24, 48 and 72 hours normalised with an early time point at 3hrs. Results indicate that MS2 stem loop insertion impairs replication, but does not abolish it. Moreover, SGR/5A-TCM+3'UTR:24xMS2 seems to replicate slightly better than the constructs with smaller inserts at day 3 post-electroporation.

that there is significant luciferase activity at all time points when compared to the HCV GND replication defective mutant. The luciferase activity of the GND mutant represents the luciferase activity translated directly from input RNA. Interestingly, the replicon containing 24 repeats of the MS2 stem loop (SGR.5A-TCM+3'UTR:MS2x24) surprisingly displayed the strongest replication potential in comparison to HCV genomes containing smaller MS2 insertions. Taken together these results demonstrate that the insertion of MS2 stem loops impairs but does not abolish replication, and moreover suggest that 24xMS2 might be the optimal insertion candidate to maximize replication and signal.

To investigate the replication fitness of these HCV genomes further we performed a colony formation assay. The rationale that underpins this assay relies on the fact that our HCV genome encodes for the Blasticidin S Deaminase (Bla) that can neutralise the toxic nucleoside antibiotic blasticidin and thus cells expressing Bla via HCV replication will be resistant to the effects of Blasticidin (cf. Chapter 2.2.10 for detailed method). The results corroborated those of the transient *Renilla* luciferase assay as we observed emergence of blasticidin resistant cell colonies following RNA electroporation with the different replicons with MS2 stem loop insertions (Figure 3.6 panel A to D). However as expected the efficiency of colony formation was significantly less than that for the parent replicon. Interestingly, the replicon containing the 24 stem loops (SGR/5A-TCM+3'UTR:MS2x24) revealed significantly higher numbers of surviving colonies (Figure 3.6 panel D) compared to other replicons. It is not immediately apparent the reasons for this however combined with the luciferase data it suggests that 24xMS2 might be the optimal insertion candidate to maximize replication and signal for imaging.

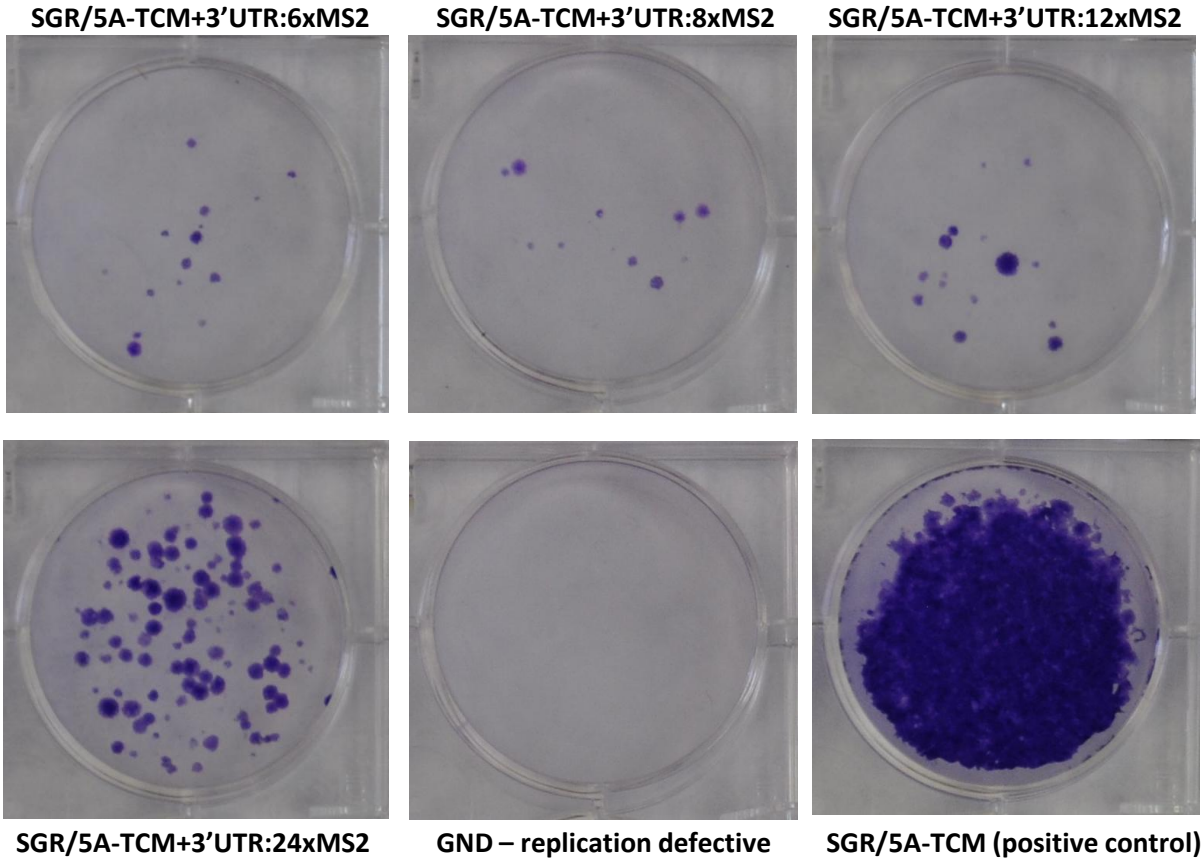


**Figure 3.6: Colony formation assay.**
Crystal violet staining of cells electroporated with the sub-genomic replicons carrying MS2 stem loops sequence (6 /8 /12 /24 repeats), the unmodified parent SGR.5A-TCM and a replication defective mutant (GND mutation in NS5B) negative control after 2 weeks of Blasticidin selection. Results confirm that MS2 stem loop insertions impairs replication. Moreover, SGR/5A-TCM+3'UTR:24xMS2 displays a replication advantage over replicon with smaller MS2 stem loop insertions after 2 weeks.

### 3.2.2 Generation of stable clones

The colony formation assay demonstrated the possibility of selecting Huh-7.5 cells stably harbouring replication of the sub-genomic replicons carrying MS2 bacteriophage stem loops. Beyond their potential application for live cell imaging of viral RNA, these clones are a precious tool to further characterise the impact of the insertion on viral replication. To generate stable Huh-7.5 cell lines harbouring the MS2 sub-genomic replicons, we used the method described in Chapter 2.4.4. Briefly, *in vitro* T7 transcribed RNA replicons were transfected into the Huh-7.5 cell line and cells were maintained under blasticidin selection for a period of 3 to 4 weeks. During this time, resistant clones were isolated using cloning rings and expanded (cf. Table 3.3 for complete list of clones). All the resistant colonies were generated as monoclonal cell lines, except one population that harboured the replicon bearing 24 repeats of MS2 stem loops that was maintained as a polyclonal cell line.

Immunofluorescence studies using pooled anti-HCV patient serum as primary antibody (cf. Chapter 2.5.3 for method and Appendix II) were used to demonstrate the presence of HCV antigens in the different clonal cell lines produced: 17 out of 22 displayed complete positivity for HCV antigens (including the 24 repeats polyclonal cell line). A sample of the immunofluorescence pictures taken is presented in Figure 3.7 and a summary of the results is presented in Table 3.3. Furthermore, Western blotting specific for NS5A viral protein were performed to confirm replication within these stable cell lines. (cf. Figure 3.8 for a sample of the clones). We observed two NS5A specific bands that correspond to the two specific forms of NS5A viral protein present during replication (p56 and p58 – cf. Chapter 1.2.6 for more information). These results strongly suggest that these cell lines harbour replicons maintaining autonomous HCV RNA replication.

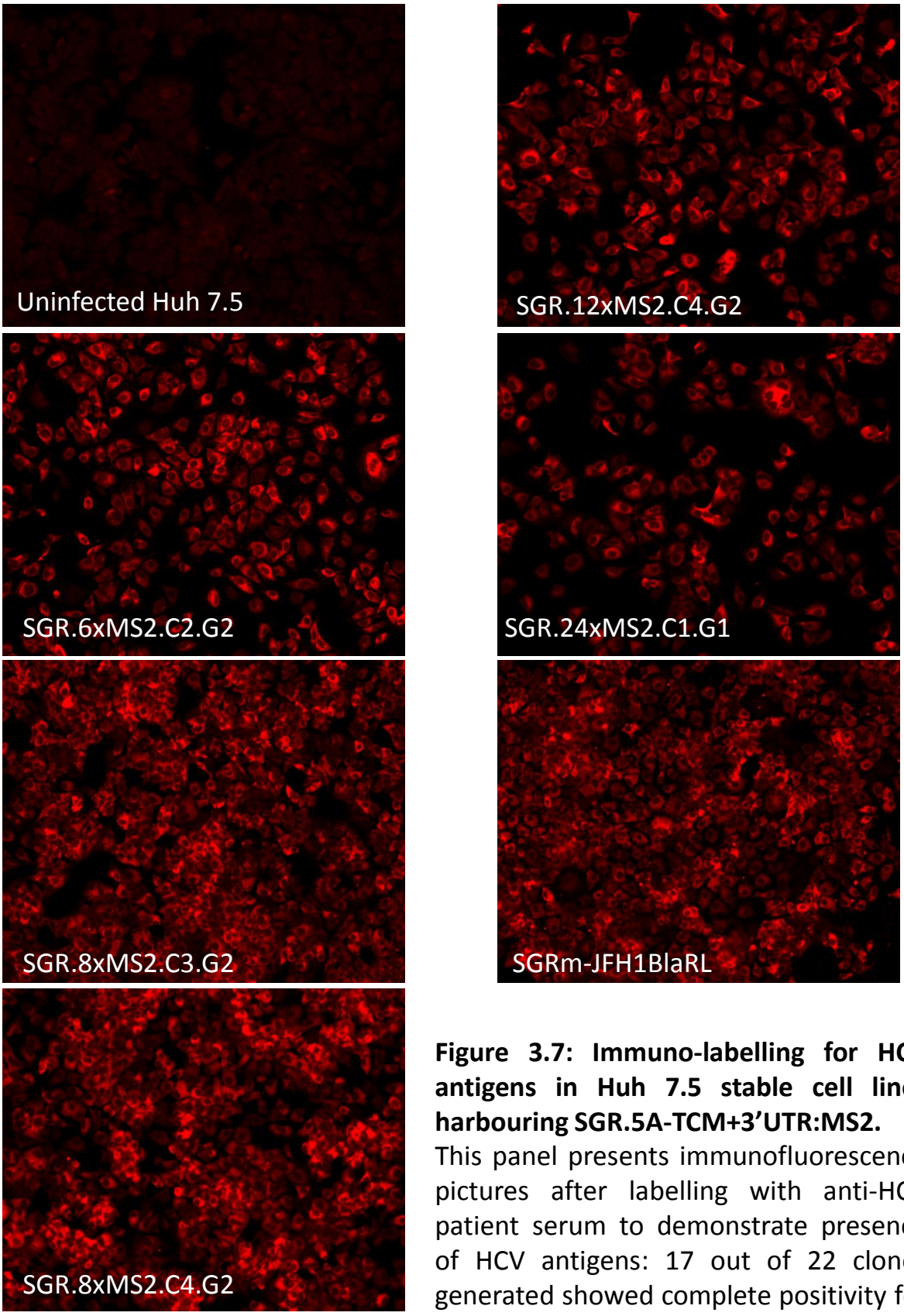


**Figure 3.7: Immuno-labelling for HCV antigens in Huh 7.5 stable cell lines harbouring SGR.5A-TCM+3'UTR:MS2.**
This panel presents immunofluorescence pictures after labelling with anti-HCV patient serum to demonstrate presence of HCV antigens: 17 out of 22 clones generated showed complete positivity for HCV antigens.

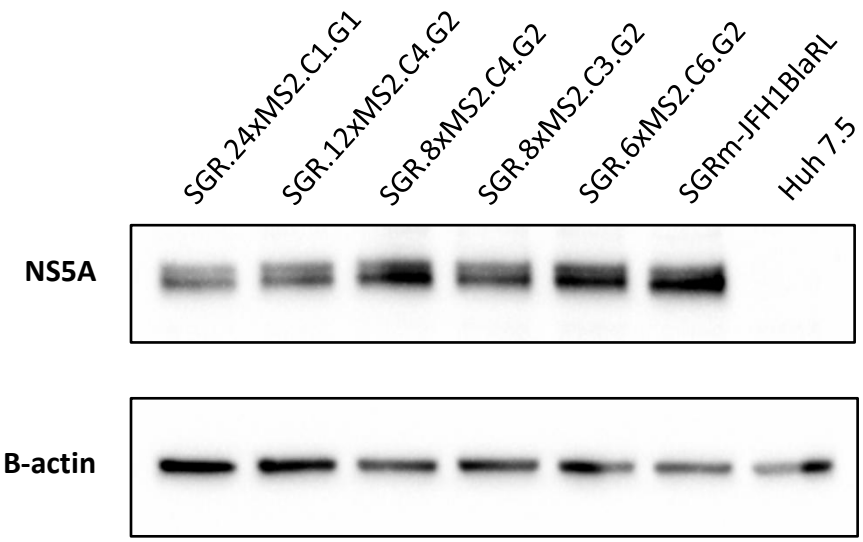


**Figure 3.8: Sample of Huh 7.5 stable monoclonal cell lines derived from SGR.5A-TCM+3'UTR:MS2 producing NS5A viral protein.**

The two bands correspond to the two specific form of NS5A viral protein present during replication (p56 and p58) and demonstrate that these cell lines harbour replicons maintaining autonomous replication.

| Stable cell lines generated from SGR/5A-TCM+6xMS2:3'UTR | | | |
|---|---|---|---|
| | | Positive for HCV antigens (Immunofluorescence) | Estimate of the insert size (PCR across the loops) |
| | 6xMS2.C1.G1 | + | *Same as control (≈800bp)* |
| | 6xMS2.C1.G2 | + | *Lower than control (≈600bp)* |
| | 6xMS2.C2.G2 | + | *Same as control (≈800bp)* |
| | 6xMS2.C3.G2 | + | *Same as control (≈800bp)* |
| | 6xMS2.C4.G2 | - | *Ø* |
| | 6xMS2.C5.G2 | - | *Ø* |
| **Stable cell lines generated from SGR/5A-TCM+8xMS2:3'UTR** | | | |
| | | Positive for HCV antigens (Immunofluorescence) | Estimate of the insert size (PCR across the loops) |
| | 8xMS2.C1.G1 | + | *Lower than control (≈600bp)* |
| | 8xMS2.C1.G2 | + | *Same as control (≈900bp)* |
| | 8xMS2.C2.G2 | + | *Lower than control (≈600bp)* |
| | 8xMS2.C3.G2 | + | *Same as control (≈900bp)* |
| | 8xMS2.C4.G2 | + | *Same as control (≈900bp)* |
| | 8xMS2.C5.G2 | + | *Lower than control (≈600bp)* |
| | 8xMS2.C6.G2 | - | *Ø* |
| **Stable cell lines generated from SGR/5A-TCM+12xMS2:3'UTR** | | | |
| | | Positive for HCV antigens (Immunofluorescence) | Estimate of the insert size (PCR across the loops) |
| | 12xMS2.C1.G1 | + | *Lower than control (≈600bp)* |
| | 12xMS2.C2.G1 | + | *2 bands one @ 600bp second@ 450 bp (=no loop)* |
| | 12xMS2.C1.G2 | + | *2 bands one @ 600bp second@ 450 bp (=no loop)* |
| | 12xMS2.C2.G2 | - | *Ø* |
| | 12xMS2.C3.G2 | + | *Lower than control (≈600bp)* |
| | 12xMS2.C4.G2 | + | *Lower than control (≈800bp)* |
| | 12xMS2.C5.G2 | - | *Ø* |
| **Stable cell lines generated from SGR/5A-TCM+24xMS2:3'UTR** | | | |
| | | Positive for HCV antigens (Immunofluorescence) | Estimate of the insert size (PCR across the loops) |
| | 24xMS2.C1.G1 | + | *Same as control (≈900bp)* |
| | 24xMS2.Polyclonal.G2 | + | *Same as control (≈900bp)* |

**Table 3.3: Summarized listing of the stable cell lines generated from SGR/5A-TCM+MS2:3'UTR in Huh7.5.**

The complete list of the stable cell lines initially generated from the sub-genomic replicons carrying MS2 stem loop repeat within their 3'UTR is presented in the table above together with results of immunofluorence study regarding HCV antigen positivity and status of the loops insertion within the 3'UTR.

### 3.2.3 Stability of the loop insertions

Previously in this chapter we have shown that the insertion of MS2 stem loops within the 3'UTR impaired viral replication to some extent. This is not surprising considering the relatively large insertions within the 3'UTR. Despite this negative pressure, we were able to generate stable Huh-7.5 monoclonal cell lines harbouring autonomous replication of the MS2 replicons. To further characterise these cell lines, we investigated how stable the insertion of MS2 stem loops remained after the blasticidin selection.

As described in the Chapter 2.1.10 and 2.1.12, total RNA was extracted and cDNA prepared from all MS2 Huh-7.5 clones. Despite considerable difficulty in amplifying regions containing the MS2 repeats, presumably due to extensive secondary structures and repetitive sequences, an optimized PCR (see Chapter 2.1.14 and Appendix V) was developed and applied to the generated cDNA to amplify a region of the 3'UTR that includes the MS2 stem loop insertion. PCR amplicons were then visualised by agarose gel electrophoresis to check the size of the insertion and assess the number of MS2 stem loops that were maintained. In Figure 3.9, a representative gel of PCR analysis is displayed with complete results summarised in Table 3.3. Initially we PCR amplified the different configurations of stem loops that are present within a plasmid backbone (Figure 3.9 Plasmid Controls). As predicted, as the number of stem loops increased so did the size of the PCR fragment in comparison to the PCR product that resulted from amplification of the HCV 3'UTR that contained no stem loops (amplicon from "empty" 3'UTR is approximately 450bp). However, while this was true for region containing up to 12 stem loops, PCR analysis of the plasmid containing 24 stem loops reliably produced an amplicon of approximately 900bp that corresponded to the amplicons produced for fragments containing 8 stem loops. Nevertheless, restriction digest

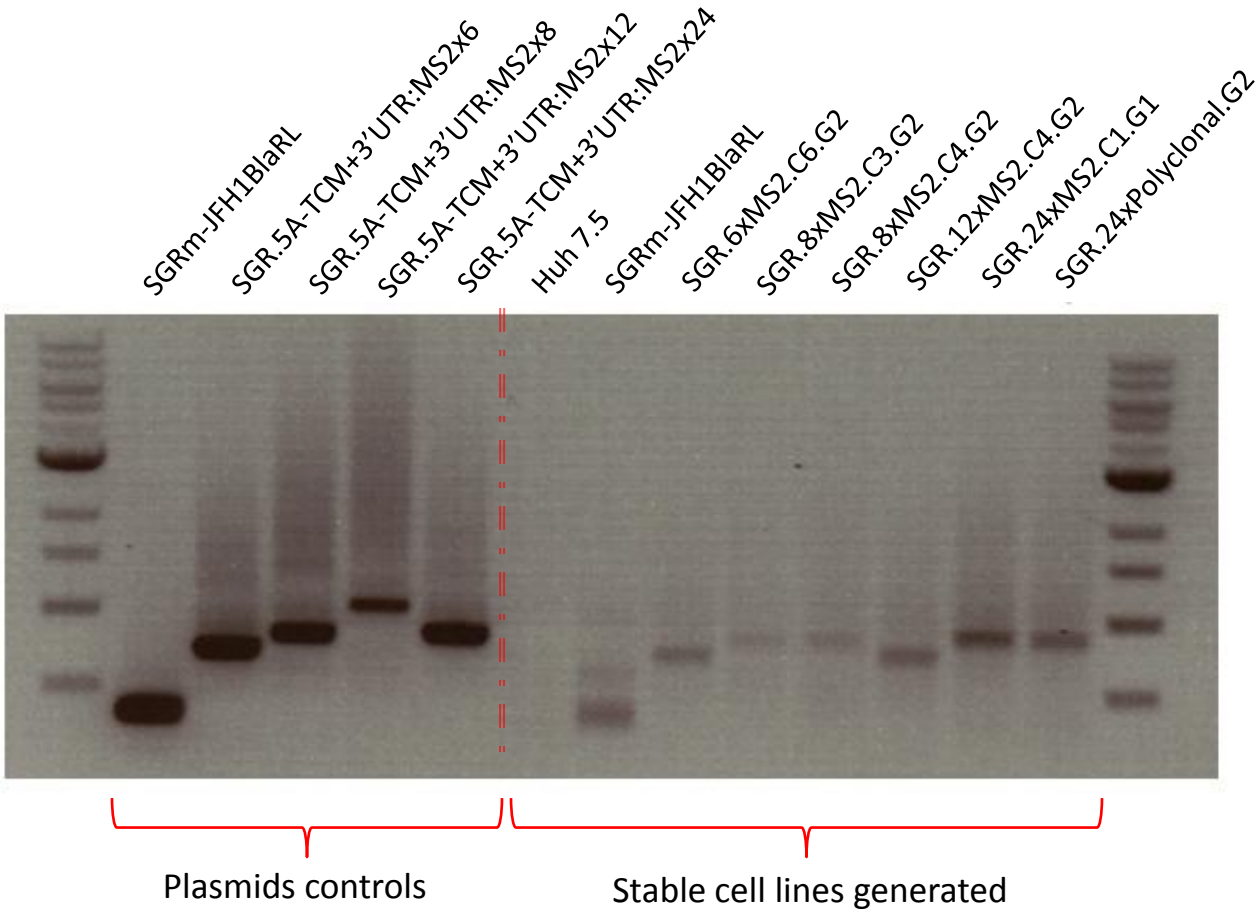


**Figure 3.9: PCR products generated after amplification of the 3'UTR from the cDNA of a sample of stable cell lines generated in Huh-7.5 from SGR/5A-TCM+3'UTR:MS2 plasmids.**

The results show a partial to complete retention of the MS2 stem loop repeats by these stable cell lines although complete loss of the insert has also been observed (data not shown). The specific case of the 24 repeats is thoroughly discussed in Chapter 3.2.3.

analysis confirmed that the 24x stem loop control plasmid contained the 24x MS2 stem loop repeats ( see Appendix VIII). It is likely that the smaller amplicon observed for templates containing 24x repeat sequences is a result of Taq polymerase 'skipping' across the loops in response to the repetition and the consequent added complexity of secondary structures involved in 24 repeats of MS2 bacteriophage stem loops.

Investigation of the stable MS2-tagged HCV replicon lines revealed PCR amplicons representing a range of sizes suggesting that for different lines stem loops were either retained, partially retained or lost. The complete array of stem loops was retained for some of stable clones carrying either 6x or 8x MS2 repeats (respectively 3 out of 4 and 3 out of 6 positive clones), however this was not the case for replicons containing 12 repeats in which the PCR amplicon corresponded to the control containing 6x MS2 repeats at best. Interestingly, clones harbouring replicons containing 24x stem loops revealed PCR amplicons that corresponded to the 24x stem loop control plasmid suggesting retention of the 24x stem loops. It is important to keep in mind that the PCR amplicon from the 24x stem loop replicon (SGR.5A-TCM+3'UTR:MS2x24) was reliably found to run at approximately 900bp which corresponds to the amplicon generated from the 24xMS2 control, although being smaller than the theoretical size of such array. Thus this strongly suggests that the cell lines that harbour the 24x stem loop replicon have retained all 24 loops and that the smaller amplicon is a result of polymerase 'skipping' across the loops during PCR. Alternatively this HCV genome could have lost approximately 16 of the stem loops but from our data and experience this seems highly unlikely. Due to difficulties in PCR amplification of regions containing MS2 stem loop repeats and, in particular, the modest processivity of enzymes used in Sanger sequencing, only partial sequences could be obtained for these regions.

From the results presented above, we can conclude that the negative pressure of the loop insertion exerted on viral replication drove some adaptation of the virus. Indeed the stable clones generated in our experiment presented different levels of adaptation (mainly partial loss of MS2 repeats). However, the high number of unaffected clones suggests that, despite this pressure, the MS2 bacteriophage stem loop insertion is relatively stable during replication. Furthermore compensatory mutations elsewhere in the genome in response to the loop insertion in the 3'UTR could also contribute to the apparent stability of the MS2 stem loop insertions.

### 3.2.4 Deep sequencing analysis of adaptive mutations

It is possible that compensatory mutations may have arisen as a result of the negative pressure exerted by the stem loop insertions. Identification of such mutations may help to develop more robust constructs and shed light on interactions between either HCV proteins or other regions of the genome with the 3'UTR. Thus, we sought to identify single nucleotide polymorphisms (SNPs) that emerged within the region coding for the viral proteins of the replicon population in comparison to the parent plasmid sequence by performing 454 Sequencing (Life Sciences, Roche). Due to both the nature of the data we wanted to gather and the high cost of the technique, we decided to centre our study on the two cell lines generated from SGR.5A-TCM+3'UTR:MS2x24 as this replicon harboured the longest MS2 stem loop array insertion (and thus is expected to enable a stronger signal) and displayed the highest replication levels. Moreover previous results (Section 3.2.3) indicate that both cell lines harbouring SGR.5A-TCM+3'UTR:MS2x24 have conserved numerous loops within the 3'UTR and we speculate that compensatory mutations could have emerged elsewhere in the coding region.

Figure 3.10 summarises the different steps and partners involved in the procedures of the deep sequencing analysis of the diversity within our stable cell. Specifically, we first harvested total RNA from both stable cell lines using the previously described method (Chapter 2.1.10) however we reduced the centrifugation speed below 9000g to avoid damage to the long RNA strands. We then prepared cDNA using SuperScript® III Reverse Transcriptase (Life Technologies) following the manufacturer's protocol (cf Chapter 2.1.15 for more information). A 6kb long PCR product was generated using SequalPrep Long PCR kit (Life Technologies) and the two primers detailed in Appendix V (primers KL_NS3P_F and KL-NS5Bc_R). PCR products were separated on a 1% agarose gel (see Chapter 2.1.6), purified (see Chapter 2.1.8) and resuspended in 10 µL of Tris buffer and sent to the Murdoch Institute for Immunology and Infectious Diseases (Perth, Australia) for Roche 454 Sequencing. The generated data set was analysed using two bioinformatical methods to call single nucleotide polymorphisms (SNPs): ShoRAH and LoFreq by Dr F. Luciani and Dr B. Betz-Stablein (UNSW, Sydney). Depending on the base call value, SNP frequency was estimated in the populations sampled.

Results were then interpreted based on the frequency determined by both base-calling methods and the presence of homopolymer regions surrounding the SNPs (region where the same base is repeated multiple times in a row). 454 Sequencing presents a much higher error rate near homopolymer regions, therefore translating into high probability for false positive SNPs. Ideally we aimed to identify SNPs called with a high frequency as an adaptive mutation(s) would become dominant amongst the population. Moreover SNPs should be called by both methods (ShoRAH and LoFreq) to be truly considered as real and not a result of sequencing errors. Finally we were particularly interested in SNPs which encoded an amino acid change, because it would

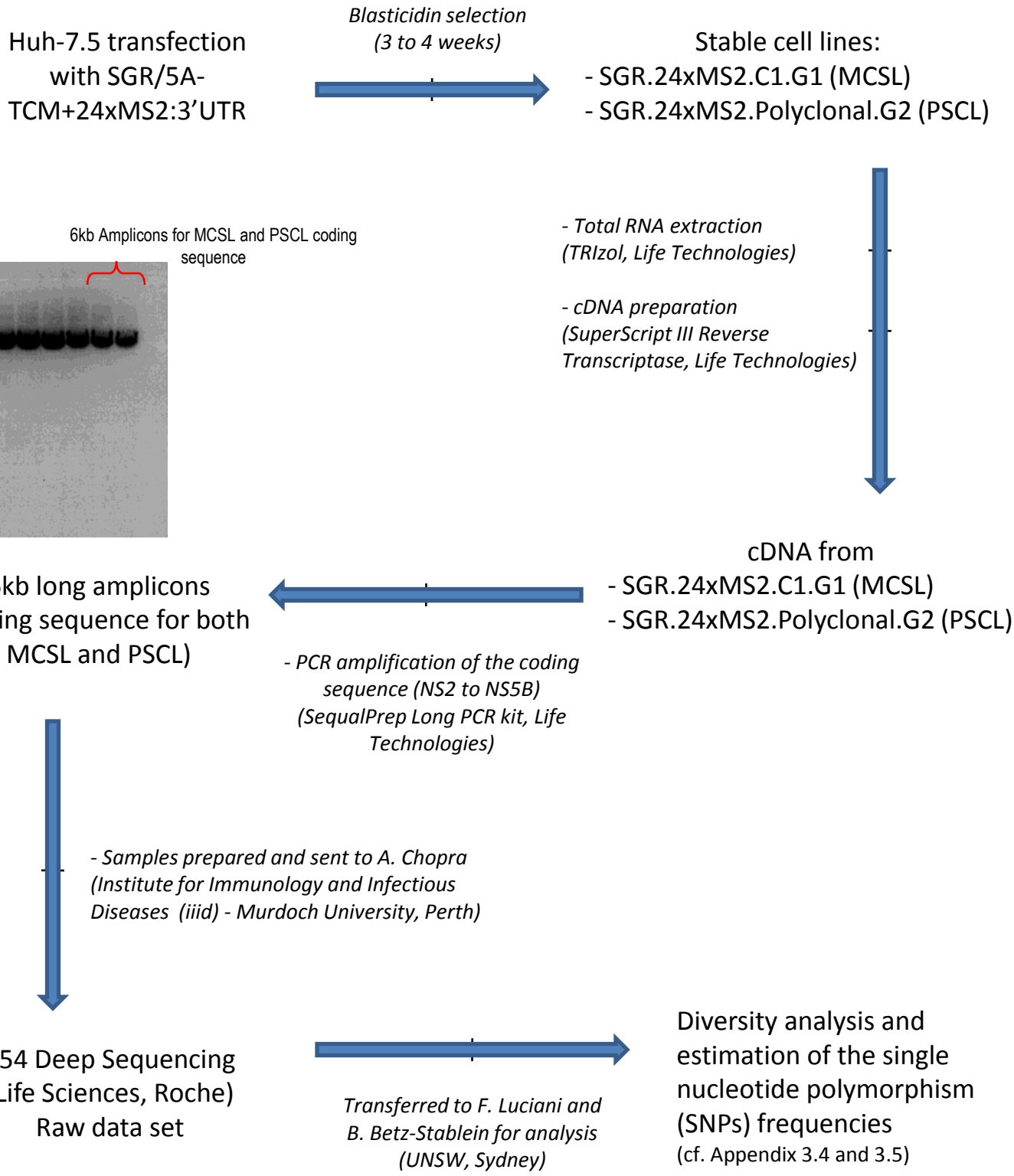


**Figure 3.10: Schematic of the deep sequencing experiment investigating MS2 sub-genomic replicon adaptive mutations.**

Diagram summarizing the different steps and partners involved in the deep sequencing project aiming to analyse diversity in the stable cell lines generated from SGR/5A-TCM+3'UTR:24xMS2.

highlight possible mechanistic changes in the viral life cycle. Complete results are presented in the table Appendix IV.

Contrary to our expectation, higher diversity was detected for the monoclonal stable cell line (MSCL) generated from SGR.5A-TCM+3'UTR:MS2x24 in comparison to the polyclonal stable cell line (PSCL) (101 SNPs in the monoclonal against 26 in the polyclonal).

None of the SNPs detected in the PSCL were called by both bioinformatics techniques. Moreover most of these SNPs (all except one: A7655G) are located in strong homopolymer regions, strongly suggesting that they are not genuine SNPs. Furthermore, the frequency of the putative A7655G SNP is fairly low (2.4%) and, if real, does not appear to be a dominant SNP.

On the other hand, 9 SNPs located away from homopolymer regions were detected by both bioinformatics methods in the case of MSCL. However, for most of these SNPs, frequencies called are lower than what would be expected for a dominant mutation. The T8740C SNP, (located within NS5B coding sequence) presents the highest frequency called with 49.6% and 18.8% (respectively with ShoRAH and LoFreq methods).This SNP is however synonymous as the base mutation does not translate into an amino acid change limiting its possible impact.

In summary, analysis of the deep sequencing results did not identify any compensatory mutations. However a broader range of monoclonal and/or polyclonal cell lines together with the conjoint studies of the 3'UTR and/or 5'UTR as well as the coding sequence could help enhance our research of possible compensatory mutations and hence improve fitness of the research model. These results and their implication are further discussed in the discussion of this chapter (Section 3.4).

## 3.3 Full-length HCV cell culture models

The insertion of MS2 bacteriophage stem loops within the 3'UTR region of the HCV replicon had a significant impact on replication efficiency, as shown above. Nevertheless, the replicon-based model displayed robust replication, while conserving the loops and displaying minimal mutation. Investigation of HCV viral RNA traffic during a full life cycle was our primary focus, although the replicon based model was a key element to bridge our understanding concerning the impact of the MS2 loops insertion on HCV viral fitness. In this section of Chapter 3, the characterisation of the full-length HCV isolate carrying 24x MS2 stem loop insertion developed in Section 3.1.1 is described.

### 3.3.1 Replication efficiency of the MS2 stem loop tagged Jc1 derivatives.

The full-length Jc1 HCV cell culture model was expected to be more sensitive to manipulation of its genome than a replicon based model as this virus completes the whole viral life cycle and introduced mutations may impact multiple stages of the life cycle. We first investigated the fitness of the cloning intermediate (Jc1/5A-TCM+3'UTR*(*EcoRI*/*BglII*)) described in Section 3.1.1. This HCV genome only carries the two restriction sites (*EcoRI* and *BglII*) introduced immediately after the NS5B stop codon by site directed mutagenesis as a precursor step to the MS2 bacteriophage stem loop insertion (cf Figure 3.2).

To assess the impact of this relatively minor modification of the 3'UTR of Jc1/5A-TCM, we compared the replication fitness of both the parent Jc1/5A-TCM and Jc1/5A-TCM+3'UTR*(*EcoRI*/*BglII*) by focus forming assay (see Chapter 2.4.3 for complete

description). Huh-7.5 cells were electroporated with T7 IVT RNA for both Jc1/5A-TCM+3'UTR*(*EcoRI*/*BglII*) and the parent construct Jc1/5A-TCM and returned to culture for 3 days after which culture supernatants were sampled and 0.45μm filtered and focus forming assay was performed. In Figure 3.11, the graph depicts the relative infectivity of both HCV genomes and thus their ability to fully go through the complete viral life cycle in cell culture. Interestingly, both constructs present similar levels of infectivity indicating that the small insertion in Jc1/5A-TCM+3'UTR*(*EcoRI*/*BglII*) had minimal impact on viral fitness.

To investigate the impact of the complete MS2 loop insertion on the full RNA imaging model, we started by reproducing the focus forming assay described above comparing Jc1/5A-TCM+3'UTR:MS2x24 /x12 /x8 /x6 to the parental construct Jc1/5A-TCM. However, Jc1/5A-TCM+3'UTR:MS2x24 /x12 /x8 /x6 constructs did not show sign of infectivity after 3 days post electroporation suggesting that these insertions were deleterious to HCV replication and/or assembly (data not shown).

Despite a lack of infectious virus production, it was possible that HCV RNA replication was occurring and viral assembly was being blocked due to the large insertion considering the replicon data above (MS2 stem loops-tagged HCV replicon replicated). We therefore investigated the presence of HCV antigens using anti-HCV patient serum as primary antibody to detect cells harbouring HCV replication (see Chapter 2.5.3). Results demonstrated reliable but limited presence of HCV antigens in the electroporated Huh-7.5 cells (3 days post-electroporation). In Figure 3.12, a side by side comparison between immunofluorescence images of Huh-7.5 cells transfected with HCV transcripts for Jc1/5A-TCM+3'UTR:MS2x24, the parent construct Jc1/5A-TCM and the replication-defective (GDD > GND mutation in NS5B) version as negative control is depicted. We observed a small percentage of cells positive for HCV

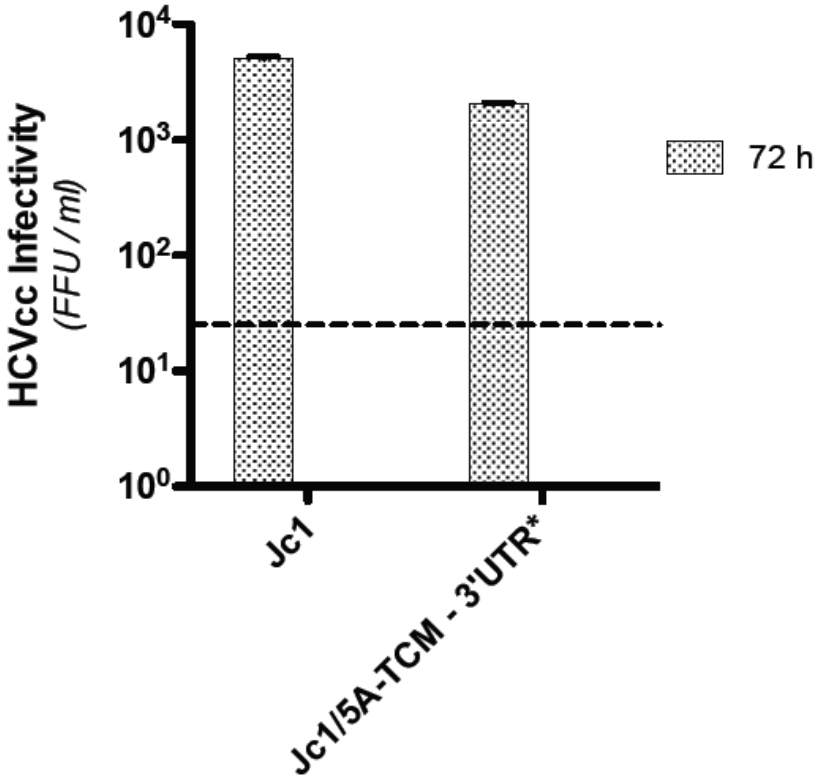


**Figure 3.11: Insertion of *EcoRI* and *BglII* in the 3'UTR causes a minor impact on infectivity of the cloning intermediate Jc1/5A-TCM+3'UTR*.**

Focus Forming Assay comparing infectivity of Jc1/5A-TCM+3'UTR* supernatant (collected 3 days post-electroporation) compared to parent on naïve huh7.5 cells.

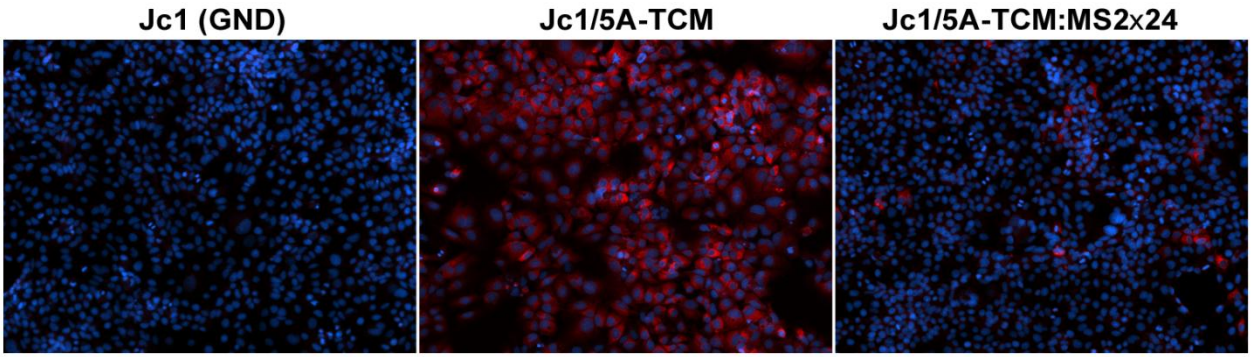


**Figure 3.12: Immunolabelling of HCV antigens (red) in electroporated Huh-7.5 cells.**

Huh-7.5 cells were electroporated with Jc1(GND), Jc1/5A-TCM or Jc1/5A-TCM+3'UTR:MS2x24. After 3 days, cells were immunolabelled for HCV antigens (red) with anti-HCV patient serum and nuclei stained with DAPI (blue). Only a small proportion of cells (quantified in Figure 3.10) appears positive with Jc1/5A-TCM+3'UTR:MS2x24.

antigens after electroporation with Jc1/5A-TCM+3'UTR:MS2x24, while the vast majority of cells were positive for the parent Jc1/5A-TCM and none were positive for the negative control.

To support this data, we manually enumerated the proportion of cells which were HCV-positive 3 days after electroporation (Figure 3.13). Approximately 3% of cells were positive for HCV antigens after being electroporated with Jc1/5A-TCM+3'UTR:MS2x24 and returned to culture for 3 days. In comparison, 92.6% of cells were positive with the parent construct Jc1/5A-TCM. Taken together, these results indicate that the insertion of 24x stem loops severely impacts upon viral fitness and probably abolishes infectivity.

### 3.3.2 Long term culture

Given the propensity of the HCV genome to adapt (a feature of positive stand RNA virus genomes) and the ability of Jc1/5A-TCM+3'UTR:MS2x24 to replicate, albeit inefficiently, we decided to investigate longer term cultures in the hope that the modified genome may adapt. Therefore we repeated the immunofluorescence study above over a longer time frame. Huh-7.5 cells were electroporated with Jc1/5A-TCM+3'UTR:MS2x24, the parent construct Jc1/5A-TCM and a replication deficient Jc1 construct (GND mutation) and returned to culture. At day 3, 6, 9 and 12, samples from these cultures were fixed, DAPI stained and immuno-labelled to detect HCV antigens as above. Results are presented in Figure 3.14.

Consistent with previous results, at day 3, HCV antigens were detected in only a small percentage of cells following electroporation with Jc1/5A-TCM+3'UTR:MS2x24, while most of the cells were positive for the parent Jc1/5A-TCM (not shown) and none

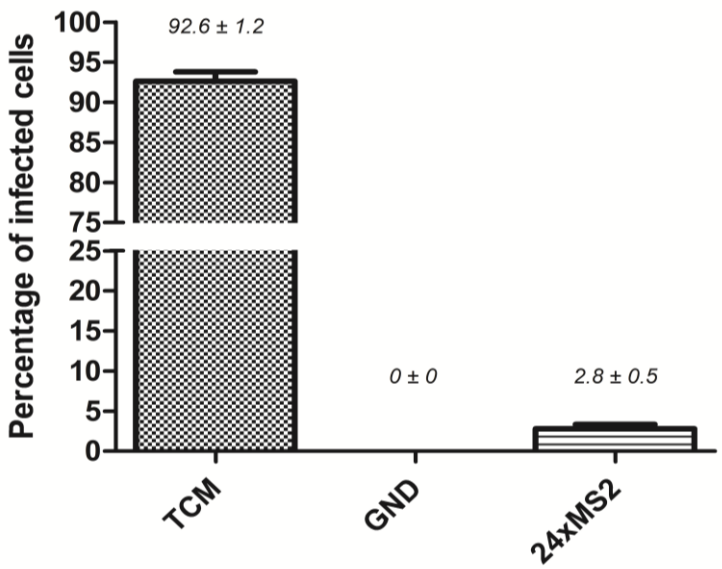


**Figure 3.13: Enumeration of HCV antigen-positive cells 3 days post-electroporation.**

Huh-7.5 cells were electroporated with Jc1(GND), Jc1/5A-TCM or Jc1/5A-TCM+3'UTR:MS2x24. Immunofluorescent labelling and manual counting of HCV antigen-positive cells shows a significant but low proportion of Jc1/5A-TCM+3'UTR:24xMS2-positive cells compared to parent Jc1/5A-TCM.

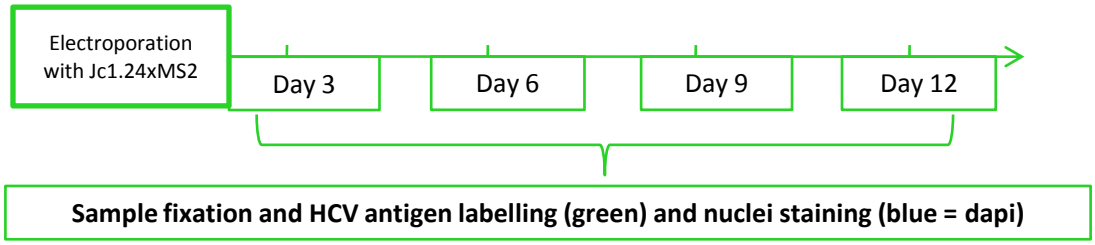


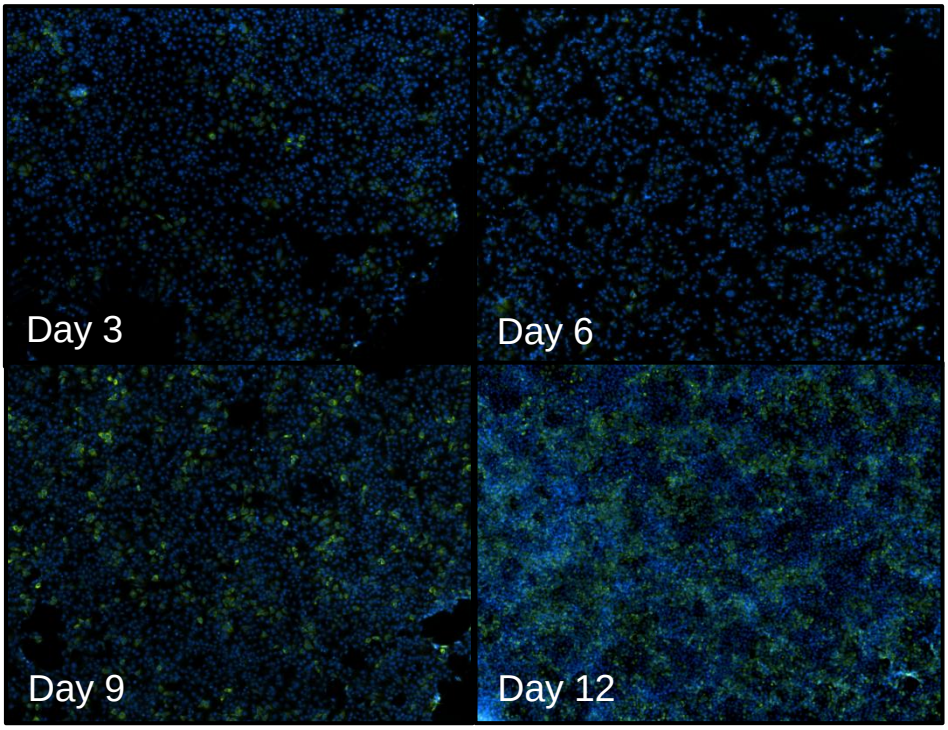


**Figure 3.14: Jc1/5A-TCM+3'UTR:24xMS2 present a reduced replication efficiency.**
Cells were immunolabelled for HCV antigens (green) with anti-HCV patient serum and nuclei stained with DAPI (blue) at days 3, 6, 9 and 12 post-electroporation.

were for the negative control (not shown). Images shown in Figure 3.14 illustrate the amount of HCV antigen-positive cells at day 3, 6, 9 and 12 after electroporation with Jc1/5A-TCM+3'UTR:MS2x24. Over the course of the 12 days, a slow and steady increase in the proportion of HCV-positive cells was observed potentially illustrating emergence of adaptive mutations We did not pursue the identity of these mutations, however a deep sequencing approach could be used as we have previously discussed to identify possible adaptive mutations. In contrast Jc1/5A-TCM-electroporated cells were entirely positive by day 6, while there was no detectable expression of HCV antigens in cells that were transfected with the replication deficient Jc1 construct (not shown). Taken together these results strongly indicate that the Jc1/5A-TCM+3'UTR:MS2x24 HCV genome could sustainably replicate at low level in Huh-7.5 cells after electroporation. Moreover, the increase in the percentage of positive cells clearly observed suggest that some sort of spreading could be occurring within the culture, either by infectious virus formation or by cell to cell spread.

### 3.3.3 Long term presence of the loops within the 3'UTR

From multiple experiments in which we electroporated Jc1/5A-TCM+3'UTR:MS2x24 RNA into Huh-7.5 cells we observed that at 5 to 8 days post-electroporation, there was an increase in the percentage of HCV antigen positive cells within our cultures. Therefore we decided to investigate the maintenance of the MS2 stem loop insertion around that time point.

Using similar methodology as before (cf. Section 3.2.3), Huh-7.5 cells were electroporated with Jc1/5A-TCM+3'UTR:MS2x24 and returned to culture. Total cellular RNA was then extracted at day 8 post-electroporation (cf. Chapter 2.1.10) and

cDNA was generated using random hexamers primers (cf. Chapter 2.1.12). The 3'UTR including the MS2 loops was then amplified using Platinium® Taq DNA polymerase High Fidelity (Life technologies) (see Chapter 2.1.13) (primers used were Jc1-9015S and Jc1-9469R – cf Appendix V for complete sequence). The plasmid Jc1/5A-TCM+3'UTR:MS2x24 was used as positive control for complete loop insertion and was thus amplified and processed the same way. An agarose gel picture presenting the PCR product is shown in Figure 3.15. We can observe that each sample is composed of a multitude of bands as is the plasmid control. This is partially due to the use of Platinium® Taq DNA polymerase instead of Deep Vent$^{R}$ polymerase as the associated 3' A overhang was critical for the rest of the experiment. Nevertheless, the band pattern seemed to differ slightly between samples and the control plasmid suggesting a heterogenous population of HCV 3'UTR with varied numbers of MS2 stem loop repeats could have been derived from the initial Jc1/5A-TCM+3'UTR:MS2x24 RNA input.

We then used the 3' A overhangs generated during the amplification with Platinium® Taq DNA polymerase (Life technologies) to allow direct ligation of the 3'UTR amplicons into pGEM®-t Easy vector (Promega). Restriction digest analysis of the resulting plasmids using NotI present on both extremities of the MCS revealed a number of clones containing insertions (an example of 3 clones per initial RNA extraction is presented in Figure 3.16). These plasmid samples were then analysed by Sanger sequencing using T7 and SP6 primers flanking the inserts (see Appendix IX).

Sequencing results showed that the initial Jc1/5A-TCM+3'UTR:MS2x24 parent diversified into a heterogenous population of viruses. Indeed some clones revealed up to retention of 7 loops while other clones had completely lost their loops. Therefore, the different sizes of inserts observed in Figure 3.15 and Figure 3.16 probably reflected

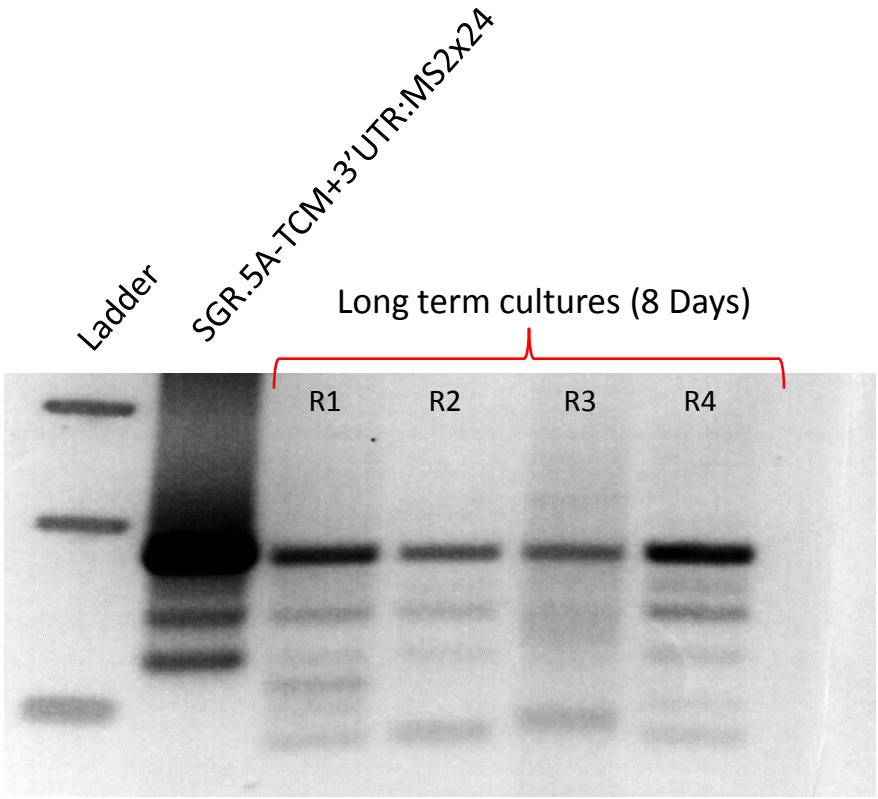


**Figure 3.15: Platinium Taq® amplification over the 3'UTR of virus cDNA from long term culture (Day 8).**
Huh-7.5 cells were electroporated with Jc1/5A-TCM+3'UTR:24xMS2 and cultured for 8 days. PCR amplification of stem loop regions from cDNA prepared from these cultures are presented and show different and more complex patterns than from the parent plasmid suggesting diversity within the cultures.

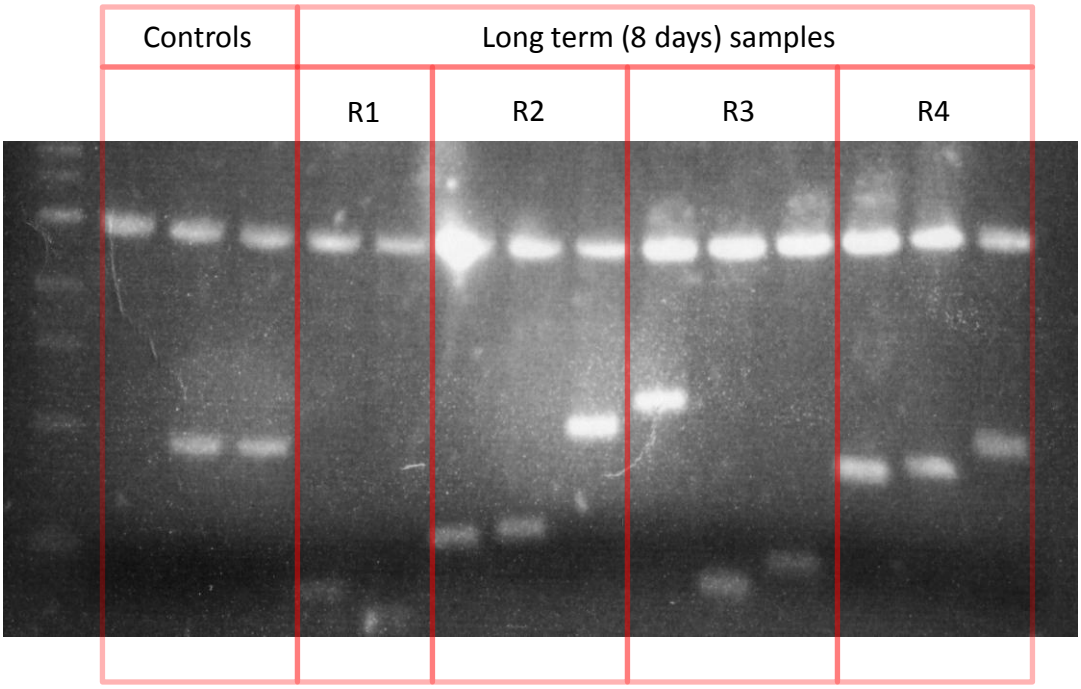


**Figure 3.16: Variability of MS2 loops insertions 8 days post-electroporation of Huh-7.5 cells with Jc1/5A-TCM+3'UTR:24xMS2.**
The four replicates (R1 to R4) generated from 8 day-cultures produced numerous clones corresponding to distinct retention of MS2 stem loop. Several clones for every replicate are presented along with control clones generated from PCR performed using the initial plasmid Jc1/5A-TCM+3'UTR:24xMS2 as template.

different numbers of MS2 stem loop repeats from different variants. Moreover, as described in Section 3.2.3, PCR amplification across the MS2 stem loop insertion for the Jc1/5A-TCM+3'UTR:MS2x24 plasmid produced a band of lower size than expected, corresponding to what would be expected for approximately 7 stem loop repeats. Furthermore this was confirmed by sequencing which showed that for the positive control only 7 loops were present after amplification. This suggests that the repeat sequences may be causing deletions during PCR amplification and that the presence of bands of a size corresponding to 7 loops for the above cDNA-derived clones could reflect in reality a virus with up to 24 repeats.

### 3.3.4 The loss of the MS2 stem loop repeats restores infectivity

In order to further characterise the evolution of the MS2 stem loop insertions into the HCV genome we extended the long-term culture of cells electroporated with the MS2-tagged HCV genomes and assessed the presence of loops over a longer period as well as the infectivity. Huh-7.5 cells were electroporated with IVT RNA of Jc1/5A-GFP+3'UTR:24xMS2, parent Jc1/5A-GFP or were mock-electroporated. Cells were returned to culture for the following three weeks. Jc1/5A-GFP+3'UTR:24xMS2 and Jc1/5A-GFP carry a GFP tag within the NS5A coding sequence in place of the TCM tag described previously, hence allowing easy visualization of the spread of the virus through the culture by fluorescence microscopy without staining.

None of the mock-electroporated cells were positive for GFP fluorescence as expected (not shown), while most of the Jc1/5A-GFP-electroporated cells were positive by 3 days after electroporation (see fluorescence imaging in Figure 3.17). In the instance of Jc1/5A-GFP+3'UTR:24xMS2 RNA-transfected cells, the proportion of HCV-positive

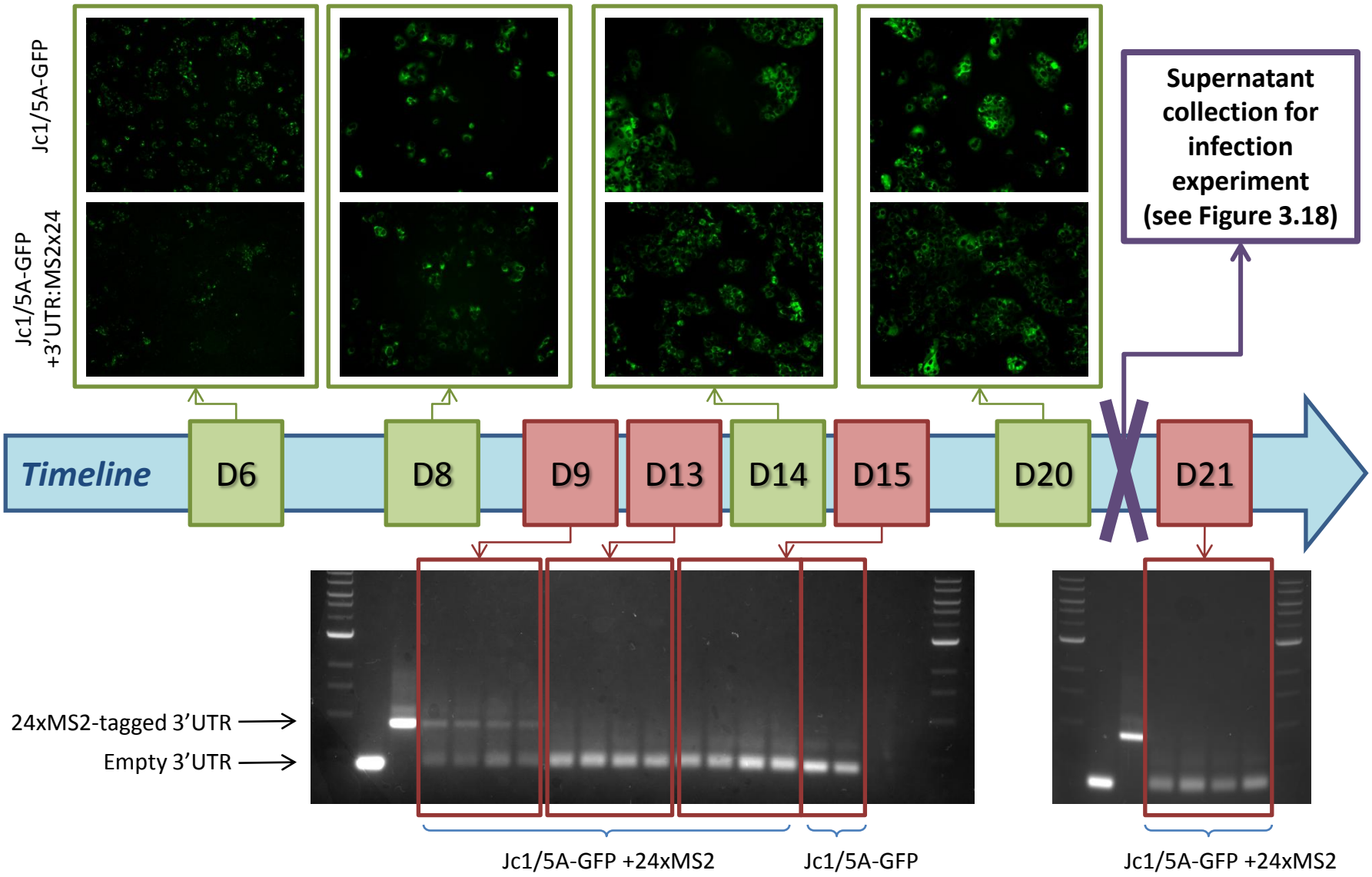


**Figure 3.17: Long-term passage of Jc1/5A-GFP+3'UTR:MS2x24 virus.** 5A-GFP fluorescence (above) and 3'UTR insertion size (below) associated with long-term culture of Jc1/5A-GFP+3'UTR:MS2x24–electroporated cells.

cells increased slowly as shown previously (see fluorescence imaging in Figure 3.17). At days 9, 13, 15 and 21 after electroporation, RNA was extracted from a sample of the Jc1/5A-GFP+3'UTR:24xMS2-electroporated cells and cDNA prepared using SuperScript III Reverse Transcriptase with the JFH1-9211_Loops cDNA primer (see Appendix V) (see method Section 2.1.12.2). PCR amplification over the loop insertion using Deep $Vent_R$ DNA polymerase and JFH1-9258FP HighTm and JFH1-9651RP HighTm primers was performed to assess the degree of retention of the MS2 stem loop repeats. Partial maintenance of the loops can be observed up to day 9, however the 3'UTR appeared to be devoid of MS2 stem loop insertions from day 13 onwards (see Figure 3.17). This time is coincidental with a relatively large increase in the number of NS5A-GFP-positive cells and could result from the emergence of specific adaptive mutation. Deep sequencing analysis of such mutation could provide further information and the nature of these potential mutations.

At 20 days post-electroporation supernatants from both Jc1/5A-GFP+3'UTR:24xMS2-electroporated and Jc1/5A-GFP-electroporated cell cultures were collected and filtered with 0.45 μm filters, before being used to infect naïve Huh-7.5 cell monolayers. Immunolabelling was performed 3 days post-infection with anti-HCV patient serum as primary antibody. Fluorescence microscopy (see Figure 3.18) revealed that a large proportion of the cell monolayers were infected in both cases. These observations indicate that infectious virus is produced at time points that coincide with loss of the MS2 stem loop repeats. This phenomenon could be related to the potentially inefficient packaging of the tagged viral genome due to the increased size (10.9 kb vs 9.6 kb). Therefore loss of the loops would restore the efficiency of the final steps of the viral life cycle enabling infectivity. Long-term passage of Jc1/5A-GFP-electroporated cells

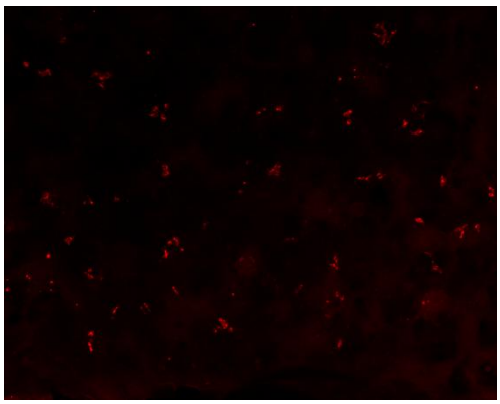

*3 days post-infection with Jc1/5A-GFP supernatant*

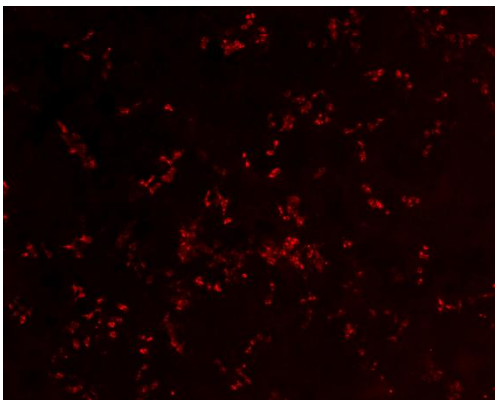

*3 days post-infection with Jc1/5A-GFP+3'UTR:24xMS2 supernatant*

**Figure 3.18: Loss of the MS2 stem loop insertion restores infectivity of the cell culture model.**

Cells were immunolabelled for HCV antigens (red) with anti-HCV patient serum 3 days post-infection with the passaged virus (both from Jc1/5A-GFP+3'UTR:MS2x24-electroporated and Jc1/5A-GFP-electroporated cultures). Long-term culture (20 days) of Jc1/5A-GFP+3'UTR:MS2x24-electroporated cells resulted in ready detection of infectious virus that coincided with loss of the MS2 loop insertion.

resulted in considerable inhibition of cell growth and viability and hence it was difficult to assess the relative infectivity of the virus produced.

## 3.4 Discussion

Hepatitis C virus replication complexes result from the association of both viral and host components and provide an environment to facilitate replication of the viral genome. An improved understanding of how precisely such host-virus interactions dynamically govern replication of HCV RNA could enable development of improved therapeutics and further our understanding of HCV replication at the molecular level. Emerging live imaging techniques have recently enabled direct visualization of HCV viral proteins in real-time (Counihan et al., 2011; Moradpour et al., 2004; Wolk et al., 2008), including work from our laboratory investigating the dynamics of NS5A during a productive infection (Eyre et al., 2014a). NS5A is a key component of HCV replication complexes and has been shown to co-localise with HCV RNA in fixed infected cells (Targett-Adams et al., 2008) and is thought to bind HCV RNA (Foster et al., 2010; Huang et al., 2005; Tellinghuisen et al., 2005). Moreover, live cell imaging of NS5A-positive structures (putative replication complexes) has revealed that these structures may be relatively large and static or small and highly motile (Eyre et al., 2014a; Wolk et al., 2008). However the relative roles of these NS5A populations are not well understood. By associating NS5A tagging and imaging techniques to the MS2 experimental model of RNA imaging we aimed to investigate the underlying connections between the NS5A structure types and RNA replication and/or traffic during the HCV life cycle.

In this chapter, we developed an MS2 bacteriophage-based system that would enable live imaging of HCV RNA in living cells. This approach was first described to visualise cellular RNA (Bertrand et al., 1998) and has more recently been used for visualization of TBEV, a related Flavivirus, RNA in the context of a replicon (Miorin et al., 2008). Inserting the MS2 stem loop arrays within the variable region of the 3'UTR we have been able to generate HCV research models which are able to sustain replication despite the negative pressure induced by such insertions. As indicated by the results from this chapter, both the sub-genomic replicon and the full-length models are able to maintain replication within Huh-7.5 cells. Published studies that have applied this technique to study HIV (Boireau et al., 2007; Jouvenet et al., 2009) or TBEV (Miorin et al., 2008; Miorin et al., 2013) were mainly focused on the use of 24 repeats of MS2 stem loops. However, a severe impact on HCV replication was expected because of the size that 24 repeats of MS2 stem loops represents (about 1.3kb while HCV genome is only 9.6 kb total) and the relative sensitivity of HCV genomes to insertions. Therefore comparisons between smaller inserts (6, 8, 12 and 24 repeats of MS2 stem loops) were initially performed. Surprisingly our data indicated that insertion of 24 MS2 stem loop repeats had a lesser impact on viral replication than the smaller inserts. Indeed both *Renilla* Luciferase assays (over 3 days) and colony formation assays (over 2 weeks) showed a significant fitness advantage of HCV constructs containing 24 repeats over those containing the smaller inserts. Moreover, as each MS2 repeat represents one potential binding site for an MS2 bacteriophage coat protein-fluorescent protein fusion (Section 1.4.3 and Figure 1.10), an insert including 24 repeats of MS2 stem loops theoretically results in a fluorescent message that is 2 times stronger than 12 repeats, 3 times stronger than 8 repeats and 4 times stronger than 6 repeats. Taken together the results demonstrated that HCV constructs bearing 24

repeats of MS2 stem loops display stronger replication than those bearing smaller MS2 stem loop insertions and are expected to enable a stronger fluorescent signal for detection by fluorescence microscopy as they carry more binding sites for the fluorescent reporter.

Although the variable region of the 3'UTR is at least partially dispensable for HCV RNA replication (Friebe and Bartenschlager, 2002; Yi and Lemon, 2003), we were concerned about the ability of the virus to retain the large MS2 stem loop insertion. With respect to the increased level of apparent replication 3 days after electroporation observed in Figure 3.9 and Figure 3.11, we investigated the possibility that the delayed kinetics of replication observed could be the consequence of viral adaptation driving a complete loss of the loops to sustain better replication. Nevertheless, our investigation showed that the majority of MS2 stem loops were maintained for numerous days (up to 8 days) after electroporation with both the full-length construct (Figure 3.12 and 3.13) and in selected stable cell lines harbouring the sub-genomic replicon (Figure 3.7).

In the stable cell lines harbouring replication of the MS2-tagged sub-genomic replicons we have observed a range of situations. MS2 stem loop insertions can be found intact or partially lost (in only 1 case out of 17 the loops were completely deleted). We have observed that the insertion including initially 12 repeats of MS2 stem loops was the most subject to loss of repeats. In contrast, 8 out of 12 stable cell lines harbouring replication of the sub-genomic replicons initially starting with 6, 8 or 24 repeats displayed an apparent deletion of the stem loop insertions.

As stated previously the amplification of the 3'UTR section including the loops has been relatively problematic by PCR when amplifying 24 repeats. Although extensive

optimization has been performed to test different conditions, additives and the use of different enzymes with improved processivity we were unable to produce a PCR product of the expected size. The amplicon resulting from the optimized PCR was consistently approximately 900 bp which is the expected size of a 7 to 8 MS2 stem loop repeat insert. Taken together our observations indicated that the apparent PCR problem was due to the highly repetitive sequence and complex secondary structures contained within 24 repeats of MS2 stem loops. After selection, both monoclonal and polyclonal stable cell lines generated from the sub-genomic replicon carrying 24 MS2 stem loop repeats displayed the specific band at 900 bp, thus indicating a high probability that the 24 repeats were stably maintained within the 3'UTR.

However in the experimental framework that is relevant to live cell imaging (within 3 to 4 days after electroporation), our results clearly demonstrates that MS2 stem loop insertions remain stable within the viral genome up to 8 days post-electroporation.

Although beyond the scope of the present study, other approaches to study the maintenance of stem loop insertions such as RNAseq and Northern blotting could reveal additional details about the nature and frequency of changes to the MS2 stem loop insertions during long term culture of these tagged genomes.

The observation made earlier concerning the evolution of the 3'UTR did not satisfactorily explain the kinetics of replication that we observed. Another hypothesis we considered was that the emergence of adaptive mutations within the coding sequence could help to compensate for the insertions. Next generation sequencing offers powerful tools to investigate such events and characterise the substitutions involved. 454 sequencing was the most relevant technique we could use to study the

emergence of single nucleotide polymorphism (SNPs) over the coding region (6kb long fragment). Indeed 454 sequencing provided the most accurate tool to generate and study long reads while reliably detecting substitutions (Shendure and Ji, 2008). Furthermore collaboration projects were developed to help with the 454 sequencing technique (Chopra A., Institute for Immunology and Infectious Disease, Murdoch University, Perth) and data analysis (Luciani F. and Betz-Stablein B., University of New South Wales, Sydney).

The two SNPs caller methods (LoFreq and ShoRAH) used to investigate diversity are based on two different algorithms to identify SNPs from the raw data set. One has tendency to overestimate SNPs values and one has tendency to underestimate it. We believe the true value of the SNPs to be somewhere in between the SNPs values called by each method. Moreover, homopolymer regions (regions with consecutive repetition of the same base) are prone to induce sequencing errors calling false positive base insertions or deletions. These events are due to the biochemical basics of the sequencing technique (Ronaghi et al., 1996) and needed to be considered when interpreting the data. The majority of the SNPs detected were present at a low frequency which strongly differs with what we would expect for an emerging compensatory mutation providing a replication advantage. The closest candidate to a compensatory mutation is the T8740C substitution (within NS5B coding region) called for 49.6% and 18.8% (respectively with ShoRAH and LoFreq methods) in the populations studied. However, this mutation is silent and thus does not translate into an amino acid change. Nevertheless, the 3' end of HCV positive-strand RNA is particularly rich in secondary structures (Blight and Rice, 1997). Multiple stem loops are organized in both the X-tail region of the 3'UTR (designated as SL1, SL2 and SL3) and in the coding sequence of NS5B (designated as SL3.2 or SL9266). Furthermore,

long range interactions between SL3.2 and the sequence around nucleotide 9110 (Tuplin et al., 2012) and between SL3.2 and SL2 (better known as kissing loops interaction) (Friebe et al., 2005) have been shown to be critical for HCV replication. However, the T>C substitution detected by deep sequencing is located relatively far away from these hotspots for secondary structure interactions and a single nucleotide substitution seems unlikely to drive the formation of unpredicted interactions of this type by itself. Taken together, the results of the deep sequencing analysis indicated that there were no dominant compensatory mutations within the NS3-NS5B coding region that enhanced the fitness of MS2-tagged HCV constructs. Although the substitution T8740C was called at a relatively high frequency in comparison to the other possible mutations, this non-coding mutation was unlikely to be a compensatory mutation developed in response to the MS2 stem loop insertion. Despite our interpretation, the reinsertion of this SNP into the original MS2-tagged full length constructs could be considered as a future direction to moderately improve the fitness of this virus.

In summary, we have developed and characterised a set of research models derived from Jc1/5A-TCM (Eyre et al., 2014a) aimed at enabling real time imaging of HCV viral RNA in living cells. Results unanimously indicate Jc1/5A-TCM+3'UTR:MS2x24 displays the best potential for replication while remaining relatively stable regarding the MS2 stem loop insertion. Moreover, Jc1/5A-TCM+3'UTR:MS2x24 also should enable the best theoretical signal for imaging HCV RNA by live cell fluorescence microscopy. Taken together, we are confident in Jc1/5A-TCM+3'UTR:MS2x24 being the best tool for HCV RNA live imaging amongst the constructs developed in this chapter and this virus is therefore mainly used in the different live cell imaging studies presented in the following chapters.

# Chapter 4:

# HCV RNA Localisation and Traffic in Living Cells

## 4.1 Introduction

Visualisation of RNA within a cell has traditionally been limited to RNA *in-situ* hybridisation studies using either radiolabelled or fluorescently labelled probes. These have limitations in that they require the fixation of cells that may distort RNA localisation. Most recently live imaging of either HIV or TBEV RNA has been achieved in living cells using the bacteriophage MS2 system (Basyuk et al., 2003; Boireau et al., 2007; Jouvenet et al., 2008; Maiuri et al., 2011; Miorin et al., 2008; Miorin et al., 2013). The MS2 bacteriophage system to tag RNA relies upon the joint expression of two elements within the experimental model (e.g. mammalian or yeast cell). The first element is the RNA of interest that has been engineered to carry the MS2 bacteriophage stem loops within an untranslated region of the sequence. In our study, as previously described in Chapter 3, we inserted an array of MS2 stem loops (6-24 repeats) within the variable region of the 3'UTR of a HCV genome designed for live imaging of NS5A. The second element is a reporter protein composed of MS2 bacteriophage coat protein fused to a fluorescent protein that needs to be expressed together with the RNA. The MS2 bacteriophage coat protein is an RNA-binding protein that specifically recognises the MS2 bacteriophage stem loops. Replication of the

tagged HCV genome in Huh-7.5 cells expressing the fusion reporter protein should induce a reorganisation of the fluorescence and allow visualisation of HCV viral RNA dynamics in real-time during viral replication for the first time.

The positive sense HCV RNA genome is readily translated into HCV viral proteins by the host cell translation machinery subsequent to its delivery into the cytoplasm. Driven primarily by NS4B (NS3/4A, NS5A and NS5B also play a role) intra-cellular endoplasmic membrane rearrangements develop to generate a complex architecture of single, double and multi-membrane vesicles termed membranous webs (Egger et al., 2002; Romero-Brey et al., 2012). These characteristic structures that occur in many positive strand RNA viral infections present a confined space where all the necessary components of the replication machinery reside. These membrane rearrangements also named replication complexes, are interconnected within a tubular network and provide a protected environment enabling viral RNA to replicate and to concentrate. Putative sites of active viral RNA replication are generally visualized using a marker for replication complexes such as NS5A. NS5A is an enigmatic viral protein with critical involvement in RNA replication as it is an important element of the replication complexes. NS5A has been shown to extensively co-localise with dsRNA (Foster et al., 2010; Targett-Adams et al., 2008) in infected cells and is predicted to bind viral RNA (Tellinghuisen et al., 2005) and therefore is considered as a reliable marker for replication complexes and thus HCV viral RNA.

In this chapter, we first describe generation and characterisation of a Huh-7.5 cell line constitutively expressing the reporter MS2Coat-mCherry protein and investigate its possible effect on replication of HCV genomes carrying the MS2 stem loops. Thereafter we describe HCV RNA dynamics in living cells in comparison to NS5A localisation and traffic.

## 4.2 Generation of an MS2.Coat–mCherry fusion protein as a reporter for tagged-HCV RNA

In this section we describe the generation of a Huh-7.5 cell line constitutively expressing the fusion protein between the MS2 bacteriophage coat protein and the mCherry fluorescent protein. The Huh-7.5 cell line was used, as this line is highly permissive for HCV infection and replication (see Section 1.3).

### 4.2.1 Stable expression of MS2.Coat-mCherry fluorescent fusion protein

In the previous chapter we described and characterised the insertion of MS2 stem loops within the 3'untranslated region of the HCV genome Jc1/5A-TCM. To enable visualization of HCV RNA with this construct, we decided to fuse MS2 coat protein to the mCherry fluorescent protein. The choice of mCherry as the fluorescent reporter protein was made to allow co-localisation studies with lipid droplets (BODIPY 493 / 503) and TCM- or GFP-tagged NS5A in previously described Jc1 derivatives (Eyre et al., 2014a).

To achieve stable expression of the MS2.Coat-mCherry fusion protein in Huh-7.5 cells, we first generated a lentiviral vector that could be used to produce lentiviral particles for transduction of Huh-7.5 cells (see Chapter 2.2.8.2 for detailed protocol). PCR amplification of the MS2 coat protein sequence using customized primers (see Table 4.1) and the plasmid pBS L30 YFP RfC 3'tk (kindly supplied by S. Boireau (IGMM, Montpellier, France)) enabled addition of *BamHI* and *NheI* restriction sites at the extremity of the RNA-binding protein sequence (respectively on 5' and 3' end) and deletion of the stop codon. The MS2 coat protein sequence used (Bertrand et al., 1998)

| Primer name | Primer sequence (5’ to 3’) | Length |
|---|---|---|
| MS2 FP1 | 5’- CCTgg atcca ccATG GCTTC TAACT TTACT CAGTT CGTTC TC-3’ | 42 nts |
| MS2 RP1 | 5’- acatg ctagc gaGTA GATGC CGGAG TTTGC TGCG -3’ | 34 nts |

**Table 4.1: Primers used for pL6[MS2.Coat-mCherry].**
Primers used to amplify MS2 Coat protein coding sequence from pBS L30 YFP RfC 3’tk and add *BamHI* and *Nhei* restriction sites at the amplicon extremities for subsequent cloning into pL6[mCherry].

is a mutant deficient in self-assembly (Lim and Peabody, 1994) (deletion of the multi-merisation signal) to avoid aggregation of the protein. After purification, the amplicon was then cloned into a lentiviral expression vector (pLenti6/V5 Directional TOPO®, Invitrogen, Life Technologies) in frame with the mCherry fluorescent protein sequence using the two restriction sites (*BamHI* and *NheI*) previously inserted. This new plasmid named pL6[MS2.Coat-mCherry] thus carries MS2.Coat protein sequence fused in frame with the mCherry sequence.

The second step of the cell line generation was the packaging of the fusion reporter protein sequence into lentiviral particles to allow transduction of Huh-7.5 cells and selection of Huh-7.5 cells into which the MS2Coat mCherry expression cassette has stably integrated. Simultaneous transfection of pL6[MS2.Coat-mCherry], and two described plasmids for production of lentiviral particles (psPAX2, a packaging vector (Addgene plasmid # 12260 ) and pMD2.G, an envelope vector (Addgene plasmid # 12259)) (Didier Trono (Laboratory of Virology and Genetics, Ecole Polytechnique Fédérale de Lausanne,Switzerland)) was performed to initiate production of the lentivirus. Transfection was performed in 293T cells using FuGENE 6 (Promega) and equal amount of each plasmid. Transfection was performed in parallel for pL6[mCherry]. In Figure 4.1, immunofluorescent images A and B illustrate the mCherry fluorescence expressed in 293T cells following transfection (for pL6[mCherry] and pL6[MS2.Coat-mCherry] respectively) during lentiviral particles packaging.

Media from transfected 293T cells (pL6[mCherry] and pL6[MS2.Coat-mCherry]) were used to infect naïve Huh-7.5 cells (See chapter 2.2.8.2). Stable insertion of the transgene cassette was then selected with Blasticidin starting 3 days after infection to generate polyclonal stable cell lines. The mCherry fluorescence expressed by the

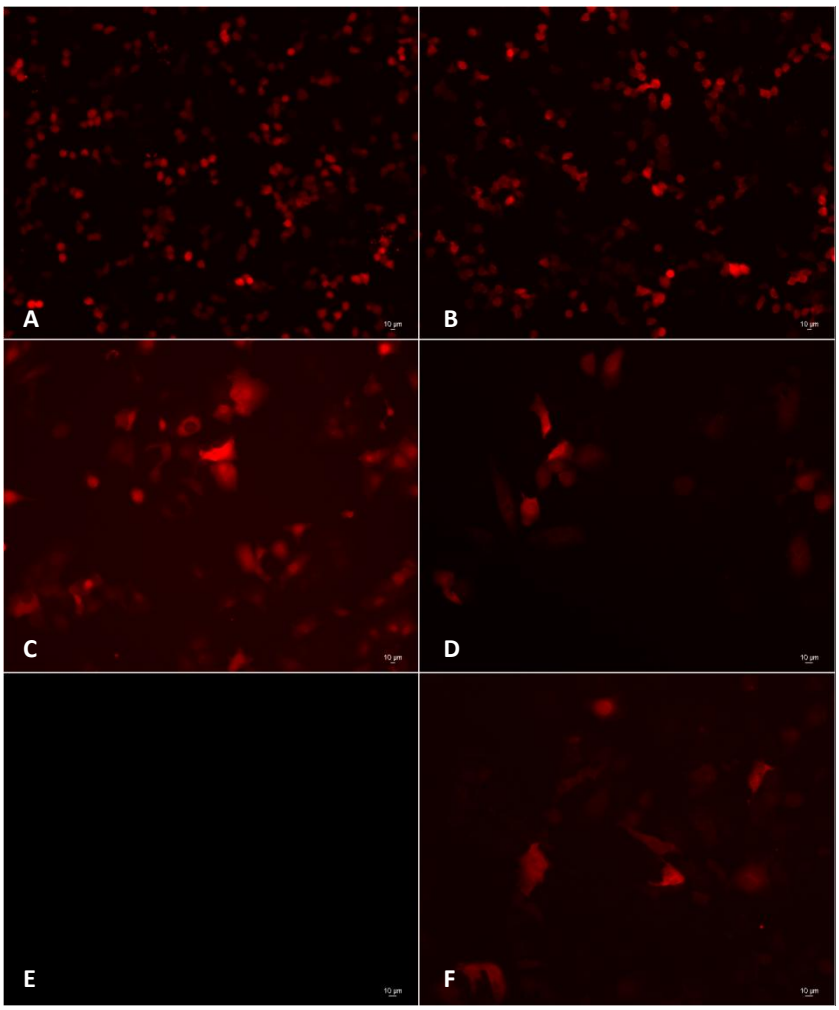


**Figure 4.1: Generation of Huh-7.5 cell lines expressing MS2.Coat-mCherry.**

(A and B) Transient expression of pL6(mCherry) (A) and pL6(MS2.Coat-mCherry) (B) in 293T cells during lentiviral packaging. (C, D and F) Representative fluorescence after 10 days of selection post lentivirus infection for (C) Huh-7.5 cells stably expressing mCherry and (D and F) Huh-7.5 cells stably expressing MS2.Coat-mCherry. (E) Huh-7.5 cells negative control.

different cell lines is illustrated in Figure 4.1, approximately 10 days post blasticidin selection. We were successful in generating stable cell lines expressing either mCherry alone (Fig 4.1C) or MS2-mCherry (Fig 4.1D & F). In comparison non-expressing Huh-7.5 cells are presented in panel E. Cell lines were maintained as polyclonal lines to maintain the diversity of Huh-7.5 cells and to maintain cells with a range of transgene expression levels.

Expression of the proteins by the respective cell lines was also verified by Western blotting using an antibody specific for mCherry. In Figure 4.2, results are presented in which the band for the Huh-7.5 cell line expressing mCherry alone (left lane) has an approximate molecular weight of 29 kDa that is consistent with that of mCherry. In contrast Huh-7.5 cells expressing MS2.Coat-mCherry fusion protein (middle lane) gave rise to a band with a molecular weight of approximately 42 kDa that is consistent with the predicted mCherry MS2 fusion protein at 42.5kDa. In comparison, naïve Huh-7.5 cells do not express anything recognised by the mCherry antibody (right lane) as expected. Collectively these results confirm expression of the MS2mCherry fusion protein in the Huh-7.5 cell line.

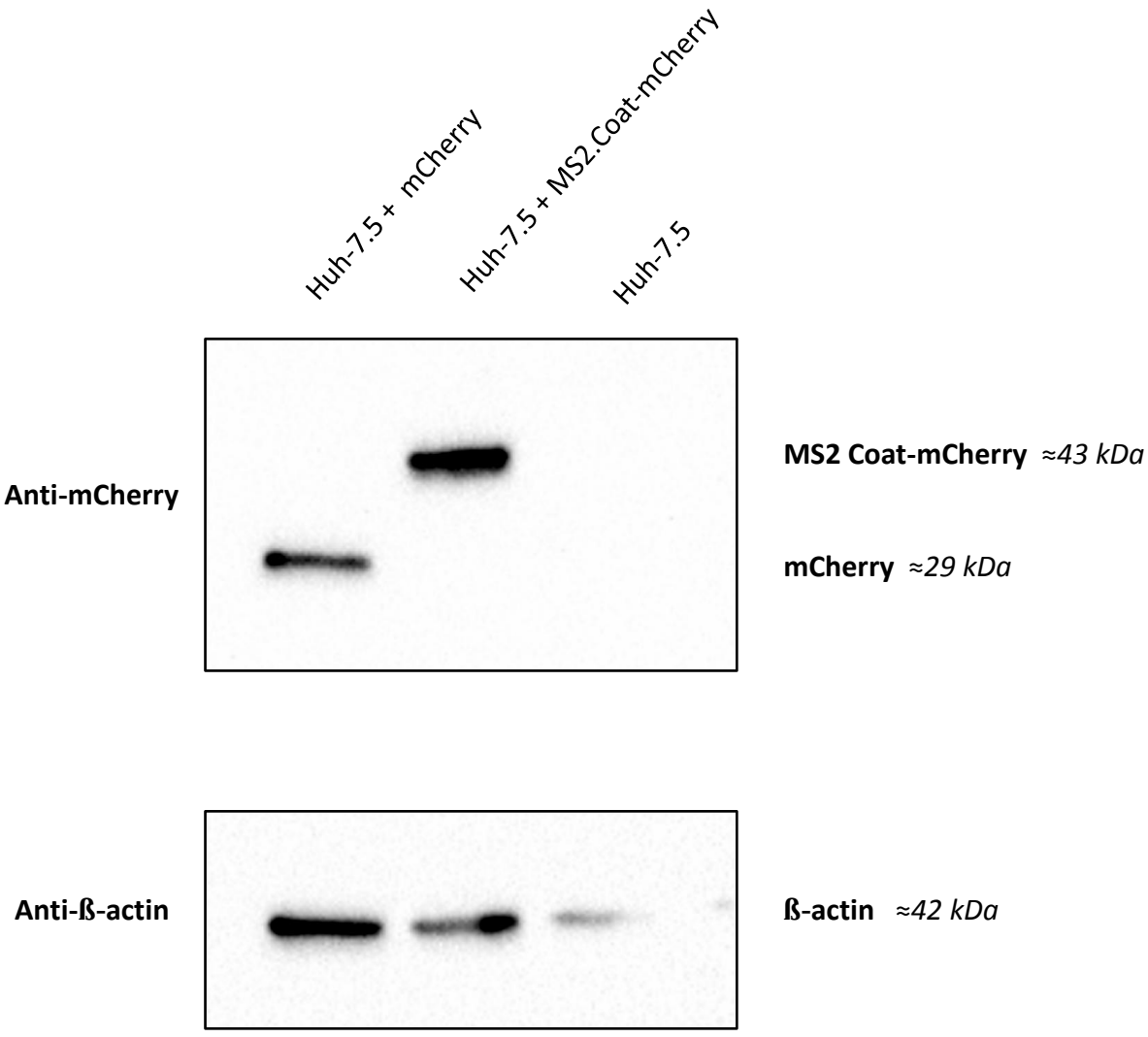


**Figure 4.2: Detection of mCherry and MS2.Coat-mCherry expression through Western blotting in the stable cell lines produced.**
Polyclonal cell lines produced were tested for expression of mCherry. In the case of Huh-7.5 cells expressing MS2 Coat-mCherry, the bands detected appear at a predicted molecular weight (≈43 kDa) characteristic of the fusion of mCherry with the MS2 bacteriophage Coat protein.

### 4.2.2 Expression of MS2.Coat-mCherry does not affect the susceptibility of cells to HCV (Jc1) infection.

Over-expression of intracellular proteins can affect the biology of the cell. Moreover, the MS2 coat protein is an active element during the MS2 bacteriophage life cycle as it acts as both a translational repressor controlling the viral replicase synthesis and as the main structural element of the MS2 viral particle (Bernardi and Spahr, 1972; Fouts et al., 1997). Expression of the MS2 coat protein has been reported in a number of cells lines with no deleterious effects, however the impact of its stable expression in Huh-7.5 cells is unknown and it is possible that it could potentially induce secondary effects in these cells not previously reported. Furthermore, the binding of the MS2 coat protein to HCV RNA (containing the MS2 stem loops) may be deleterious to HCV RNA replication.

We did not observe any significant changes in cellular morphology or growth rates of Huh-7.5 cells expressing MS2.Coat-mCherry protein when compared to mCherry alone indicating that the MS2 protein had no major impact on cell viability. Furthermore these cells could be serially passaged with no loss of mCherry expression. Next we sought to assess the suceptibility of these cells to HCV infection despite over-expression of the fusion protein MS2.Coat-mCherry. We compared the replication fitness of the HCV Jc1 in different Huh-7.5 cells lines: the original parent Huh-7.5 cell line, the Huh-7.5 cell line expressing MS2.Coat-mCherry and the Huh-7.5 cell line expressing mCherry alone. Cells were electroporated with *in vitro* transcribed HCV Jc1 RNA and returned to culture for 3 days (see Chapter 2.4.2.1 for methods) after which culture supernatants were sampled (0.45 μm filtered) and a focus forming assay performed using Huh-7.5 cells. In Figure 4.3 is presented the relative infectivity of

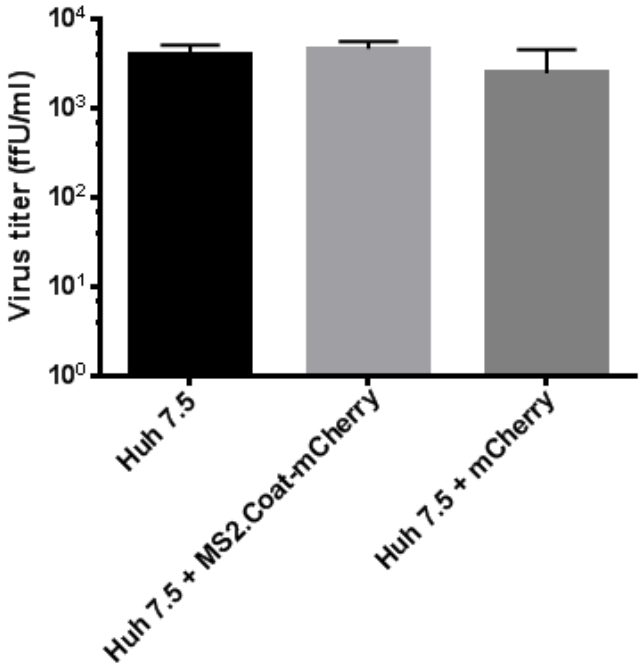


**Figure 4.3: Over-expression of MS2.Coat-mCherry does not alter the susceptibility of Huh-7.5 cells to HCV Jc1 infection.**
Focus forming assay comparing the relative infectivity of HCV Jc1 with respect to stable expression of MS2.Coat-mCherry or mCherry by Huh-7.5. Parametric unpaired Student's t-test (n=3) indicates that none of the groups were significantly different from each other.

HCV Jc1 isolated from the different Huh-7.5 cell lines. Interestingly the presence of mCherry or MS2-mCherry has no impact on the replication capacity of HCV Jc1 and thus these lines present a suitable model to visualise the traffic of HCV RNA during a productive infection.

### 4.2.3 MS2.Coat – mCherry fluorescent fusion protein binds to HCV RNA containing MS2 stem loops

Binding of MS2 coat protein to the MS2 bacteriophage stem loop represents a high affinity interaction and has been used with a range of different experimental models including MLV (Basyuk et al., 2003), HIV-1 (Boireau et al., 2007; Jouvenet et al., 2008; Maiuri et al., 2011) and TBEV (an HCV related Flavivirus) (Albornoz et al., 2014; Miorin et al., 2008; Miorin et al., 2013). However, the use of this system in the context of the HCV life cycle to visualize sites of active replication is a new application.

The complex architecture of HCV induced single, double and multi-membrane vesicles termed the membranous web (see Chapter 1.2.6 for a detailed description) form an intricate network of membranes where the replication complexes are harboured and where the RNA is synthesised. Moreover, it is thought that replication complexes have only a limited exposure to the cytoplasm and it is hypothesised that this shields the virus to prevent triggering an immune response by the host cell. It was hypothesised that this compartmentalisation of the HCV replication complex may limit accessibility of viral RNA to the MS2 coat protein. Therefore we investigated if it was possible for the MS2 coat protein to physically interact with the HCV containing the MS2 stem loop structures.

In order to demonstrate binding of MS2.Coat-mCherry reporter protein to HCV RNA during viral replication, we adapted a published protocol of immunoprecipitation of mRNA-protein complexes (Peritz et al., 2006; Zielinski et al., 2006). Using this technique the putative RNA binding protein is immunoprecipitated from the sample, RNA is extracted and reverse transcription is performed before PCR amplification of the gene of interest. The presence of an amplicon indicates the binding between the protein and the RNA. A detailed procedure is presented in Chapter 2.1.20. Huh-7.5 cells expressing MS2.Coat-mCherry were electroporated with T7 IVT HCV RNA from Jc1/5A-GFP+3'UTR:24xMS2, parent Jc1/5A-GFP and a replication deficient HCV genome Jc1 (GND) and returned to culture for 3 days. Handling in RNAse-free conditions, a total protein extract was collected using ice cold polysome lysis buffer (NP40 based lysis buffer containing RNAse inhibitors – described in Appendix I). Extracts were then homogenised and cellular debris were cleared by centrifugation. Lysates were then incubated with pre-cleared A/G agarose beads to remove any non specific association. Finally, after clearing the samples of these beads, lysates were then incubated with anti-mCherry antibody. Precipitation of the anti-mCherry antibody and the associated protein was achieved by addition of pre-cleared A/G agarose beads. After extraction of the beads, subsequent washes were performed to eliminate any non specific binding to RNA. Washed beads were then directly resuspended in Trizol (Life Technologies) and RNA extraction was performed as previously described (see Chapter 2.1.10). Finally, cDNA was prepared as described in Chapter 2.1.12.2, followed by amplification of the HCV genome spanning the non-structural viral proteins (NS2 to NS5B fragment - 6kb) (see section 2.1.15) to visualize the presence of bound near-full-length RNA at the time of extraction. We were successful in recovering RNA and generating a PCR amplicon of the correct size from Huh-7.5 cells electroporated with

Jc1/5A-GFP+3'UTR:24xMS2 (Figure 4.4). No PCR amplicon was detected for both control Jc1 (GND) and Jc1/5A-GFP indicating the specificity of the reaction to genomes containing MS2 stem loops. These results indicate that during viral replication the MS2.Coat-mCherry fusion protein can specifically bind to HCV viral RNA that contains MS2 stem loop repeats.

### 4.2.4 MS2.Coat – mCherry fluorescent fusion protein does not interfere with HCV replication

The active regulatory role of the MS2 coat protein in the MS2 viral life cycle involves binding of MS2 RNA stem loops with a relatively strong affinity. Furthermore it was considered that the relatively high number of repeats of these stem loops in the untranslated region of our tagged genomes could interfere with the HCV life cycle. Therefore possible effects of expression of the MS2.Coat-mCherry fluorescent protein on replication of HCV genomes carrying repeats of MS2 stem loops were investigated using a sub-genomic HCV replicon carrying the MS2 stem loops and a *Renilla* luciferase gene to allow for simple quantification of HCV replication.

*Renilla* luciferase activity of the sub-genomic HCV genomes carrying 6, 8, 12 and 24 repeats of the MS2 stem loops (respectively named SGR/5A-TCM+3'UTR:MS2x6/ x8/ x12/ x24 and described in Section 3.2) was monitored in Huh-7.5 cells stably expressing MS2.Coat-mCherry at days 3 and 4 post-electroporation. Variation between transfection efficiency was normalised to luciferase activity 3 hours post electroporation that represents luciferase activity from input RNA. In Figure 4.5 (A), the four replicon constructs carrying MS2 stem loop insertions (6-24) were compared to a replication-defective HCV genome (GDD > GND mutation in the NS5B RdRp)

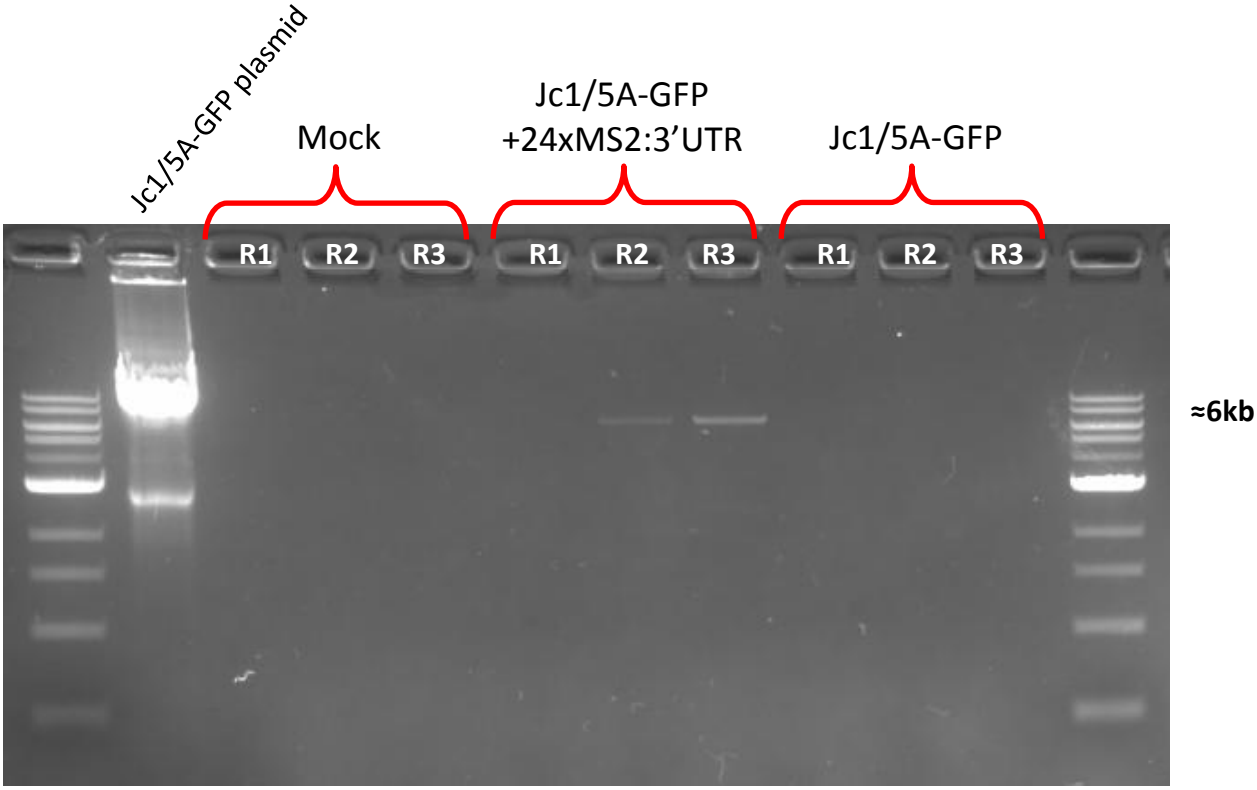


**Figure 4.4: Association of MS2 stem loop-tagged HCV RNA with MS2.Coat-mCherry as determined by immunoprecipitation and RT-PCR.** Following electroporation of Huh-7.5+MS2.Coat-mCherry cells with the indicated HCV RNA transcript in triplicate (R1, R2 and R3) and culture for 3 days, cell lysates were processed for mCherry immunoprecipitation, RNA was extracted and cDNA prepared. RT-PCR was then performed using primers specific for the NS3-5B coding region. Plasmid DNA for pJc1/5A-GFP served as a positive control template for NS3-5B PCR. As can be seen, bands of the expected size (≈6kb) were only detected in Jc1/5A-GFP+3'UTR:24xMS2 samples.

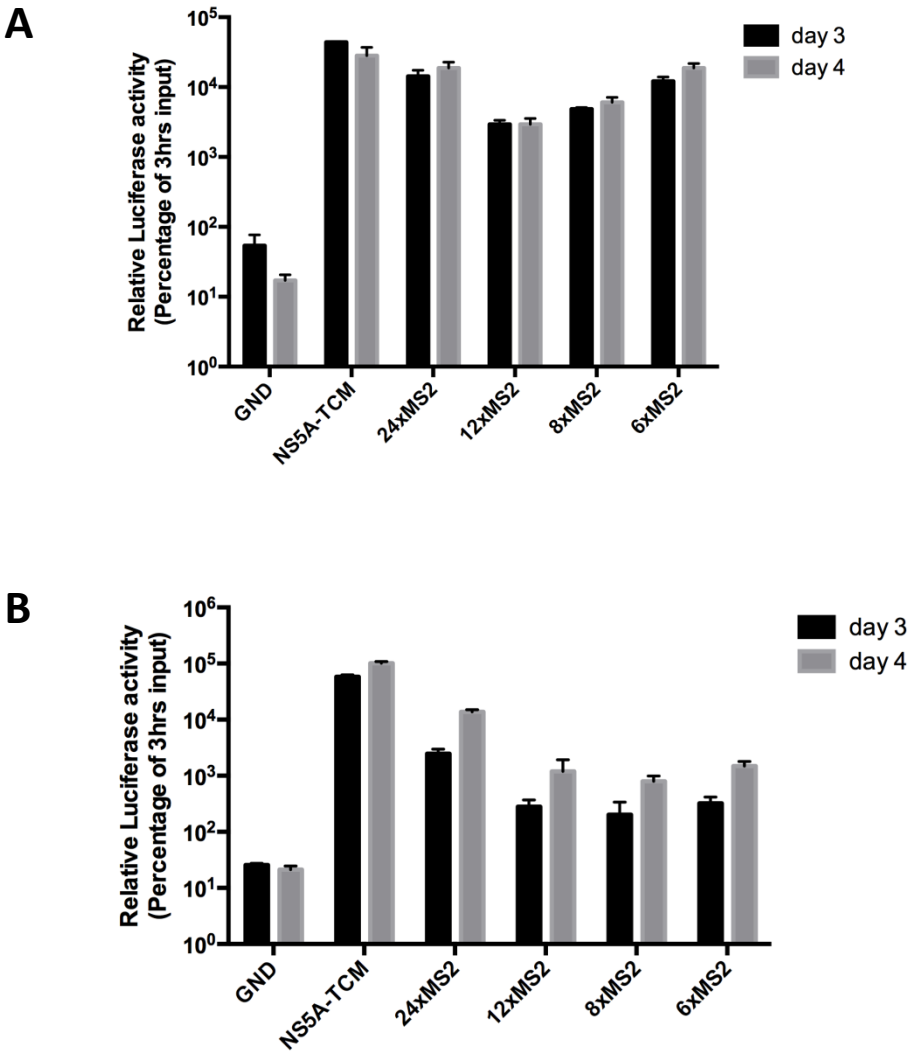


**Figure 4.5: Stable expression of MS2.Coat-mCherry in Huh-7.5 cells does not impair replication of the SGR/5A-TCM+3'UTR:MS2 sub-genomic replicons.**

HCV RNA-encoded *Renilla* luciferase activity was compared between the sub-genomic replicons carrying MS2 stem loop arrays (6 /8 /12 /24 repeats) and SGR/5A-TCM and SGR.GND (replication deficient mutant) controls in Huh-7.5 cells expressing MS2.Coat-mCherry (A) or mCherry (B). Data show luciferase activity of the different constructs after 72 and 96 hours, normalised to an early time point at 3hrs. Results indicate that MS2.Coat-mCherry does not impair HCV RNA replication despite binding to the RNA.

(Krieger et al., 2001) and the parent replicon without stem loop insertions (SGR/5A-TCM). A parallel experiment was conducted in Huh-7.5 cells expressing mCherry alone as a control (Figure 4.5 (B)).

Results show that replication of SGR/5A-TCM+3'UTR:MS2 genomes is generally not impaired in the background of the stable expression of MS2.Coat-mCherry fusion protein despite the binding of MS2 coat to the HCV viral RNA. Furthermore if the binding of the MS2 coat protein to the HCV viral RNA had an effect on replication (negative or positive), we would expect for it to logically correlate to the number of loops inserted. Therefore the genomes carrying more repeats would be expected to display greater effects than HCV genomes carrying fewer loops. However this effect was not observed as the relative levels of activity of each replicon was similar to those observed in Huh-7.5 (Figure 3.5) and Huh-7.5 stably expressing mCherry alone (Figure 4.5 (B)). This indicates that the binding of the MS2 coat protein to the HCV RNA does not have a direct effect on the replication of these genomes. This now establishes that the MS2 coat system for the detection of RNA can be used to study HCV RNA localisation during active viral RNA replication.

## 4.3 NS5A as a marker for HCV replication

As previously discussed most of the HCV non-structural proteins and a number of host factors have been described to be localised within the HCV replication complex and as such are often considered to be markers of active sites of HCV replication. The HCV NS5A protein is one of the most widely accepted markers of replication complexes. Using a specific antibody that detects dsRNA, co-labelled NS5A was found to co-localise with dsRNA in infected cells (Targett-Adams et al., 2008). Similarly NS5A has been shown to co-localise with nascent RNA in fixed cells harbouring replication of a Con1 replicon (Moradpour et al., 2004). These observations together with the fact that NS5A has a predicted RNA binding motif (Tellinghuisen et al., 2005) and binds HCV RNA *in vitro* (Foster et al., 2010) have designated NS5A as a strong marker for HCV replication complexes. However the above mentioned studies have all examined NS5A localisation in fixed samples. Work from our laboratory and others has shown that in live imaging experiments in which the NS5A protein has been tagged with either a TCM or GFP tag, NS5A is predominantly enriched in both small structures that can be observed to traffic sporadically throughout the cytoplasm and in larger relatively static structures that were predominantly located around the nucleus (Eyre et al., 2014a; Wolk et al., 2008). Nevertheless, it was unclear if one or both pools of NS5A represent active replication complexes and/or sites of delivery of HCV RNA. A significant aim of this thesis was to determine if one or both pools of NS5A contain HCV RNA that may shed light on the function on these distinct pools of NS5A.

### 4.3.1 TCM insertion into NS5A enables its imaging with minimal impact on viral fitness.

To characterise HCV replication complexes in live cells, we investigated visualization of the associated protein NS5A. The HCV construct Jc1/5A-TCM developed in our laboratory enabled visualization of NS5A during a fully productive infection (Eyre et al., 2014a). As described in Chapter 3, this Jc1 chimera was the precursor to the development of Jc1/5A-TCM+3'UTR:MS2 genomes.

Insertion of the optimised tetracysteine motif (TCM) (Hoffmann et al., 2010) within the Domain III of NS5A coding sequence enabled Jc1/5A-TCM to maintain replication levels comparable to the wild type parent HCV Jc1 chimera. In Figure 4.6, we quantified intracellular levels of HCV RNA (showed as percentage of the wild type Jc1 level) through qRT-PCR at days 1, 2, 3 and 4 after electroporation. Comparison between the wild type parent HCV Jc1, Jc1/5A-TCM and Jc1(GND) a replication-defective negative control (GDD > GND mutation in the NS5B RdRp) (Krieger et al., 2001) illustrate the minimal impact of the TCM insertion on viral fitness. Results were further confirmed through infectivity assay as published in (Eyre et al., 2014a). These results suggest that insertion of a TCM within domain III of NS5A has little impact on HCV replication and assembly.

The specificity and reliability of labelling of tetracysteine motifs with membrane permeable biarsenical fluorescent dyes such as FlAsH-EDT (green) or ReAsH-EDT (red) has been extensively characterised (Hoffmann et al., 2010). Usage of such tagging techniques in the context of the study of HCV viral life cycle has emerged as a powerful tool to visualize HCV core and NS5A protein traffic in a productive infection (Coller et al., 2012; Counihan et al., 2011; Eyre et al., 2014a).

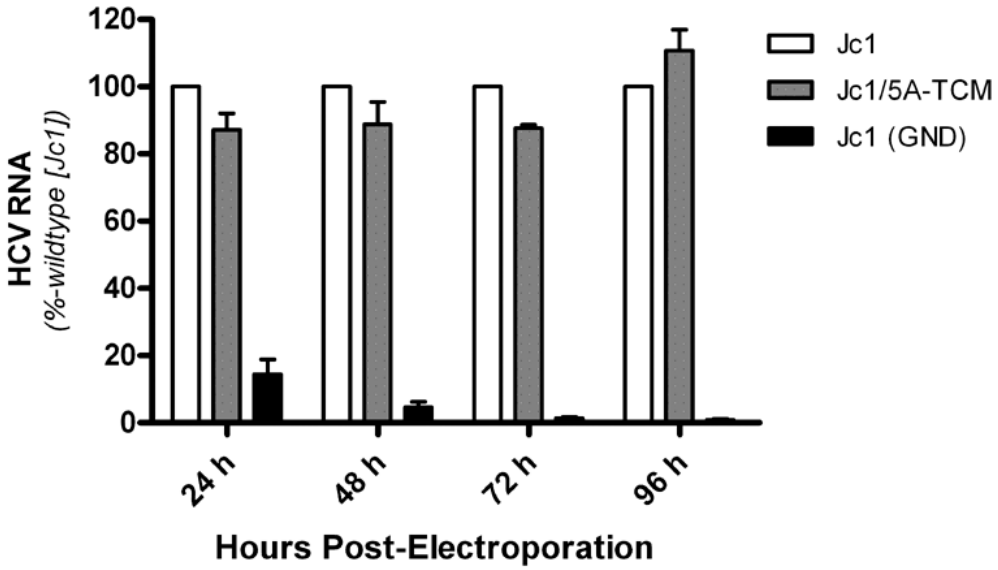


**Figure 4.6: Intracellular HCV RNA levels** (Eyre et al., 2014).
Real time RT-PCR was performed to compare intracellular HCV RNA levels. Data were normalized to *RPLPO* mRNA levels and expressed as a percentage of those of WT Jc1 (n=3). No statistically significant difference in intracellular HCV RNA levels was observed between Jc1- and Jc1/5A-TCM-infected cells at any time-point ($P > 0.05$; unpaired Student's t-test).

We initially wished to determine the specificity of NS5A labelling with FlAsH in the context of HCV viral replication. This was achieved by electroporating Huh-7.5 cells with Jc1/5A-TCM *in vitro* transcribed RNA after which cultures were cultured for 3 days to allow establishment of HCV replication. Thereafter, cells were labelled with FlAsH (green) (see Chapter 2.6.2 for complete protocol), then processed for immunofluorescence labelling using anti-NS5A antibody (9E10 antibody) and finally visualized using a Nikon TiE inverted microscope (Figure 4.7). Fluorescence from both FlAsH (green) and anti-NS5A (red) overlapped extensively with minimal background indicating the high specificity of the TCM NS5A labelling.

One concern in any procedure that manipulates live cultures is the issue of cellular toxicity. The toxicity of reagents involved in the FlAsH and/or ReAsH labelling process (especially the washing steps) has raised some concerns. Although toxicity has previously been observed in isolated cells by us and others (Hoffmann et al., 2010), the majority of the cell population remained apparently healthy and produced comparable levels of infectious virus compared to mock-labelled cells in the 24h following labelling (not shown). Moreover previous studies have shown that numerous cell signalling pathways, cellular functions, proteins synthesis and normal cell division are unaffected by labelling with FlAsH and/or ReAsH (Hoffmann et al., 2010).

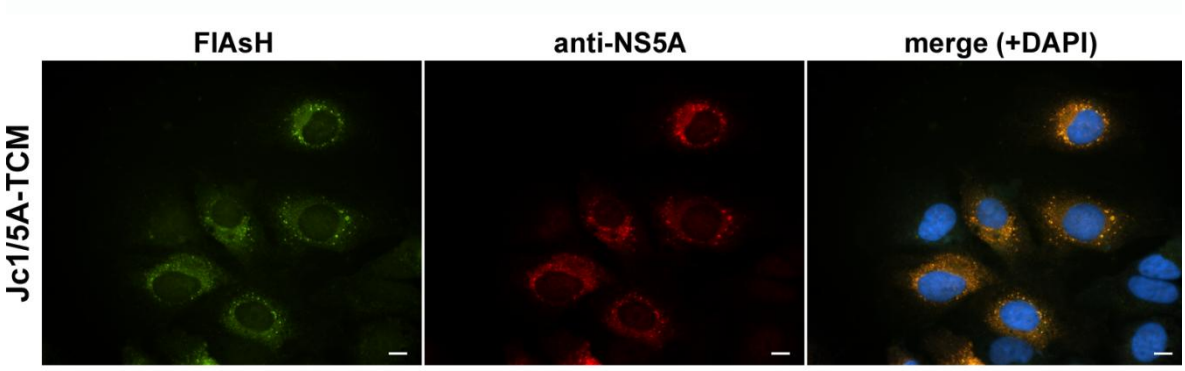


**Figure 4.7: Specificity of tetracysteine-tagged NS5A protein labelling with biarsenical dye FlAsH-EDT** (Eyre et al., 2014).
Jc1/5A-TCM electroporated Huh-7.5 cells were labelled with FlAsH-EDT (green) 3 days post-electroporation, then fixed and processed for indirect immunofluorescence labelling using anti-NS5A antibody (red). Merged images show colocalization (yellow) and DAPI-stained nuclei (blue).

### 4.3.2 Localisation and traffic of NS5A in living cells during a productive infection.

We next examined the localization and traffic of NS5A in living cells during a productive HCV infection. Visualization of NS5A viral protein was achieved using FlAsH labelling (green fluorescence) in Huh-7.5 cells harbouring replication of Jc1/5A-TCM. Cells were electroporated with IVT RNA for HCV Jc1/5A-TCM. Cells were labelled with the biarsenical dye FlAsH (See Chapter 2.6.2 for detailed procedure) 24 hours after electroporation and then returned to culture overnight before visualization by fluorescence microscopy. Images were collected every 3 seconds for 3 minutes, then assembled to reconstitute a movie using the NIS-Element imaging software (Figure 4.8 - Movie 4.1). These studies revealed that NS5A is localised to both relatively static and highly motile foci in the cytoplasm of infected cells as previously described (Eyre et al., 2014a)

FlAsH-labeled NS5A-TCM was predominantly found in large, relatively static structures and smaller highly motile structures that shuttle throughout the cytoplasm in a sporadic manner. Their movement appeared directional and they could often be observed to traffic back along the same path. The inset from Movie 4.1 (also presented in Figure 4.8) illustrates an example of the movement of this type of structure. The fast moving structure presented can be observed to travel in a directional manner over 20 μm in under 30 sec.

In a recent study from our laboratory, FlAsH labelled mobile NS5A-TCM positive structures were manually tracked during their movement throughout the cytoplasm 3 days after electroporation with IVT RNA for HCV Jc1/5A-TCM (Eyre et al., 2014a). Recording the path of these small motile structures (Figure 4.9) revealed displacement characterised by strong accelerations with velocities in the order of 1 μm/s in a directional manner, sometimes moving backward along the exact same path.

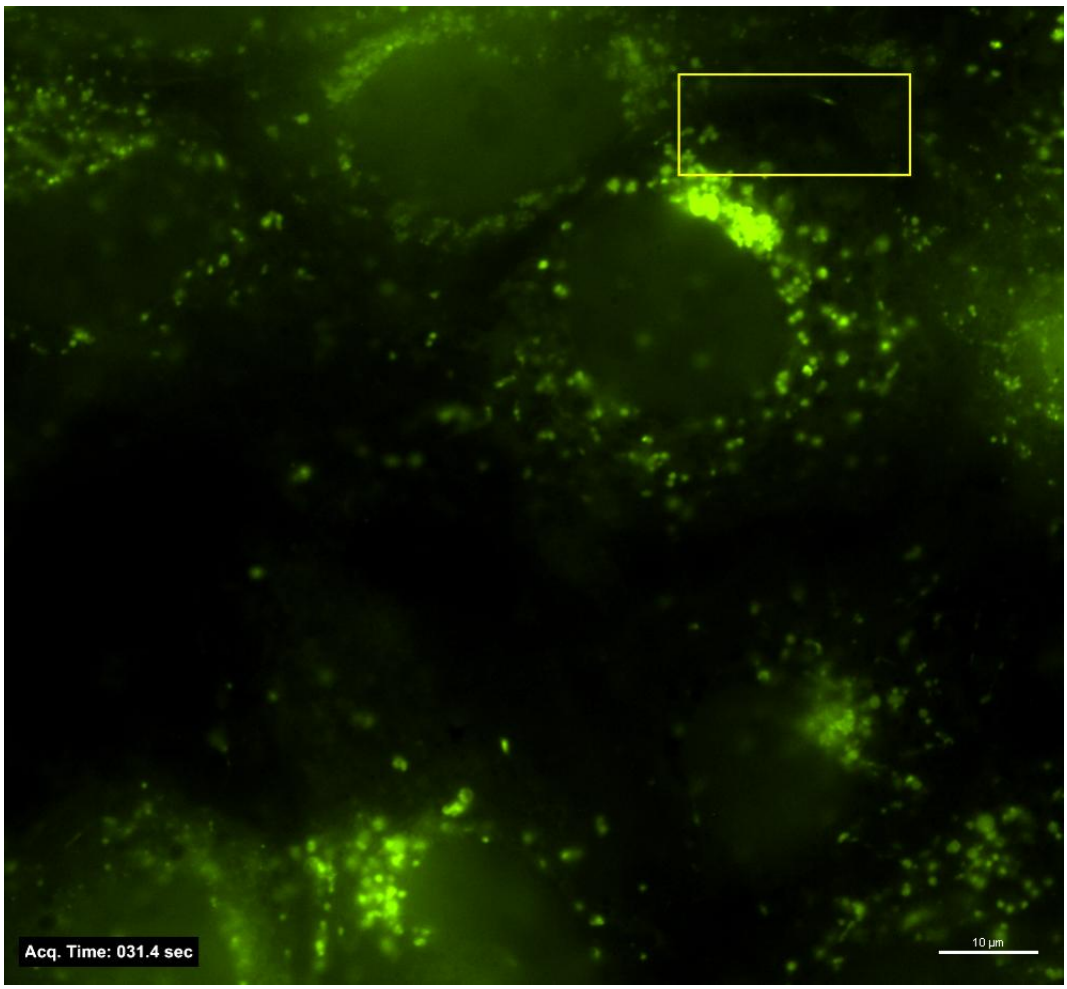


**Inset**

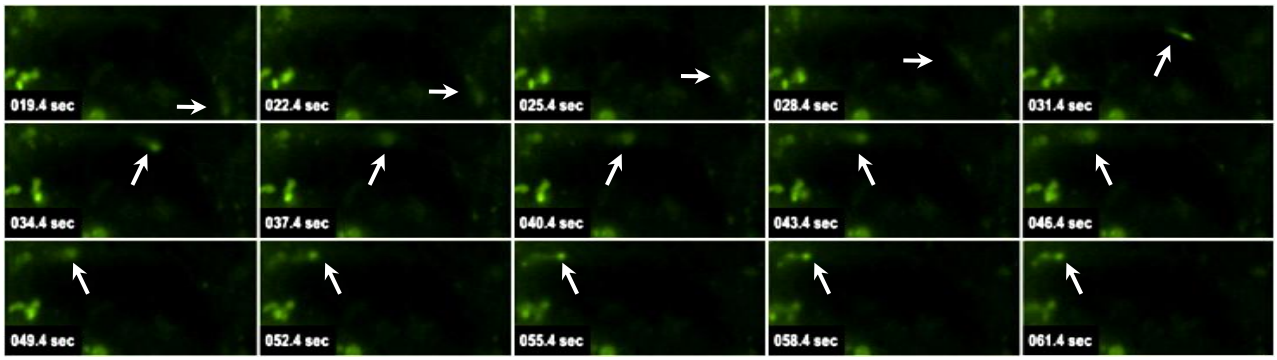


**Figure 4.8: FlAsH labelled NS5A-TCM traffic in living cells (movie 4.1).**
Jc1/5A-TCM electroporated Huh-7.5 cells were labelled with FlAsH (green) 24 hours post-electroporation, returned to culture overnight and visualized by time-lapse wide-field fluorescence microscopy. Images were collected every 3 seconds for 3 minutes.

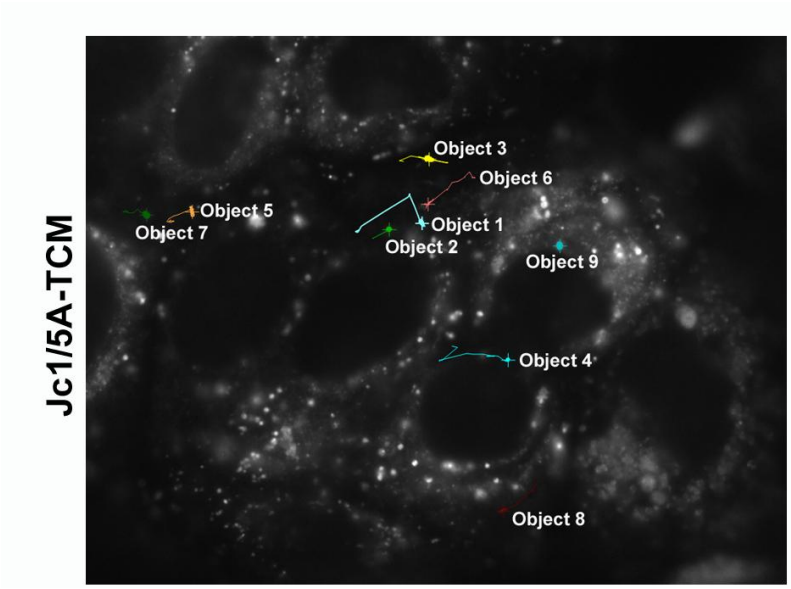


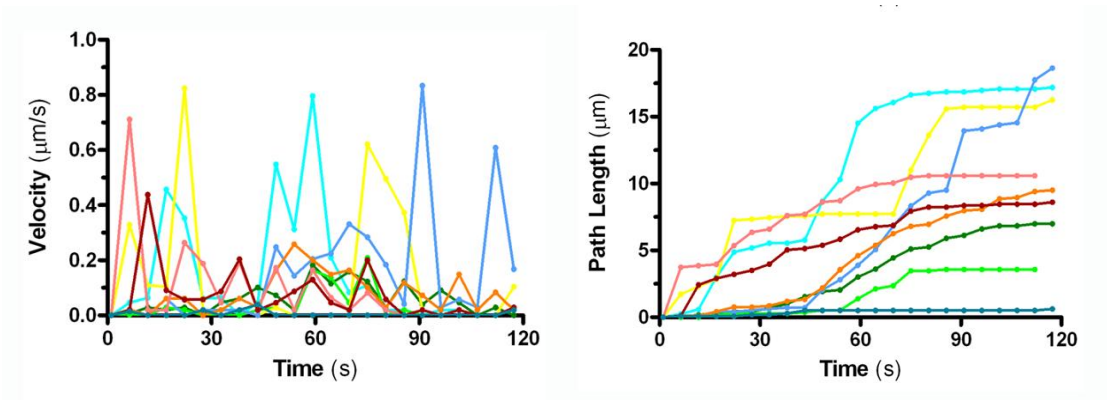


**Figure 4.9: NS5A-positive motile structures traffic analysis** (Eyre et al., 2014).

Huh-7.5 cells were electroporated with Jc1/5A-TCM and labelled with FlAsH 48hrs after. Traffic of small motile NS5A-positive structures was then visualized 3 days after electroporation by time-lapse wide-field fluorescence microscopy. Images were collected every 5.3 seconds for 2 minutes.

Manual tracking analysis (NIS Elements software) revealed that small fluorescent RNA structures traffic sporadically throughout the cytoplasm at speeds of up to 1 µm / s and over 5 to 20 µm in 2 minutes

Furthermore using the microtubule depolymerisation agent Nocodazole and inhibitors of microtubule motor protein dynein, studies by Dr Eyre demonstrated that the MT network and the associated motor protein dynein were involved in long range NS5A traffic and critical to HCV replication cycle (Eyre et al., 2014a).

On the other hand, the relatively static structures varied greatly in size. Live cell imaging analysis revealed that these structures often appeared to be formed of multiple smaller units clustered together. Moreover, these structures do not appear to be fully inert and small motile structures can be observed to travel towards and transiently interact with them. More interestingly, movement within these static structures can be distinguished. The structures units and sub-units display confined movement, as might be expected if their movement was restricted by their anchoring within a membranous network. Although predominantly found in the perinuclear region of the cells harbouring HCV replication, these structures can also be identified in the periphery of the cytoplasm near the plasma membrane.

Acquired following the same experimental methodology as above, Movie 4.2 (Figure 4.10) illustrates the traffic of another set of NS5A foci within cells labelled this time 48 hours after electroporation. In this example larger static structures are less represented, however static structures can still be observed towards the plasma membrane. Inset 3 especially depicts numerous small and highly motile structures while some static structures composed of only few subunits can also be observed.

The main advantage of the TCM tagging approach is that the amino acid motif that constitutes the TCM is small (FLNCCPGCCMEP) in contrast to relatively large more conventional tags such as GFP. However, several HCV replicons have been described in which the NS5A protein contains a GFP insertion within domain III and remains

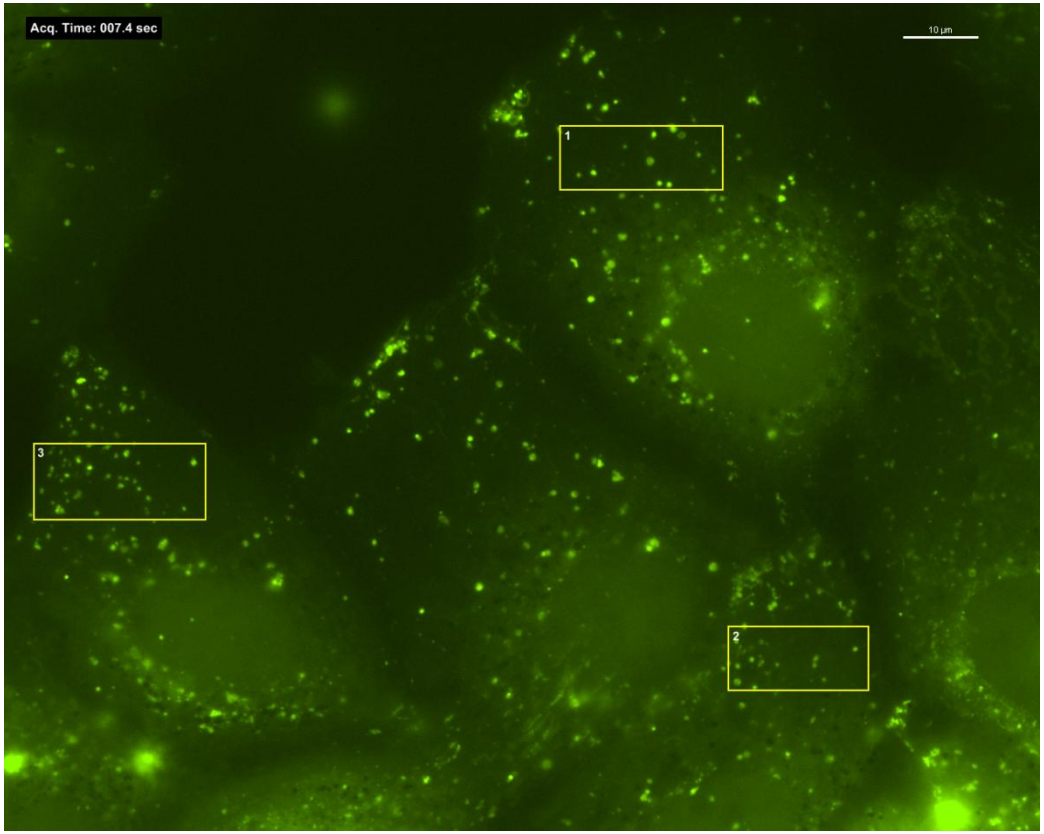


**Inset 1**

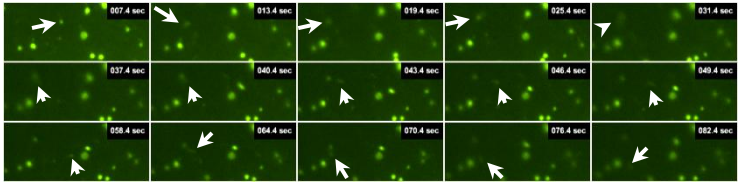


**Inset 2**

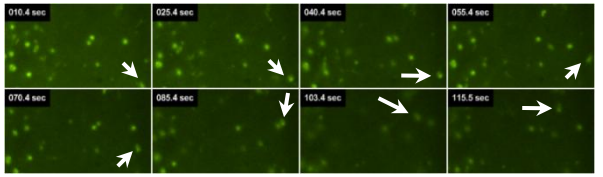


**Inset 3**

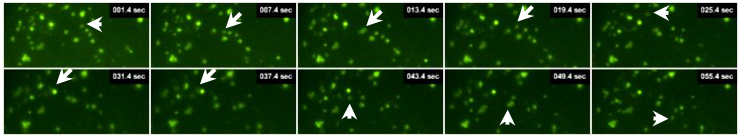


**Figure 4.10: FlAsH labelled NS5A-TCM traffic in living cells (Movie 4.2).**
Jc1/5A-TCM electroporated Huh-7.5 cells were labelled with FlAsH (green) 2 days post-electroporation, returned to culture overnight and visualized by time-lapse wide-field fluorescence microscopy. Images were collected every 3 seconds for 3 minutes.

replication competent (Moradpour et al., 2004; Wolk et al., 2008). Furthermore a chimeric HCV genome based on Jc1 carrying the GFP coding sequence within NS5A (Schaller et al., 2007) and an adaptive mutation [K1402Q] to enhance virus production in Huh-7.5 cells has also been described (Reiss et al., 2011). An analogous genome termed Jc1/5A-GFP[K1402Q] was also previously developed and characterised by our laboratory (Eyre et al., 2014a). Jc1/5A-GFP[K1402Q] is infectious although it displays slightly delayed kinetics of infectious virus production (Eyre et al., 2014a).

The advantage of this GFP-tagged HCV genome is that visualization of NS5A protein via detection of GFP does not require any labelling procedures. After electroporation with IVT RNA for Jc1/5A-5A-GFP[K1402Q], Huh-7.5 cells were then returned to culture for 3 days, after which visualization by fluorescence microscopy of NS5A was performed with images were collected every 3 seconds for 47 sec. Results are presented in the Movie 4.3 and Figure 4.11. Although these cells harbour a considerable larger amount of large static structure in their cytoplasm and especially around the nucleus, the behaviour of both small highly motile and static large structures were comparable to the one previously reported and described. Nevertheless both inserts illustrate examples of motile NS5A positive structures travelling towards large and static structure where they pause.

In summary, two different sub-types of NS5A-positive structures can be differentiated with respect to their mobility: one remaining relatively static while the second travel throughout the cytoplasm via the MT network. Based on previous studies, the large static structures may represent the RCs while the roles of the smaller motile ones remain unknown.

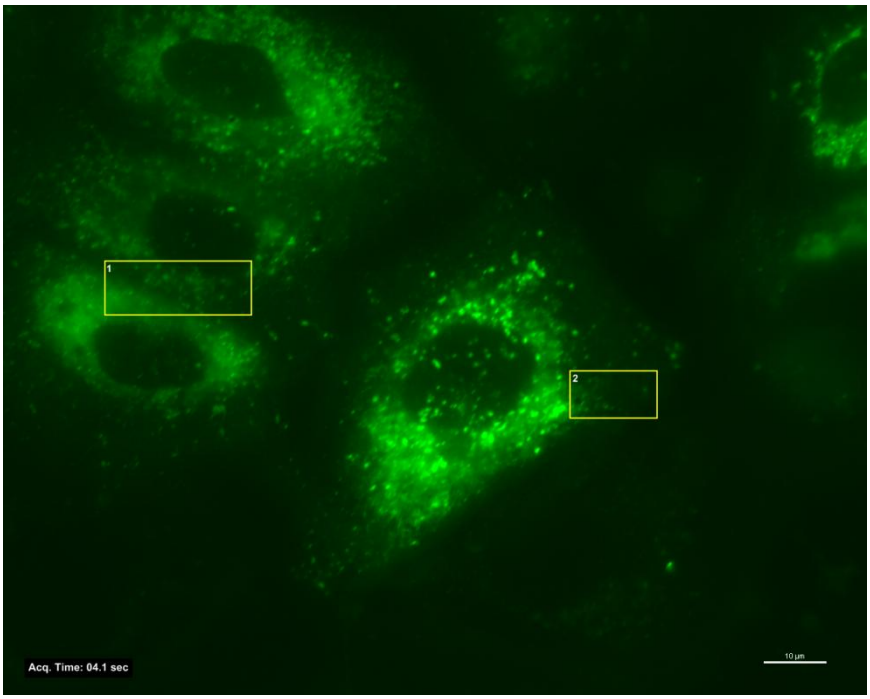


**Inset 1**

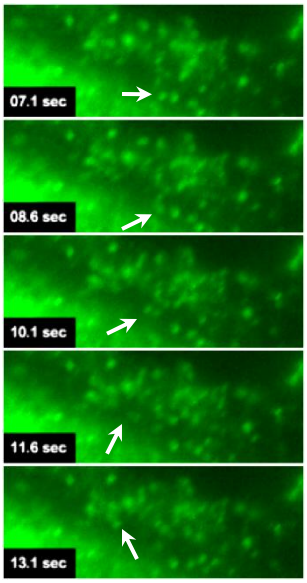


**Inset 2**

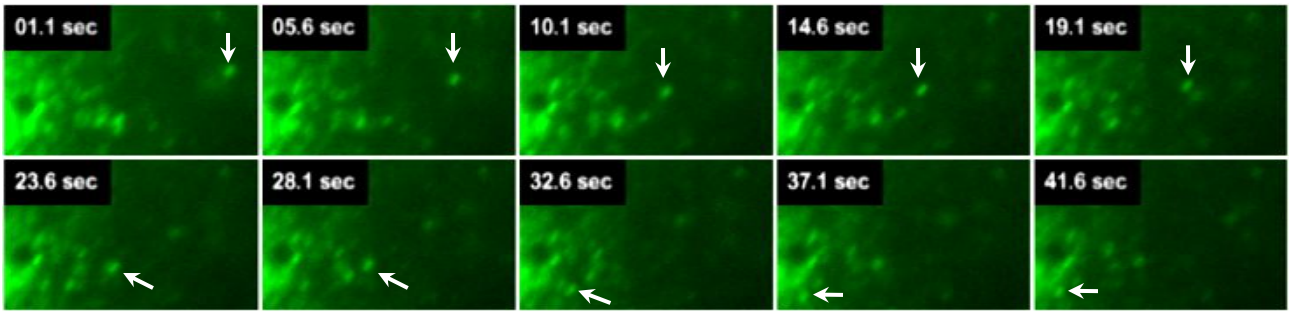


**Figure 4.11 : NS5A GFP traffic in living cells (Movie 4.3).**
Jc1/5A-GFP electroporated Huh-7.5 cells were visualized by time-lapse wide-field fluorescence microscopy 3 days post-electroporation. Images were collected every 3 seconds for 47 sec.

## 4.4 HCV RNA imaging in live cells

Visualization of RNA through the use of the MS2 system has been used to show reliable RNA detection in living cells. After first starting with the observation of overexpressed mRNA in living cells (Bertrand et al., 1998; Fusco et al., 2003; Shav-Tal et al., 2004a; Shav-Tal et al., 2004b), the technique has now developed so that viral research models can be engineered to allow visualization of viral RNA localisation and traffic in real-time. For instance, most recently the system has successfully been used in HIV research to investigate viral RNA biogenesis as well as the viral transcription cycle using an HIV vector carrying 24 repeats of MS2 stem loops which was able to produce viral mRNA after integration in the cell genome (Boireau et al., 2007). Furthermore application of the system towards study of TBEV, a flavivirus related to HCV, has enabled visualization of the replication compartments associated with ER membrane reorganisation (Miorin et al., 2008; Miorin et al., 2013). In the absence of the MS2 stem loops the fluorescent reporter MS2 coat protein circulates freely within the the cytoplasm and exhibits a homogenous cellular distribution. However in the presence of an RNA carrying MS2 stem loops there is concentration of the MS2 coat protein and hence fluorescence localised at RNA enriched sites. This intensification of the fluorescence signal allows for visualization of the RNA foci.

### 4.4.1 Redistribution of mCherry fluorescence

Having established the necessary tools to investigate HCV RNA localisation we next investigated the effect of the replication of an HCV genome carrying the MS2 stem loops on the diffuse fluorescence pattern observed within the Huh-7.5 cell line stably expressing MS2.Coat-mCherry by fluorescence microscopy. These cells were electroporated with IVT RNA of Jc1/5A-TCM+3'UTR:24xMS2, the parent HCV genome Jc1/5A-TCM and Jc1 (GND) a replication-defective (GDD > GND mutation in NS5B). Cells were returned to culture for 3 days after which they were observed under live cell imaging conditions using a wide-field fluorescence microscope as previously described.

As illustrated in Figure 4.12, there was striking reorganisation of the MS2 coat mCherry with the presence of distinct cytoplasmic foci of intense red fluorescence in cells harbouring replication of the HCV genome Jc1/5A-TCM+3'UTR:24xMS2. These foci were predominantly (but not exclusively) located in a perinuclear region. Furthermore the size of the foci varied greatly such that a distinction between two subsets of foci could be made based on size. On one hand large fluorescent structures varying in size were densely located around the nucleus although occasionally found in the periphery of the cytoplasm towards the cell membrane (Figure 4.12 [arrow]). Interestingly the perinuclear region has been observed in previous studies to harbour the active site of HCV replication complexes (Ferraris et al., 2010; Romero-Brey et al., 2012). On the other hand, smaller punctate foci were generally observed spread throughout the cytoplasm (Figure 4.12 [arrowheads]). Furthermore these punctate foci also displayed sporadic movement throughout the cell that will be described in the following sections. Most importantly, specific foci were not observed following

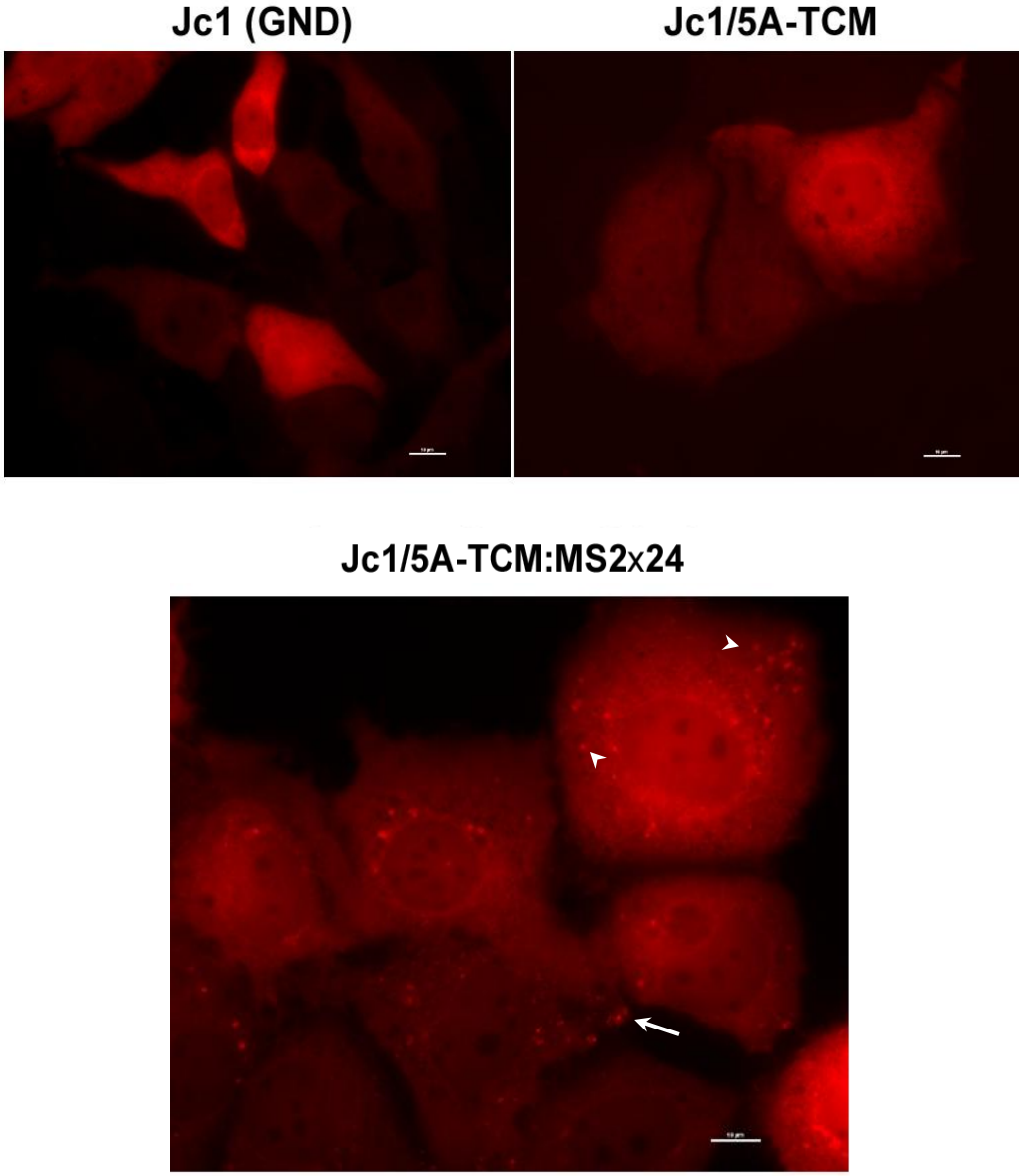


**Figure 4.12: Jc1/5A-TCM+24xMS2:3'UTR replication in Huh-7.5+ MS2.Coat-mCherry cells induces a specific reorganisation of mCherry fluorescence to cytoplasmic foci.**

Live cell imaging of MS2coat-mCherry distribution in Huh-7.5 cells that stably express MS2coat-mCherry and were electroporated with the indicated HCV transcripts. Cells were observed using a wide-field fluorescence microscope 3 days after electroporation. Re-distribution of MS2coat-mCherry diffuse fluorescence to cytoplasmic foci was only evident in cells that were electroporated with Jc1/5A-TCM+3'UTR:24xMS2 transcripts**.**

electroporation with Jc1/5A-TCM or Jc1(GND) indicating the specificity of the MS2 coat protein for Jc1/5A-TCM+3'UTR:24xMS2.

In contrast to other published reports, we noted that not all of the MS2.Coat-mCherry signal was relocating to specific puncta within the cell, resulting in a low level of background fluorescence. It has been described that low levels of expression of the MS2 coat fluorescent reporter protein together with adequate levels of expression the RNA of interest are crucial to the reliable usage of this experimental technique (Park et al., 2010). Indeed over-expression of the MS2 coat fluorescent reporter can induce aggregation as a fluorescent complex. This type of fluorescent artefact was occasionally observed in those cells with very high expression and was easily distinguished from the foci of RNA due to their larger spherical shape and absence of movement.

### 4.4.2 HCV RNA traffic

Having observed fluorescence redistribution in the presence of MS2coat mCherry and HCV replication in still images we next investigated the traffic of viral RNA in the context of the viral life cycle. Similar to the previous experimental procedure, Huh-7.5 cells expressing MS2.Coat-mCherry were electroporated with IVT RNA of Jc1/5A-TCM+3'UTR:24xMS2 and returned to culture. Fluorescence microscopy was performed at 2 or 3 days after (as described in the figures legend) using a wide-field fluorescence microscope under live cell imaging (37°C) conditions. Frames were acquired every 3 or 7 sec over the course of 3 mins and subsequently used to reconstitute the movies (and associated figures).

As reported in the previous section, HCV RNA positive structures are predominantly large and perinuclear or small and dispersed. When observed over time, these structures display major differences in their behaviour as illustrated in Movie 4.4 and the associated Figure 4.13. In a strikingly similar fashion to NS5A, HCV RNA is predominantly detected in smaller and often motile structure (depicted in Inset of Movie 4.4 / Figure 4.13) or larger and relatively static structures (Figure 4.13).

As seen in Movie 4.5 and the associated Figure 4.14, the small structures travel sporadically throughout the cytoplasm and do not appear to be restricted to any particular area of the cell. Inset 1 of Movie 4.5 depicts an example of a small structure that travels towards a larger structure and pauses for an extended period of time. In another example from the previous Movie 4.4, small structures can be observed to traffic towards a larger static structure (bottom left of the inset) but instead of stopping bounce back and return towards their origin.

In contrast larger HCV RNA-positive structures are characterized by confined movement within the cytoplasm. In a similar fashion to NS5A this structure type seems to be preferentially located around the nucleus (as illustrated in Movie 4.4/ Figure 4.13) or less frequently can be found further away in the cytoplasm (as illustrated in Movie 4.5/ Figure 4.14). In Movie 4.6/ Figure 4.15, the large static structures occupy a significant portion of the cytoplasm and often appeared composed of an association of smaller sub-units that display confined movement that is not capable of driving net movement of the larger structure within the cell.

Finally, as presented in the Inset of Movie 4.6 / Figure 4.15, rare examples of larger motile structures have been observed. For instance, the motile structures represented in this inset appear to be composed of two or more smaller structures travelling together.

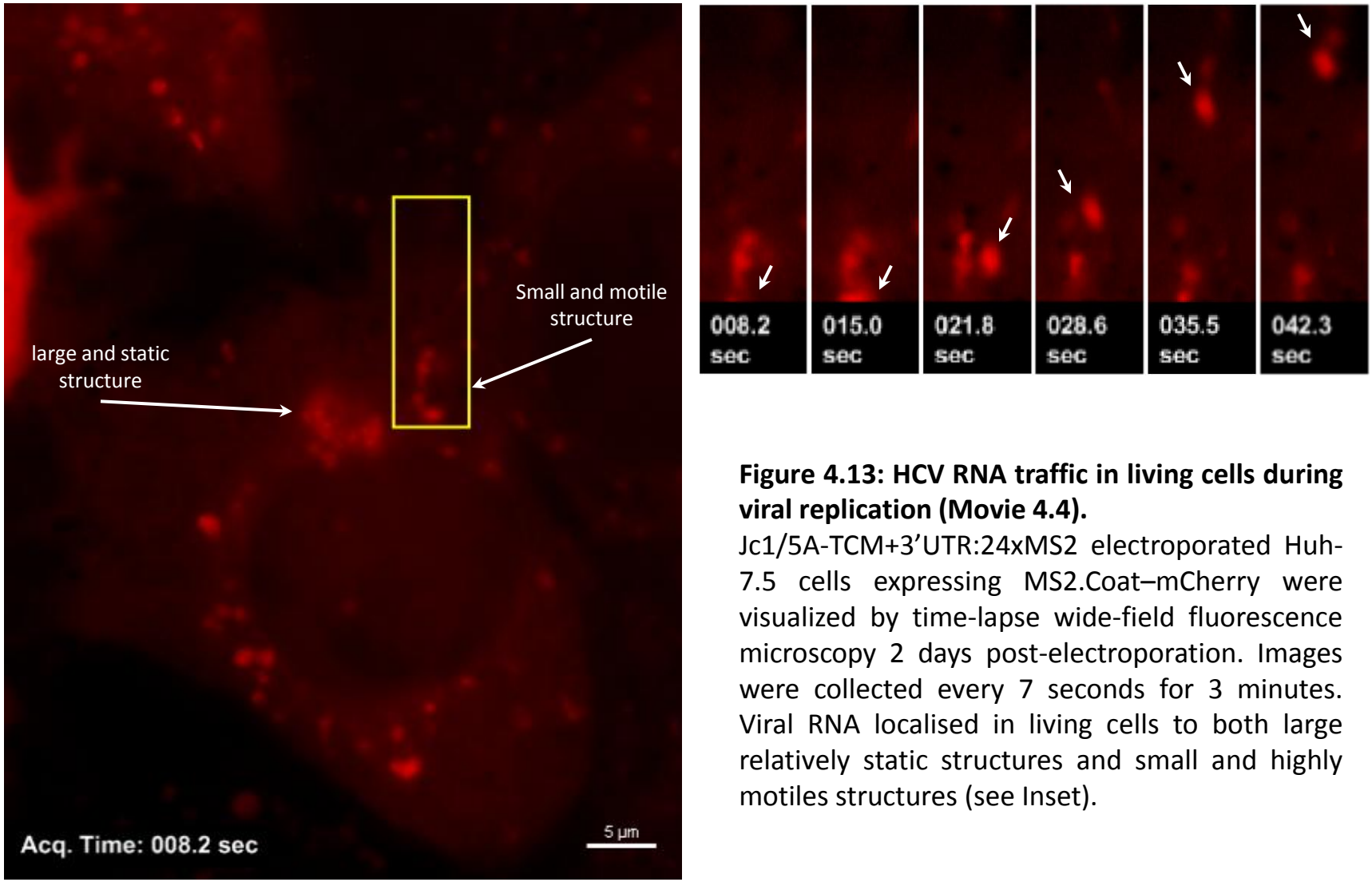


**Figure 4.13: HCV RNA traffic in living cells during viral replication (Movie 4.4).**
Jc1/5A-TCM+3'UTR:24xMS2 electroporated Huh-7.5 cells expressing MS2.Coat–mCherry were visualized by time-lapse wide-field fluorescence microscopy 2 days post-electroporation. Images were collected every 7 seconds for 3 minutes. Viral RNA localised in living cells to both large relatively static structures and small and highly motiles structures (see Inset).

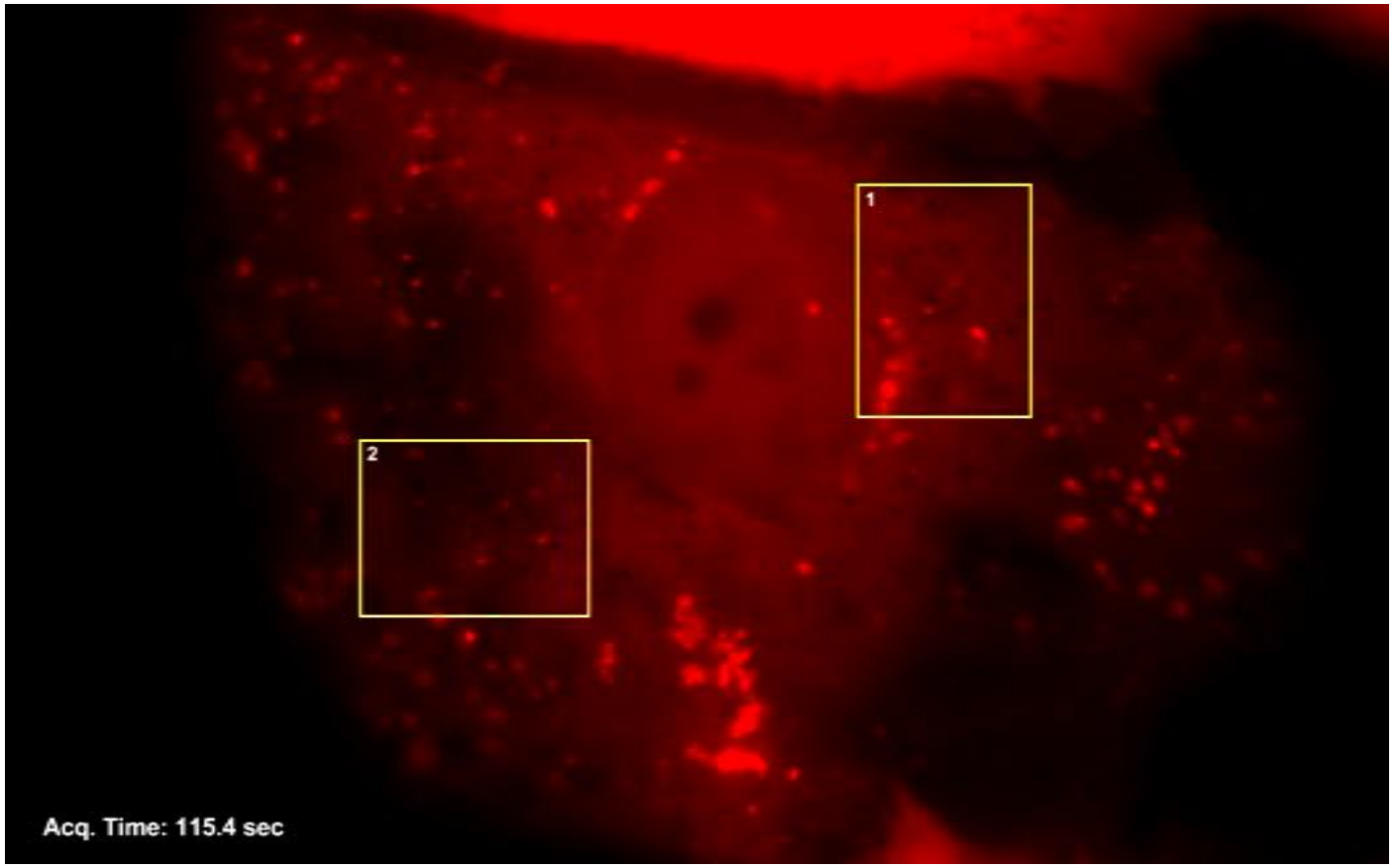


**Figure 4.14: HCV RNA traffic in living cells during viral replication (Movie 4.5).**
Jc1/5A-TCM+3'UTR:24xMS2 electroporated Huh-7.5 cells expressing MS2.Coat–mCherry were visualized by time-lapse wide-field fluorescence microscopy 2 days post-electroporation. Images were collected every 3 seconds for 3 minutes. Viral RNA localises to both large relatively static structures and small and highly motiles structures.

Inset 1

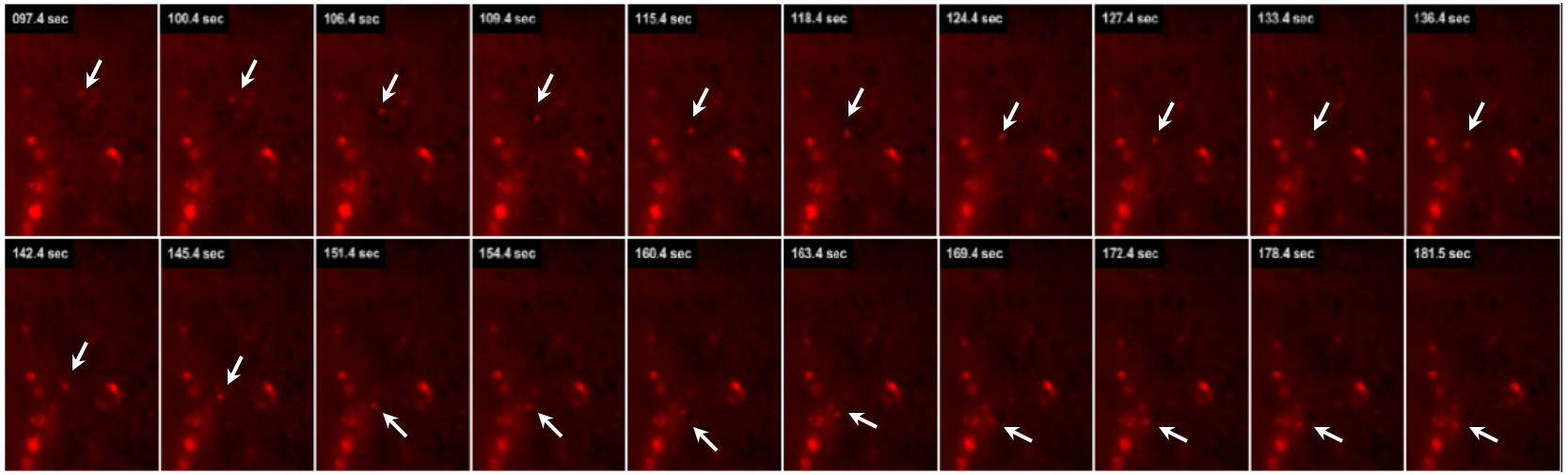


**Figure 4.14 Insets: Inset presenting HCV RNA traffic in living cells during viral replication (Inset from Movie 4.5).**

The time-lapse sequences presented here depict HCV RNA-positive structure traffic from the insets in Figure 4.14. The arrows point at particularly motile structures.

Inset 2

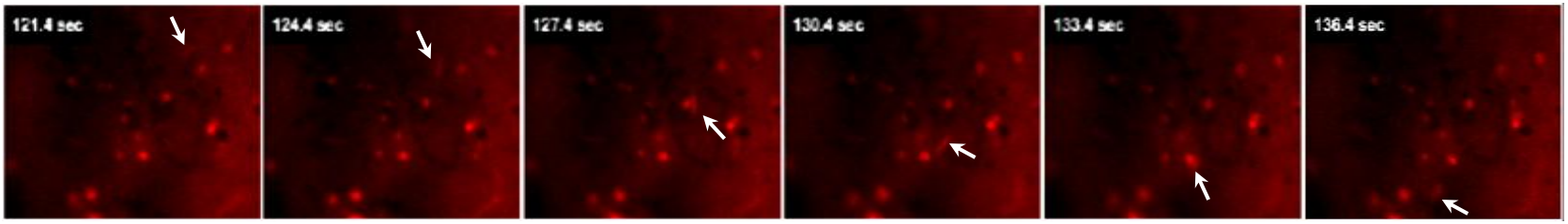

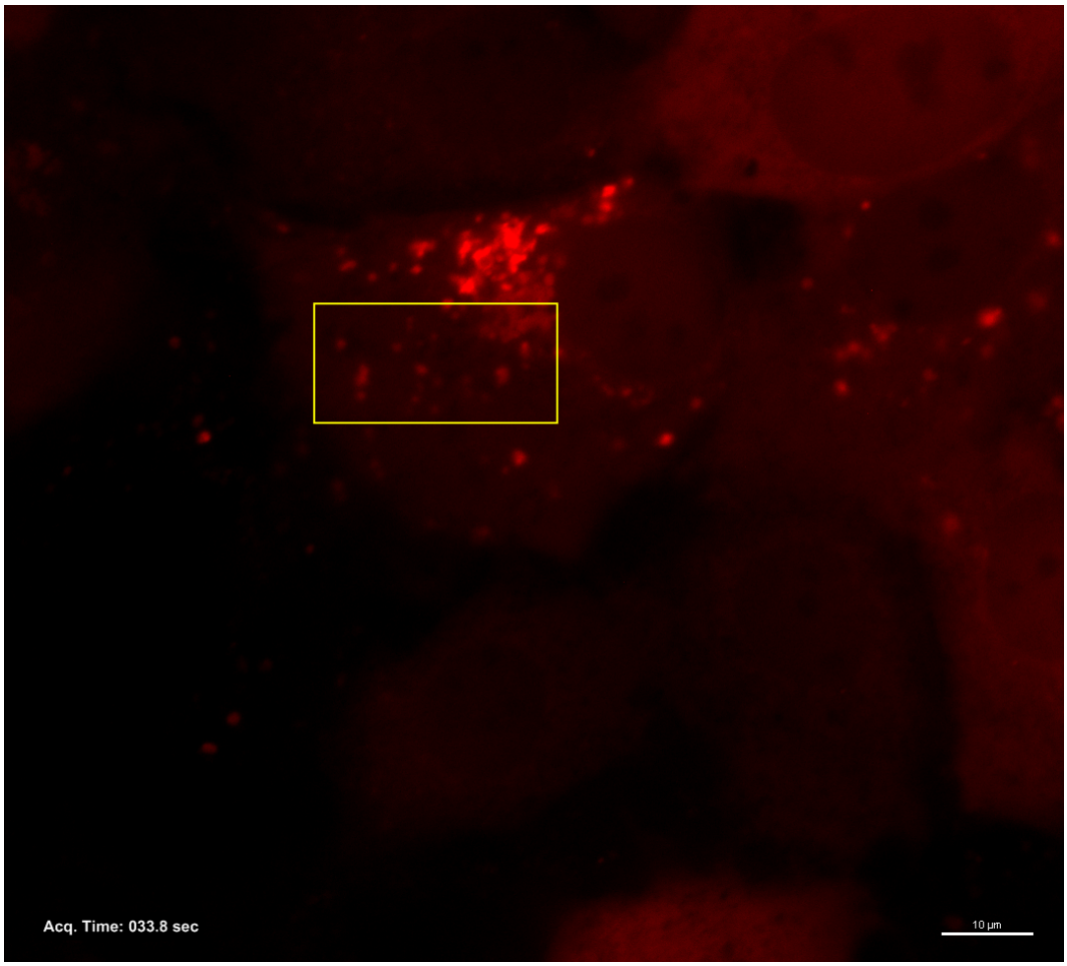


**Inset**

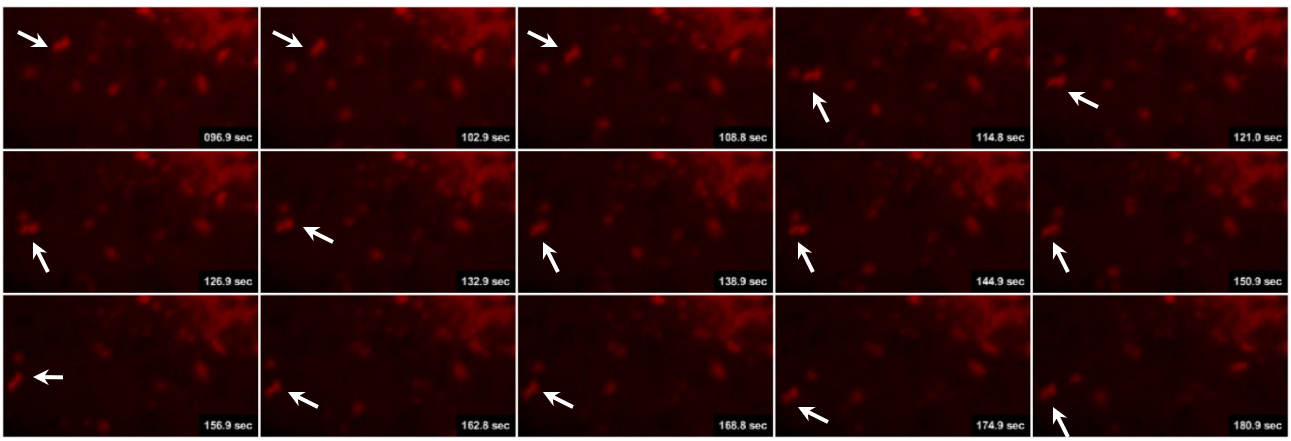


**Figure 4.15: HCV RNA traffic in living cells during viral replication (Movie 4.6).**

Jc1/5A-TCM+3'UTR:24xMS2-electroporated Huh-7.5 cells expressing MS2.Coat–mCherry were visualized by time-lapse wide-field fluorescence microscopy 3 days post-electroporation. Images were collected every 3 seconds for 3 minutes.

Association during travel is relatively rarely observed but an interesting point when related to the spasmodic and confined movement of smaller sub-units within large static structures as described for both HCV RNA and NS5A imaging.

### 4.4.3 Analysis of movement

Manual tracking analysis was performed for a representative sample of small RNA-positive structures from the Movie 4.5. Figure 4.16 presents the paths that these particles trafficked along (A) with their position at the time of snap-shot. Figure 4.16 (C) depicts the path lengths corresponding to these trafficking patterns. The movement adopted by these structures is characterised by the rapid acceleration they display. Figure 4.16 (B) presents the velocity of the different objects recorded over time and illustrates the bursts of speed which are observed.

The analysis revealed that small highly motile structures move sporadically throughout the cytoplasm and display rapid acceleration to reach velocities of up to 1μm/s. Moreover they can travel across large distances (10-30 μm in 3 minutes). These trafficking characteristics are very similar to those of motile NS5A-positive structures (Eyre et al., 2014a). The close similarities between NS5A and RNA during the viral life cycle are striking both in terms of localisation and traffic and in terms of organization. Given the central role of NS5A during replication and assembly and previous demonstration that NS5A binds HCV RNA with high affinity (Foster et al., 2010; Huang et al., 2005), it was considered likely that NS5A and RNA may shuttle jointly throughout the cytoplasm. In the next chapter we investigate this hypothesis by combining TCM labelling of NS5A with the MS2 tagging system to visualize the two RC components at the same time during the HCV life cycle.

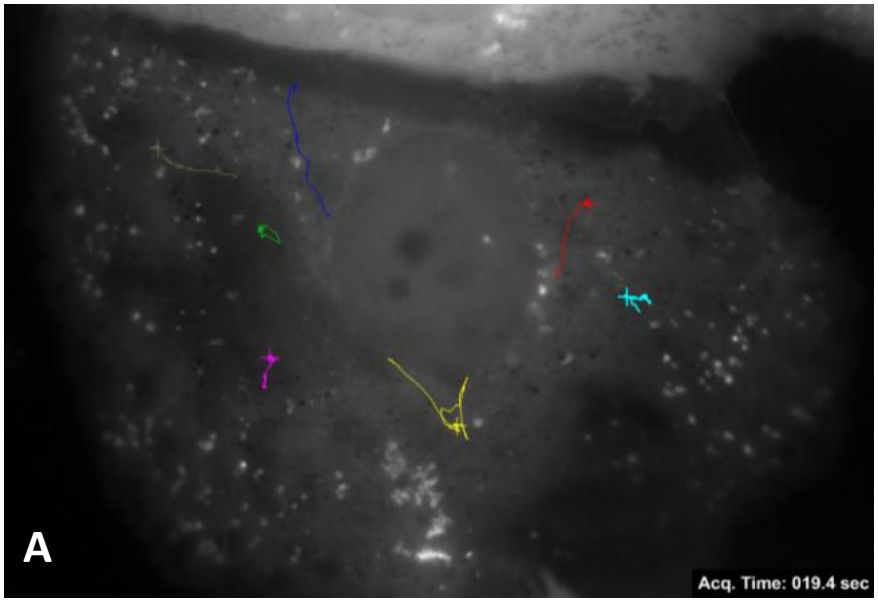


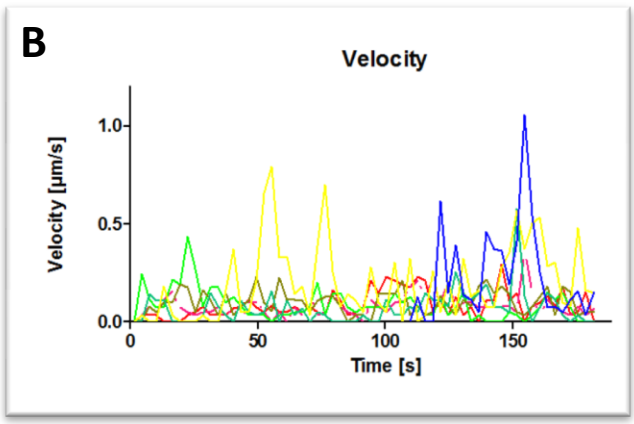


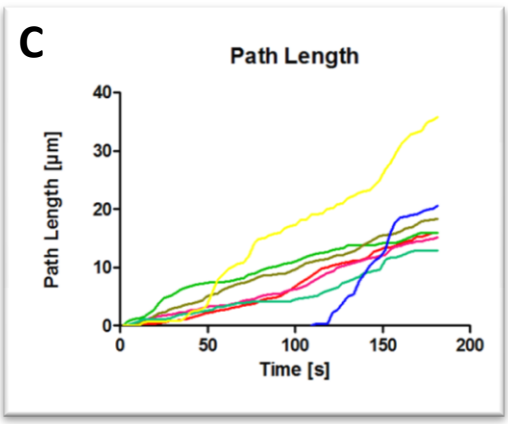


**Figure 4.16: Small and motile RNA structure traffic analysis.**
Traffic of small and motile structures of HCV RNA were visualized 2 days after electroporation of Huh-7.5 cells expressing MS2.Coat–mCherry with Jc1/5A-TCM+3'UTR:MS2x24 by time-lapse wide-field fluorescence microscopy. Each colour represent a single tracked RNA structure. Images were collected every 4 seconds for 3 minutes. Manual tracking analysis (NIS-Elements Advanced Research software) revealed that small fluorescent RNA structures traffic sporadically throughout the cytoplasm at speeds of up to 1 µm / s and over 10 to 30 µm in 3 minutes.

## 4.5 Signal-to-Noise Ratio (SNR) improvement

While we could demonstrate relocalisation of MS2.Coat-mCherry in Huh-7.5 harbouring Jc1/5A-TCM+3'UTR:MS2x24 replication, there was a level of unbound MS2.Coat-mCherry that may confound interpretation of bound fluorescence. According to the results presented in the previous sections, optimal real-time visualization of HCV RNA would require a close equilibrium between the expression of the reporter protein and the MS2-tagged RNA. An inadequate proportion of one in comparison of the other would be expected to limit the sensitivity of RNA detection, as the detection of the signal is limited to the amount of redistributed fluorescence with respect to the amount which is freely diffuse throughout the cytoplasm. In addition as replication of the MS2-tagged viruses is somewhat impaired, detection of the fluorescent signal over the diffuse cytoplasmic fluorescence can be challenging. Considering this we attempted to improve the SNR by selecting clones with lower fluorescence from the existing Huh-7.5-MS2.Coat-mcherry cell line or adding a nuclear localisation signal to MS2 coat reporter fluorescent protein to 'clear' the cytoplasm of the diffuse fluorescence.

### 4.5.1 Flow cytometry

Initially we endeavoured to improve the utility of the polyclonal cell line stably expressing MS2.Coat-mCherry that we generated in Chapter 4.2. Fluorescence levels appeared to be an important factor in our observation of HCV RNA traffic, therefore in an initial attempt to improve the experimental system we sorted the established cells using flow cytometry and selected cell populations with respect to the level of

fluorescence they expressed. Fluorescence-activated cell sorting (FACS) was performed in order to extract from the polyclonal cell line several cell populations characterised by different ranges of intracellular mCherry fluorescence. Using a Beckman Coulter Epics Altra HyperSort coupled with the Expo MultiComp Software version 1.2B (Beckman Coulter, Miami, FL, USA), we sorted cells expressing “low” and “medium” mCherry fluorescence (See Chapter 2.2.9 for more details). Figure 4.17 A represents the experimental distribution of a representative sample of the polyclonal cell line and the gating applied (the two areas designated by C and D respectively demarcate “low” and “medium” levels). Separation of the gates was spaced with a significant gap to improve the visual difference in intracellular fluorescence.

Despite the effort made to obtain clear differences in terms of fluorescence levels with the gating, following return of the sorted cells to culture the differences observed in mCherry expression were limited. Furthermore the two cell lines produced still displayed variability in expression of mCherry as observed in Figure 4.17 B. Indeed, populations sorted as “low” and “medium” contained cells with high levels of fluorescence and also cells without any observable fluorescence. Moreover the limited difference initially observed and the homogeneity of the fluorescence level only grew weaker over time. Therefore, we hypothesized that intracellular levels of diffuse fluorescence could be relatively dependent on each cells stage within the cell cycle, and consequently the fluorescence might be cycling through a range of fluorescence. Similarly analysis of numerous monoclonal cell lines derived from the original polyclonal cell line revealed varying levels of fluorescence within and between cell lines (not shown). As such we abandoned this approach to isolate cells for optimal MS2.Coat-mCherry expression and decided to generate another cell line model where

**A**

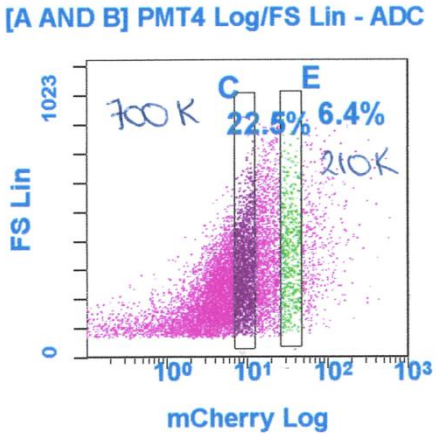


[A AND B] PMT4 Log/FS Lin

| Region | Number | %Total | %Gated | X-Mean | Y-Mean |
|---|---|---|---|---|---|
| C | 2252 | 17.58 | 22.52 | 9.4 | 296.6 |
| E | 644 | 5.03 | 6.44 | 34.6 | 358.9 |

**B**

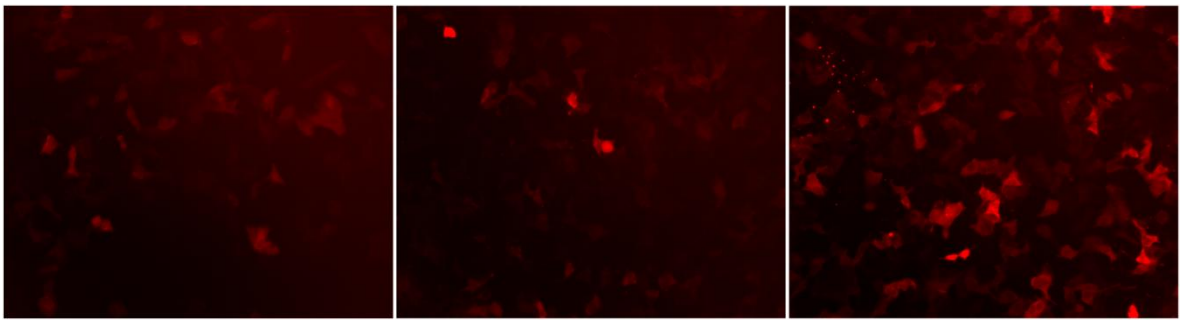

Not sorted | Low Fluorescence | Mid-Fluorescence

**Figure 4.17: FACS sorting of Huh 7.5 + MS2.Coat-mCherry cells.**

A. Sorting gate used to extract cell of different fluorescence level (panel C – low intensity of fluorescence, panel E – medium intensity of fluorescence).

B. Fluorescence images of the sorted cell lines.

the fluorescence was not diffuse in the uninfected state but instead was localised into the nucleus.

### 4.5.2 Incorporation of a nuclear localisation signal into MS2.Coat-mCherry fusion

Previous work investigating intracellular RNA traffic using the MS2 bacteriophage system has shown that a nuclear localisation signal fused to the MS2.Coat-Fluorescent protein could help redirect unbound fluorescence from the cytoplasm to concentrate it within the nucleus. This approach was initially used to track cellular mRNA and HIV mRNA which originate from the nucleus and thus traffic in close proximity to the concentrated reporter protein (Bertrand et al., 1998; Jouvenet et al., 2009). Recently the same principle was successfully applied to a TBEV replicon that enabled reduction of background MS2 coat fluorescence (Miorin et al., 2013). In this instance, TBEV RNA localised to the cytoplasm bound the MS2 coat fluorescent reporter while unbound fluorescent MS2 coat concentrated within the nucleus.

To implement such modification within our experimental system, a nuclear localisation signal (NLS) was inserted within the MS2.Coat-mCherry expression plasmid using an oligo duplex strategy. Two oligos coding for a nuclear localisation signal (NLS) were commercially synthesised with a phosphate on their 5' end (Geneworks, Adelaide, SA, Australia) (Table 4.2). After annealing of the two oligos into a duplex (See Chapter 2.1.22 for details), a *BamHI* restriction site, Antarctic phosphatase (NEB) and ligation were used to insert the NLS immediately preceding the MS2 coat protein within the plasmid pL6[MS2.Coat-mCherry] (described in Chapter 4.2.1) to generate pL6[NLS-MS2.Coat-mCherry].

| **TOP STRAND OLIGO** | **NLS_MS2coatTOP** |
|---|---|
| 5’- gatccacc ATG GAT CCA AAA AAG AAG AGA AAG GTA g -3’ | |
| | |
| **BOTTOM STRAND OLIGO** | **NLS_MS2coatBOT** |
| 5’- GATCCTACCTTTCTCTTCTTTTTTGGATCCATggtg -3’ | |
| | |
| **Oligo Duplex** | |
| *5’*- gatccacc ATGGATCCAAAAAAGAAGAGAAAGGTA g *-3’*<br>*3’*- gtgg TACCTAGGTTTTTT CTTCTC TTTCC AT CCTAG *-5’* | |
| | |
| **Encodes** | **Protein** |
| Gatccaaaaaagaagagaaaggta | D P K K K R K V |

**Table 4.2: Oligo duplex strategy for pL6[NLS-MS2.Coat-mCherry]**

Similar to the generation of the original MS2.Coat-mCherry expressing cell line, a lentiviral approach was used to achieve stable expression of the NLS-MS2.Coat-mCherry fusion protein in Huh-7.5 cells. Packaging of the fusion reporter protein transgene into lentiviral particles (details in Chapter 2.2.8) allowed transduction in Huh-7.5 cells and further selection of Huh-7.5 cells constitutely expressing NLS-MS2.Coat-mCherry using blasticidin. The mCherry fluorescence pattern displayed by the stable cell line is illustrated in Figure 4.18 A.

Although mCherry fluorescence was relatively concentrated in the nucleus, a significant number of cells displayed additional diffuse red fluorescence throughout their cytoplasm. Moreover, presence of fluorescent artefacts throughout the cell cytoplasm was observed at times contrary to what has been reported previously (Miorin et al., 2013) and seemed to be accentuated depending on the confluency. Finally preliminary results indicated that reorganisation of the fluorescence from the nucleus to the cytoplasm during viral replication of the HCV MS2 chimera was not reliably induced. We hypothesised that this could be due to the low levels of replication of the Jc1/5A-TCM+3'UTR:24xMS2 and limited recruitment of the nuclear MS2.Coat reporter.

In summary none of the model optimisation approaches produced significant or reliable advantages over the existing model. Nevertheless improvement of the experimental system is an ongoing focus to enable sensitive and minimally disruptive labelling of HCV RNA for advanced applications such as super-resolution microscopy.

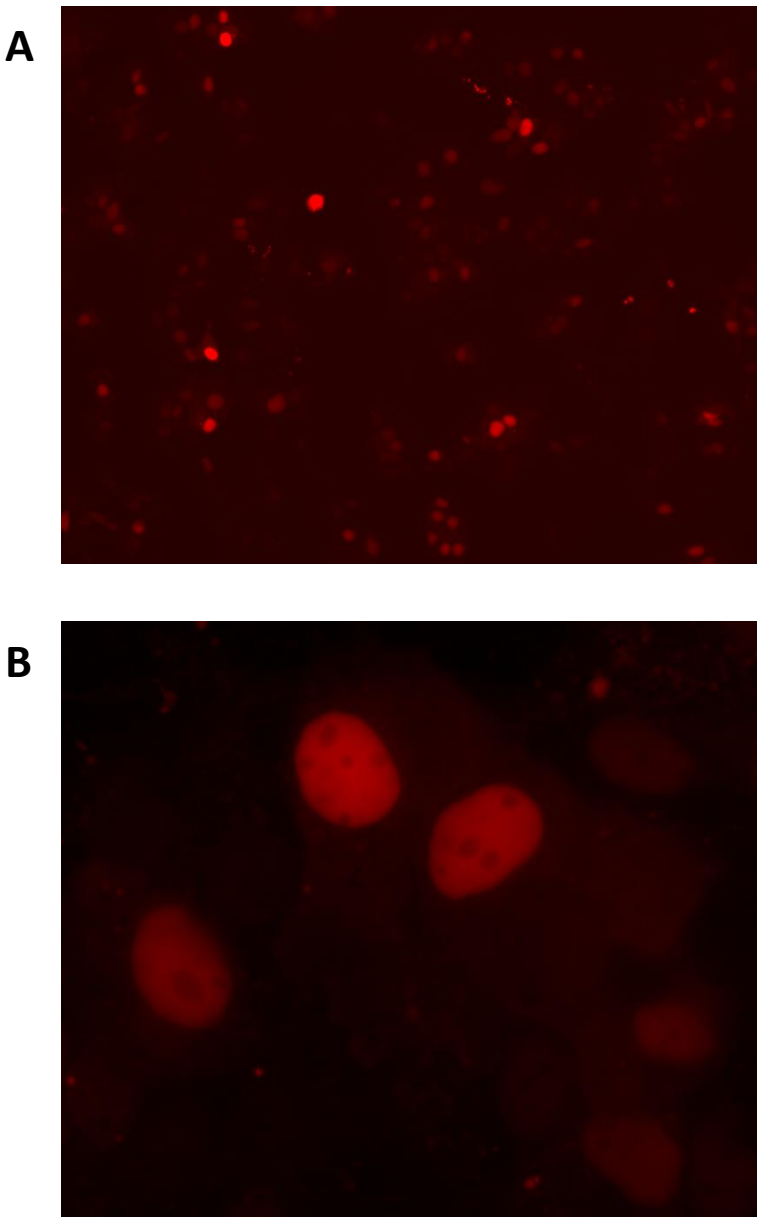


**Figure 4.18: Fluorescence of Huh 7.5 +NLS-MS2.Coat-mCherry cells.**
Live fluorescence displayed by the Huh 7.5+NLS-MS2.Coat-mCherry cells with 10x (A) and x60 (B) objectives.

## 4.6 Discussion

As previously mentioned, the MS2 bacteriophage system to tag and track mRNA in living cells required the joint usage of two elements (Bertrand et al., 1998). First we described in Chapter 3 the insertion of repeats of the MS2 bacteriophage stem loops within the 3'UTR of a chimera genome of HCV. In this chapter we then described the use of MS2.Coat-mCherry as the reporter protein which localises to the foci of RNA during viral replication due to its affinity for the tagged viral RNA. After showing that the specific binding of the reporter protein to the viral RNA does not have any major impact on viral replication, we then described the fluorescence pattern induced by viral replication and the parallel with NS5A localisation and traffic during the viral life cycle. This constitutes the first visualization of positive strand HCV RNA traffic in the context of a full-length virus genome replication in real time.

The initial choice of working with a polyclonal cell line was driven by multiple factors. First of all, as described previously, expression levels of the reporter protein and of the tagged RNA are crucial (Park et al., 2010). Over-expression of these elements can induce aggregation of the fluorescent reporter despite the removal of the multimerisation signal in the MS2 coat coding sequence. As described in Chapter 3, the HCV genomes with the MS2 stem loop insertions display low levels of replication and delayed kinetics of replication in comparison to the parent. Although using electroporation can help to initiate a semi-synchronous replication cycle, using a full-length virus inherently induces cell to cell variation and variation between experiments. Accordingly polyclonal MS2.Coat-mCherry-expressing cell lines were employed to

enable a range of reporter expression levels to suit a variety of tagged genome replication levels.

The HCV RNA results presented in this chapter were produced using the HCV full-length chimera carrying 24 repeats of MS2 stem loops (Jc1/5A-TCM+3'UTR;24xMS2) as it displayed better fitness levels than variants with fewer MS2 stem loops and the most potential for strength of the fluorescence signal, as thoroughly discussed in Chapter 3. Nevertheless, experiments with the constructs containing fewer MS2 stem loops repeats (6, 8 and 12 repeats) were also performed. The use of these viruses did not improve fluorescent RNA labelling. As stated previously, their delayed replication kinetics and lower levels of peak replication also suggest their limited utility in imaging experiments. Moreover, previous studies generally employ 24 repeats of MS2 stem loops as the minimal number of repeats required to visualize fluorescently tagged RNA (Fusco et al., 2003; Shav-Tal et al., 2004a).

Although it was not reported with other viral imaging models using the MS2 bacteriophage-based system for RNA live imaging, it was considered possible that binding of the MS2.Coat-mCherry protein to the MS2-tagged HCV RNA during viral replication would have a deleterious impact on HCV replication. Indeed the high affinity binding could induce jamming of the NS5B viral polymerase or interfere with the NS3 viral helicase activity. Nevertheless, results presented in this chapter (Section 4.2.4) indicated that there was no negative impact on viral replication induced by binding of the MS2 fusion reporter protein.

The emergence of strongly fluorescent foci induced by the replication of Jc1/5A-TCM+3'UTR:24xMS2 enabled reliable detection of two major types of structures of RNA foci. The first was described as small and often highly motile while the second was described as relatively static and larger. The size of the relatively static structures varied significantly between cells and experiments. Moreover the larger structures often appeared to be composed of smaller sub-units that displayed spasmodic and confined movement. Their association together could impose a restriction on the independent movements of these smaller sub-units. Taken together with the example presented in the Inset of Movie 4.6 of a motile structure composed of at least two associated particles moving throughout the cytoplasm, one can easily draw the conclusion that the larger and static structures are composed of former small and motile ones which by an unknown process associate together and become restricted in their movement.

Furthermore tagged RNA induced fluorescence reorganisation reveals that although the small and motile structures are always present, larger relatively static structures can be absent from the cell or vary in size. Moreover as mentioned in the results section, smaller structures when travelling towards larger structures can pause indefinitely in their close proximity, although they have also been observed to bounce back towards their origin. These events may relate to the hypothesised formation of larger structures as a result of association of smaller structures with one another. However, it remains unknown whether certain sub-classes of structure are more likely to harbour active HCV RNA replication or participate in other aspects of the HCV life cycle, such as viral polyprotein translation and virion assembly. Although technically challenging, further investigation studying negative strand HCV RNA by inserting reverse complement version of the MS2 stem loops within the 3'UTR would enhance our observations by specifically identifying RCs from potential trafficking RNA.

Observations were occasionally limited by presence of background fluorescence or fluorescent artefacts associated with unbound reporter fluorescent protein and would benefit from an improvement of the Signal-to-Noise Ratio (SNR). Viral fitness was partially responsible for the noise observed as the balance between expression of the MS2 protein and viral RNA expression levels would work in concert to generate the fluorescent signal observed. An increase in viral fitness would result in a larger proportion of the diffuse MS2.Coat-mCherry fluorescence binding to the MS2 stem loop-tagged HCV RNA. This could potentially be achieved by either increasing viral fitness (e.g. through adaptation) or regulating the expression of the MS2.Coat-mCherry protein. Regarding the latter, suppression of the cytoplasmic background through the insertion of a nuclear localisation signal (NLS) within the reporter fluorescent protein has shown in the past to be efficient to relocate the MS2 reporter fluorescence into the nucleus (Miorin et al., 2013). However in our hands the addition of one NLS to MS2.Coat-mCherry was not sufficient to result in a complete and stable nuclear localisation of the MS2.Coat-mCherry in naïve cells. It is possible that insertion of a second NLS may overcome cytoplasmic localisation and future experiments should test this strategy (see Appendix VI). Future strategies could include the use of an expression system such as the tetracycline-controlled transcriptional activation (tet-on/off) systems (Appendix III), to enable tight regulation of the expression level of MS2.Coat-mCherry.

Finally conversion of our system towards a split fluorescent protein technology such as split-GFP or split-Venus (improved version of YFP (Nagai et al., 2002)) could potentially drastically reduce background fluorescence (Ozawa et al., 2007; Rackham and Brown, 2004; Valencia-Burton and Broude, 2007; Valencia-Burton et al., 2007). This technique is based on two reporter proteins instead of one, each being the fusion

of one RNA-binding protein with one complementary half of the fluorescent protein. The binding of the RNA-binding proteins on two closely adjacent sequences triggers a conformational change enabling juxtaposition of the two complementary halves of the fluorescent protein thus generating a fluorescent complex only at the site of RNA localisation. This method drastically removes diffuse fluorescence background because the fluorescence theoretically only occurs at the specific RNA foci. Nevertheless, the split-FP strategy requires two binding sequences instead of one for the traditional MS2-tagging system. Therefore the fluorescent signal induced by an insertion of the same size would be half as strong using the split-fluorescent protein technique.

In the imaging presented throughout this chapter a strong parallel can be drawn between fluorescently labelled NS5A-positive structures and RNA-positive structures revealed by the reorganisation of the MS2.Coat-mCherry reporter protein. Both structures display similar subcellular localisation and trafficking patterns. This observation is not inconceivable as NS5A is known to play a role in both RNA replication and assembly and as such would be associated with HCV RNA during these processes. In regards to motile structures, both NS5A and RNA foci can be observed to travel throughout the cytoplasm with sporadic acceleration, achieving speeds of up to 1 μm/s. These observations raised questions as to the functions of each class of NS5A-positive structure and RNA-positive structure within the viral life cycle. In the next chapter, imaging of HCV RNA with respect to NS5A and intracellular organelles was undertaken to help us understand the relative roles of each class of structure.

# Chapter 5

# HCV RNA Traffic with Respect to Intracellular Organelles

## 5.1 HCV RNA and NS5A localisation and traffic in living cells

### 5.1.1 Introduction

HCV RNA replication is a tightly regulated step of the viral life cycle occurring within replication complexes (RCs) formed by the association of both viral proteins and host factors tethered within reorganised endoplasmic reticulum membrane compartments termed the membranous web (MW) (Egger et al., 2002; Ferraris et al., 2010; Gosert et al., 2002; Romero-Brey et al., 2012). Figure 5.1 depicts a schematic representation of the RCs with the principal players involved (adapted from (Chukkapalli and Randall, 2014)). Therefore RNA replication is governed by numerous factors involved in a cohesive and sequential manner that is even today only partially understood.

HCV non-structural proteins are synthesised at the ER and remain directly anchored into the ER membrane, except NS3 whose ER localisation is mediated by a direct interaction with NS4A. While NS4B has been associated as the prime HCV protein that induce membranous web formation, recent studies have shown that HCV NS3/4A, NS5A and NS5B also play a role (Ferraris et al., 2013; Gouttenoire et al., 2010;

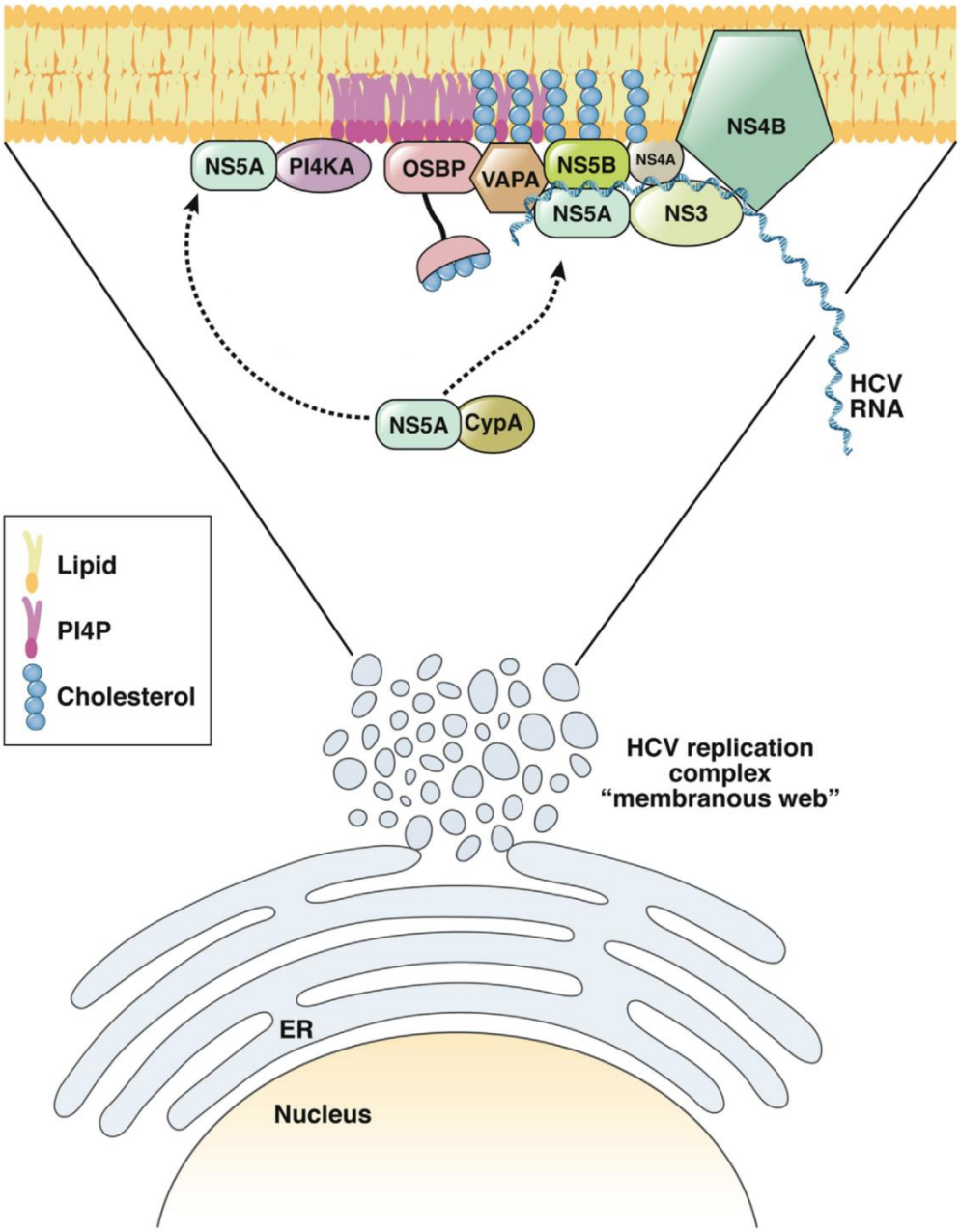


**Figure 5.1: Schematic of the HCV Replication Complex.**
Adapted from (Chukkapalli and Randall, 2014).
In this schematic the complex association of the multiple viral and host components of the HCV RCs is represented .

Romero-Brey et al., 2012) which harbour RCs (Egger et al., 2002; Gosert et al., 2003; Gosert et al., 2002). Replication complexes are also known to recruit specific host factors such as PI4KIIIα (Berger et al., 2011; Reiss et al., 2011), Rab5A (Berger et al., 2009) and VAP-A and VAP-B (Gao et al., 2004; Hamamoto et al., 2005); each playing critical but partially understood roles in RNA replication including through direct interactions with viral NS proteins such as NS5A. Identification of the RCs within the MW as the site of RNA replication was initially hypothesised by labelling of de novo-synthesized RNA using 5-bromouridine 5'-triphosphate (BrUTP) subsequent to actinomycin D treatment that inhibits all cellular DNA dependent RNA polymerase derived RNA (Gosert et al., 2002). It is hypothesised that during the Flavivirus replication cycle dsRNA is present in the form of negative and positive strand duplexes (termed replication intermediates [RI]) allowing for visualization of active RNA replication and thus active RCs with antibodies that specifically recognise dsRNA. Kunjin-West Nile virus (WNV), another related Flavivirus, employs a replication strategy involving a replication intermediate (RI) with both negative and positive RNA strands attached (Chu and Westaway, 1985) allowing RCs to be characterised by indirect visualisation of the RI using a dsRNA-specific antibody (Westaway et al., 1999; Westaway et al., 1997). Similarly, the specific antibody against dsRNA, 'J2' (Schonborn et al., 1991) has been used to further characterise HCV RCs and revealed that dsRNA partially co-localises with HCV NS5A and core viral proteins in JFH-1-electroporated cells in an immunofluorescence study (Targett-Adams et al., 2008). In contrast to conventional static imaging, the differences highlighted in NS5A live imaging studies provided an insight to the complexity of the temporal and spatial coordination of NS5A traffic (Eyre et al., 2014a; Wolk et al., 2008). Collectively the

dynamics of NS5A traffic emerged as a critical factor in HCV replication and in the later stages of the HCV life cycle.

Live cell imaging discussed in Chapter 4 displayed strikingly similar cytoplasmic movement between HCV NS5A and HCV RNA. Both NS5A and HCV (+)RNA indeed were organised predominantly in either static and larger structures in the perinuclear region of the cell or in smaller structures that can often be observed to travel throughout the cytoplasm in a directional manner, often changing trajectory to move backward along the same path.

In the present section a combination of immunofluorescence studies were performed, confirming specific aspects of HCV RCs that are further characterised in subsequent studies using live cell imaging techniques to investigate the co-traffic of HCV NS5A and RNA. Furthermore the traffic of HCV RNA with respect to cellular organelles is then investigated in the following sections. Taken together, the data presented will shed light for the first time to characterise the intersection of HCV replication at the RC and assembly at the lipid droplet interface.

### 5.1.2 HCV RNA and NS5A partially colocalise in fixed Huh-7.5 cells

Initially we sought to examine the localization of different components of the HCV RCs such as NS3, NS5A and dsRNA in cells harbouring replication of Jc1/5A-FLAG. This J6/JFH-1 (‘Jc1’) derived chimera incorporates a FLAG tag within the NS5A sequence and is capable of a productive HCV infection with similar kinetics to that of WT Jc1 (Eyre et al., 2014a). Cells were electroporated with IVT RNA for HCV Jc1/5A-FLAG and returned to culture. Supernatant was collected 3 days post-electroporation, filtered with a 0.45 μm filter and used to infect naïve Huh-7.5 cells.

After 2 days, cells were then fixed using acetone:methanol solution (1:1) at 4°C for 5 mins. Finally samples were prepared for indirect immuno-labelling (see Section 2.5.3) using the antibodies specified in Appendix II.

Figure 5.2 illustrates the co-localisation of NS3 and NS5A viral proteins (Pearson's correlation coefficient = 0.89) where NS3 (Red) is identified using a monoclonal antibody raised against the viral non-structural protein while NS5A (Green) is detected using an antibody against the FLAG epitope inserted within the NS5A coding sequence. Both viral proteins present a very similar localisation as they predominantly co-localise in a dense and seemingly MW-bound network (Figure 5.2 Inset 1 and 2). This co-localisation is consistent with the understanding that both proteins are produced from the same polyprotein at the ER and that they both are interacting components of the RCs (Lai et al., 2008). Moreover, NS5A also displays a ring-like fluorescent pattern in some instances (particularly noticeable in Figure 5.2 - Inset 1 [arrow]) that seem to be devoid of NS3. The NS5A-positive ring-like structures are putative lipid droplets and have been identified as a crucial platform for viral assembly where it is postulated that NS5A interacts with core as an initial step of new virion biogenesis (Camus et al., 2013; Masaki et al., 2008). Furthermore RCs are believed to be in close proximity to the assembly platform at the lipid droplet surface (Miyanari et al., 2007). Moreover discrete NS3-positive foci appear in the periphery of the putative LDs (Figure 5.2 - Inset 1 [arrowhead]) and could illustrate the hypothesised involvement of NS3 helicase activity in viral RNA encapsidation. Nevertheless it is not apparent if NS5A directly interacts with other RCs components at that step of the viral life cycle or if only independent NS5A would interact with core.

The relative position of putative RCs (dsRNA) with respect to the NS5A network is further illustrated in Figure 5.3. dsRNA was visualized using the J2 anti-dsRNA

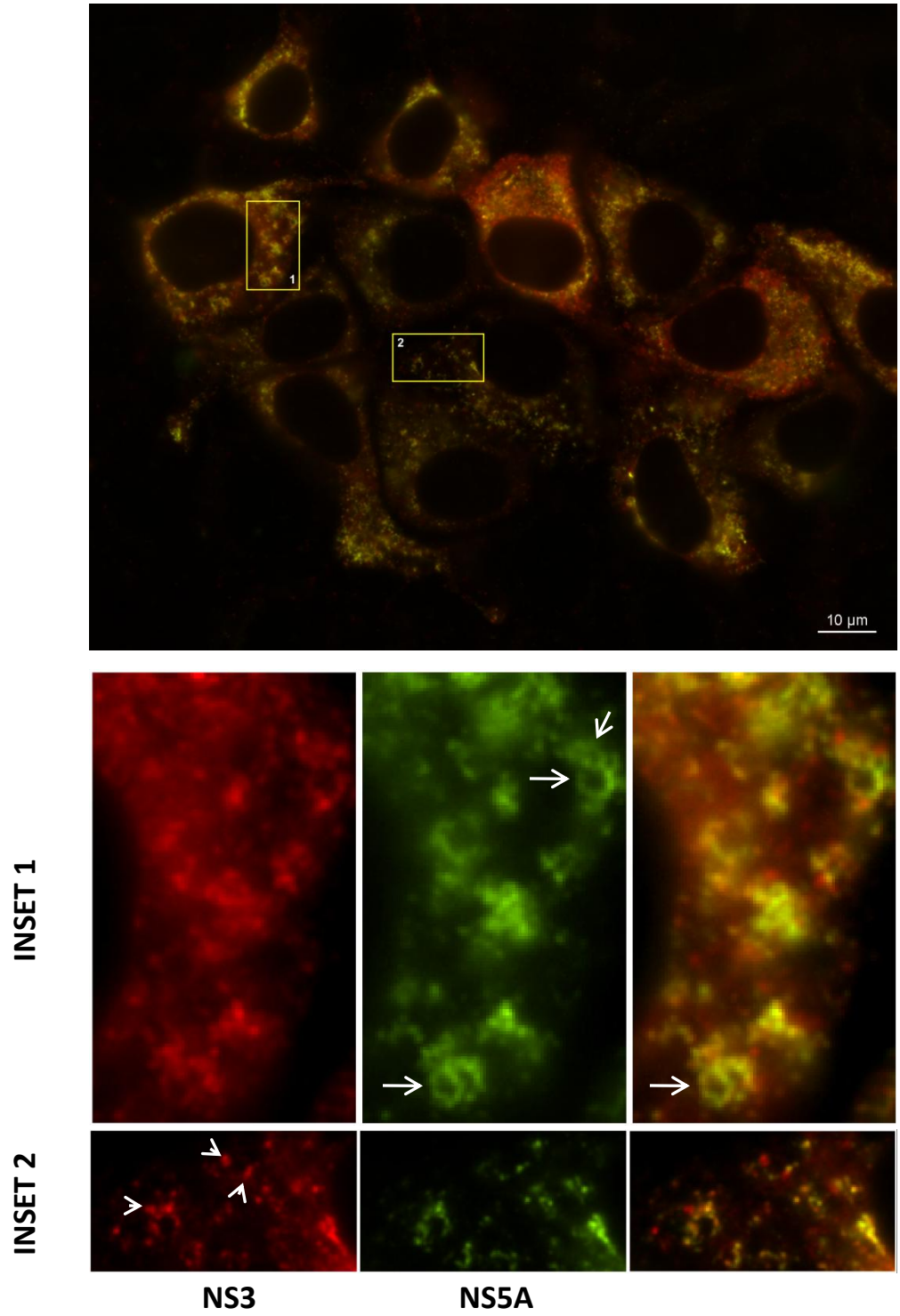


**Figure 5.2: Immuno-labelling of NS5A and NS3 in infected Huh-7.5 cells.**
Cells were fixed 2 days post-infection with Jc1/5A-FLAG and immuno-labelled with anti-FLAG (green) and anti-NS3 (red).
Arrows indicate NS5A ring-like structures (putative lipid droplets). Arrowheads indicate NS3 single discrete positive foci.

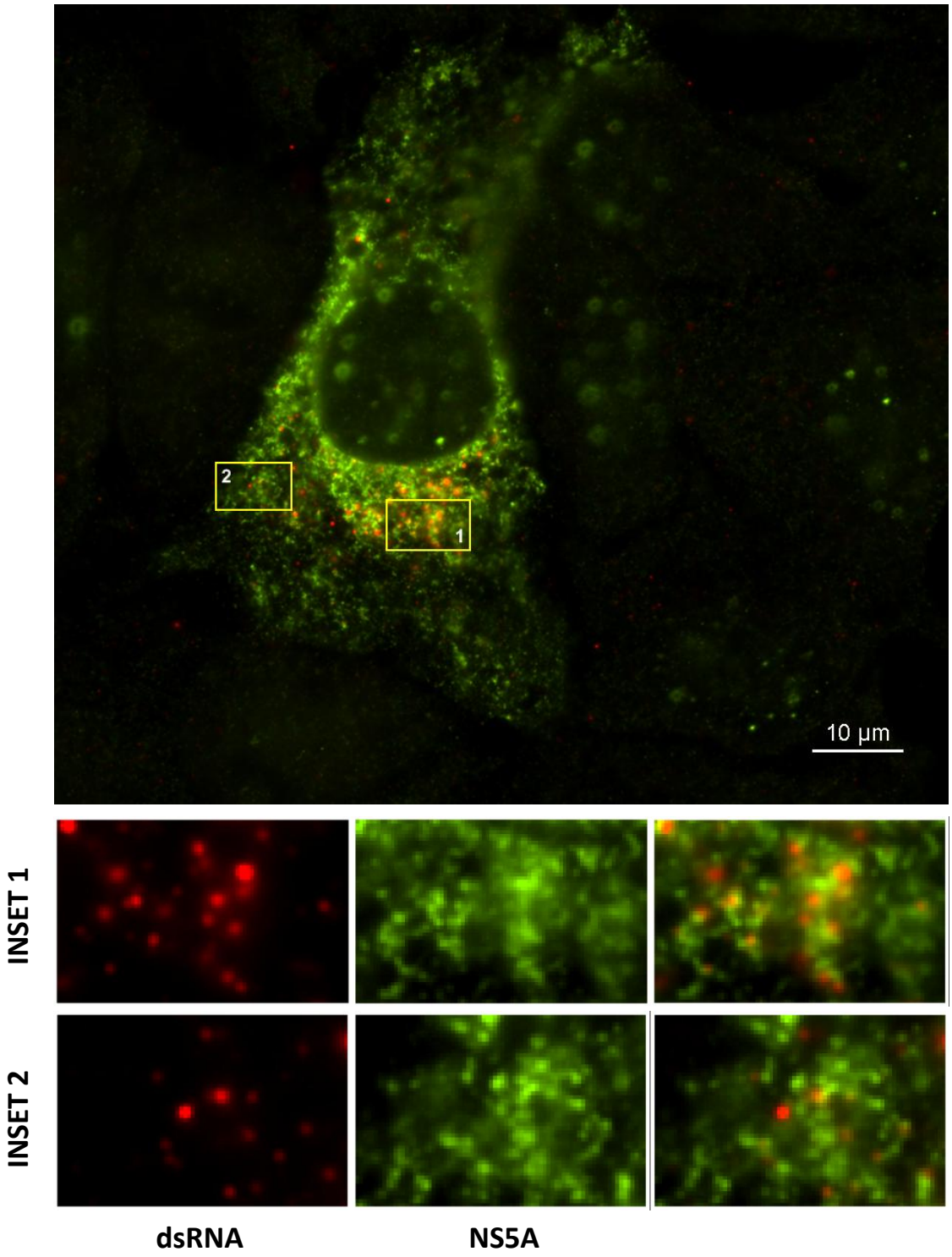


**Figure 5.3: Immuno-labelling of NS5A and dsRNA in infected Huh-7.5 cells.**

Cells were fixed 2 days post-infection with Jc1/5A-FLAG and immuno-labelled with anti-FLAG (green) and J2 anti-dsRNA (red) antibodies.

(Schonborn et al., 1991) antibody to detect putative replication intermediates (RIs) and further characterise active replication complexes similar to the work of Targett-Adams and colleagues (Targett-Adams et al., 2008). dsRNA is depicted in this image by the red fluorescence. On the other hand, NS5A-FLAG visualisation is mediated by labelling with the same anti-FLAG antibody used in Figure 5.2 and appears in green. dsRNA appear strongly concentrated in the perinuclear region consistent with the predicted localisation of the RCs (see Figure 5.3). Furthermore, direct overlap of dsRNA foci signal with NS5A signal appears limited (Pearson's correlation coefficient = 0.45) and in most cases was juxtaposed. Nevertheless, dsRNA always localised in close proximity of NS5A. To extend our imaging, a z-stack of 70 images was processed for deconvolution to eliminate noise signal using the deconvolution module of NIS-Elements imaging software (see Section 2.5.8) (Figure 5.4 A). Then 3D reconstruction of the fluorescence depicting both NS5A and dsRNA within the cell was generated using Nikon NIS-Elements software (Figure 5.4 B and Movie 5.1). Generation of this model enabled a deeper insight of dsRNA distribution with respect to NS5A. There seems to be two populations of NS5A and dsRNA. In general as in Figure 5.3 the majority of dsRNA was localised in juxtaposition to NS5A while in some instances there was strong co-localisation (Figure 5.4 C).

Finally we investigated the position of putative RCs through indirect immunolabelling of dsRNA with respect to the HCV core protein which is critical for virion assembly. In Figure 5.5, localisation of dsRNA (using J2 monoclonal antibody – red fluorescence) relative to HCV core protein (using RR-8 core rabbit polyclonal antibody (generously provided by Michinori Kohara (Tokyo Metropolitan Institute of Medical Science, Tokyo, Japan)) – green fluorescence) is displayed in Huh-7.5 cells 2 days after HCV Jc1/5A-FLAG infection. Core protein displayed a different pattern of localisation to

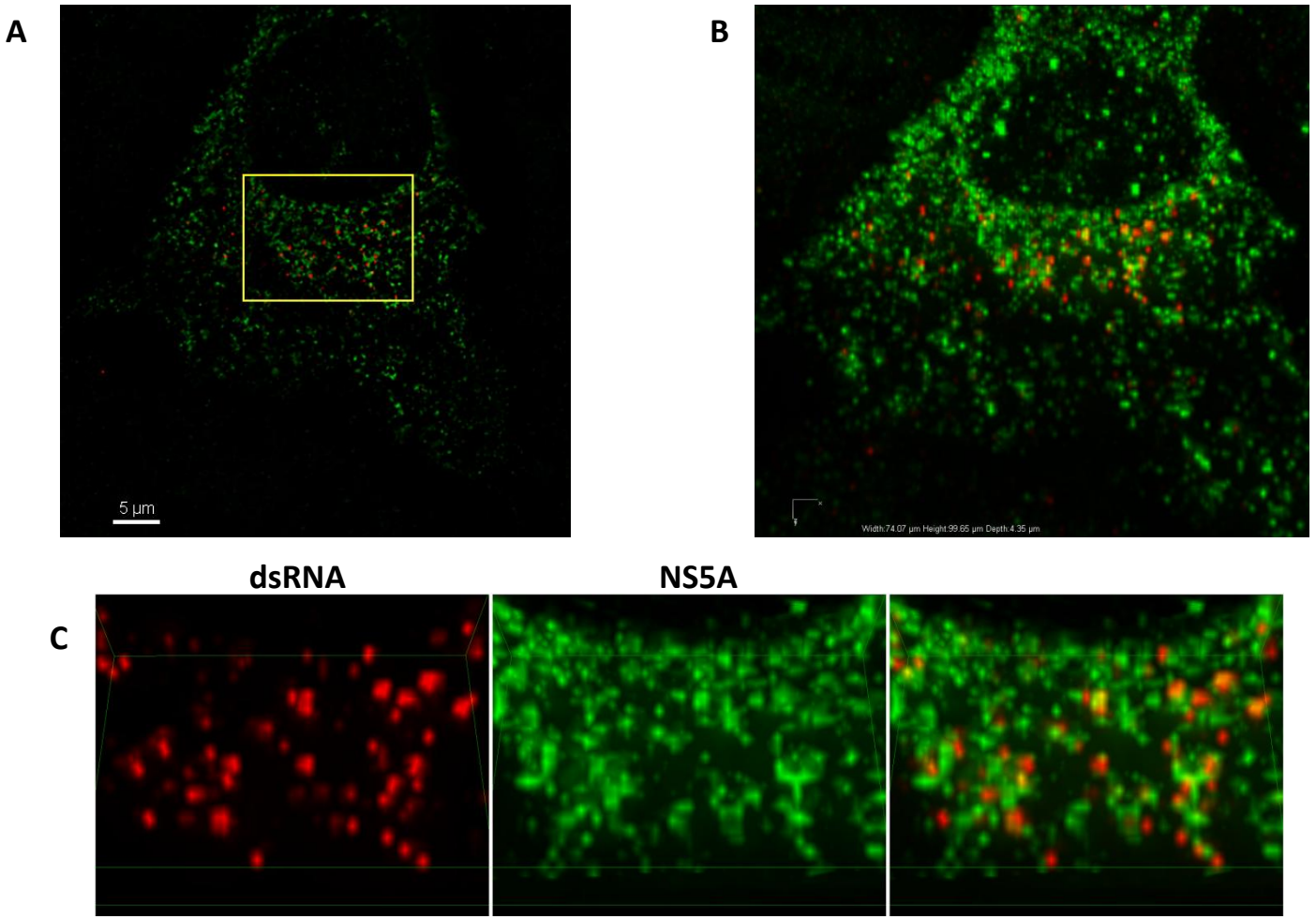


**Figure 5.4: 3D-Model of the relative position of dsRNA with respect to NS5A-FLAG (Movie 5.1).**
(A) Deconvolved image generated from a 70-image z-stack. (B) 3D model generated from the deconvolved z-stack. [Movie 5.1 presents the 3D-model rotation along the y-axis to translate a better perception of the association within the model depth] (C) Zoom of the peri-nuclear region (inset in A) within the 3D model.

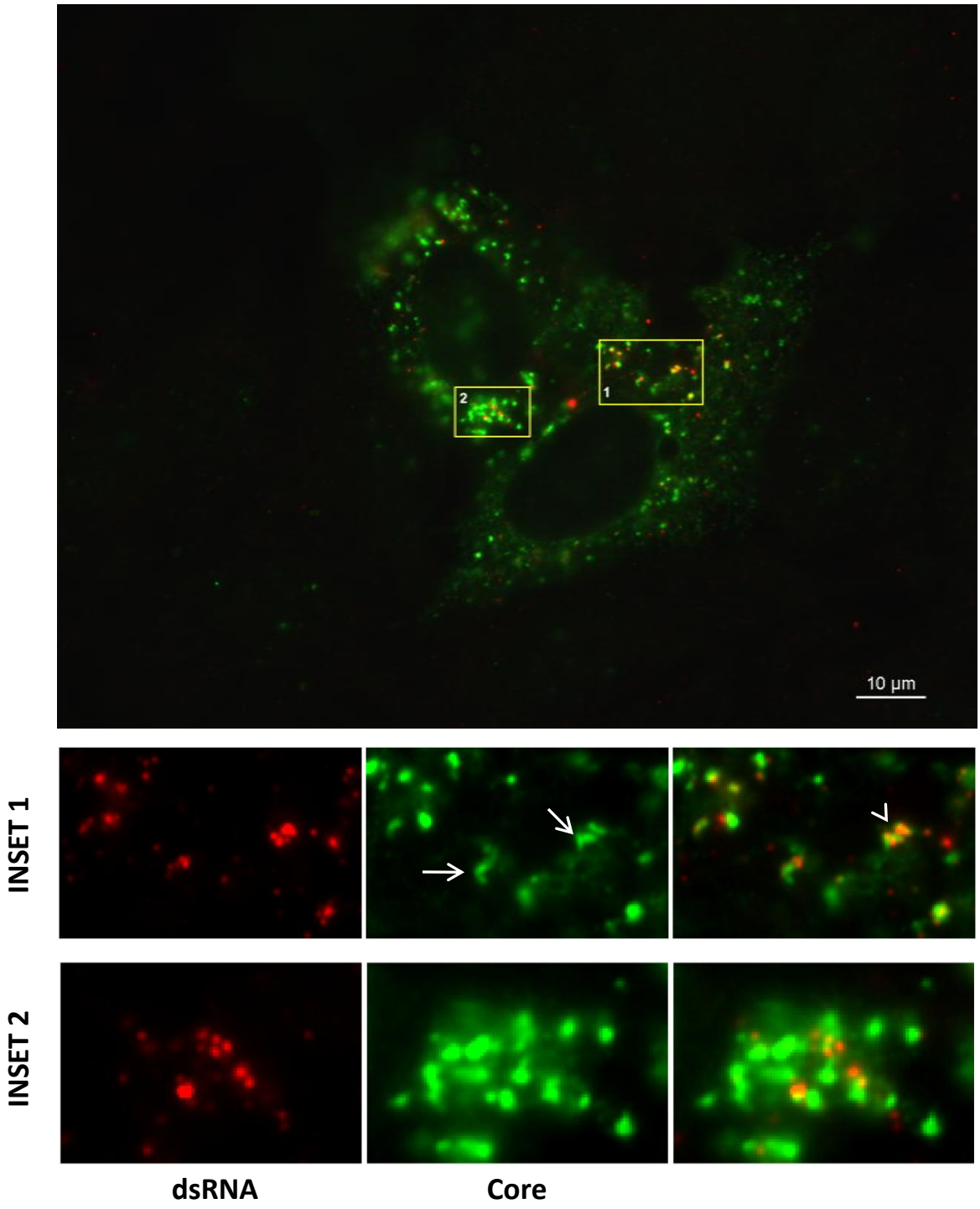


**Figure 5.5: Immuno-labelling of core and dsRNA in infected Huh-7.5 cells.**

Cells were fixed 2 days post-infection with Jc1/5A-FLAG and immuno-labelled with anti-core (green) and J2 anti-dsRNA (red) antibodies.

Arrows indicate cap-like core-positive structures. The arrowhead indicates dsRNA that strongly co-localises with core-positive structures.

that of from NS5A or NS3 as would be expected. Indeed core localised to distinct single foci or was present as a semi-circular cap stucture (see Figure 5.5 [arrow]). Moreover, core foci were found spread throughout the cytoplasm although they were more concentrated in the perinuclear region. dsRNA can be found in relative close proximity to core. In some instances, dsRNA is localised adjacent to core cap-like structures and in other instances they even can be observed to co-localise (see Figure 5.5 [arrowhead]). Moreover, dsRNA foci appear to often localise around larger core foci (Inset 1). Core protein has been shown to localise to the lipid droplet (LD) surface (Barba et al., 1997; Boulant et al., 2005; Counihan et al., 2011; Shavinskaya et al., 2007) which consequently accumulate in the perinuclear region in close proximity to the cisternae face of the ER network (Boulant et al., 2008). This mechanism is thought to induce close proximity between the RCs at the ER and the assembly platform onto the LDs and thus enable easy access for RNA delivery (Miyanari et al., 2007).

The J2 dsRNA antibody recognises long dsRNA helices, however it hypothesised that the J2 dsRNA antibody could cross-react with ssRNA adopting a helical secondary structure conformation over a long (>9-11 bp) homopolymer regions for instance (Schonborn et al., 1991). Although no RNA helix secondary structure is reported for HCV genome (Targett-Adams et al., 2008), Paul and colleagues highlighted the risk of false-positive binding of the dsRNA antibody towards complex secondary structures of RNA viruses such as Coronavirus with which false positive detection has been observed (Hagemeijer et al., 2012; Paul et al., 2013). Furthermore, neither details of the mechanistic management of HCV RNA encapsidation nor the resulting RNA spatial conformation consequences is known, but we can hypothesise that this step of the viral life cycle induces HCV RNA to develop a higher degree of secondary structure and thus could potentially cross-react with J2 dsRNA antibody. Thereafter this type of false

positive could indicate assembly sites at the surface of the LD and therefore explain the presence of “dsRNA” at the surface of the core-capped LDs observed in Figure 5.5.

In summary the static images of dsRNA presented herein show that dsRNA localises with or in close proximity to NS5A in what could constitute replication complexes. Moreover detection of dsRNA foci in close proximity to the HCV core protein could either be a sign of cross interaction of the J2 dsRNA antibody to highly folded (+) RNA during the encapsidation process or occasional close localisation of +/- RNA intermediates within RCs to sites of viral RNA encapsidation.

### 5.1.3 HCV RNA co-traffic with NS5A

Static images only provide a snap-shot of the state of the cell at the time of fixation, hence intracellular dynamics of virus-host interactions involved can not be appreciated. Spatial and temporal organisation of steps within the HCV life cycle are key in the investigation of the mechanisms involved in replication and packaging of viral RNA, highlighting the advantage that live imaging can provide.

Using the system we developed as described in Chapter 4, we examined the simultaneous localization and traffic of NS5A and HCV RNA in living cells during HCV replication. Cells were electroporated with IVT RNA for HCV Jc1/5A-TCM+3’UTR:24xMS2 to allow simultaneous visualization of both NS5A and HCV RNA. Similar to the experiments described in Section 4.3, electroporated cells were labelled with the dye FlAsH to allow for NS5A live imaging (See Chapter 2.6.2 for details) 2 days after electroporation and then returned to culture for 8 hours before visualization by fluorescence microscopy. Visualization of HCV RNA is mediated by the reorganisation of the MS2.Coat-mCherry fluorescent protein after binding to the

MS2 stem loop tag within the viral RNA and thus does not require external labelling. HCV RNA and NS5A fluorescence were successively recorded every 3 seconds for 3 minutes as described previously. Every merged image is composed of two fluorescent images acquired sequentially to investigate co-traffic (TxRed filter: RNA, FITC filter: NS5A). Pictures were then merged and assembled to reconstitute a movie using the Nikon NIS-Elements imaging software.

Figure 5.6A depicts HCV RNA (red) and NS5A (green) cellular localisation at a particular time point from the Movie 5.2. Also presented are the time lapse sequences from Insert 1 and 2 depicting the traffic of both HCV RNA and NS5A (Figures 5.6 B and C respectively). Analysis of images reveals the co-localisation and simultaneous traffic of HCV RNA and NS5A (Movie 5.2 and Figure 5.6 A and Inset 1 and 2). The majority of the structures are double positive for both NS5A and HCV RNA fluorescence. However in some instances NS5A-positive RNA-negative motile structures can be observed suggesting that not all motile NS5A structures contain HCV RNA.

Inset 1 (Figure 5.6 B and Movie 5.2_Inset 1) highlights the co-traffic between HCV RNA with NS5A in which both can be observed to move simultaneously with a high degree of coordination indicating co-traffic and complete association. The live imaging (together with the time-lapse sequence) particularly illustrates the pattern we previously observed for NS5A (see Chapter 4.3.2 and 4.4.3) as the double-positive structure (Figure 5.6 B [arrow]) is trafficking, pausing, and then moving again in an opposite direction. This behaviour is characteristic of microtubule (MT)-dependent traffic as discussed Chapter 4.3.2 and 4.4.3. At various times during the movement we observed that NS5A appeared to pull ahead of HCV RNA. This artefact is due to the technical limitation of the microscope and camera system used for imaging in which there is a

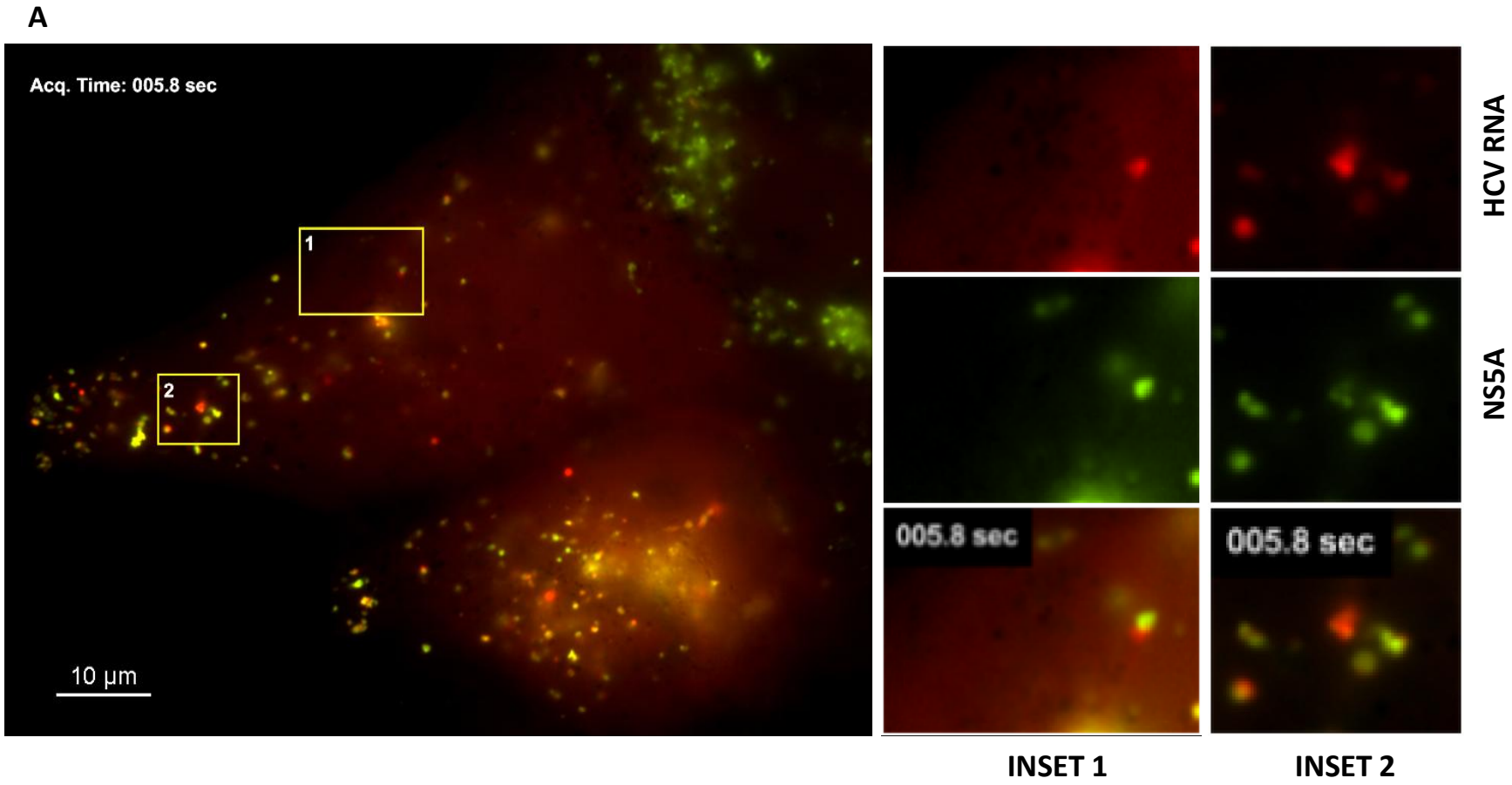


**Figure 5.6: Co-imaging of HCV RNA and NS5A in living Huh-7.5+MS2.Coat-mCherry cells (Movie 5.2)**
Jc1/5A-TCM+3'UTR:24xMS2-electroporated Huh-7.5+MS2.Coat-mCherry cells were labelled with FlAsH (green) 2 days post-electroporation, returned to culture for 2hrs and visualized by time-lapse wide-field fluorescence microscopy.

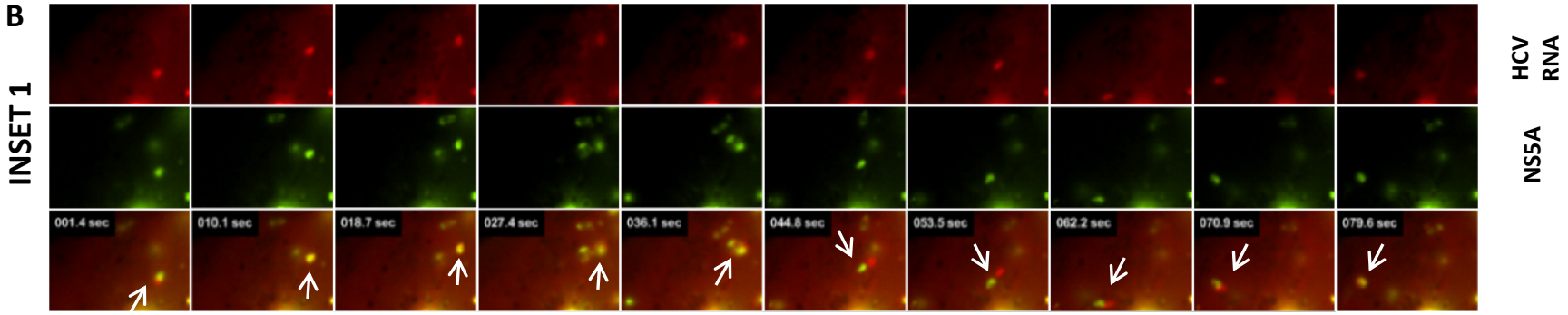


**Figure 5.6 Insets sequence: Co-imaging of HCV RNA and NS5A in living Huh-7.5 +MS2.Coat-mCherry cells (Movie 5.2)**

Figure 5.6 B and C present time-lapse sequences of the insets from in Figure 5.6 A. Inset 1 illustrates NS5A and HCV RNA co-traffic. In Inset 2 we can observe that double-positive structures can display higher levels of red or green fluorescence suggesting variable composition. Moreover NS5A-positive, RNA-negative structures can be observed (Figure 5.6 C [arrowheads]) while HCV RNA-positive, NS5A-negative structures were not detected.

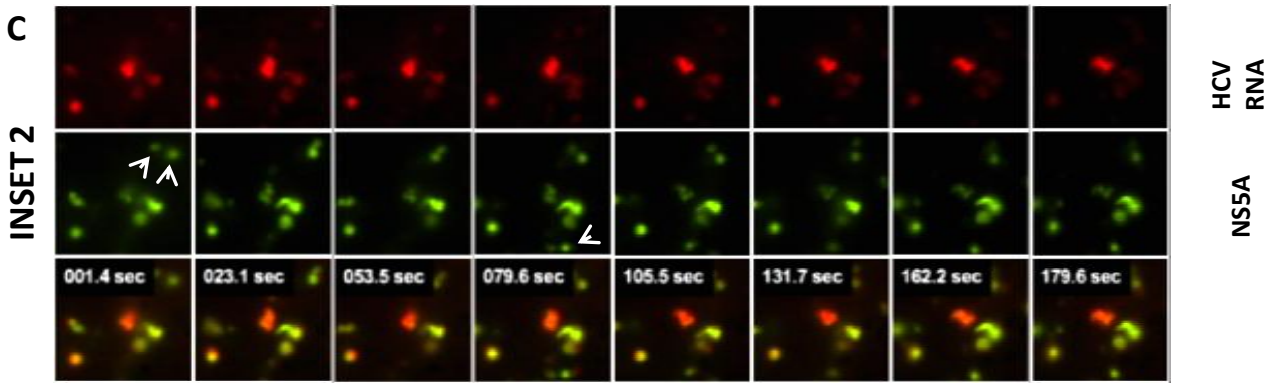

slight lag between acquiring the images for both channels (detailed explanations are provided in Chapters 2.6.5 and 2.6.6). Moreover, static structures appear double positive for NS5A and HCV RNA suggesting that they may also represent RCs as have previously outlined in static image analysis (Figure 5.6_C and Movie 5.2_Inset 2).

Furthermore, both motile and static structures are present in which there seems to be a greater abundance of either NS5A or HCV RNA. These observations indicate the possibility that the composition of the double-positive structures is not fixed and may vary over time. Furthermore on occasion motile NS5A-positive structures were devoid of HCV RNA. However, this was not the case for HCV RNA-positive structures in which RNA always localised with NS5A both in motile and static structures. These observations indicate that HCV RNA traffic is coincident with the presence of HCV NS5A, whereas NS5A is capable of associating directly or indirectly to the MT network to traffic throughout the cytoplasm even in the absence of detectable HCV RNA in these foci. This suggests that HCV RNA is dependent on NS5A and that this association may contribute to the traffic of viral RNA between the intracellular sites of replication and assembly.

### 5.1.4 Immunoprecipitation of HCV RNA via NS5A

The HCV RNA-binding capacity of NS5A was proposed in 2005 with the resolution of the crystal structure of its zinc-binding domain (Tellinghuisen et al., 2005) and the demonstration of its ability to bind the 3'UTR of both HCV positive-strand and negative-strand RNA *in vitro* (Huang et al., 2005). This ability of NS5A was further confirmed *in vitro* by showing that all three NS5A domains contribute to HCV RNA 3'UTR binding (Foster et al., 2010). Using the RNA-protein complex immuno-precipitation technique described in Chapter 4.2.3 to demonstrate binding of MS2.Coat-mCherry to the tagged-HCV RNA, we endeavoured to specifically extract HCV RNA via GFP-tagged NS5A to confirm the interaction in cell culture during viral replication.

Huh-7.5 cells expressing MS2.Coat-mCherry were electroporated with T7 IVT HCV RNA from Jc1/5A-GFP+3'UTR:24xMS2, parent Jc1/5A-GFP and a replication deficient HCV genome Jc1 (GND) and returned to culture for 3 days. Total protein extracts were collected using ice cold polysome lysis buffer (see Appendix I). Extracts were then homogenised and cellular debris were cleared by centrifugation. Lysates were first incubated with pre-cleared A/G agarose beads to remove any non specific association. After clearing the samples of the beads, lysates were then incubated with biotinylated anti-GFP antibody. Precipitation of the anti-GFP antibody and the associated protein was achieved by addition of pre-cleared A/G agarose beads. After extraction of the beads and subsequent washes, beads were resuspended in Trizol and RNA extraction was performed (see Chapter 2.1.10). Finally, cDNA was prepared as described in Chapter 2.1.12.2 and the HCV NS5B coding sequence was PCR-amplified using AmpliTaq Gold and primers (JFH1-8337S and KL.NS5Bc_R – see Appendix V). Amplification results are presented in Figure 5.7.

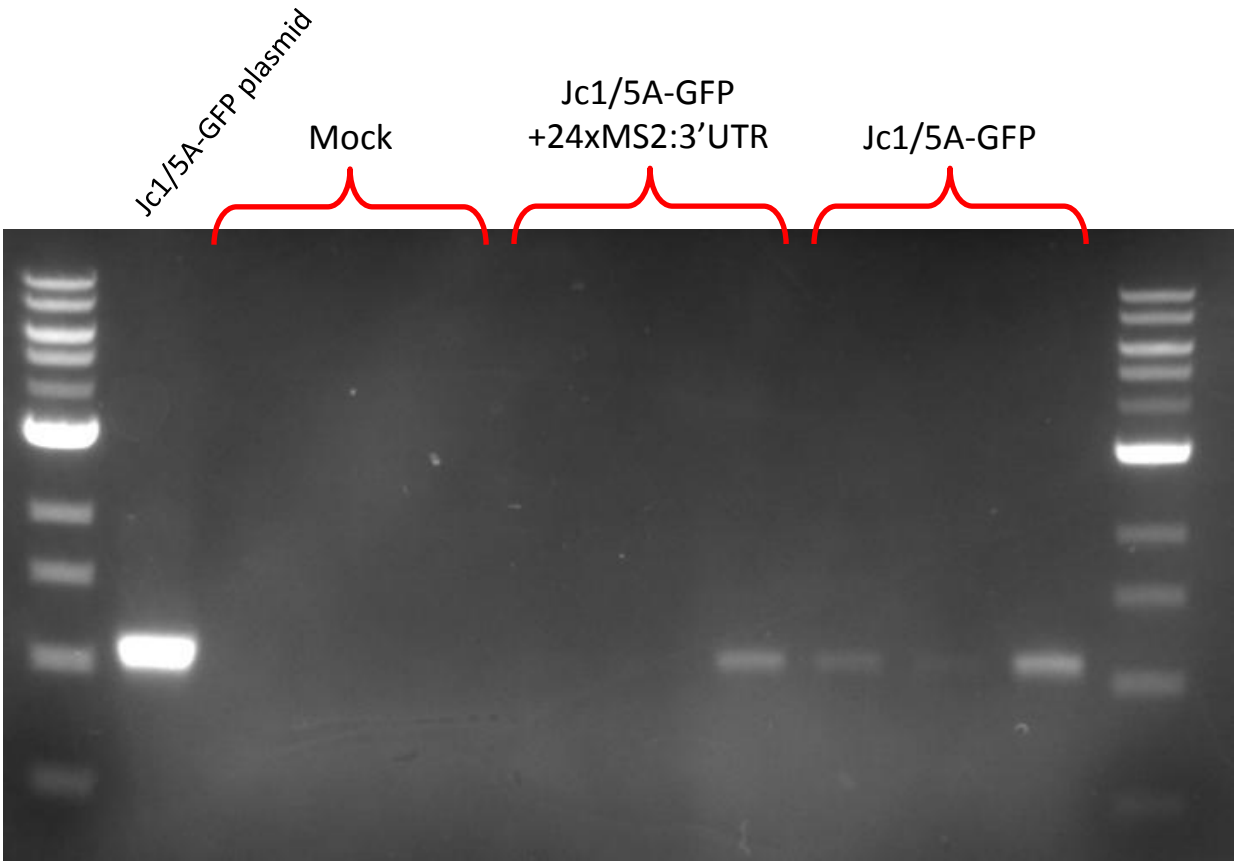


**Figure 5.7: HCV RNA immunoprecipitation via GFP-tagged NS5A during viral replication.**

Following electroporation of Huh-7.5+MS2.Coat-mCherry cells with the indicated HCV RNA transcript and culture for 3 days, NS5A-GFP was immunoprecipitated and associated RNA was extracted and cDNA prepared. RT-PCR was then performed using primers specific for the NS5B coding region. Plasmid DNA for pJc1/5A-GFP served as a positive control template for NS5B PCR. As can be seen, bands of the expected size (≈1.1kb) were only detected in samples prepared from cells electroporated with Jc1/5A-GFP+3'UTR:MS2x24 and Jc1/5A-GFP.

The presence of an amplicon of the expected size (≈ 1.1 kb) indicates successful extraction of HCV RNA via immunoprecipitation of NS5A. Although the efficacy of the HCV RNA immunoprecipitation was limited for the instance of Jc1/5A-GFP+3'UTR:24xMS2 (1 out of 3 samples was positive), parent Jc1/5A-GFP enabled much stronger detection of NS5A-associated HCV RNA (at least 2 out 3 positive). This might be due to the lower fitness of Jc1/5A-GFP+3'UTR:24xMS2 in comparison to the parent Jc1/5A-GFP. These results suggest confirmation of the interaction of NS5A and HCV RNA during the viral life cycle either by direct binding or another intermediate protein binding both to NS5A and HCV RNA (e.g. extraction of the full replication complexes). These experiments should be repeated incorporating a negative control virus in which NS5A is not tagged with GFP such as the Jc1/5A-TCM or the Jc1 wild-type viruses. Moreover Western blot analysis of the immunoprecipitated samples for other components of the replication complex such as NS5B or NS3 would help to investigate if the RNA-protein complex immunoprecipitated indicates direct binding *in vivo* of HCV RNA by NS5A.

## 5.2 HCV RNA and Lipid Droplets

### 5.2.1 Introduction

Following synthesis and maturation, the core protein localises to LDs (Barba et al., 1997; Counihan et al., 2011; McLauchlan et al., 2002; Moradpour et al., 1996), potentially aided by its interaction with host factors such as cytosolic phospholipase A2 (cPLA2) (Menzel et al., 2012), diacylglycerol O-acetyltransferase 1 (DGAT1) (Herker et al., 2010), and Ras-related protein 18 (Rab18) (Dansako et al., 2014). On the other hand NS5A is predominantly found within the RCs despite also having been shown to bind the LD surface through the amphipathic α-helix in the domain 1 (Hinson and Cresswell, 2009). NS5A phosphorylation is believed to be a critical factor towards NS5A targeting at the LDs surface (Appel et al., 2008; Kim et al., 2011; Masaki et al., 2008; Tellinghuisen et al., 2008a). Moreover relocation of NS5A has been shown to be promoted by DGAT1 (Camus et al., 2013) and Rab18 (Salloum et al., 2013). Finally core could be the main driving factor by actively recruiting NS5A alone or associated with viral RNA and/or complete replication complexes to the cLD surface where they interact (Masaki et al., 2008; Miyanari et al., 2007; Pietschmann et al., 2009; Tellinghuisen et al., 2008a). This interaction between core and NS5A represents an essential step of viral particle assembly and is necessary to the subsequent re-localisation of core (Appel et al., 2008; Masaki et al., 2008; Miyanari et al., 2007).

Retrieving of core from the cLD surface is mediated by a variety of host factors such as AP2M1 (clathrin assembly protein complex 2 medium chain) (Neveu et al., 2012) and more importantly other HCV viral proteins. Interaction between NS2 and p7 is critically involved in assembly (Jirasko et al., 2010; Popescu et al., 2011) and enables NS2 to further interact with NS3/4A complex also promoting core relocation to the ER

membrane where viral particle budding is hypothesised to occur within the ER (Counihan et al., 2011). Moreover, the NS3/4A complex plays a critical role in the assembly process through NS3 helicase activity as detrimental mutations severely handicap assembly of new virions (Jirasko et al., 2010; Jones et al., 2011; Ma et al., 2008; Phan et al., 2009). Therefore NS3 helicase could possibly be involved in RNA packaging. In addition, it is not known if the encapsidation of HCV RNA within newly formed core-composed capsids is concomitant with the budding process expected to occur within the ER for the biogenesis of the HCV virion (see Figure 1.8).

The highly dynamic nature of the transition between HCV RNA replication within the RCs to the packaging of the viral RNA into new virions has made this process difficult to study with current static imaging techniques. However, most recently live cell imaging studies have started to indirectly enable study of these dynamic events (Coller et al., 2012; Counihan et al., 2011; Eyre et al., 2014a). With the development of the MS2-HCV system to visualize HCV RNA in real-time we hope to unveil some of the exact details of this process.

In this section of Chapter 5, an immunofluorescence study to illustrate the relative localisation of putative RCs and assembly platforms in fixed cells is presented. Secondly investigation of HCV RNA in living cells is presented together with live imaging of lipid droplets to further investigate the dynamics of HCV RNA transition between replication and assembly sites.

### 5.2.2 HCV RNA localisation with respect to lipid droplets in fixed cells

The current understanding of HCV replication would suggest that there is transfer of HCV RNA from the RC to core coated lipid droplets to initiate assembly. In this section, the relative localization of HCV viral components involved in both RNA replication and new virion assembly were examined with respect to lipid droplets in cultured Huh-7.5 cells. Huh-7.5 cells harbouring HCV replication were fixed and prepared for indirect immuno-labelling (see Section 2.5.3 and 2.5.4) using the antibodies or organelle marker specified in Appendix II. While a number of studies have suggested the HCV core/LD interaction it was important to establish this relationship in our model system.

In Figure 5.8, core localisation is presented with respect to lipid droplets. Similar to immunofluorescence studies in Section 5.1.2, Huh-7.5 cells were labelled 2 days after infection with Jc1/5A-FLAG virus. HCV core protein was labelled with RR-8 anti-core polyclonal antibody (red fluorescence) while LD localisation is displayed using BODIPY 493 (Listenberger and Brown, 2007; Spangenburg et al., 2011). HCV core displays a characteristic pattern of localisation in accordance with the previous observations from Figure 5.5 in which it appears to concentrate in the perinuclear region while often adopting a ring-like structure. When related to LD localisation, core appears to locate on the LD surface in a cap-like fashion in the majority of instances (Miyanari et al., 2007).

To highlight the localisation of NS5A with respect to the LDs, we electroporated Huh-7.5 cells with Jc1 IVT RNA and returned the cells to culture for 2 days. Thereafter, samples were fixed, prepared and processed for indirect immuno-labelling to visualize HCV NS5A (using 9E10 monoclonal antibody – red fluorescence) and lipid droplets (using BODIPY 493 – green fluorescence). As illustrated in Figure 5.9, NS5A-positive

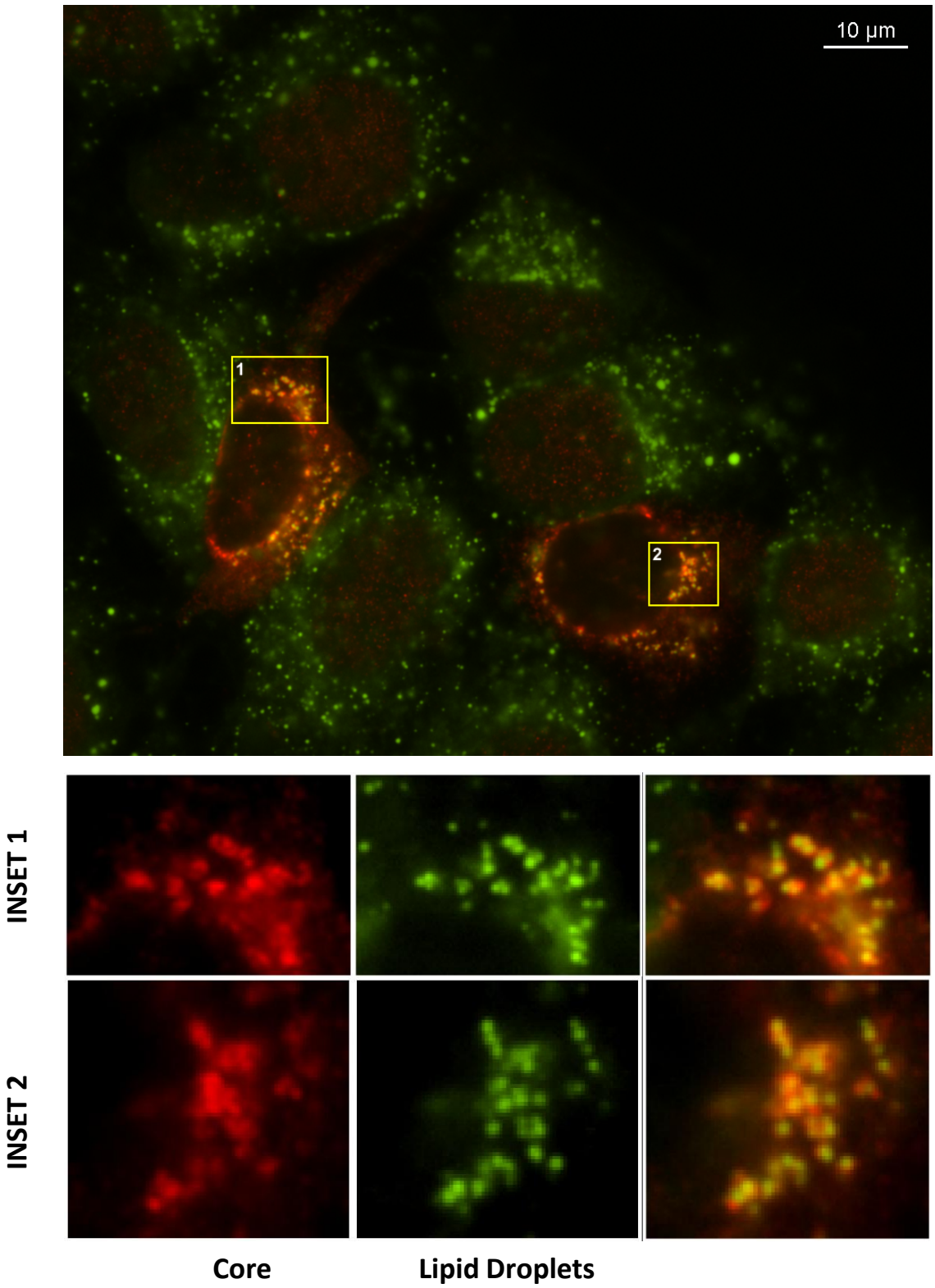


**Figure 5.8: Labelling of core and lipid droplets in infected Huh-7.5 cells.**

Cells were fixed 2 days post-infection with Jc1/5A-FLAG and immuno-labelled with anti-core (red) antibody and BODIPY 493/503 (green).

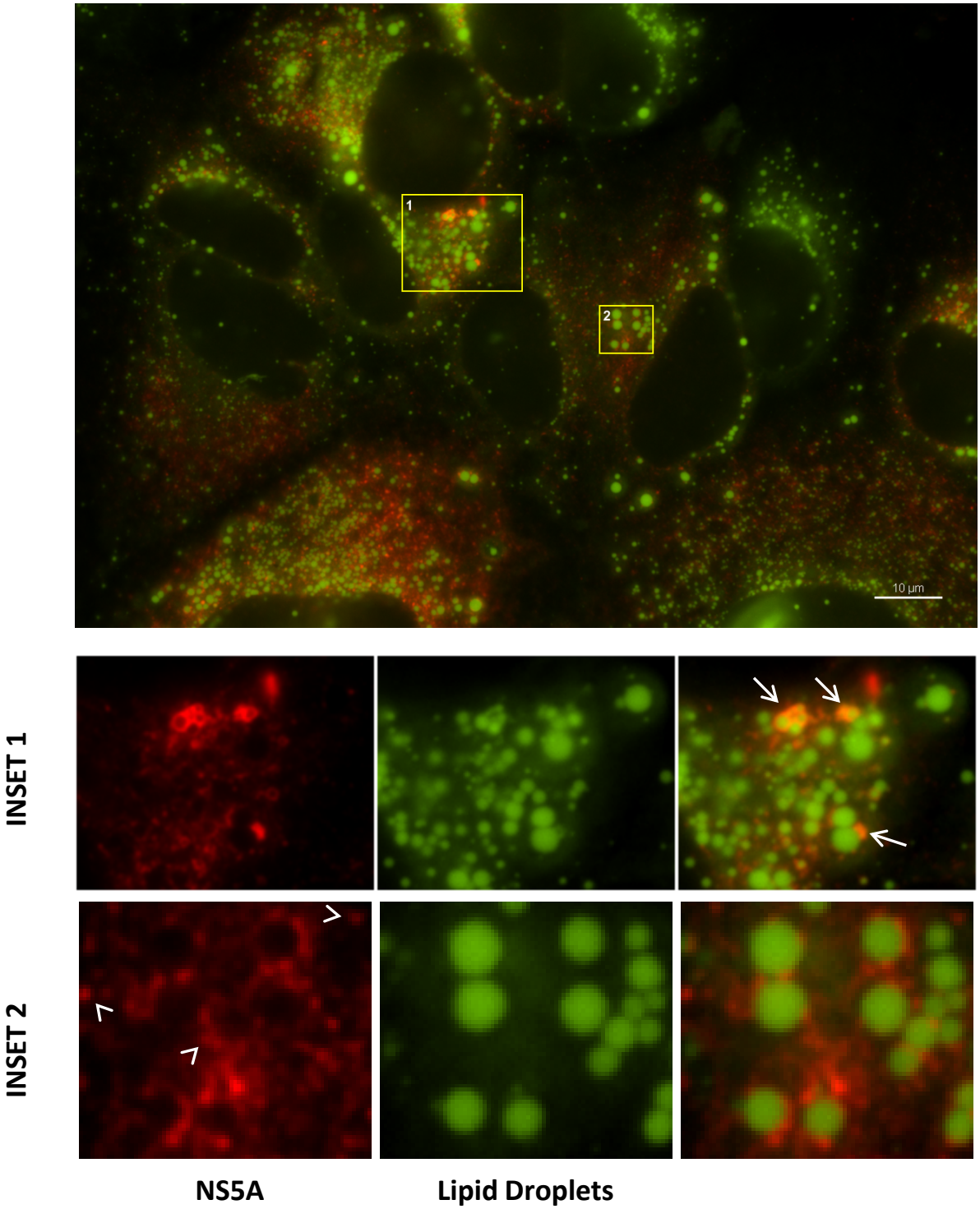


**Figure 5.9: Labelling of NS5A and lipid droplets in infected Huh-7.5 cells.**
Cells were fixed 3 days post-infection with Jc1 and immuno-labelled with anti-NS5A (red) antibody and BODIPY 493/503 (green).
Arrow indicate NS5A ring-like structures that coat lipid droplets. Arrowhead indicate discrete NS5A-positive foci.

foci displayed two distinctive patterns of fluorescence. In some instances, NS5A was observed to localise to the LD surface (see Figure 5.9 Inset 1 [arrows]) while the remainder of the NS5A-positive foci displayed a punctate cytoplasmic localisation (see Figure 5.9 Inset 2 [arrowheads]). While the MW location is characteristic of the role of NS5A in genome replication, the localisation at the LD surface is consistent with the interaction of NS5A with core at these sites and the possible delivery of viral RNA from the MW.

Based on current understanding one would expect HCV RNA to also locate to the LD. Therefore we examined the localisation of dsRNA with respect to LDs in Figure 5.10. Using the same settings as previously, dsRNA was labeled using the J2 antibody (visualized in red) and the lipid droplets using BODIPY 493/503 (green fluorescence) in Huh-7.5 cells harbouring Jc1/5A-FLAG replication 2 days after infection. Occasionally dsRNA-positive foci were observed in close proximity of the LD surface as illustrated in Figure 5.10 Inset 1 (Arrows). In this instance dsRNA was present as discrete foci, often limited to one or two foci per lipid droplet. In contrast the remainder of the dsRNA signal, comprising the vast majority of the dsRNA-positive structures, was detected in cytoplasmic foci that were distinct from LD. The relatively infrequent co-localisation of dsRNA and LDs displayed here is consistent with the observations made previously from Figure 5.5 in relation to dsRNA and HCV core protein (see Section 5.1.2).

Taken together these data support the role of lipid droplets as a platform for HCV particle assembly and a site of convergence of HCV RNA replication and assembly stages of the HCV life cycle. Beyond the multiple roles of LDs in cellular biology, they also represent the central platform of numerous critical interactions conditioning HCV RNA encapsidation and new virion biogenesis. However it is unknown if this

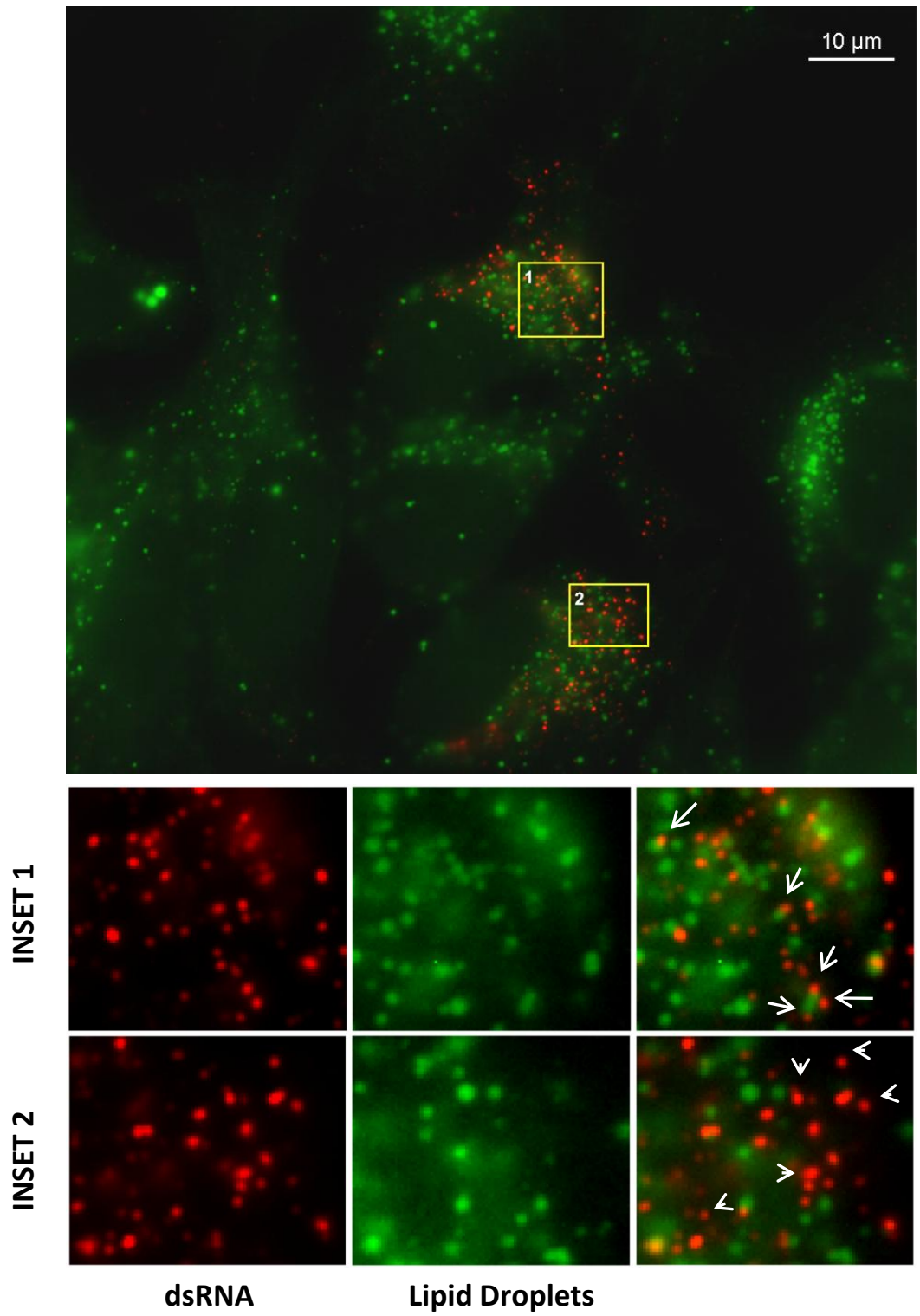


**Figure 5.10: Labelling of dsRNA and lipid droplets in infected Huh-7.5 cells.**

Cells were fixed 2 days post-infection with Jc1/5A-FLAG and immuno-labelled with anti-dsRNA (red) antibody and BODIPY 493/503 (green). Arrows indicate dsRNA in close proximity/co-localising at the surface of the lipid droplets. Arrowheads indicate dsRNA localised away from lipid droplets and putative virion assembly sites

NS5A/RNA interaction with the LD is a permanent association or if it is transient in nature. To answer this question we investigated the dynamics of these interactions in the following section using live imaging.

### 5.2.3 HCV RNA traffic with respect to lipid droplets

Investigation of HCV RNA traffic and localisation with respect to lipid droplets was then performed in living cells. Huh-7.5 cells constitutively expressing MS2.Coat-mCherry were electroporated with IVT RNA for Jc1/5A-TCM+3'UTR:24xMS2 and returned to culture. While HCV RNA is passively labelled through the binding of MS2 coat protein to the MS2-tagged viral RNA, staining of the lipid droplet was performed using BODIPY 493 / 503 (Spangenburg et al., 2011) (see Chapter 2.6.3). Cells were then returned to culture for 2 hours and visualized using the Nikon Ti inverted fluorescent microscope. Similar to previous live cell imaging experiments, images of HCV RNA and lipid droplet-associated fluorescence were acquired every 3 seconds for 3 minutes, images were merged and movies generated using NIS-Element imaging software.

Figure 5.11 represents a snapshot from the live cell imaging experiments (Movie 5.3) with two insets provided for greater clarity of the potential interactions between HCV RNA and the LDs. As can be seen from these images there is significant association between the HCV RNA and the LD (Figure 5.11 A Inset 1 and Inset 2 [arrows]), nevertheless HCV RNA could also be seen not associated with the LDs (Figure 5.11 A Inset 1 and Inset 2 [arrowheads]). In the instances where RNA-LD association was apparent, HCV RNA often displayed a cap-like structure on the LD surface very reminiscent of the characteristic HCV core-positive and NS5A-positive structures

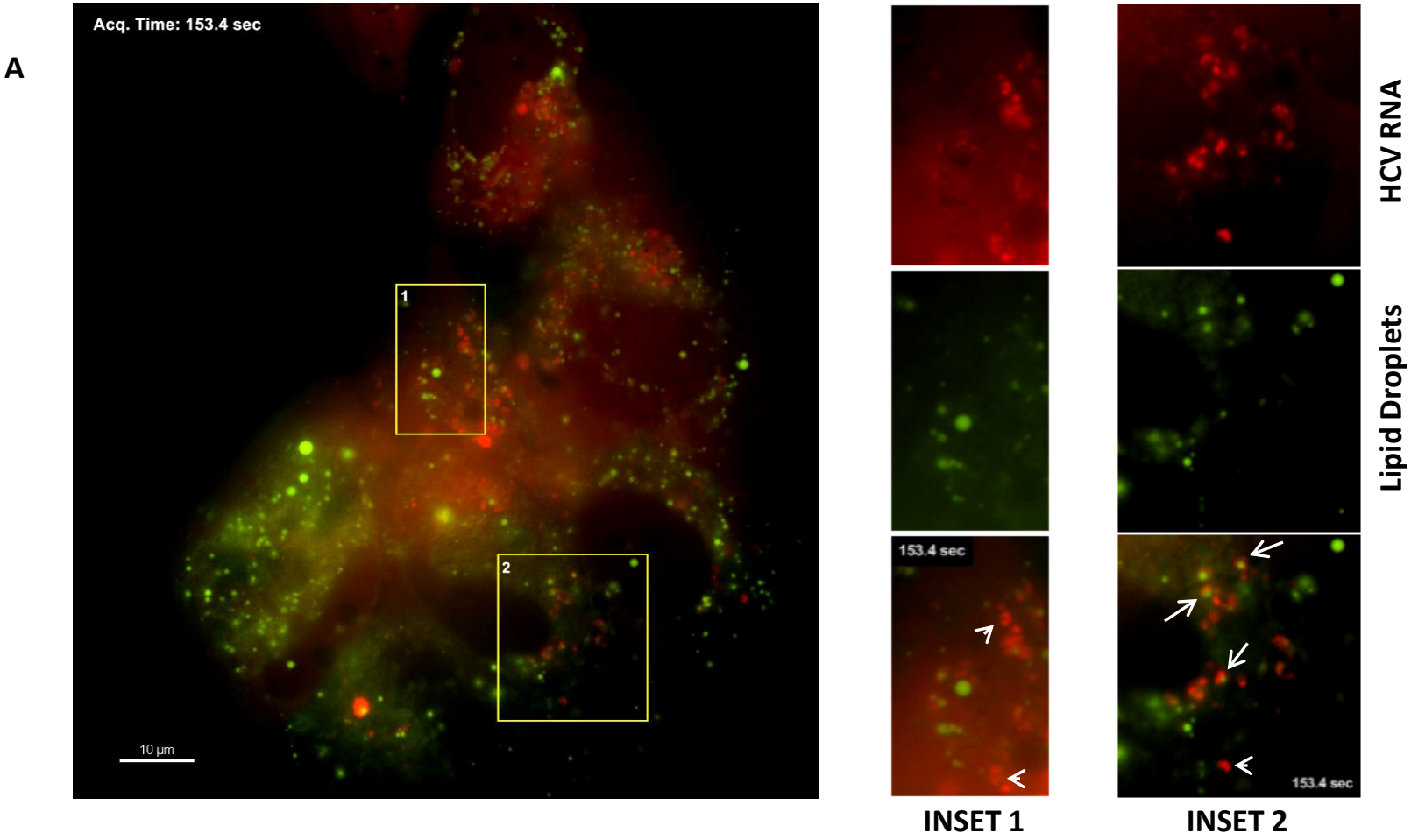


**Figure 5.11: Co-imaging of HCV RNA and lipid droplets in living Huh-7.5 +MS2.Coat-mCherry cells (Movie 5.3).**

Jc1/5A-TCM+3'UTR:24xMS2-electroporated Huh-7.5+MS2.Coat-mCherry cells were labelled with BODIPY 493/503 3 days post-electroporation, returned to culture for 2hrs and visualized by time-lapse wide-field fluorescence microscopy.

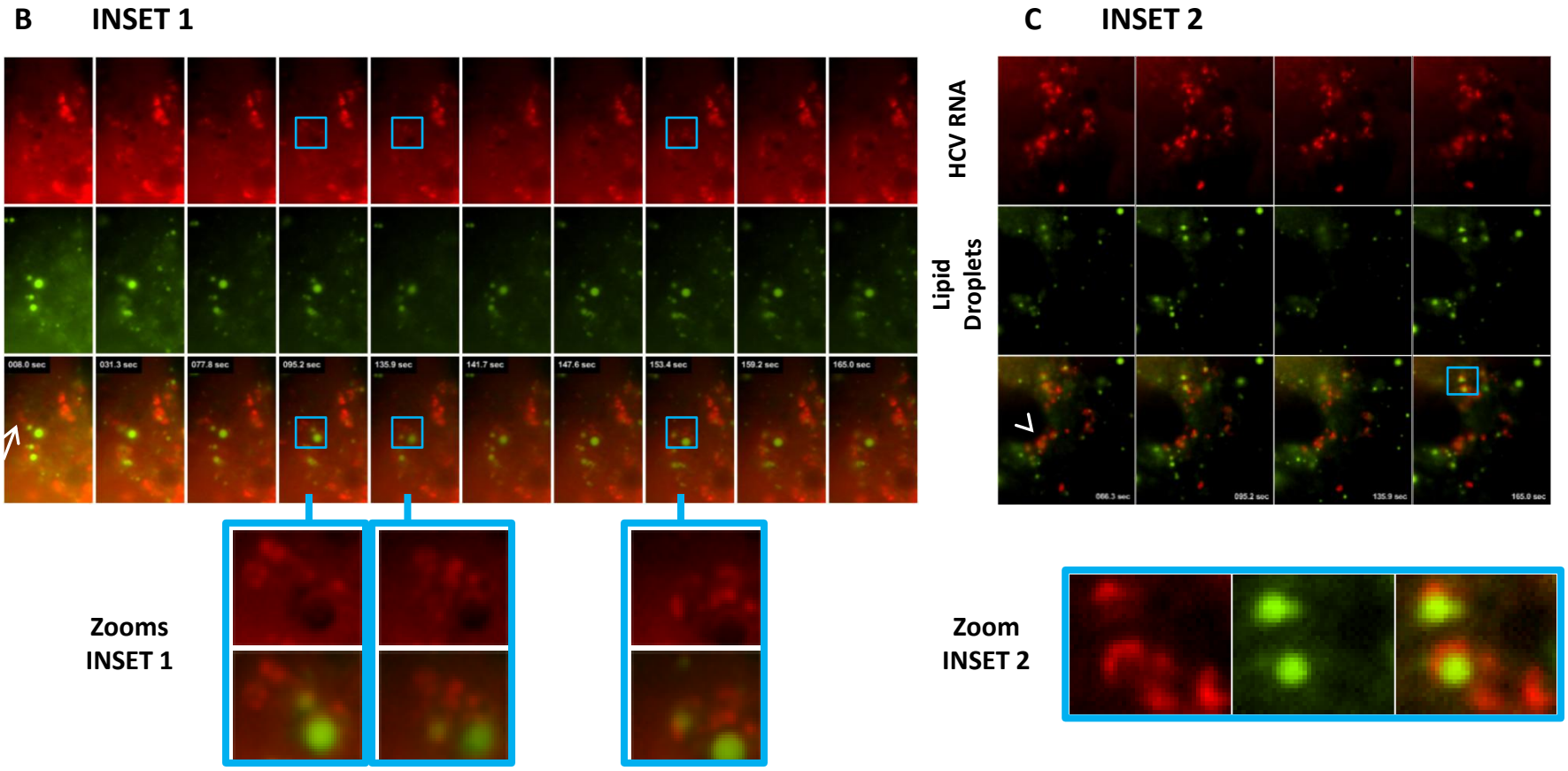


**Figure 5.11: Co-imaging of HCV RNA and lipid droplets in living Huh-7.5 +MS2.Coat-mCherry cells (Movie 5.3).**

Figure 5.11 B and C present time-lapse sequence of the insets from in Figure 5.11 A. The zoom of Inset 2 particularly depicts the cap-like structure that HCV RNA displays at the LD surface while Inset 1 illustrates an example of potential delivery of HCV RNA to LDs.

coating the LD surface (for example see Figure 5.8 and Figure 5.9). The presence of HCV RNA cap-like structures is especially apparent in the Zoom Inset of Figure 5.11 C.

Figure 5.11 B depicts the time-lapse sequence associated to the Inset 1 of Movie 5.3. In this particular example, an HCV RNA-positive structure (designated by an arrow in the initial frame) can be observed travelling towards a lipid droplet. The RNA-positive structures seem to coalesce as they move towards the LD. Especially remarkable is the last moments where the structure seemed to adopt a cap-like shape in the process of associating with the lipid droplet. This is consistent with the model of HCV RNA delivery to the lipid droplet and it is possible that for the first time we have visualized this interaction.

Moreover, when associated to the LD surface, HCV RNA seems to concentrate on one face of the LD rather than being distributed around the complete circumference of the LD. The resulting apparent polarisation of the HCV RNA is a phenomenon observed previously for HCV core capping of the LDs as previously discussed.

In summary, we have visualized HCV RNA in living cell with respect to the LD marker BODIPY. Three categories of HCV RNA-positive structures were noted: one was highly motile, one was static and associated with the lipid droplets and the third one was static in association with putative RCs. Interestingly all HCV RNA was associated with NS5A highlighting a central role for NS5A protein in the biology of HCV RNA replication and assembly. Taken together with the association of NS5A with HCV RNA and the central role of the LDs as a hub for initiation of the assembly process, we hypothesise that NS5A may deliver HCV RNA to the LD to initiate viral RNA encapsidation while still maintaining a replication function within the MW.

## 5.3 Rab18

### 5.3.1 Introduction

LDs are important organelles conserved amongst all eukaryotic and some prokaryotic cells. They have been thought to only function as inert lipid storage compartments but have now gained attention as an essential and dynamic cellular organelle (Gross and Silver, 2014; Pol et al., 2014). Indeed they appear to play multiple roles in cellular processes such as membrane organization and synthesis, trafficking of LD-bound proteins, cellular signalling, and regulation of lipid homeostasis by assembling, storing and supplying lipids in response to cellular needs (extensively reviewed in (Farese and Walther, 2009; Martin and Parton, 2006; Walther and Farese, 2009)). Furthermore as we have discussed previously they are also important in HCV assembly process. LDs are spherical organelles originating from the ER (Pol et al., 2014). They are mainly comprised of cholesterol esters and triglycerides at the core, a phospholipid monolayer and a range of LD-bound proteins relative to the different functions managed by the LDs. Of particular interest in this study were the adipocyte differentiation-related protein (ADRP) and the Ras-related small GTPase Rab18 that are LD-bound proteins involved in regulation of LD traffic.

With the advent of live cell imaging it became apparent that the LD is a dynamic organelle that naturally uses the microtubule network to traffic throughout the cytoplasm (Bostrom et al., 2005; Kunwar et al., 2011; Targett-Adams et al., 2003). This traffic is mediated by dynein and kinesin motors to shuttle to and from the microtubule organizing centre (MTOC) (Gross et al., 2007; Gross et al., 2000; Kulic et al., 2008; Welte, 2004). Both ADRP and Rab18 have been linked to lipid droplet localisation (Ozeki et al., 2005), with Rab18 appearing to displace ADRP from the LDs. Moreover

both over-expression of Rab18 and knock-down of ADRP induce an accumulation of LDs towards the cisternae membranes derived from the rough ER (Ozeki et al., 2005).

This morphological change in the localisation of the LDs is very similar to the one we and many others reported in the context of HCV infection. Moreover Rab18 has been shown to directly interact with NS5A (Salloum et al., 2013). Furthermore core protein has been shown to migrate to the LDs following maturation (Barba et al., 1997; McLauchlan et al., 2002; Moradpour et al., 1996) and consequently induces displacement of ADRP and subsequent accumulation of the LDs to ER-derived cisternae membranes similar to Rab18 (Counihan et al., 2011). Although conflicting reports emerged on that matter, HCV core has been shown to interact with Rab18 and Rab18 could be critically involved in core recruitment to the LD surface (Dansako et al., 2014). The growing list of evidence indicating that Rab18 plays an important role(s) in dynamic aspects of HCV assembly drove our investigation towards examining Rab18 using live imaging. We sought to investigate HCV RNA and NS5A traffic with respect to Rab18 using Rab18-GFP expressing cell lines. However due to time constraints we were unable to study potential HCV RNA-Rab18 interactions and in the following section only the results of studies investigating NS5A and Rab18 are presented.

### 5.3.2 Generating cell lines expressing Rab18-GFP

To further investigate the dynamic events occurring at the intersection between HCV RNA replication and initiation of the virus assembly process, we generated a cell line expressing labelled Rab18. Direct transfection of Huh-7.5 cells with an expression plasmid encoding Rab18-GFP (pRab18-EGFP plasmid (Ozeki et al., 2005)) was first performed using FuGene 6 reagent (see Chapter 2.2.8.1). Geneticin selection for approximately 3 weeks enabled selection of a polyclonal cell line expressing Rab18-GFP.

Flow cytometry was then used to perform fluorescence-activated cell sorting (FACS-sorting) with respect to the green fluorescence expressed by the cells. Cell sorting was performed using a MoFlo Astrios High Speed Cell Sorter and the Summit Software version 6.2 (Beckman Coulter, Miami, FL, USA) (See Chapter 2.2.9 for more details). Biological consequences of Rab18 ectopic expression are not fully understood despite the apparent promotion of LDs juxtaposition to the cisternae membrane of the ER (Ozeki et al., 2005), therefore FACS-sorting of Rab18-GFP-expressing cells without selection of any specific level of expression was performed to outline potential unknown side-effects.

In Figure 5.12, live fluorescence images of the cell line stably expressing Rab18-GFP are presented (Figure 5.12 A and B). Rab18 is enriched in ring-like structures as it locates to the LD surface. Rab18-GFP covered lipid droplets were predominantly found in the perinuclear region while Rab18-GFP positive structure were also less frequently distributed to the periphery of the cytoplasm. Finally a wide range of GFP fluorescence levels was observed (Figure 5.12 A) with some LDs displaying much stronger fluorescence and/or much more resilience against bleaching.

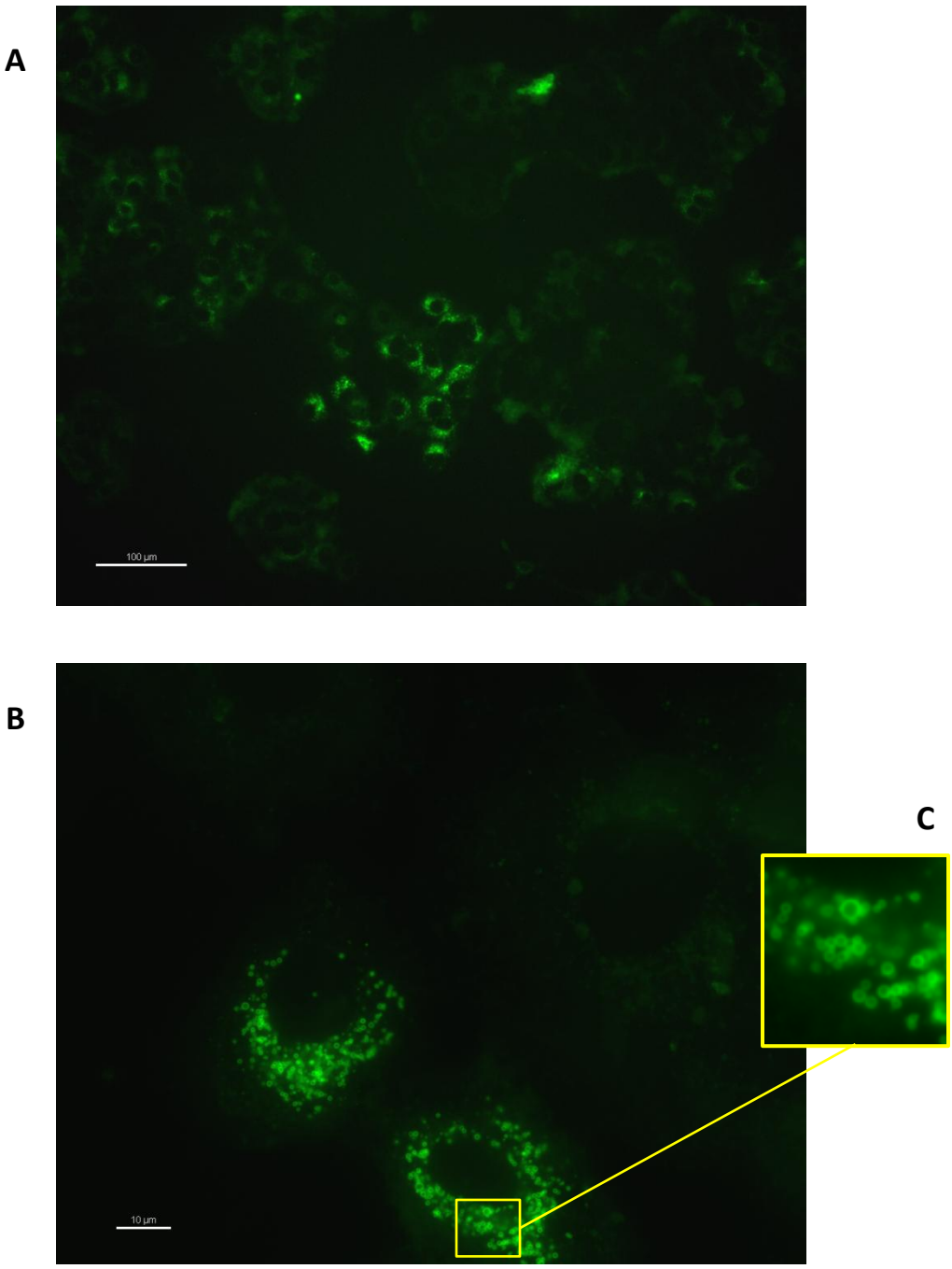


**Figure 5.12: Live fluorescence of the Huh-7.5 + Rab18-GFP cell line.**
(A) 10x objective. (B) 60x objective (C) Inset zoom
Rab18-GFP localises to ring-like structure around lipid droplets.

### 5.3.3 NS5A traffic with respect to Rab18

The generation of a Rab18-GFP cell line precluded analysis of LD and NS5A interaction using Jc1/5A-GFP as both express GFP. To overcome this we used Jc1/5A-SNAP, previously described in (Eyre et al., 2014a). This HCV Jc1 chimera derived from Jc1/5A-GFP [K1402Q] carryies a SNAP tag in place of the GFP coding sequence. This virus is able to undergo the full life cycle with minimal impact on virus production and NS5A processing. The SNAP tag enables specific labelling in living cells with a variety of fluorescently coloured dyes in a simple and non-toxic labelling process (see Section 2.6.4).

Jc1/5A-SNAP virus particles were first produced by electroporating naïve Huh-7.5 with IVT RNA and collecting supernatant after 3 days of culture. Virus samples were filtered (0.45μm) and used to infect (approx. MOI: 0.1) naive Huh-7.5 stably expressing Rab18-GFP (described Section 5.3.2). Cells were labelled at 48 hours post-infection using SNAP-Cell TMR-Star (New England Biolabs, USA) (Red fluorescence) (see Section 2.6.4) and then returned to culture for approximately 1h before imaging. Live imaging was performed using the Nikon Ti inverted fluorescent microscope as described previously (see Chapter 2.6.5 and 2.6.6).

We first examined ‘Mock’-infected cells to visualize how the Rab18-GFP coated lipid droplets were behaving in real time. LDs appeared relatively concentrated in the broad perinuclear region as previously noted. In Movie 5.4 and Figure 5.13, movement of Rab18-GFP positive structures is illustrated. Rab18 coated LDs displayed both long directional movement and more confined movement. Furthermore no relationship between their size, motility or localisation was obvious.

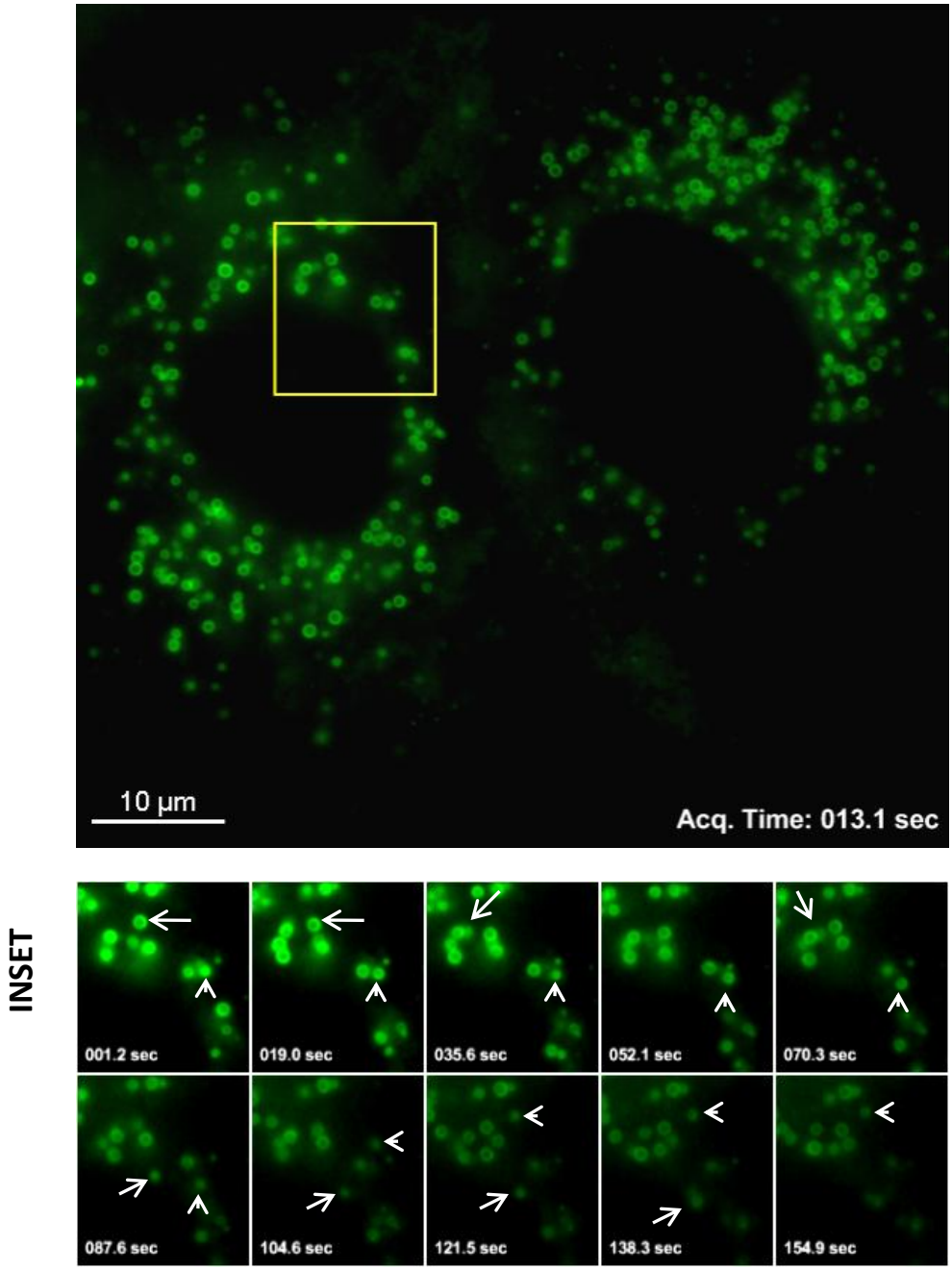


**Figure 5.13: Movement of Rab18-GFP coated lipid droplets (Movie 5.4).**

Rab18-GFP displayed both long directional movement and more confined movement in mock infected cells. Arrows and arrowheads indicate two structures displaying fast acceleration.

Next we investigated the relationship between HCV NS5A and LD in a productive infection. Figure 5.14 A and Movie 5.5 present a Jc1/5A-SNAP infected cell and depict the representative localisation and traffic of NS5A with respect to Rab18-GFP coated LDs. Static foci of NS5A-positive structures can be observed stably locating on the Rab18-GFP-positive LDs (Figure 5.14 A Inset [Arrows]). In comparison to previous observations with ADRP (Eyre et al., 2014a), NS5A localisation on LDs seemed relatively stronger. Nevertheless this observation is coherent with the published study reporting that Rab18 over-expression promotes NS5A localisation at the LDs surface (Salloum et al., 2013).

Furthermore numerous small trafficking NS5A-positive foci appear to dynamically interact with lipid droplets (Figure 5.14 B Inset [Arrowheads]). Mobile structures were observed trafficking towards and away from lipid droplets, sometimes pausing at the LD surface for various durations after which they would move away. These observations outline the potential for transient interactions of NS5A and putative RCs with Rab18-positive LDs. Exact mechanisms inducing more stable binding of NS5A to the LD surface in comparison to NS5A foci that only transiently interact before resuming traffic is not understood. Knowing that NS5A interacts with core at the LD surface in a critical step to trigger initiation of HCV assembly, it is possible that NS5A in association with HCV RNA dynamically ‘samples’ the LD population prior to more stable association with core-coated LDs to deliver RNA and initiate the last steps of the viral life cycle.

Due to time constraints imaging of HCV RNA in conjunction to Rab18 was not performed but will be pursued in future studies as it may provide a greater understanding of the events occurring at Rab18-positive virus assembly sites.

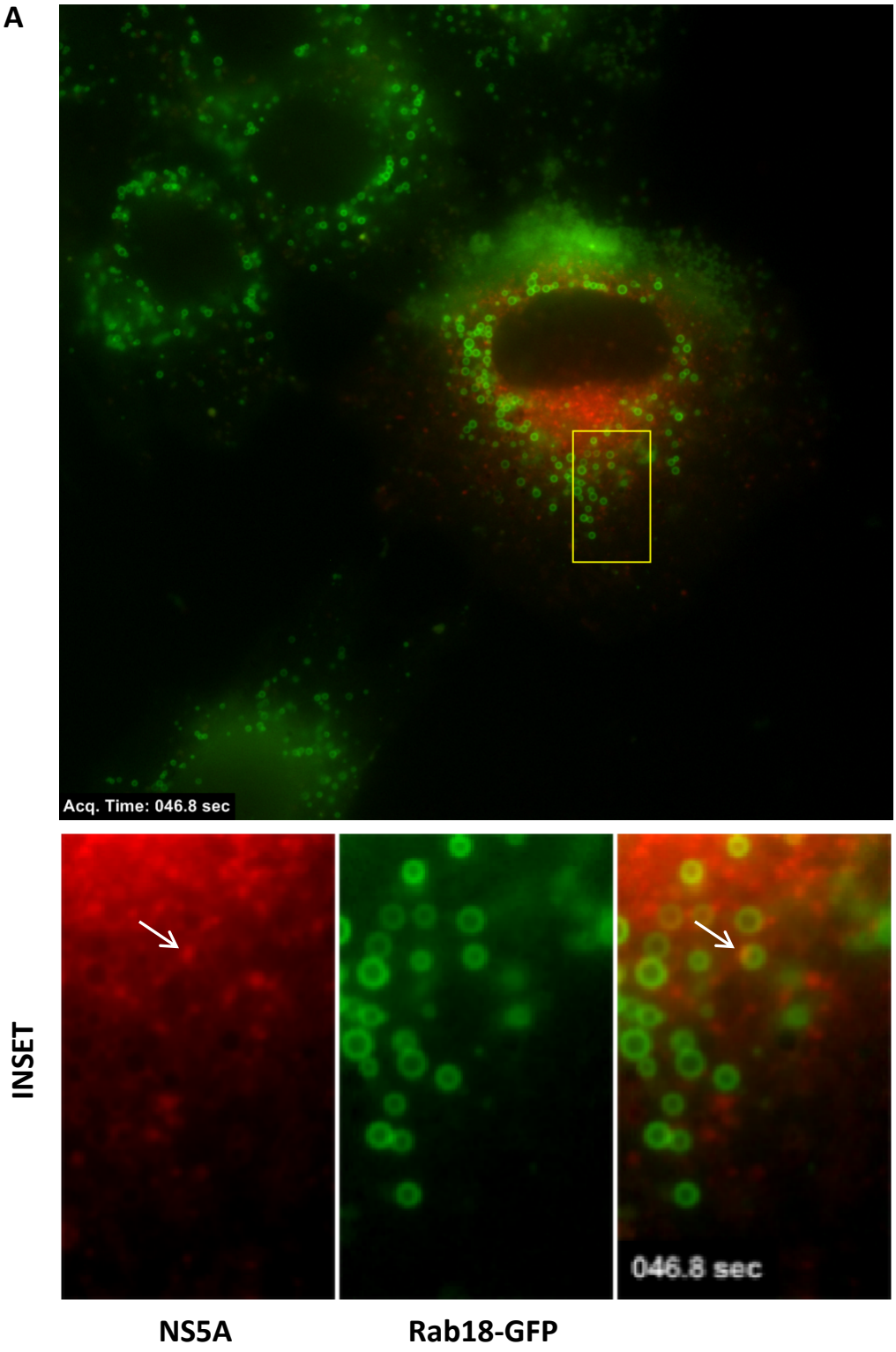


**Figure 5.14: Co-imaging of NS5A and Rab18-GFP in living Huh-7.5+Rab18-GFP cells (Movie 5.5)**

Jc1/5A-SNAP-infected Huh-7.5+Rab18-GFP cells were labelled with SNAP-Cell TMR-Star (red) 2 days post-infection, returned to culture for 1hr and visualized by time-lapse wide-field fluorescence microscopy.

**B** **Figure 5.14: Co-imaging of NS5A and Rab18-GFP in living Huh-7.5+Rab18-GFP cells (Movie 5.5)**
Figure 5.14 B presents a time lapse sequence of the Inset from Figure 5.14 A.

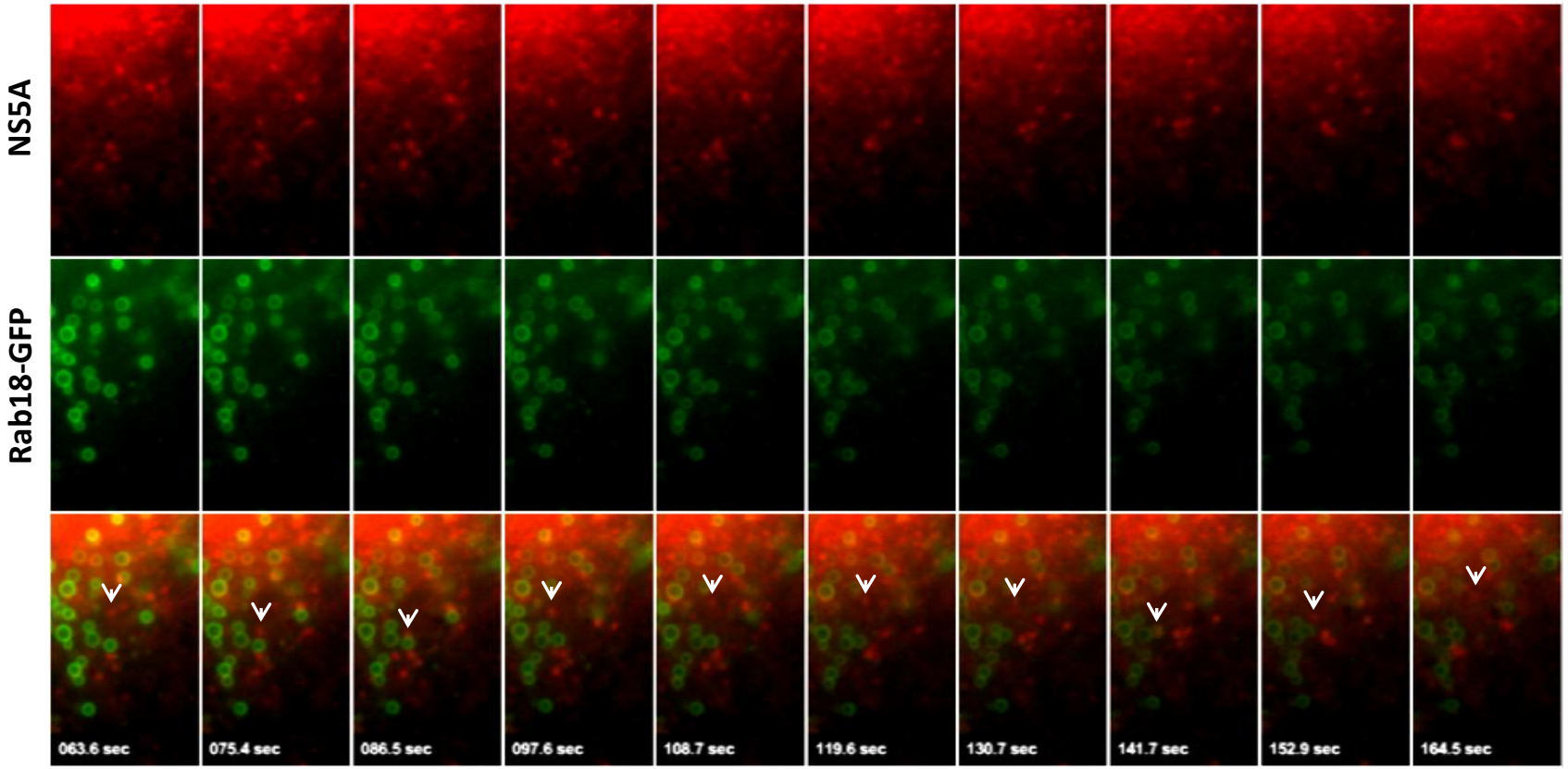

## 5.4 Discussion

Hepatitis C virus displays a wide range of intricate mechanisms to hijack natural intracellular pathways to its advantage. The use of live cell imaging to investigate viral life cycles and viral-host interactions have previously reported new insights that could not be appreciated outside of the real-time experimental models developed (Boireau et al., 2007; Miorin et al., 2008). In the case of HCV research, division of NS5A into subclasses depending on their dynamics has only been highlighted by live cell imaging (Eyre et al., 2014a; Wolk et al., 2008). To further enhance our understanding of the underlying biological properties of each class of NS5A dynamics previously observed, we generated an HCV chimera to enable visualization of HCV RNA during the life cycle and thus uncover further details of the NS5A structures. In this chapter we have used the MS2 based system in conjunction with tagged-NS5A, BODIPY 493 / 503 and tagged-Rab18 in order to illustrate aspects of the viral life cycle at the intersection of RNA replication and initiation of assembly stages.

Similarities between NS5A and RNA positives structures were striking in single colour analysis in the previous chapter. Imaging of HCV RNA with respect to NS5A illustrated that all RNA-positive structures visibly appeared positive for NS5A whatever their size or movement. However a small proportion of trafficking NS5A structures was not enriched with viral RNA, although this second category of NS5A displayed the same apparent characteristics as the HCV RNA-positive subclass of small motile units. We hypothesised that two different categories of small NS5A-positive mobile structures could be actually distinguished depending on their RNA content, where double positive structures could dictate delivery of RNA through NS5A and single NS5A structures could perform another specific function. Alternatively NS5A

structures devoid of HCV RNA could actually carry small amount of HCV RNA lower than the detection threshold.

Lipid droplets have been shown to be critically involved as a transitory platform necessary for assembly of new virions, especially hosting the determining core-NS5A interaction occurring before viral RNA encapsidation. Simultaneous visualization of HCV RNA and LDs displayed a specific localisation pattern of HCV RNA. First of all, RNA was associating strongly with LDs and accumulated on one side of the LDs. Moreover static structures were also observed that were not directly in contact or in close proximity to LDs suggesting two different subclasses of static structures could possibly co-exist and perform different biological roles. Integration of these observations with what is known of the HCV life cycle suggests that the static HCV RNA structure devoid of LDs (see Section 5.2.3) could represent the accumulation of HCV RNA produced by the RC. Moreover the motile double-positive structures could represent the delivery of HCV RNA (see Section 5.1.3) to the sites of core-NS5A interaction at the LDs surface. These observations were supported by visualization of NS5A traffic with respect to Rab18-GFP in Section 5.3.3. Replication of Jc1/5A-SNAP virus in Huh-7.5 cells stably expressing Rab18-GFP illustrated the potential for dynamic and transient interactions of NS5A-positive small and motile structures trafficking back and forth towards and away from LDs. While many instances displayed potential short-term interactions where NS5A structures bounced back and resumed traffic, numerous static NS5A-positive foci could be distinguished that were juxtaposed to the LD surface.

However, observations generated using the Rab18-GFP model were hindered by the relatively quick bleaching of GFP. Replacing GFP with a more robust fluorophore could represent a useful optimisation, but GFP is a relatively bright and photo-stable

fluorescent protein and this would technically only achieve a marginal improvement. Therefore improvement associated with the use of a more sensitive system for microscopy may enable long-term imaging and investigation of the fate of LDs once recruited to the perinuclear region. Further work, especially imaging of HCV RNA in the Huh-7.5 cell line expressing both Rab18-GFP and MS2.Coat-mCherry will help us further understand the interactions at play. Moreover performing live imaging using combinations of more than two fluorophores would especially enhance our understanding of the interactions and dynamics involved. For instance, HCV RNA could be observed simultaneously with LDs and NS5A to reveal more details about HCV RNA delivery at the LD interface during early assembly events.

# Chapter 6:

# Discussion and Future Directions

Hepatitis C virus induced liver disease (fibrosis, cirrhosis, HCC) is a major worldwide health problem with 2-3% of the world population being infected and between 350,000 and 500,000 people dying every year according to the WHO. Despite development of direct acting antiviral (DAA) combination therapies (reviewed in (Chukkapalli and Randall, 2014; Eyre et al., 2014b)) and the associated improvement in management of HCV infection, there is the possibility for the emergence of DAA resistance mutations. This results as the HCV genome can mutate in the face of selective pressure resulting in drug resistance mutations and together with the high cost of DAA therapy these factors will likely impact upon the success of these therapies in the immediate future. Collectively this highlights the need for basic research that underpins therapeutic innovations through a better understanding of the intricate virus-host interactions involved in the HCV life cycle.

Our understanding of the HCV life cycle at the molecular level has made significant progress since the discovery of the virus in 1989 (Choo et al., 1989). However it took approximately 10 years until we could study HCV replication in cultured cells with the development of the first HCV replicon system in 1999. HCV replicons enable autonomous replication of HCV RNA and expression of viral non-structural proteins in Huh-7 cells and provide a way of investigating the molecular basis underpinning HCV

RNA replication and translation (Lohmann et al., 1999). Furthermore, with the development of the HCV JFH-1 infectious cell culture model in 2005, the entire HCV life cycle could be studied in detail at the molecular level (Lindenbach et al., 2005; Wakita et al., 2005; Zhong et al., 2005). Collectively this step-wise progress to study HCV replication *in vitro* resulted in an understanding of HCV replication and protein function at the molecular level that facilitated development of the current wave of DAAs.

Virus-host interactions are key components involved at every step of the HCV life cycle. However the study of the dynamic nature of these interactions is often limited by the use of conventional methods such as static imaging of fixed samples that provide information at a particular point in time. Therefore emergence of live imaging techniques enabling real-time visualization of viral proteins together with host factors in single infected cells have galvanized our understanding of the intricate cross-talk between host and viral factors. For instance, sequential redistribution of HIV-1 GAG protein was characterised using tetracysteine labelling technology in the context of real-time imaging (Perlman and Resh, 2006). This study revealed for the first time the traffic of the retroviral GAG protein from the perinuclear compartment where it is synthesised, through multi-vesicular bodies (MVB) to the plasma-membrane. In respect to HCV and this thesis, we have used live cell imaging to investigate both the dynamic nature of HCV RNA and NS5A protein to reveal new insights into their interactions as it relates to the viral life cycle. NS5A's lack of enzymatic activity and the crucial although not fully understood roles in both RNA replication and virion assembly has generated speculation with respect to its precise functions in these processes. Using live cell imaging, work from our laboratory and others has revealed that NS5A segregates into two specific compartments and is involved dynamically with host factors such as

VAP-A and Rab5A (Eyre et al., 2014a; Wolk et al., 2008). NS5A localised to structures that generally accumulated around the nucleus and remained relatively static (Eyre et al., 2014a; Wolk et al., 2008). Secondly, NS5A is also enriched in smaller foci that displayed sporadic movement along the microtubule network punctuated by burst of rapid accelerations (Eyre et al., 2014a; Wolk et al., 2008). This raises the question as to the relative roles of these different populations of NS5A. It is well known that NS5A is present within the RC fulfilling roles in HCV RNA replication, however based on current literature, it is not clear which class of structures, static or motile, most likely represent active replication complexes. Furthermore the function of the fast moving small structures is unknown and it is possible that the mobility of these structures may represent a mechanism whereby HCV RNA is transported from RC to sites of assembly. If this is the case then these fast moving structures should contain HCV RNA. To further characterise NS5A's role in HCV life cycle and investigate the composition of these fast motile NS5A structures we endeavoured to generate a system to simultaneously track in the context of live cell imaging HCV RNA and NS5A in real-time and hence this was a major focus of this thesis.

The ability of NS5A to bind HCV RNA has been shown on multiple occasions as NS5A has a predicted RNA binding motif (Tellinghuisen et al., 2005) and furthermore can bind HCV RNA *in vitro* (Foster et al., 2010; Huang et al., 2005). In addition, results from our RNA-protein complex immunoprecipitation studies described in Chapter 5 would further confirm that NS5A is associated with HCV RNA during the viral life cycle. Moreover NS5A was found to co-localise in fixed cells with HCV RNA detected using an antibody directed against dsRNA (putative RI) in HCV JFH-1 infected cells (Targett-Adams et al., 2008) and nascent RNA in fixed cells harbouring a Con1 replicon (Moradpour et al., 2004). Furthermore the fate of the viral RNA at the

site of synthesis within the RCs and at the site of virion biogenesis remains a vastly unexplored subject due to limitations of the current techniques. Indeed visualization of HCV RNA has been limited to fixed samples by either *in situ* hybridization (ISH), fluorescent *in situ* hybridization (FISH), immunofluorescence labelling with anti-dsRNA antibody (Targett-Adams et al., 2008), or actinomycin D-coupled broad RNA labelling such as BrUTP (Moradpour et al., 2004; Paul et al., 2013), Click-iT® chemistry RNA imaging (Life Technologies) (Coller et al., 2012), or RiboGreen® in live cells (Life Technologies) (Coller et al., 2012). While these studies have been informative, they do not greatly enhance our understanding of the dynamic nature of RNA synthesis and traffic.

To overcome the above limitations and in order to further characterize the composition of the NS5A-positive structures with regards to HCV RNA and the dynamics of the spatial and temporal organisation of the HCV life cycle at the intersection of replication and assembly, we generated for the first time a novel tagged-HCV construct capable of reporting in real-time the localisation and traffic of the full-length replicating HCV RNA.

In 1998, visualization of cellular mRNA in living yeast cells was achieved for the first time by E. Bertrand and colleagues (Bertrand et al., 1998) using a system based on the MS2 bacteriophage. As we detailed in previous chapters this system is based on the high affinity of the MS2 bacteriophage coat protein for the stem loop carried by the bacteriophage RNA genome (Figure 1.10). Since its inception this technique has been used to study a number of cellular and viral RNAs including murine leukaemia virus (MLV) RNA traffic (Basyuk et al., 2003), the human immunodeficiency virus type 1 (HIV-1) transcription cycle (Boireau et al., 2007; Maiuri et al., 2011) and HIV-1 mRNA biogenesis (Jouvenet et al., 2008). In particular relevance to this thesis is the

work by Miorin and colleagues who engineered MS2 stem loop insertion into the closely related flavivirus TBEV to observe TBEV RNA localisation (Miorin et al., 2008; Miorin et al., 2013). These TBEV experiments indicated that in fact a flavivirus genome could tolerate MS2 stem loop insertion and prompted us to investigate HCV RNA localisation in infected cells. In order to observe HCV RNA in living cells, we inserted MS2 bacteriophage stem loop repeats within the 3' untranslated region of the viral genome (Figure 3.3) and initiated replication within a Huh-7.5 cell line expression the fusion reporter protein between the mCherry fluorescent protein and the MS2 bacteriophage coat protein.

MS2 stem loop-tagged HCV genomes maintained replication both in the context of a HCV subgenomic replicon and in a HCV full-length Jc1 model despite the impact on fitness induced by such a substantial insertion. Although the longest array of repeats (24x ≈ 1.3 kb) should have theoretically presented the greatest impact in comparison to the smaller arrays that range from 6 to 12 MS2 stem loop repeats, it interestingly induced the smallest handicap on viral fitness. The mechanisms that underpin this observation are not fully understood, but we hypothesise that this could be related to a potential change in the secondary structure of the viral RNA induced by the inserted stem loops. The HCV 3' untranslated regions is composed of a series of complex secondary structures (as explained previously in Chapter 1.2.5 and Chapter 3.4) (Blight and Rice, 1997), composed of 3 different regions: the variable region, the Poly-U tract and the X-region containing three stem loops (namely SL1, SL2 and SL3). The long range interaction between SL2 and SL3.2 (located in the coding sequence of NS5B) better known as the kissing-loop interaction was shown to be of critical importance for HCV replication (Friebe et al., 2005). It is not inconceivable that insertion of 24 stem loops is better suited to the retention of this kissing-loop interaction than that of the

smaller insertions. One could envisage that above a certain number of MS2 stem loop repeats, the increased flexibility associated could result in the restoration of the long range interaction of the kissing-loop explaining the higher fitness encountered with an insertion of 24 stem loops. This type of interpretation could be verified using computational biology to predict the 3-dimensional models of the HCV RNA depending on the number of insertions. Consequently, further optimization could be performed both in terms of the minimal number of insertions and more importantly in terms of flexibility of the oligonucleotide linker between the stem loops to minimize overall the impact on viral fitness.

RNA viruses are believed to be genuinely intolerant towards insertion and especially unnecessary coding sequence. However the capacity of HCV chimeras to maintain the MS2 stem loop arrays after more than 8 days is remarkable. In accordance a recent study using transposon induced mutagenesis to randomly insert a 15-nt tag throughout the HCV genome highlighted numerous sites which were tolerant for insertion (Remenyi et al., 2014). This revealed that the HCV genome is more plastic than was initially thought. Interestingly, the site within the HCV 3'UTR used for our MS2 stem loops insertion was also detected by this study. It is also possible that the MS2 stem loop insertion may induce compensatory mutations within the HCV genome to either enhance protein-protein interactions or alter RNA secondary structure. This led us to perform a deep sequencing analysis of two cell lines harbouring 24xMS2-tagged HCV JFH-1-based genomes (See Chapter 3.2.4). However none of the single nucleotide polymorphism (SNP) identified by deep sequencing were classified as predominant amongst the viral population. Broader investigations involving more clones and different insertion sizes could yield refined results providing determinant SNPs associated with improved viral fitness. Alternatively, it is possible that adaptations in

the 5'UTR or 3'UTR (which were not subjected to deep sequencing analysis) may have occurred to compensate for the MS2 stem loop-induced changes in the size and secondary structure of the 3'UTR. Investigation of the nature and impact of such changes could also enable development of MS2 stem loop-tagged genomes with improved fitness. Nevertheless, such studies would be technically challenging due the complexity of the HCV 3'UTR such as the high degree of secondary structure and the repetitive polyU sequence.

Replication of the MS2-tagged HCV genomes drove specific reorganisation of the MS2 coat diffuse fluorescence in what is the first real-time visualization of replicative HCV RNA in living cells. Interestingly, the HCV RNA discrete foci displayed striking similarities to that of NS5A-positive structures (Eyre et al., 2014a; Wolk et al., 2008) in terms of structure motility, with small discrete foci often displaying saltatory movement characteristic of MT network-associated traffic and larger and relatively static structures occasionally displaying spasmodic and confined movement. The simultaneous imaging of HCV RNA and NS5A in living cells further explained these similarities as HCV RNA and NS5A were shown to co-localise in both small and larger structures and to co-traffic in mobile discrete foci (Figure 5.6 and Movie 5.2). More precisely, all HCV RNA-positive structures were also positive for NS5A whereas in contrast a subset of NS5A-positive structures was devoid of viral RNA. These observations taken with the literature previously discussed are consistent with evidence that NS5A has a strong affinity for HCV RNA (Foster et al., 2010; Huang et al., 2005; Tellinghuisen et al., 2005) and suggests that viral RNA traffic is conditional on that of NS5A and/or other RC components. In conclusion the two different subsets of NS5A-

positive structures characterised by their HCV RNA content are probably fulfilling two different roles or participating in different stages in the HCV life cycle.

To address this question we initiated a study to investigate the dynamic interactions of NS5A and HCV RNA with the lipid droplets (LD), a cellular organelle known to be essential for HCV assembly (Miyanari et al., 2007). Real-time visualisation of HCV RNA simultaneously with the LD enabled us to distinguish two sub-types of static structures in living cells: one being associated in a cap-like fashion at the LD surface while the second was not associated with LDs (Figure 5.11 and Movie 5.3). Moreover from the previous live imaging performed we have shown that all of the HCV RNA-positive foci are NS5A positive as well including these two subtypes of static structures. This distinction is consistent with the HCV life cycle model displaying two potential static sites: the RCs harbouring RNA replication (Paul et al., 2013; Romero-Brey et al., 2012; Targett-Adams et al., 2008) and the LDs where core and NS5A accumulates in order to initiate new virion assembly (Appel et al., 2008; Masaki et al., 2008; Miyanari et al., 2007; Paul et al., 2014; Salloum et al., 2013).

Consequently, we hypothesise that the static HCV RNA structure observed at the LD surface is HCV RNA ready for (or in) the process of encapsidation. This hypothesis is supported by the live imaging from the Zoom of Figure 5.11 Inset 1 where an HCV RNA-positive structure appears to shift in the direction of a LD and pre-emptively shape in a semi-circular manner adjusting to the LD surface before appearing to dock onto it. Moreover co-imaging of NS5A with the LD marker Rab18 enabled illustration of the dynamics of NS5A and its transient interaction with the LD surface. Although in some instances NS5A is anchored on the LD surface, numerous NS5A-positive motile foci can be observed travelling throughout the cytoplasm and transiently localising to the LD surface. We hypothesised that this short-term contact may be relevant to NS5A

is proposed HCV RNA-delivery function where NS5A may sample the LD surface prior to interaction with core to initiate the assembly process (Appel et al., 2008; Masaki et al., 2008). According to the existing model, core would then be retrieved towards the ER membrane where the budding of new virions occurs (Miyanari et al., 2007). Deeper insights into the interactions at play could be achieved by further quantification of the segregations observed such as the proportion of RNA localised at the LD surface, or the exact proportion HCV RNA-negative NS5A-positive structures. Furthermore, long-term imaging experiments and/or additional labelling and imaging of other relevant viral and/or host cell factors could help to distinguish HCV RNA localisation and interactions that are characteristic of productive HCV assembly events.

The MS2-tagging system for real-time RNA visualization enables observation of all viral positive-strand RNA genomes in comparison to the anti-dsRNA immunofluorescence studies such as that of Targett-Adams and colleagues (Targett-Adams et al., 2008) or in Chapter 5 which identify replication intermediates (i.e. sign of active replication). Consequently the MS2-based technique is limited to visualization of both active and inactive RCs, with respect to HCV RNA replication. Although it would be technically challenging, tagging the negative strand of HCV RNA to selectively visualize active RCs would provide a deeper understanding of the properties of active RCs and their evolution over time. In an extension of the published morphological studies of RCs (Ferraris et al., 2010; Paul et al., 2013; Romero-Brey et al., 2012), real-time imaging of HCV RNA coupled with a transmission electron microscopy (TEM) study (e.g. through correlative EM) would greatly enhance our understanding of the fate of RCs and their possible inactivation during the HCV life cycle. Moreover investigating the localisation of both positive- and negative-strand RNA would be

interesting to enable greater distinction between replication and assembly associated events.

Furthermore the technique of fluorescence recovery after photobleaching (FRAP) could be employed to study the degree of mobility of the HCV RNA specific sub-types using similar method as in (Miorin et al., 2013). For instance by performing FRAP on HCV RNA-positive static foci (putative RCs) or on HCV RNA-positive cap-like structures localised around LDs we could study the accessibility and the degree of diffusion of the HCV RNA within the RCs or the rate of delivery of HCV RNA to assembly sites at the LD surface.

Investigation of additional cellular organelle(s), host protein(s) and viral protein(s) markers would also contribute greatly towards a better understanding of the HCV life cycle with the potential to study new facets of the processes involved. In an instance particularly relevant to this thesis, the study of the E1-E2 heterodimer complex would provide extensive information on the fate of the HCV RNA-NS5A-core complex, as the E1-E2 dimer locates on the viral particle membrane and together with core is a critical marker of the biogenesis of the new virions. As explained in Chapter 1.2.7, glycoproteins E1 and E2 form heterodimers which are incorporated on newly formed virions (Brazzoli et al., 2005; Michalak et al., 1997; Op De Beeck et al., 2000; Patel et al., 2001; Yi et al., 1997). Tracking of the E1-E2 complex in live imaging would indubitably reveal important aspects of the dynamics of HCV virion biogenesis. In order to generate this new model we propose to adapt the split fluorescent technology to the E1-E2 heterodimer by identifying sites in E1 and E2 permissive for insertion (such as the described for E1 in (Merz et al., 2011)). This could be achieved by insertion of the complementary halves of one fluorescent protein in E1 and E2 coding sequences according to the predicted three-dimensional model of the E1-E2 complex

(Nayak et al., 2014). Interaction subsequent to correct folding of the functional complex would generate fluorescence and therefore specifically report the localisation of E1-E2 heterodimers. In addition targeting precise host factors whose role or cellular localisation are relevant to specific stages of the viral life cycle would enhance our understanding of these events. For example apolipoprotein E (ApoE) is a host factor essential for HCV virion production (Chang et al., 2007). ApoE has been shown to interact with NS5A (Benga et al., 2010) and is incorporated into the HCV lipoviral particle (Gastaminza et al., 2008). Due to its relevance in assembly, ApoE has previously been visualized in real-time in the context of viral particle secretion (Coller et al., 2012). Nevertheless live cell imaging of ApoE with respect to HCV RNA and NS5A localisation and traffic would greatly enhance our understanding of the sequential organisation of HCV RNA encapsidation and viral budding stages.

Finally real-time visualisation of fluorescence resonance energy transfer (FRET) between two interacting adequately tagged-proteins in living cells could be another interesting extension of the live cell imaging of HCV RNA. Furthermore the recent published functional map of the HCV genome (Remenyi et al., 2014) has revealed a number of candidate sites for fluorescent tagging of viral proteins. This map potentially enables insertion of FRET donor/acceptor pairs in different interacting-partners within the HCV genome. Hence multiple interactions could be investigated such as HCV RNA interacting-partners in real-time or visualization of HCV RNA traffic with respect to protein-protein interaction (viral and/or host proteins). Using such techniques we could for instance study the dynamics of the HCV core-NS5A interaction at the LD with respect to HCV RNA traffic and putative delivery. This approach has the potential to reveal new details about the sequential and spatial organisation of stages of the HCV life cycle and would only be limited by the number of fluorophore available.

In summary, live cell imaging has proven to be a powerful tool to investigate the HCV life cycle by providing a direct insight into the dynamic events occurring that are not readily apparent using conventional static microscopy. Tracking viral RNA during the complete HCV replication cycle enables the opportunity to study all the events linking RNA replication to the viral assembly. We have shown here interactions at play between NS5A, LDs and HCV RNA and potentially illustrate the delivery of RNA to putative sites of RNA encapsidation for the first time. This is summarised in Figure 6.1 in which we propose that after synthesis within the RCs, HCV RNA travels via the MT-network in association with NS5A towards core-coated LDs which are juxtaposed on the cisternae face the ER. There core-NS5A interaction would enable delivery of HCV RNA to initiate its subsequent encapsidation followed by virion morphogenesis mediated by budding into the ER and the later stages of viral egress. Simultaneous imaging of other viral proteins and/or host factors together with HCV RNA will provide further detailed understanding of the events involved in HCV RNA replication and virus particle assembly and secretion. Finally, the techniques and understanding developed here may be readily translated to similar studies of other RNA viruses.

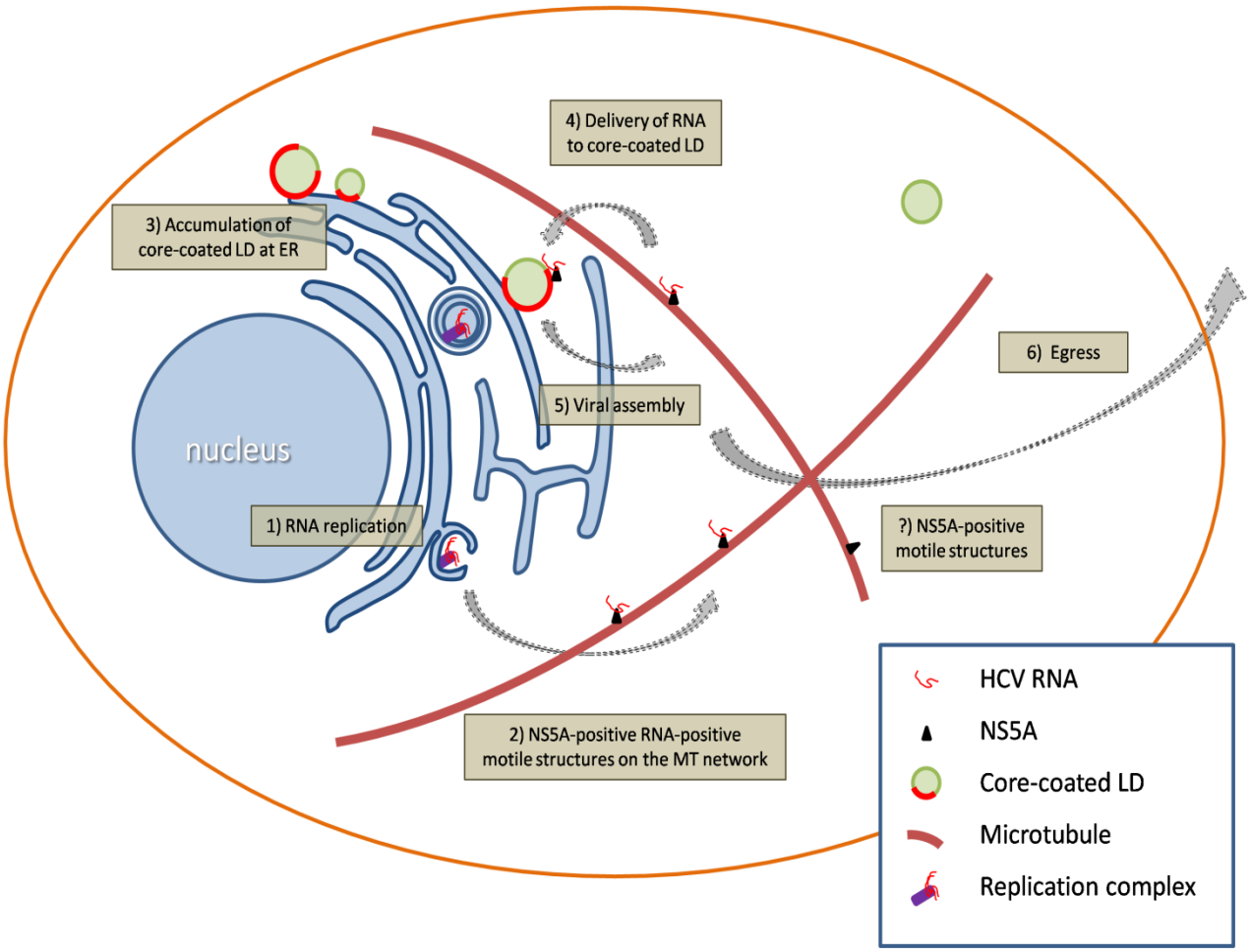


**Figure 6.1: Schematic model of HCV replication and assembly.**
(1) HCV RNA is synthesised by the RCs. (2-3) HCV RNA travels via the MT-network in association with NS5A towards core-coated LDs which are juxtaposed on the cisternae face of the ER. (4) There core-NS5A interaction enables delivery of HCV RNA to initiate subsequent encapsidation, followed by virion morphogenesis mediated by budding into the ER (5) and the later stages of viral egress (6).

# Appendix I – Buffers and Solutions

**Solutions obtained from the CSU (Central Services Unit), School of Biological Sciences, the University of Adelaide:**

- FCS (Foetal Calf Serum)
- 20% Glucose solution
- 10x GTS buffer
- 1M KCl solution
- Luria agar plates
- Luria agar + Ampicillin plates
- Luria broth
- 1M $MgCl_2$ solution
- 1x and 20x PBS (phosphate buffered saline) solutions
- 0.85% saline solution
- SOC Medium
- 4M NaCl solution
- 20x TAE buffer
- 10x TBS buffer
- Tris solutions (different concentration and pH)
- Tryptan Blue
- Trypsin-EDTA

**Solution composition:**

| | |
|---|---|
| Cell Lysis Buffer<br>*(Western blot)* | 50 mM of Tris (from pH=8 solution)<br>150 mM of NaCl<br>1 % IGEPAL CA-630 |
| SDS-PAGE Running Buffer<br>*(Western blot)* | 1x GTS solution in $dH_2O$<br>(14.4 g Glycine)<br>(30 g Tris)<br>(10 g SDS) |
| SDS-PAGE Transfer Buffer<br>*(Western blot)* | 0.3 % tris(hydroxymethyl)aminomethane [Tris]<br>1.44 % Glycine<br>20 % (v/v) Methanol |
| 5x Laemmli Sample Buffer (50 mL)<br>*(Western Blot)* | 3.8 mL of $dH_2O$<br>1 mL of 0.5 M Tris-HCl (pH = 6.8)<br>0.8 mL of glycerol<br>1.6 mL of 10 % SDS (w:v)<br>0.4 mL of 2-mercaptoethanol<br>0.4 mL of 1 % bromophenol blue (w:v) |

| | |
|---|---|
| 10x TBS solution<br>(1 L) | 87.66 g NaCl<br>30.28 g Tris<br>Prepared in MQ Water (pH = 7.5) |
| T-TBS washing solution<br>*(Western blot)* | 1x TBS buffer in $dH_2O$<br>0.1 % Tween® 20 |
| Polysome Lysis Buffer<br>*(Protein-RNA complex immunoprecipitation)* | 100 mM of KCL<br>5 mM of $MgCl_2$<br>0.5 % of IGEPAL CA-630<br>1 mM of DTT (DiThioThreitol)<br>10 mM HEPES<br>100 U/mL of RNAse inhibitor<br>25 U/mL of Protease inhibitor cocktail |
| TE Buffer<br>(*Deep sequencing*) | 10 mM Tris-Cl<br>1 mM EDTA<br>pH 8.0 |
| FlAsH labelling solutions<br>(*Live cell imaging*) | HBSS[Glucose] - Preparation detailed in Chapter 2.6.2.1<br>FlAsH Staining solution - Preparation detailed in Chapter 2.6.2.2<br>FlAsH Washing solution - Preparation detailed in Chapter 2.6.2.3 |

**Competent cell used for transformation:**

The *E.coli* α-Select Chemically Competent Cells (Bioline$^{TM}$) of the genotype deoR endA1 recA1reIA1 gyrA96 hsdR17($r_k^- m_k^-$) supE44 thi-1 Δ(lacZY-argFV169) Φ80δlacZΔM15F$^-$y$^-$ were used for bacterial transformation.

# Appendix II - Antibodies

| Target antigen | Type | Concentration | Origin |
|---|---|---|---|
| **Primary** | | | |
| FLAG | Rabbit anti-FLAG antibody (#F7425) | 1 in 200 | Sigma-Aldrich |
| NS3 | Mouse anti-NS3 antibody | 1 in 200 | Biovision |
| dsRNA | Mouse anti-dsRNA antibody (J2) | 1 in 200 | English and Scientific Consulting Kft. |
| Core | RR8 - Rabbit anti-Core | 1 in 200 | Generously provided by Michinori Kohara (Tokyo Metropolitan Institute of Medical Science, Tokyo, Japan) |
| NS5A | 9E10 - Mouse anti-NS5A antibody | 1 in 200 | Generously provided by Charles Rice (Rockefeller University, New York, USA) |
| HCV antigens | Human anti-HCV antiserum | | Prepared as previously described (Eyre et al., 2009) |
| β-Actin *(Western blot)* | anti- β-Actin (AC-15) | 1 in 15,000 | Sigma-Aldrich |
| mCherry *(Western blot)* | anti-mCherry | 1 in 15,000 | Biovision (#5993-100) |

| | | | |
|---|---|---|---|
| **Secondary** | | | |
| Rabbit antibody | Alexa Fluor anti-rabbit 488 | 1 in 200 | Life Technologies |
| Mouse antibody | Alexa Fluor anti-mouse 555 | 1 in 200 | Life Technologies |
| Mouse antibody | HRP-conjugated anti-mouse antibody | 1 in 10,000 | Thermo Scientific |
| **Dye** | | | |
| DAPI | | | |
| Tetracysteine -tag | FlAsH | Detailed in Chapter 2.6.2 | Generously provided by Stuart Turville (The Kirby Institute, Sydney, Australia) |
| Lipid Droplets | BODIPY 493 (neutral lipid stain) | Detailed in Chapter 2.6.3 | Sigma-Aldrich |
| SNAP-tag | SNAP-Cell TMR-Star | Detailed in Chapter 2.6.4 | NEB |

# Appendix III - Plasmids

- ***pGEM®-T Easy Vector (Promega):***

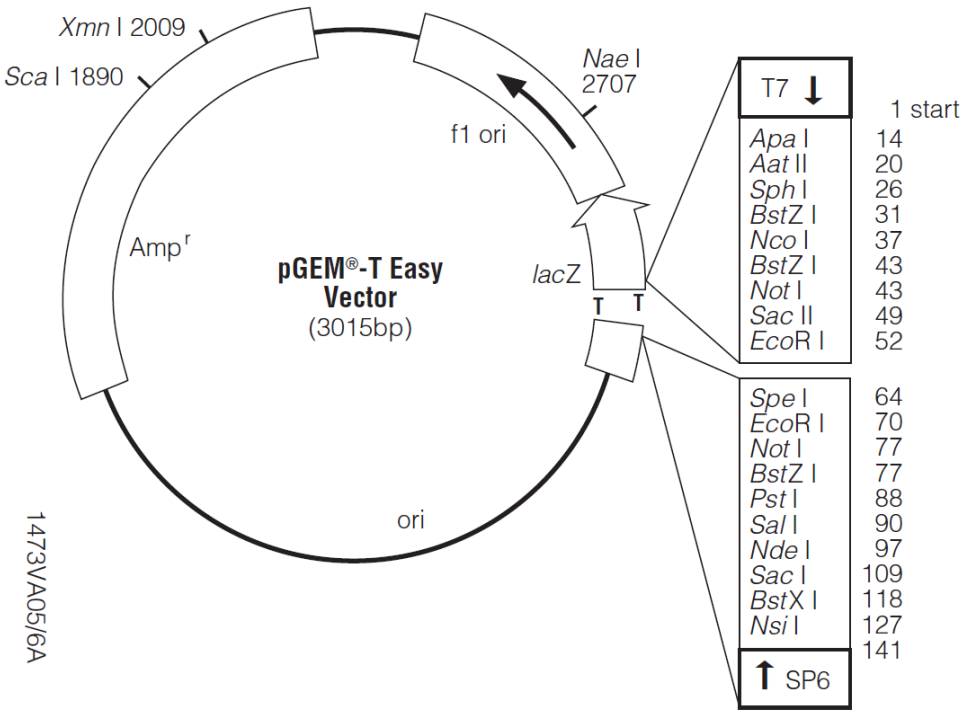


**pGEM®-T Easy Vector Sequence reference points:**

| | |
|---|---|
| T7 RNA Polymerase transcription initiation site | 1 |
| multiple cloning region | 10–128 |
| SP6 RNA Polymerase promoter (–17 to +3) | 139–158 |
| SP6 RNA Polymerase transcription initiation site | 141 |
| pUC/M13 Reverse Sequencing Primer binding site | 176–197 |
| *lac*Z start codon | 180 |
| *lac* operator | 200–216 |
| β-lactamase coding region | 1337–2197 |
| phage f1 region | 2380–2835 |
| *lac* operon sequences | 2836–2996, 166–395 |
| pUC/M13 Forward Sequencing Primer binding site | 2949–2972 |
| T7 RNA Polymerase promoter (–17 to +3) | 2999-3 |

***(Reference documents – Promega)***

- ***pLenti6/V5-Directional-TOPO® (Invitrogen by Life Technologies)***

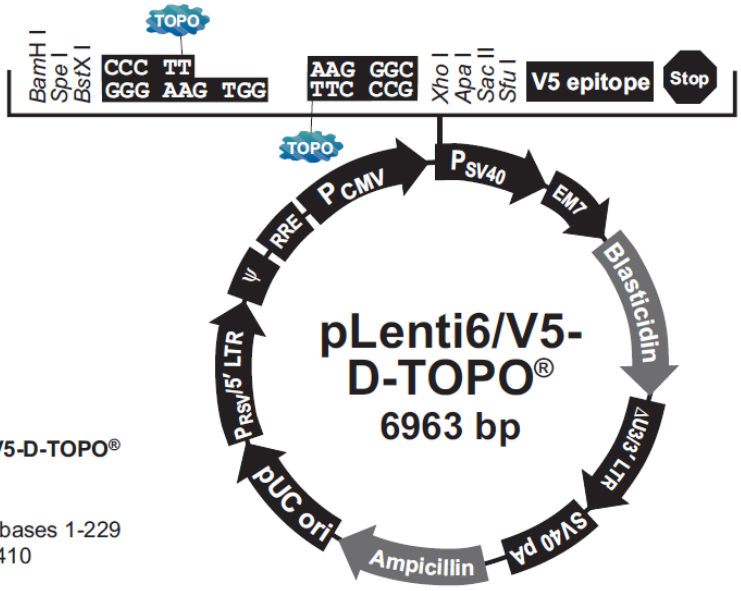


**Comments for pLenti6/V5-D-TOPO®**
**6963 nucleotides**

RSV enhancer/promoter: bases 1-229
HIV-1 5′ LTR: bases 230-410
5′ splice donor: base 520
HIV-1 psi (ψ) packaging sequence: bases 521-565
HIV-1 Rev response element (RRE): bases 1075-1308
3′ splice acceptor: base 1656
3′ splice acceptor: base 1684
CMV promoter: bases 1809-2392
CMV forward priming site: bases 2274-2294
Directional TOPO® site: bases 2431-2444
V5 epitope: bases 2473-2514
V5(C-term) reverse priming site: bases 2482-2502
SV40 early promoter and origin: bases 2569-2877
EM7 promoter: bases 2932-2998
Blasticidin resistance gene: bases 2999-3397
ΔU3/HIV-1 3′ LTR: bases 3484-3717
ΔU3: bases 3484-3536
Truncated HIV-1 3′ LTR: bases 3537-3717
SV40 polyadenylation signal: bases 3789-3920
*bla* promoter: bases 4779-4877
Ampicillin (*bla*) resistance gene: bases 4878-5738
pUC origin: bases 5883-6556

invitrogen™

***(Reference documents – Life Technologies)***

- ***pTRIPz Inducible Lentiviral vector (Dharmacon$^{TM}$)***

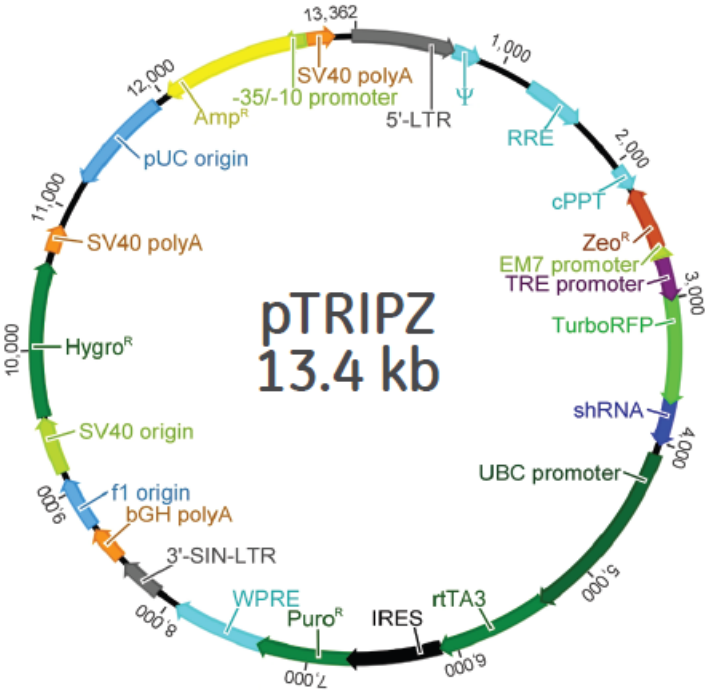


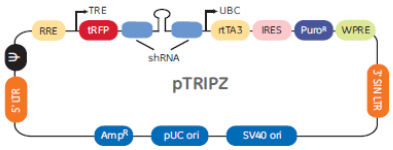


| Vector Element | Utility |
|---|---|
| TRE | Tetracycline-inducible promoter |
| tRFP | TurboRFP reporter for visual tracking of transduction and shRNA expression |
| shRNA | microRNA-adapted shRNA (based on miR-30) for gene knockdown |
| UBC | Human ubiquitin C promoter for constitutive expression of rtTA3 and puromycin resistance genes |
| rtTA3 | Reverse tetracycline-transactivator 3 for tetracycline-dependent induction of the TRE promoter |
| Puro$^R$ | Puromycin resistance permits antibiotic-selective pressure and propagation of stable integrants |
| IRES | Internal ribosomal entry site allows expression of rtTA3 and puromycin resistance genes in a single transcript |
| 5' LTR | 5' long terminal repeat |
| 3' SIN LTR | 3' self-inactivating long terminal repeat for increased lentivirus safety |
| Ψ | Psi packaging sequence allows viral genome packaging using lentiviral packaging systems |
| RRE | Rev response element enhances titer by increasing packaging efficiency of full-length viral genomes |
| WPRE | Woodchuck hepatitis posttranscriptional regulatory element enhances transgene expression in the target cells |

***(Reference documents – Dharmacon$^{TM}$)***

# Appendix IV – Full Listing of SNPs Obtained After Deep Sequencing Analysis

**Legend**

| |
|---|
| Blue text indicates SNP was seen in both samples |
| Yellow highlight shows SNP was identified by both SNP callers |

**Single Nucleotide polymorphisms (SNPs) obtained from deep sequencing analysis of the monoclonal cell line of Huh-7.5 +SGR/5A-TCM + 3'UTR:24xMS2:**

| | Position (nt) | SNP | Method | Freq-ShoRAH | Frq-LoFreq | Homopl | NonSyn | wtAA | mtAA |
|---|---|---|---|---|---|---|---|---|---|
| 1 | 3511 | A>G | LoFreq | NA | 0.004 | 0 | 0 | T | T |
| 2 | 3544 | A>G | LoFreq | NA | 0.004 | 0 | 0 | T | T |
| 3 | 3550 | T>C | LoFreq | NA | 0.005 | 0 | 0 | S | S |
| 4 | 3610 | C>T | LoFreq | NA | 0.008 | 0 | 0 | G | G |
| 5 | 3648 | A>G | LoFreq | NA | 0.004 | 0 | 1 | Q | R |
| 6 | 3730 | A>G | LoFreq | NA | 0.011 | 0 | 0 | G | G |
| 7 | 3802 | A>G | ShoRAH | 0.012 | NA | 1 | 0 | G | G |
| 8 | 3853 | G>C | ShoRAH | 0.01 | NA | 1 | 0 | G | G |
| 9 | 3883 | T>C | LoFreq | NA | 0.021 | 1 | 0 | V | V |
| 10 | 3950 | A>G | LoFreq | NA | 0.006 | 0 | 1 | T | A |
| 11 | 4000 | A>G | LoFreq | NA | 0.02 | 0 | 0 | P | P |
| 12 | 4039 | T>C | LoFreq | NA | 0.006 | 0 | 0 | H | H |

| | | | | | | | | | |
|---|---|---|---|---|---|---|---|---|---|
| 13 | 4054 | T>C | LoFreq | NA | 0.008 | 0 | 0 | S | S |
| 14 | 4145 | G>T | ShoRAH | 0.031 | NA | 1 | 1 | G | W |
| 15 | 4294 | A>G | LoFreq | NA | 0.011 | 0 | 1 | I | M |
| 16 | 4312 | T>C | LoFreq | NA | 0.005 | 0 | 0 | A | A |
| 17 | 4411 | G>T | ShoRAH | 0.01 | NA | 1 | 0 | G | G |
| 18 | 4412 | T>C | ShoRAH | 0.026 | NA | 1 | 1 | S | P |
| 19 | 4626 | T>C | LoFreq | NA | 0.006 | 0 | 1 | I | T |
| 20 | 4795 | T>C | LoFreq | NA | 0.005 | 0 | 0 | A | A |
| 21 | 4797 | T>C | LoFreq | NA | 0.004 | 0 | 1 | V | A |
| 22 | 4807 | T>C | LoFreq | NA | 0.007 | 0 | 0 | S | S |
| 23 | 4873 | A>G | LoFreq | NA | 0.006 | 0 | 0 | R | R |
| 24 | 4879 | A>G | LoFreq | NA | 0.007 | 0 | 0 | S | S |
| 25 | 4972 | A>G | LoFreq | NA | 0.006 | 0 | 0 | R | R |
| 26 | 5117 | T>C | LoFreq | NA | 0.009 | 0 | 1 | Y | H |
| 27 | 5153 | C>T | ShoRAH | 0.043 | NA | 1 | 1 | P | S |
| 28 | 5361 | T>C | ShoRAH& LoFreq | 0.07 | 0.026 | 0 | 1 | V | A |
| 29 | 5368 | A>G | ShoRAH& LoFreq | 0.061 | 0.028 | 0 | 0 | A | A |
| 30 | 5381 | A>G | LoFreq | NA | 0.008 | 0 | 1 | T | A |
| 31 | 5399 | A>G | ShoRAH | 0.004 | NA | 0 | 1 | I | V |
| 32 | 5408 | T>C | ShoRAH | 0.004 | NA | 0 | 0 | L | L |
| 33 | 5414 | G>C | LoFreq | NA | 0.006 | 0 | 1 | V | L |
| 34 | 5424 | G>A | LoFreq | NA | 0.005 | 0 | 1 | R | Q |
| 35 | 5435 | G>A | ShoRAH | 0.004 | NA | 0 | 1 | A | T |
| 36 | 5446 | G>T | LoFreq | NA | 0.014 | 0 | 1 | K | N |
| 37 | 5470 | T>C | LoFreq | NA | 0.013 | 0 | 0 | D | D |
| 38 | 5496 | C>G | ShoRAH | 0.011 | NA | 1 | 1 | A | G |
| 39 | 5497 | G>C | ShoRAH | 0.011 | NA | 1 | 0 | A | A |

| | | | | | | | | | |
|---|---|---|---|---|---|---|---|---|---|
| 40 | 5876 | A>G | ShoRAH& LoFreq | 0.04 | 0.021 | 0 | 1 | I | V |
| 41 | 5962 | T>A | LoFreq | NA | 0.013 | 0 | 0 | S | S |
| 42 | 6082 | G>A | ShoRAH | 0.011 | NA | 1 | 0 | E | E |
| 43 | 6181 | T>C | LoFreq | NA | 0.004 | 0 | 0 | R | R |
| 44 | 6260 | A>G | ShoRAH | 0.018 | NA | 1 | 1 | I | V |
| 45 | 6321 | A>G | ShoRAH | 0.005 | NA | 0 | 1 | D | G |
| 46 | 6358 | G>A | ShoRAH | 0.004 | NA | 0 | 0 | K | K |
| 47 | 6385 | T>C | ShoRAH | 0.005 | NA | 1 | 0 | C | C |
| 48 | 6452 | A>G | ShoRAH& LoFreq | 0.026 | 0.021 | 0 | 1 | N | D |
| 49 | 6578 | A>G | ShoRAH | 0.022 | NA | 1 | 1 | T | A |
| 50 | 6594 | C>A | ShoRAH | 0.006 | NA | 0 | 1 | A | D |
| 51 | 6612 | C>G | ShoRAH | 0.006 | NA | 0 | 1 | A | G |
| 52 | 6647 | T>C | LoFreq | NA | 0.006 | 0 | 1 | Y | H |
| 53 | 6745 | T>C | ShoRAH& LoFreq | 0.059 | 0.032 | 0 | 0 | H | H |
| 54 | 6838 | T>C | LoFreq | NA | 0.009 | 0 | 0 | C | C |
| 55 | 6974 | G>T | LoFreq | NA | 0.009 | 0 | 1 | A | S |
| 56 | 7020 | A>G | LoFreq | NA | 0.007 | 0 | 1 | D | G |
| 57 | 7026 | A>G | LoFreq | NA | 0.008 | 0 | 1 | D | G |
| 58 | 7057 | C>T | LoFreq | NA | 0.015 | 1 | 0 | G | G |
| 59 | 7074 | A>G | LoFreq | NA | 0.005 | 0 | 1 | E | G |
| 60 | 7101 | A>G | LoFreq | NA | 0.009 | 1 | 1 | D | G |
| 61 | 7140 | A>G | LoFreq | NA | 0.016 | 1 | 1 | E | G |
| 62 | 7149 | T>C | LoFreq | NA | 0.02 | 0 | 1 | I | T |
| 63 | 7149 | T>G | LoFreq | NA | 0.009 | 0 | 1 | I | R |
| 64 | 7160 | T>C | ShoRAH& LoFreq | 0.007 | 0.02 | 0 | 1 | C | R |

| | | | | | | | | | |
|---|---|---|---|---|---|---|---|---|---|
| 65 | 7163 | A>G | LoFreq | NA | 0.008 | 0 | 1 | M | V |
| 66 | 7164 | T>C | LoFreq | NA | 0.012 | 0 | 1 | M | T |
| 67 | 7218 | A>G | LoFreq | NA | 0.01 | 0 | 1 | Y | C |
| 68 | 7254 | A>G | ShoRAH | 0.007 | NA | 0 | 1 | D | G |
| 69 | 7346 | A>G | LoFreq | NA | 0.018 | 0 | 1 | S | G |
| 70 | 7361 | T>C | LoFreq | NA | 0.007 | 0 | 1 | S | P |
| 71 | 7586 | C>A | ShoRAH | 0.041 | NA | 1 | 1 | Q | K |
| 72 | 7587 | A>C | ShoRAH | 0.045 | NA | 1 | 1 | Q | P |
| 73 | 7588 | G>C | ShoRAH | 0.013 | NA | 1 | 1 | Q | H |
| 74 | 7589 | G>A | ShoRAH | 0.104 | NA | 1 | 1 | G | R |
| 75 | 7634 | T>C | LoFreq | NA | 0.013 | 0 | 1 | C | R |
| 76 | 7641 | A>G | LoFreq | NA | 0.016 | 0 | 1 | E | G |
| 77 | 7644 | A>G | LoFreq | NA | 0.02 | 0 | 1 | E | G |
| 78 | 7647 | A>G | LoFreq | NA | 0.008 | 0 | 1 | D | G |
| 79 | 7649 | G>A | LoFreq | NA | 0.007 | 0 | 1 | D | N |
| 80 | 7650 | A>G | LoFreq | NA | 0.007 | 0 | 1 | D | G |
| 81 | 7652 | A>G | LoFreq | NA | 0.045 | 0 | 1 | T | A |
| 82 | 7655 | A>G | LoFreq | NA | 0.081 | 0 | 1 | T | A |
| 83 | 7658 | G>A | LoFreq | NA | 0.025 | 0 | 1 | V | M |
| 84 | 7659 | T>A | LoFreq | NA | 0.011 | 0 | 1 | V | E |
| 85 | 7659 | T>C | LoFreq | NA | 0.014 | 0 | 1 | V | A |
| 86 | 7661 | T>A | LoFreq | NA | 0.015 | 0 | 1 | C | S |
| 87 | 7661 | T>C | LoFreq | NA | 0.091 | 0 | 1 | C | R |
| 88 | 7667 | T>A | LoFreq | NA | 0.009 | 0 | 1 | S | T |
| 89 | 7768 | T>C | LoFreq | NA | 0.005 | 0 | 0 | H | H |
| 90 | 7780 | C>T | LoFreq | NA | 0.005 | 0 | 0 | Y | Y |
| 91 | 7783 | T>C | LoFreq | NA | 0.005 | 0 | 0 | C | C |
| 92 | 7924 | G>A | LoFreq | NA | 0.007 | 0 | 0 | E | E |
| 93 | 8126 | A>T | ShoRAH | 0.009 | NA | 1 | 1 | K | * |

| | | | | | | | | | |
|---|---|---|---|---|---|---|---|---|---|
| 94 | 8427 | A>G | LoFreq | NA | 0.011 | 0 | 1 | H | R |
| 95 | 8497 | A>G | LoFreq | NA | 0.004 | 0 | 0 | R | R |
| 96 | 8740 | T>C | ShoRAH& LoFreq | 0.496 | 0.188 | 0 | 0 | Y | Y |
| 97 | 8970 | T>C | ShoRAH& LoFreq | 0.077 | 0.038 | 0 | 1 | V | A |
| 98 | 8973 | A>G | LoFreq | NA | 0.008 | 0 | 1 | Q | R |
| 99 | 8974 | A>G | ShoRAH& LoFreq | 0.116 | 0.051 | 0 | 0 | Q | Q |
| 100 | 9030 | A>G | LoFreq | NA | 0.012 | 0 | 1 | N | S |
| 101 | 9325 | C>T | LoFreq | NA | 0.011 | 0 | 0 | V | V |

**Single Nucleotide polymorphisms (SNPs) obtained from deep sequencing analysis of the polyclonal cell line of Huh-7.5 +SGR/5A-TCM + 3'UTR:24xMS2:**

| | Position | SNP | Method | Freq-ShoRAH | Frq-LoFreq | Homopl | NonSyn | wtAA | mtAA |
|---|---|---|---|---|---|---|---|---|---|
| 1 | 3511 | A>G | LoFreq | NA | 0.005 | 0 | 0 | T | T |
| 2 | 4411 | G>T | ShoRAH | 0.008 | NA | 1 | 0 | G | G |
| 3 | 4737 | T>C | LoFreq | NA | 0.005 | 0 | 1 | V | A |
| 4 | 4795 | T>C | LoFreq | NA | 0.005 | 0 | 0 | A | A |
| 5 | 5019 | A>G | ShoRAH | 0.005 | NA | 1 | 1 | E | G |
| 6 | 5034 | T>C | ShoRAH | 0.005 | NA | 1 | 1 | V | A |
| 7 | 5070 | T>A | ShoRAH | 0.005 | NA | 0 | 1 | L | H |
| 8 | 5153 | C>T | ShoRAH | 0.068 | NA | 1 | 1 | P | S |
| 9 | 5911 | A>G | LoFreq | NA | 0.006 | 0 | 0 | A | A |
| 10 | 6082 | G>A | ShoRAH | 0.01 | NA | 1 | 0 | E | E |
| 11 | 6452 | A>G | LoFreq | NA | 0.009 | 0 | 1 | N | D |
| 12 | 6578 | A>G | ShoRAH | 0.018 | NA | 1 | 1 | T | A |
| 13 | 7273 | T>C | ShoRAH | 0.007 | NA | 0 | 0 | V | V |
| 14 | 7586 | C>A | ShoRAH | 0.075 | NA | 1 | 1 | Q | K |
| 15 | 7588 | G>A | ShoRAH | 0.313 | NA | 1 | 0 | Q | Q |
| 16 | 7588 | G>C | ShoRAH | 0.049 | NA | 1 | 1 | Q | H |
| 17 | 7589 | G>A | ShoRAH | 0.146 | NA | 1 | 1 | G | R |
| 18 | 7652 | A>G | LoFreq | NA | 0.007 | 0 | 1 | T | A |
| 19 | 7655 | A>G | LoFreq | NA | 0.024 | 0 | 1 | T | A |
| 20 | 7658 | G>A | LoFreq | NA | 0.009 | 0 | 1 | V | M |
| 21 | 7659 | T>C | LoFreq | NA | 0.007 | 0 | 1 | V | A |
| 22 | 7661 | T>C | LoFreq | NA | 0.028 | 0 | 1 | C | R |

| | | | | | | | | | |
|---|---|---|---|---|---|---|---|---|---|
| 23 | 8114 | G>C | ShoRAH | 0.011 | NA | 1 | 1 | A | P |
| 24 | 8427 | A>G | LoFreq | NA | 0.005 | 0 | 1 | H | R |
| 25 | 8620 | T>C | LoFreq | NA | 0.005 | 0 | 0 | D | D |
| 26 | 8970 | T>C | LoFreq | NA | 0.009 | 0 | 1 | V | A |

# Appendix V - Primers

| | Method section |
|---|---|
| ***Deep Sequencing and RNA-Protein complex Immunoprecipitation*** | |
| ***cDNA using SuperScript® III Reverse Transcriptase (Life Technologies)*** | 2.1.12.2 |
| **NS5Bend_R** | |
| 5’ to 3’: AC CGA GCG GGG AGT AGG AAG | |
| **JFH1-9211_Loops cDNA** | |
| 5’ to 3’: AGGGAAAGCG GCCGTTTGCG | |
| ***PCR using SequalPrep Long PCR kit (Life Technologies)*** | 2.1.15 |
| ***or AmpliTaq Gold (Life Technologies)*** | 2.1.13 |
| **KL_NS3P_F** | |
| 5’ to 3’: GCT CCC ATC ACT GCT TAT GCC | |
| **KL-NS5Bc_R (9400 to 9377)** | |
| 5’ to 3’: TAG GAG TAG GCC GAA GAG TAA TGA | |

**JFH1-8337S**

5’ to 3’: TTT CGT ATG ATA CCC GAT GCT T

## *PCR across MS2 stem loop repeats*

***Deep Vent$_R$™ DNA polymerase (NEB)*** 2.1.14

**JFH1-9258FP HighTm**

5’ to 3’: AGA CCA AGC TCA AAC TCA CTC CAT TGC CGG AGG CGC GCC TAC TGG

**JFH1-9651RP HighTm**

5’ to 3’: GCA CTC TCT GCA GTC ATG CGG CTC ACG GAC CTT TCA CAG CTA GC

## *Cloning in pGEM-T EASY*

***Platinium Taq® DNA Polymerase High Fidelity (Life Technologies)*** 2.1.13

**Jc1-9015S**

5’ to 3’: CAGTATACTCCGTGAATCCTTTGGACC

**Jc1 – 9469R**

5’ to 3’: TAT GGA GTG TAC CTA GTG TGT GCC G

## *Real-Time Quantitative PCR* 2.1.16

### *HCV primer set*

**HCVF**

5’ to 3’: TCTTCACGCAGAAAGCGTCTAG

**HCVR**

5’ to 3’: GGTTCCGCAGACCACTATGG

### *Housekeeping gene primer set*

**36B4-F**

5’ to 3’: AGATGCAGCAGATCCGCAT

**36B4-R**

5’ to 3’: GGATGGCCTTGCGCA

# Appendix VI – Cloning Strategy for pLenti6[NLS-MS2.Coat-NLS-mCherry]

| **TOP STRAND OLIGO** | **NLS_MS2coat NheI_TOP** |
|---|---|
| 5’- ctagcaGGTGATCCAAAAAAGAAGAGAAAGGTAGGAg -3’ | |
| | |
| **BOTTOM STRAND OLIGO** | **NLS_MS2coat NheI_BOT** |
| 5’- ctagCTCCTACCTTTCTCTTCTTTTTTGGATCACCtg -3’ | |
| | |
| **Oligo Duplex** | |
| 5’-cta gca GGTGATCCAAAAAAGAAGAGAAAGGTAGGAg -3’<br>3’- gt CCAC TAGGTTTT TT CTT CTC TTT CC ATCCTCgatc-5’ | |
| | |
| **Encodes** | **Protein** |
| GATCCAAAAAAGAAGAGAAAGGTA | D P K K K R K V |

# Appendix VII – Sequences of the MS2 Stem Loop Repeats

***6x MS2 stem loop repeat sequence, Length: 342bp (purchased from GenScript)***

Vector Name: pUC57

Cloning site: EcoRI-HindIII

GAATTCTCCTAAGGTACCTAATTGCCTAGAAAACATGAGGATCACCCATGT
CTGCAGGTCGACTCTAGAAAACATGAGGATCACCCATGTCTGCAGTATTCC
CGGGTTCATTAGATCCTAAGGTACCTAATTGCCTAGAAAACATGAGGATCA
CCCATGTCTGCAGGTCGACTCTAGAAAACATGAGGATCACCCATGTCTGCA
GTATTCCCGGGTTCATTAGATCCTAAGGTACCTAATTGCCTAGAAAACATG
AGGATCACCCATGTCTGCAGGTCGACTCTAGAAAACATGAGGATCACCCAT
GTCTGCAGTATTCCCGGGTTCATTAGATCTAAGCTT

***Gene Name: 8x MS2 stem loop repeat sequence, Length: 448bp (ordered through GenScript)***

Vector Name: pUC57

Cloning site: EcoRI-HindIII

GAATTCTCCTAAGGTACCTAATTGCCTAGAAAACATGAGGATCACCCATGT
CTGCAGGTCGACTCTAGAAAACATGAGGATCACCCATGTCTGCAGTATTCC
CGGGTTCATTAGATCCTAAGGTACCTAATTGCCTAGAAAACATGAGGATCA
CCCATGTCTGCAGGTCGACTCTAGAAAACATGAGGATCACCCATGTCTGCA
GTATTCCCGGGTTCATTTCCTAAGGTACCTAATTGCCTAGAAAACATGAGG
ATCACCCATGTCTGCAGGTCGACTCTAGAAAACATGAGGATCACCCATGTC
TGCAGTATTCCCGGGTTCATTAGATCCTAAGGTACCTAATTGCCTAGAAAA
CATGAGGATCACCCATGTCTGCAGGTCGACTCTAGAAAACATGAGGATCAC
CCATGTCTGCAGTATTCCCGGGTTCATTAGATCTAAGCTT

***Gene Name: 12x MS2 stem loop repeat sequence, Length: 669bp (ordered through GenScript)***

Vector Name: pUC57

Cloning site: EcoRI-HindIII

GAATTCTCCTAAGGTACCTAATTGCCTAGAAAACATGAGGATCACCCATGT
CTGCAGGTCGACTCTAGAAAACATGAGGATCACCCATGTCTGCAGTATTCC
CGGGTTCATTAGATCCTAAGGTACCTAATTGCCTAGAAAACATGAGGATCA
CCCATGTCTGCAGGTCGACTCTAGAAAACATGAGGATCACCCATGTCTGCA

GTATTCCCGGGTTCATTAGATCCTAAGGTACCTAATTGCCTAGAAAACATG
AGGATCACCCATGTCTGCAGGTCGACTCTAGAAAACATGAGGATCACCCAT
GTCTGCAGTATTCCCGGGTTCATTAGATCCTAAGGTACCTAATTGCCTAGAA
AACATGAGGATCACCCATGTCTGCAGGTCGACTCTAGAAAACATGAGGATC
ACCCATGTCTGCAGTATTCCCGGGTTCATTAGATCCTAAGGTACCTAATTGC
CTAGAAAACATGAGGATCACCCATGTCTGCAGGTCGACTCTAGAAAACATG
AGGATCACCCATGTCTGCAGTATTCCCGGGTTCATTAGATCCTAAGGTACCT
AATTGCCTAGAAAACATGAGGATCACCCATGTCTGCAGGTCGACTCTAGAA
AACATGAGGATCACCCATGTCTGCAGTATTCCCGGGTTCATTAGATCTAAG
CTT

***Gene Name: 24x MS2 stem loop repeat sequence, Length: 448bp (kindly provided by S. Boireau (IGMM, Montpellier, France).***

Vector Name: pTRIP-MS2x24(deltaU3)-1

Cloning site: EcoRI-HindIII

GAATTCGAATGGCCATGGGACGTCGACCTGAGGTAATTATAACCCGGGCCC
TATATATGGATCCTAAGGTACCTAATTGCCTAGAAAACATGAGGATCACCC
ATGTCTGCAGGTCGACTCTAGAAAACATGAGGATCACCCATGTCTGCAGTA
TTCCCGGGTTCATTAGATCCTAAGGTACCTAATTGCCTAGAAAACATGAGG
ATCACCCATGTCTGCAGGTCGACTCTAGAAAACATGAGGATCACCCATGTC
TGCAGTATTCCCGGGTTCATTAGATCCTAAGGTACCTAATTGCCTAGAAAA
CATGAGGATCACCCATGTCTGCAGGTCGACTCTAGAAAACATGAGGATCAC
CCATGTCTGCAGTATTCCCGGGTTCATTAGATCCTAAGGTACCTAATTGCCT

AGAAAACATGAGGATCACCCATGTCTGCAGGTCGACTCTAGAAAACATGA

GGATCACCCATGTCTGCAGTATTCCCGGGTTCATTAGATCCTAAGGTACCTA

ATTGCCTAGAAAACATGAGGATCACCCATGTCTGCAGGTCGACTCTAGAAA

ACATGAGGATCACCCATGTCTGCAGTATTCCCGGGTTCATTAGATCCTAAG

GTACCTAATTGCCTAGAAAACATGAGGATCACCCATGTCTGCAGGTCGACT

CTAGAAAACATGAGGATCACCCATGTCTGCAGTATTCCCGGGTTCATTAGA

TCCTAAGGTACCTAATTGCCTAGAAAACATGAGGATCACCCATGTCTGCAG

GTCGACTCTAGAAAACATGAGGATCACCCATGTCTGCAGTATTCCCGGGTT

CATTAGATCCTAAGGTACCTAATTGCCTAGAAAACATGAGGATCACCCATG

TCTGCAGGTCGACTCTAGAAAACATGAGGATCACCCATGTCTGCAGTATTC

CCGGGTTCATTAGATCCTAAGGTACCTAATTGCCTAGAAAACATGAGGATC

ACCCATGTCTGCAGGTCGACTCTAGAAAACATGAGGATCACCCATGTCTGC

AGTATTCCCGGGTTCATTAGATCCTAAGGTACCTAATTGCCTAGAAAACAT

GAGGATCACCCATGTCTGCAGGTCGACTCTAGAAAACATGAGGATCACCCA

TGTCTGCAGTATTCCCGGGTTCATTAGATCCTAAGGTACCTAATTGCCTAGA

AAACATGAGGATCACCCATGTCTGCAGGTCGACTCTAGAAAACATGAGGAT

CACCCATGTCTGCAGTATTCCCGGGTTCATTAGATCCTAAGGTACCTAATTG

CCTAGAAAACATGAGGATCACCCATGTCTGCAGGTCGACTCTAGAAAACAT

GAGGATCACCCATGTCTGCAGTATTCCCGGGTTCATTAGATCT

# Appendix VIII – Digestion of 24xMS2 Plasmids

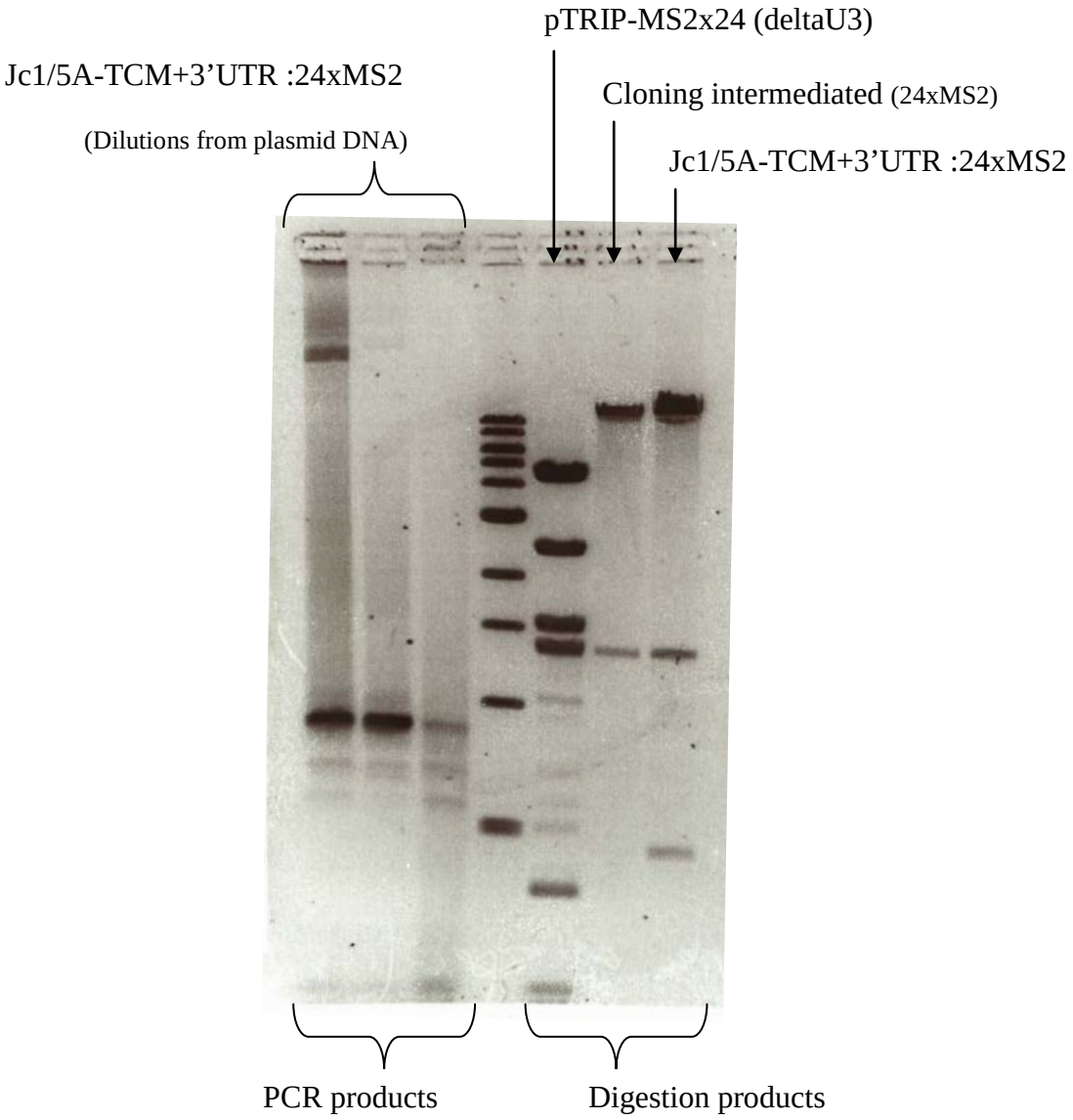

# Appendix IX – Sequencing of Long-Term (8 Days) Cultures

## *Primers used:*

***SP6 - Forward primer***

5’ - GATTTAGGTGACACTATAG - 3’

***T7 - Reverse primer***

5’ - TAATACGACTCACTATAGGG - 3’

## *Sequencing results:*

***Replicate 1 – Colonie A***

- Sp6

GGGGCGCCGTGAAAAGACGATGTTCGGGCTCGCCGTATGGTCACTGCATTT
TATTGAGATTCAGAGTGATTTTTAGTGGGAGGTTGATGGTGAACATCAATT
CTGTGTTCTAAAAAAATTAAAATCCTGCGGAGTATGCACTGGATCAGCGGA
ATCCA

- T7

TGTAGAGCACTATGCGAGTCGCTGCTCCGGCCGCCATGGCGGCCGCGGGAA
TTCGATTATGGAGTGTACCTAGTGTGTGCTGGGCTCCAGTGTAGACTGGGC
CTTGCCCAAAACAGGTAAGCAGAGGCTCAGGAGCAAAGGGTGGGAGTGGG
GCGGAGGGCAAAGCGAATAATTGTGTTGACTTCAACTGGACTACCAATTAA
TACACATAAGGGGCCTGTGTCGGGGAGTGGAAGGCAACTGTGGGTGGCAC

***Replicate 1 – Colonie C***

- Sp6

CCCGTTTTGTATCAAACGCGTTGGGAGCTCTCCCATATGGTCGACCTGCAGG
CGGCCGCGAATTCACTAGTGATTTATGGAGTGGGAGGGTGCGGGCCGTCCT
CATTCTCCCCTGTCCTTACAGACATCTGAGCGCTCGGGCGTGCTCCGGTGGT
CGTCCCTTTGCCTTTGCCTGCTGCCGTATTGTCTGCTTTGCTCC

- T7

GACAAGAGTCGCATGCTCCGGCCGCCATGGCGGCCGCGGGATTCTTTTTAT
GGATGTACAAATTGAGTGTGGTAAAGAAGGGGTTTGCTGGATTAGTATGAC
TCGGGTGTTCATATAAGCAATTCTCCTCCTTCTCCGCATTATACATGTTTATC
TTTTTGCACAACTATGTCTTTGATGAGTTTACTGCA

***Replicate 2 – Colonie A***

- Sp6

GGAATTTAGCTCCACGCGTTGGGAGCTCTCCCATATGGTCGACCTGCAGGC
GGCCGCGAATTCACTAGTGATCAGTATACTCCGTGAATCTTTGGACCTTCCA
GCCATAATTGAGAGGTTACACGGGCTTGACGCCTTTTCTATGCACACATACT
CTCACCACGAACTGACGCGGGTGGCTTCAGCCCTCAGAAAACTTGGGGCGC
CACCCCTCAGGGTGTGGAAGAGTCGGGCTCGCGCAGTCAGGGCGTCCCTCA
TCTCCCGTGGAGGGAAAGCGGCCGTTTGCGGCCGATATCTCTTCAATTGGG
CGGTGAAGACCAAGCTCAAACTCACTCCATTGCCGGAGGCGCGCCTACTGG
ACTTATCCAGTTGGTTCACCGTCGGCGCCGGCGGGGGCGACATTTTTCACA
GCGTGTCGCGCGCCCGACCCCGCTCATTACTCTTCGGCCTACTCCTACTTTT
CGTAGGGGTAGGCCTCTTCCTACTCCCCGCTCGGTAGAGCGGCACACACTA
GGTACCCTCCATAAGTCGAATTCCCGCGGCTTCCATGGCGGCCGG

- T7

TTAGCGAGTCGCATGCTCCGGCCGCCTGGCGGCCGCGGGAATTCGATTTAT
GGAGTGTACCTAGTGTGTGCCGCTCTACCGAGCGGGGAGTAGGAAGAGGC
CTACCCCTACGATAAGCCTGAGTTCGCCGATCAGCCTGACCGGGGTCGGGT
GCGCAATTCTTTGTGAAAATTGAGTTCATCGCCGTATATTTAGTGAACCAAT
TGTATCATCGAGGTGAAGCCCCTCTGTCTTGGATTGACTTGCA

***Replicate 1 – Colonie B***

- Sp6

AAATATTAGCATCCACGCGTTGGGAGCTCTCCCATATGGTCGACCTGCAGG
CGGCCGCGAATTCACTAGTGATTAGTGTACCTAGTGTGTGCCGCTATGGCC
ATTCGAATTCCTACCGAGCGGGGAGTAGGAAGAGGCCTACCCCTACGAAA
AGTAGGAGTAGGCCGAAGAGTAATGAGCGGGGTCGGGCGCGCGACACGCT
GTGAAAAATGTCGCCCCCGCCGGCGCCGACGGTGAACCAACTGGATAAGTC
CAGTAGGCGCGCCTCCGGCAATGGAGTGAGTTTGAGCTTGGTCTTCACCGC
CCAATTGAAGAGATATCGGCCGCAAACGGCCGCTTTCCCTCCACGGGAGAT
GAGGGACGCCCTGACTGCGCGAGCCCGACTCTTCCACACCCTGAGGGGTGG
CGCCCCAAGTTTTCTGAGGGCCGAAGCCACCCGCGTCAGTTCGTGGTGAGA
GTATGTGTGCATAGAAAAGGCGTCAAGCCCGTGTAACCTCTCAATTATGGC
TGGAAGGTCCAAAGGATTCACGGAGTATACTGAATCGAATTCCCGCGGCCG
CCATGGCGGCCGGGAGCATGCGACGTCGGGCCCAATTCGCCCTATAGTGAG
TCGTATTACAATTCACTGGCCGTCGTTTTACAACGTCGTGACTGGGAAAAA
CCCTGGCGTTACCCAACTTAAT

- T7

GCAGCGAGTCGCATGCTCCGGCCGCCATGGCGGCCGCGGGAATTCGATTCA
GTATACTCCGTGAATCCTTTGGACCTTCCAGCCATAATTGAGAGGTTACACG
GGCTTGACGCCTTTTCTATGCACACATACTCTCACCACGAACTGACGCGGGT
GGCTTCGGCCCTCAGAAAACTTGGGGCGCCACCCCTCAGGGTGTGGAAGAG
TCGGGCTCGCGCAGTCAGGGCGTCCCTCATCTCCCGTGGAGGGAAAGCGGC
CGTTTGCGGCCGATATCTCTTCAATTGGGCGGTGAAGACCAAGCTCAAACT
CACTCCATTGCCGGAGGCGCGCCTACTGGACTTATCCAGTTGGTTCACCGTC
GGCGCCGGCGGGGGCGACATTTTTCACAGCGTGTCGCGCGCCCGACCCCGC
TCATTACTCTTCGGCCTACTCCTACTTTTCGTAGGGGTAGGCCTCTTCCTACT
CCCCGCTCGGTAGGAATTCGAATGGCCATAGCGGCACACACTAGGTACACT
AATCACTAGTGAATTCGCGGCCGCCTGCAGGTCGACCATATGGGAGAGCTC
CCAACGCGTTGGATGCATAGCTTGAGTATTCTATAGTGTCACCTAAATAGCT
TGGCGTAATCATGGTCATAGCTGTTTCCTGTGTGAAATTGTTATCCGCTCAC
AATTCCACACAACATACGAGCCGGAAGCATAAAGTGTAAAGCCTGGGGTG
CCTAATGAGTGAGCTAACTCACATTAATTGCGTTGCGCTCACTGCCCGCTTT
CCAGTCGGGAAACCTGTCGTGCCAGCTGCATTAATGAATCGGCCAACGCGC
GGGAGAGGCGGTTTGCGTATTGGGGCGCTCTTCCGCTTCCTCGCTCACTGAC
TCCCTGCGCTCGGGTCGTTCGGCTGCGGCGAGCCGGTATCAGCTCACTCAA
AGCGGTAATACGGTTATCCACAGAATCAGGGGATAACGCAGGAAAAAACA
TGTGACCAAAGGGCCAGCAAAGGCCAGGAACCGTAAAAGGCGGCGTTGCT
GGCGTTTTTCCATAGGGCTTCCGCCCTCCGGACGAACTATCCAAAAATCGA

***Replicate 2 – Colonie C***

- Sp6

GATTCAGCATCAACGCGTTGGGAGCTCTCCCATATGGTCGACCTGCAGGCG
GCCGCGAATTCACTAGTGATTTGTGGAGTGTACCTAGTGTGTGCCGCTAGA
TCTAATGAACCCGGGAATACTGCAGACATGGGTGATCCTCATGTTTTCTGG
AGTCGACCTGCAGACATGGGTGATCCTCATGTTTTCTAGGCAATTAGGTAC
CTTAGGATCTAATGAACCCGGGAATACTGCAGACATGGGTGATCCTCATGT
TTTCTAGAGTCGACCTGCAGACATGGGTGATCCTCATGTTTTCTAGGCAATT
AGGTACCTTAGGATCTAATGAACCCGGGAATACTGCAGACATGGGTGATCC
TCATGTTTTCTAGGCAATTAGGTACCTTAGGATCTAATGAACCCGGGAATA
CTGCAGACATGGGTGATCCTCATGTTTTCTAGAGTCGACCTGCAGACATGG
GTGATCCTCATGTTTTCTAGGCAATTAGGTACCTTAGGATCCATATATAGGG
CCCGGGTTATAATTACCTCAGGTCGACGTCCCATGGCCATTCGAATTCCTAC
CGAGCGGGGAGTAGGAAGAGGCCTACCCCTACGAAAAGTAGGAGTAGGCC
GAAGAGTAATGAGCGGGGTCGGGCGCGCGACACGCTGTGAAAAATGTCGC
CCCCGCCGGCGCCGACGGTGAACCAACTGGATAAGTCCAGTAGGCGCGCCT
CCGGCAATGGAGTGAGTTTGAGCTTGGTCTCCACCGCCCAATTGAAGAGAT
ATCGGCCGCAAACGGCCGCTTTCCCTCCACGGGAGATGAGGGACGCCCTGA
CTGCGCGAGCCCGACTCTTCCACACCCTGAGGGGTGGCGCCCCAAGTTTTC
TGAGGGGCTGAAGCCACCCGCGTCAGTTCGTGGTGAGAGTATGTGTGCATA
GAAAAGGCGTCAAGCCCGTGTAACCTCTCAATTATGGCTGGGAAGTCCAAG
GATTCACGGAGTATACTGAATCGAATTCCCGCGGCCGCCATGGCGGCCGGA
GCATGCGACGTCGGGCCCAATTCGCCTTATATTGAGTCGTATTACATTCACT
GACGTCGTTTACAAACGTCTGACTGGAACCCTTGCGTTACCCACTTAATCGC
CCTTGCAGCACATCCCCTTCCAACTGCTAAGCGAAAAGCCCCGCACGAATG
CCTTCCACAGATGCCACCTGAATGCCGATGATACGCTCTAGT

- T7

GGAGAGTCGCATGCTCCGGCCGCCATGGCGGCCGCGGGAATTCGATTCAGT
ATACTCCGTGAATCCTTGGACCTTCCAGCCATAATTGAGAGGTTACACGGG
CTTGACGCCTTTTCTATGCACACATACTCTCACCACGAACTGACGCGGGTGG
CTTCAGCCCTCAGAAAACTTGGGGCGCCACCCCTCAGGGTGTGGAAGAGTC
GGGCTCGCGCAGTCAGGGCGTCCCTCATCTCCCGTGGAGGGAAAGCGGCCG
TTTGCGGCCGATATCTCTTCAATTGGGCGGTGGAGACCAAGCTCAAACTCA
CTCCATTGCCGGAGGCGCGCCTACTGGACTTATCCAGTTGGTTCACCGTCGG
CGCCGGCGGGGGCGACATTTTTCACAGCGTGTCGCGCGCCCGACCCCGCTC
ATTACTCTTCGGCCTACTCCTACTTTTCGTAGGGGTAGGCCTCTTCCTACTCC
CCGCTCGGTAGGAATTCGAATGGCCATGGGACGTCGACCTGAGGTAATTAT
AACCCGGGCCCTATATATGGATCCTAAGGTACCTAATTGCCTAGAAAACAT
GAGGATCACCCATGTCTGCAGGTCGACTCTAGAAAACATGAGGATCACCCA
TGTCTGCAGTATTCCCGGGTTCATTAGATCCTAAGGTACCTAATTGCCTAGA

AAACATGAGGATCACCCATGTCTGCAGTATTCCCGGGTTCATTAGATCCTA
AGGTACCTAATTGCCTAGAAAACATGAGGATCACCCATGTCTGCAAGTCGA
CTCTAGAAAACATGAGGATCACCCCATGTCTGCAGTATTCCCGGGTTCATT
AGATCCTAAGTACCTAATTGCCTAGAAAACATTGAGGATCACCCATGTCTG
CAGGTCGACTCCAGAAAAACATGAAGGATCACCCATGTCTGCAGTATTCCC
GGGTCCATTAGATCTAGCGGCACACACTAGGTACATTCCACAAATTCCCTA
GTGAATTTCCCGGCCGCCTGCAGGTCGAC

***Replicate 3 – Colonie A***

- Sp6

GTCGGCTAGAATCCACGCGTTGGGAGCTCTCCCATATGGTCGACCTGCAGG
CGGCCGCGAATTCACTAGTGATTCAGTATACTCCGTGAATCCTTTGGACCTT
CCAGCCATAATTGAGAGGTTACTGTCTGCAGTATTCCCGGGTTCATTAGATC
TAGCGGCACACACTAGGTACACTCCATAGCACTCCACTCGCCCGGGCTGCC
TGGGAAACAGTTAGACACTCCCCTATCAATTCATGGCTGGGAAACATCATC
CAGTATGCTGTATACTCCGTGAATCCTTTGGACCTTCCAGCCATAATTGAGA
GGTTACACGGGCTTGACGCCTTTTCTATGCACACATACTCTCACCACGAACT
GACGCGGGTGGCTTCAGCCCTCAGAAAACTTGGGGCGCCACCCCTCAGGGT
GTGGAAGAGTCGGGCTCGCGCAGTCAGGGCGTCCCTCATCTCCCGTGGAGG
GAAAGCGGCCGTTTGCGGCCGATATCTCTTCAATTGGGCGGTGAAGACCAA
GCTCAAACTCACTCCATTGCCGGAGGCGCGCCTACTGGACTTATCCAGTTG
GTTCACCGTCGGCGCCGGCGGGGGCGACATTTTTCACAGCGTGTCGCGCGC
CTGACCCCGCCCATTACTCTTCGGCCTACTCCTACTTTTTCTTAGGGGTAGG
CCTCTTCCTA

- T7

AGACGGAGTCGCATGCTCCGGCCGCCATGGCGGCCGCGGGAATTCGATTTA
TGGAGTGTACCTAGTGTGTGCCGCTAGATCTAATGAACCCGGGAATACTGC
AGACATGGGTGATCCTCATGTTTTCTGGAGTCGACCTGCAGACATGGGTGA
TCCTCATGTTTTCTAGGCAATTAGGTACCTTAGGATCTAATGAACCCGGGAA
TACTGCAGACATGGGTGATCCTCATGTTTTCTAGGCAATTAGGTACCTTAGG
ATCTAATGAACCCGGGAATACTGCAGACATGGGTGATCCTCATGTTTTTTA
GGCAATTAGGTACCTTAGGATCTAATGAACCCGGGAATACTGCAGACATGG
GTGATCCTCATGTTTTCTAGAGTCGACCTGCAGACATGGGTGATCCTCATGT
TTTCTAGGCAATTAGGTACCTTAGGATCCATATATAGGGCCCGGGTTATAAT
TACCTCAGGTCGACGTCCCATGGCCATTCGAATTCCTACCGAGCGGGGAGT
AGGAAGAGGCCTACCCCTACGAAAAGTAGGAGTAGGCCGAAGAGTAATGG
GCGGGGTCAGGCGCGCGACACGCTGTGAAAAATGTCGCCCCCGCCGGCGC

CGACGGTGAACCAATTGGATAAGTCCAGTAGGCGCGCCTCCGGCAATGGA
GTGACTTTGAGCT

***Replicate 3 – Colonie B***

- Sp6

CCAACCTACTCCACGCGTTGGGAGCTCTCCCATATGGTCGACCTGCAGGCG
GCCGCGAATTCACTAGTGATTCAGTATACTCCGTGAATCCTTTGGACCTTCC
AGCCATAATTGAGAGGTTACTGTCTGCAGTATTCCCGGGTTCATTAGATCTA
GCGGCACACACTAGGTACACTCCATAGCACTCCACTCGCCCGGGCTGCCTG
GGAAACAGTTAGACACTCCCCTATCAATTCATGGCTGGGAAACATCATCCA
GTATGCTGTATACTCCGTGAATCCTTTGGACCTTCCAGCCATAATTGAGAGG
TTACTGTCTGCAGTATTCCCGGGTTCATTAGATCTAGCGGCACACACTAGGT
ACACTCCATAAATCGAATTCCCGCGGCCGCCATGGCGGCCGGGAGCATGCG
ACGTCGGGCCCAATTCGCCCTATAGTGAGTCGTATTACAATTCACTGGCCGT
CGTTTTACAACGTCGTGACTGGGAAAACCCTGGCGTTACCCAACTTAATCG
CCTTGCAGCACATCCCCCTTTCGCCAGCTGGCGTAATAGCGAAGAGGCCCG
CACCGATCGCCCTTCCCAACAGTTGCGCAGCCTGAATGGCGAATGGACGCG
CCCTGTAGCGGCGCATTAAGCGCGGCGGGTGTGGTGGTTACGCGCAGCGTG
ACCGCTACACTTGCCAGCGCCCTAGCGCCCGCTCCTTTCGCTTTCTTCCCTT
CCTTTCTCGCCACGTTCGCCGGCTTTCCCCGTCAAGCTCTAATCGGGGGCTC
CCTTTAGGGTTCCGATTTAGTGCTTTACGGCACCTCGACCCCAAAAAACTTG
ATTAGGGTGATGGTTCACGTAGTGGGCCATCGCCCTGATAGACGGTTTTTTC
GCCCTTTGACGTTGGAGTCCACGTTCTTTAATAGTGGGACTCTTGTTCAAAC
TGGAACAACACTCAACCCCTATCTCGGTCTAATTC

- T7

AGGTGTATGAGTCGCATGCTCCGGCCGCCATGGCGGCCGCGGGAATTCGAT
TTATGGAGTGTACCTAGTGTGTGCCGCTAGATCTAATGAACCCGGGAATAC
TGCAGACAGTAACCTCTCAATTATGGCTGGAAGGTCCAAAGGATTCACGGA
GTATACAGCATACTGGATGATGTTTCCCAGCCATGAATTGATAGGGGAGTG
TCTAACTGTTTCCCAGGCAGCCCGGGCGAGTGGAGTGCTATGGAGTGTACC
TAGTGTGTGCCGCTAGATCTAATGAACCCGGGAATACTGCAAACAGTAACC
TCTCGATTATG

***Replicate 3 – Colonie C***

- Sp6

CCCACCTTGCATCCACGCGTTGGGAGCTCTCCCATATGGTCGACCTGCAGG
CGGCCGCGAATTCACTAGTGATTCAGTATACTCCGTGAATCCTTTGGACCTT
CCAGCCATAATTGAGAGGTTACTGTCTGCAGTATTCCCGGGTTCATTAGCA
GTATACTCCGTGAATCCTTTGGACCTTCCAGCCATAATTGAGAGGTTACTGT
CGGCAGTATTCCCGGGTTCATTAGATCTAGCGGCACACACTAGGTACACTC
CATAGCACTCCACTCGCCCGGGCTGCCTGGGAAACAGTTAGACACTCCCCT
ATCAATTCATGGCTGGGAAACATCATCCAGTATGCTGTATACTCCGTGAAT
CCTTTGGACCTTCCAGCCATAATTGAGAGGTTACTGTCTGCAGTATTCCCGG
GTTCATTAGATCTAGCGGCACACACTAGGTACACTCCATAATCGAATTCCC
GCGGCCGCCATGGCGGCCGGGAGCATGCGACGTCGGGCCCAATTCGCCCTA
TAGTGAGTCGTATTACAATTCACTGGCCGTCGTTTTACAACGTCGTGACTGG
GAAAACCCTGGCGTTACCCAACTTAATCGCCTTGCAGCACATCCCCCTTTCG
CCAGCTGGCGTAATAGCGAAGAGGCCCGCACCGATCGCCCTTCCCAACAGT
TGCGCAGCCTGAATGGCGAATGGACGCGCCCCTGTAGCGGCGCATTAAGCG
CGGCGGGTGTGGTGGTTACGCGCAGCGTGACCGCTACACTTGCCAGCGCCC
TAGCGCCCGCTCCTTTCGCTTTCTTCCCTTCCTTTCTCGCCACGTTCGCCGGC
TTTCCCCGTCAAGCTCTAAATCGGGGGGCTCCCTTTAGGGTTCCGATTTAGT
GCTTTTACGGC

- T7

GGATGAGAGTCTATGCTCCGGCCGCATGTATACATAATATATTAGAAATTA
CAATGGGATATAGGGGGGATTTATCTTTAAAGAAAGGTTATGTTCCTATAA
AAAATTCTTCACCTTTGGGTTTTGAAGATGTCACCATGATGAGATTAATACC
TTCCGTCAATGGGGTTCACAAACACCAGGTCATCATAATTTGGAATACGGC
AAGA

***Replicate 4 – Colonie A***

- Sp6

CCACCCTGCATCCACGCGTTGGGAGCTCTCCCATATGGTCGACCTGCAGGC
GGCCGCGAATTCACTAGTGATTCGTATACTCCGTGAATCCTTTGGACCTTCC
AGCCATAATTGAGAGGTTACACGGGCTTGACGCCTTTTCTATGCACACATA
CTCTCACCACGAACTGACGCGGGTGGCTTCAGCCCTCAGAAAACTTGGGGC
GCCACCCCTCAGGGTGTGGAAGAGTCGGGCTCGCGCAGTCAGGGCGTCCCT
CATCTCCCGTGGAGGGAAAGCGGCCGTTCGCGGCCGATATCTCTTCAATTG
GGCGGTGAAGACCAAGCTCAAACTCACTCCATTGCCGGAGGCGCGCCTACT
GGACTTATCCAGTTGGTTCACCGTCGGCGCCGGCGGGGGCGACATTTTTCA

CAGCGTGTCGCGCGCCCGACCCCGCTCATTCCTCTTCGGCCTACTCCTACTT
TTCGTAGGGGTAGGCCTCTTCCTACTCCCCGCTCGGTAGGAATTCGAATGGC
CATGGGACGTCGACCTGAGGTAATTATAACCCGGGCCCTATATATGGATCC
TAAGGTACCTAATTGCCTAGAAAACATGAGGATCACCCATGTCTGCAGGTC
GACTCTAGAAGACATGAGGATCACCCATGTCTGCAGTATTCCCGGGTTCAT
TAGATCCTAAGGTACCTAATTGCCTAGAAAACATGAGGATCACCCCATGTC
TGCAGGTCCGACTCCAGAAAACATGAGGATCACCCCATGTCTGCAGTATTC
CCGGGTTCATTTAGATCTAGCGGCACACACTAGGTACACTTCCATAAATCG
AATTCCCCGCGGCCGCCATGGCGGCCGGGAGCATGCCGACGTCGGGCCCAA
TTCCCCCCTATAGTGAGTC

- T7

GATGAGTCGCATGCTCCGGCCGCCATGGCGGCCGCGGGAATTCGATTTATG
GAGTGTACCTAGTGTGTGCCGCTAGATCTAATGAACCCGGGAATACTGCAG
ACATGGGTGATCCTCATGTTTTCTGGAGTCGACCTGCAGACATGGGTGATC
CTCATGTTTTCTAGGCAATTAGGTACCTTAGGATCTAATGAACCCGGGAAT
ACTGCAGACATGGGTGATCCTCATGTCTTCTAGAGTCGACCTGCAGACATG
GGTGATCCTCATGTTTTCTAGGCAATTAGGTACCTTAGGATCCATATATAGG
GCCCGGGTTATAATTACCTCAGGTCGACGTCCCATGGCCATTCGAATTCCTA
CCGAGCGGGGAGTAGGAAGAGGCCTACCCCTACGAAAAGTAGGAGTAGGC
CGAAGAGGAATGAGCGGGGTCGGGCGCGCGACACGCTGTGAAAAATGTCG
CCCCCGCCGGCGCCGACGGTGAACCAACTGGATAAGTCCAGTAGGCGCGCC
TCCGGCAATGGAGTGAGTTTGAGCTTGGTCTTCACCGCCCAATTGAAGAGA
TATCGGCCGCGAACGGCCGCTTTCCCTCCACGGGAGATGAGGGACGCCCTG
ACTGCGCGAGCCCGACTCTTCCACACCCTGAGGGGTGGCGCCCCAAGTTTT
CTGAGGGCTGAAGCCACCCGCGTCAGTTCGTGGGTGAGAGTATGTGTGCAT
AGAAAAGGCGTCAAGCCCGTGTAACCTCTCAATTATGGCTGGAAGGTCCAA
AGGATTCACGGAGTATACGAATCACTAGTGAAATTCGCGGCCGCCTGCAGG
TCGACCATATGGGAGAGCTCCCAACGCGTTTGGATGCATAGCTTGAGTATT
CTATAGTGTCACCTAAATAGCTTTGCCGTAATCATGGGTCATAGCTGTTTCC
TGTGTGAAATTGTTATCCGCTCACAATTTCCACACACCTTACGA

***Replicate 4 – Colonie B***

- Sp6

GGGCAATCTTGCCTCCACGCGTTGGGAGCTCTCCCATATGGTCGACCTGCA
GGCGGCCGCGAATTCACTAGTGATTTATACTCCGTGAATCCTTTGGACCTTC
CAGCCATAATTGAGAGGTTACACGGGCTTGACGCCTTTTCTATGCACACAT
ACTCTCACCACGAACTGACGCGGGTGGCTTCAGCCCTCAGAAAACTTGGGG
CGCCACCCCTCAGGGTGTGGAAGAGTCGGGCTCGCGCAGTCAGGGCGTCCC

TCATCTCCCGTGGAGGGAAAGCGGCCGTTTGCGGCCGATATCTCTTCAATT
GGGCGGTGAAGACCAAGCTCAAACTCACTCCATTGCCGGAGGCGCGCCTAC
TGGACTTATCCAGTTGGTTCACCGTCGACCTGAGGTAATTATAACCCGGGC
CCTATATATGGATCCTAAGGTACCTAATTGCCTAGAAAACACGAGGATCAC
CCATGTCTGCAGGTCGGCTCTAGAAAACATGAGGATCACCCATGTCTGCAG
TATTCCCGGGT

- T7

GGTGCGAGTCGCATGCTCCGGCCGCCATGGCGGCCGCGGGAATTCGATTAT
GGAGTGTACCTAGTGTGTGCCGCTAGATCTAATGAACCCGGGAATACTGCA
GACAAGGGTGATCCTCATGTTTTCTGGAGTCGACCTGCAGACATGGGTGAT
CCTCATGTTTTCTAGGCAATTAGGTACCTTAGGATCTAATGAACCCGGGAAT
ACTGCAGACATGGGTGATCCTCATGTTTTCTAGAGTCGACCTGCAGACATG
GGTGATCCTCATGTTTTCTAGGCAATTAGGTACCTTAGGATCTAATGAACCC
GGGAATACTGCAGACATGGGTGATCCTCATGTTTTCTAGGCAATTAGGTAC
CTTAGGATCTAATGAACCCGGGAATACTGCAGACATGGGTGATCCTCATGT
TTTCTAGAGCCGACCTGCAGACATGGGTGATCCTCGTGTTTTCTAGGCAATT
AGGTACCTTAGGATCCATATATAGGGCCCGGGTTATAATTACCTCAGGTCG
ACGGTGAACCAACTGGATAAGTCCAGTAGGCGCGCCTCCGGCAATGGAGT
GAGTTTGAGCTTGGTCTTCACCGCCCAATTGAAGAGATATCGGCCGCAAAC
GGCCGCTTTCCCTCCACGGGAGATGAGGGACGCCCTGACTGCGCGAGCCCG
ACTCTTCCACACCCTGAGGGGTGGCGCCCCAAGTTTTCTGAGGGCTGAAGC
CACCCGCGTCAGTTCGTGGGTGAGAGTATGTGTGCATAGAAAAGGCGTCAA
GCCCGTGTAACCTCTCAATTATGGCTGGAAGG

***Replicate 4 – Colonie C***

- Sp6

GGGGGCGGTAGGCTCCACGCGTTGGGAGCTCTCCCATATGGTCGACCTGCA
GGCGGCCGCGAATTCACTAGTGATTCAGTATATTCCGTGAATCTTTGGACCT
TCCAGCCATAATTGAGAGGTTACACGGGCTTGACGCCTTTTCTATGCACAC
ATACTCTCACCACGAACTGACGCGGGTGGCTTCAGCCCTCAGAAAACTTGG
GGCGCCACCCCTCAGGGTGTGGAAGAGTCGGGCTCGCGCAGTCAGGGCGTC
CCTCATCTCCCGTGGAGGGAAAGCGGCCGTTTGCGGCCGATATCTCTTCAA
TTGGGCGGTGAAGACCAAGCTCAAACTCACTCCATTGCCGGAGGCGCGCCT
ACTGGACTTATCCAATTGGTTCACCGTCGGCGCCGGCGAGGGCGACAAATT
TCACAAAGTGGCGCGCGTTCGACCCCCCTCA

- T7

TAGCGAGTCGCATGCTCCGGCCGCCATGGCGGCCGCGGGAATTCGATTTAT
GGAGTGTACCTAGTGTGTGCCGCTAGATCTAATGAACCCGGGAATACTGCA
GACATGGGTGATCCTCATGTTTTCTGGAGTCGACCTGCAGACATGGGTGAT
CCTCATGTTTTCTAGGCAGTTAGGTACCTTAGGATCTAATGAACCCGGGAAT
ACTACAGACATGGGTGATCCTCATGTTTTCTAGAGTCGACCTGCAGACATG
GGTGATCCTCATGTTTTCTAGGCAATTAGGTACCTTAGGATCTAATGAACCC
GGGAATACTGCAGACATGGGTGATCCTCATGTTTTCTAGGCAATTAGGTAC
CTTAGGATCTAATGAACCCGGGAATACTGCAGACATGGGTGATCCTCATGT
TTTCTAGAGTCGACCTGCAGACATGGGTGATCCTCATGTTTTCTAGGCAATT
AGGTACCTTAGGATCCATATATAGGGCCCGGGTTATAATTACCTCAGGTCG
ACGTCCCATGGCCATTCGAATTCCTACCGAGCGGGGAGTAGGAAGAGGCCT
ACCCCTACGAAAAGTAGGAGTAGGCCGAAGAGTAATGAGCGGGGTCGGGC
GCGCGACACGCTGTGAAAAAATGTCCCCCCCGCCGGCGCCGACGGTGAACC
AACTGGATAAGTCCAGTAAGGCGCGCCTCCCGGCAATGGAATGAGTTTTGA
GCTT

***Control 2***

- Sp6

GAAGGTATGTATCCACGCGTTGGGAGCTCTCCCATATGGTCGACCTGCAGG
CGGCCGCGAATTCACTAGTGATTCAGTATACTCCGTGAATCCTTGGACCTTC
CAGCCATAATTGAGAGGTTACACGGGCTTGACGCCTTTTCTATGCACACAT
ACTCTCACCACGAACTGACGCGGGTGGCTTCAGCCCTCAGAAAACTTGGGG
CGCCACCCCTCAGGGTGTGGAAGAGTCGGGCTCGCGCAGTCAGGGCGTCCC
TCATCTCCCGTGGAGGGAAAGCGGCCGTTTGCGGCCGATATCTCTTCAATT
GGGCGGTGAAGACCAAGCTCAAACTCACTCCATTGCCGGAGGCGCGCCTAC
TGGACTTATCCAGTTGGTTCACCGTTGGCGCCGGCTGGGGCGAC

- T7

GGGGCGAGTCGCATGCTCCGGCCGCCATGGCGGCCGCGGGAATTCGATTTA
TGGAGTGTACCTAGTGTGTGCCGCTAGATCTAATGAACCCGGGAATACTGC
AGACATGGGTGATCCTCGTGTTTTCTGGAGTCGACCTGCAGACATGGGTGA
TCCTCATGTTTTCTAGGCAATTAGGTACCTTAGGATCTAATGAACCCGGGAA
TACTGCAGACATGGGTGATCCTCATGTTTTCTAGAGTCGACCTGCAGACAT
GGGTGATCCTCATGTTTTCTAGGCAATTAGGTACCTTAGGATCTAATGAACC
CGGGAATACTGCAGACATGGGTGATCCTCATGTTTTCTAGGCAATTAGGTA
CCTTAGGATCTAATGAACCCGGGAATACTGCAGACATGGGTGATCCTCATG
TTTTCTAGAGTCGACCTGCAGACATGGGTGATCCTCATGTTTTCTAGGCAAT
TAGGTACCTTAGGATCCATATATAGGGCCCGGGTTATAATTACCTCAGGTC

GACGTCCCATGGCCATTCGAATTCCTACCGAGCGGGGAGTAGGAAGAGGCC
TACCCCTACGAAAAGTAGGAGTAGGCCGAAGAGTAATGAGCGGGGTCGGG
CGCGCGACACGCTGTGAAAAATGTCGCCCCCGCCGGCGCCGACGGTGAACC
AACTGGATAAGTCCAGTAGGCGCGCCTCCGGCAATGGAGTGAGTTTGAGCT
TGGTCTTCACCGTCCAATTGAAGAGATATCGGCCCGCAAACGGCCGCTTTC
CCTCCACGGGGAAATGAGGGACGCCCTGACTGCGCGAGCCCCAACTCTTTC
CACACCCTGAGGGGGGGGCGCCCCAAGTTTTCTGAGGCTGAACCCACCCCC
CGTCAATTTCCTGGTGAA

***Control 3***

- Sp6

GTCATTAGCATCCACGCGTTGGGAGCTCTCCCATATGGTCGACCTGCAGGC
GGCCGCGAATTCACTAGTGATTATACTCCGTGAATCCTTTGGACCTTCCAGC
CATAATTGAGAGGTTACACGGGCTTGACGCCTTTTCTATGCACACATACTCT
CACCACGAACTGACGCGGGTGGCTTCAGCCCTCAGAAAACTTGGGGCGCCA
CCCCTCAGGGTGTGGAAGAGTCGGGCTCGCGCAGTCAGGGCGTCCCTCATC
TCCCGTGGAGGGAAAGCGGCCGTTTGCGGCCGATATCTCTTCAATTGGGCG
GTGAAGACCAAGCTCAAACTCACTCCATTGCCGGAGGCGCGCCTACTGGAC
TTATCCAGTTGGTTCACCGTCGGCGCCGGCGGGGGCGACATTTTTCACAGC
GTGTCGCGCGCCCGACCCCGCTCATTACTCTTCGGCCTACTCCTACTTTTCG
TAGGGGTAGGCCTCTTCCTACTCCCCGCTCGGTAGGAATTCGAATGGCCAT
GGGACGTCGACCTGAGGTAATTATAACCCGGGCCCTATATATGGATCCTAA
GGTACCTAATTGCCTAGAAAACATGAGGATCACCCATGTCTGCAGGTCGAC
TCTAGAAAACATGAGGATCACCCATGTCTGCAGTATTCCCGGGTTCATTAG
ATCCTAAGGTACCTAATTGCCTAGAAAACATGAGGATCACCCATGTCTGCA
GTATTCCCGGGTTCATTAGATCCTAAGGTACCTAATTGCCTAGAAAACATG
AGGATCACCCATGTCTGCAGGTCGACTCTAGAAAACATGGGATCACCCATG
TCTGCAGTATTCCCGGGTTCATTAGATCCTAAGGTACCTTATTGCCTAGAAA
ACATGAGATCACCCATGTCTGCAGTCGACTCCAGAAAACATGAGGATCACC
CATGTCTGCAGTATTCCCGGGTTCATAGATCTAGCGGCACACACCTAGTAC
CACTCCATAAATCGAATTCCCCGCGGCGGCATGGCGGCCGGGTAGCAATGC
GAACGTCGGCCCAATTTCGCCTATAGGAAGTCTATTACAGTCACCTGGACG
TCGTTAAAACGTCTGACCTGGGAAAACCCTGGCGTTACCCAACTAATGCGC
TTGGAGACAAATCCCCTTTCGCCAGCATGGCGGTAATGCGAGAGCTGCACG
GAATTGCTTTCCTACATGGCAACCTGGAATGGCAAAGTGA

- T7

TGACGAGTCGCATGCTCCGGCCGCCATGGCGGCCGCGGGAATTCGATTTAT
GGAGTGTACCTAGTGTGTGCCGCTAGATCTAATGAACCCGGGAATACTGCA
GACATGGGTGATCCTCATGTTTTCTGGAGTCGACCTGCAGACATGGGTGAT
CCTCATGTTTTCTAGGCAATTAGGTACCTTAGGATCTAATGAACCCGGGAAT
ACTGCAGACATGGGTGATCCTCATGTTTTCTAGAGTCGACCTGCAGACATG
GGTGATCCTCATGTTTTCTAGGCAATTAGGTACCTTAGGATCTAATGAACCC
GGGAATACTGCAGACATGGGTGATCCTCATGTTTTCTAGGCAATTAGGTAC
CTTAGGATCTAATGAACCCGGGAATACTGCAGACATGGGTGATCCTCATGT
TTTCTAGAGTCGACCTGCAGACATGGGTGATCCTCATGTTTTCTAGGCAATT
AGGTACCTTAGGATCCATATATAGGGCCCGGGTTATAATTACCTCAGGTCG
ACGTCCCATGGCCATTCGAATTCCTACCGAGCGGGGAGTAGGAAGAGGCC

# Appendix X – Related Publication: Dynamic Imaging of the Hepatitis C Virus NS5A Protein During a Productive Infection.

## Statement of Authorship

| | |
|---|---|
| Title of Paper | Dynamic imaging of the hepatitis C virus NS5A protein during a productive infection |
| Publication Status | Published |
| Publication Details | Eyre, N.S., Fiches, G.N., Aloia, A.L., Helbig, K.J., McCartney, E.M., McErlean, C.S., Li, K., Aggarwal, A., Turville, S.G., Beard, M.R., 2014a. Dynamic imaging of the hepatitis C virus NS5A protein during a productive infection. Journal of virology 88, 3636-3652 |

By signing the Statement of Authorship, each author certifies that permission is granted for the publication to be included in the candidate thesis.

| | |
|---|---|
| Name of Principal Author | N.S. Eyre |
| Signature | |
| Date | 12-3-15 |

| | |
|---|---|
| Name of Co-Author (candidate) | G.N. Fiches |
| Signature | |
| Date | 11/03/2015 |

| | |
|---|---|
| Name of Co-Author | A.L. Aloia |
| Signature | |
| Date | 22/3/15 |

| | |
|---|---|
| Name of Co-Author | K.J. Helbig |
| Signature | |
| Date | 12/3/2015 |

| Name of Co-Author | E.M. McCartney |
|---|---|
| Signature | |
| Date | 17/3/15 |

| Name of Co-Author | C.S. McErlean |
|---|---|
| Signature | |
| Date | 12/3/2015. |

| Name of Co-Author | K. Li |
|---|---|
| Signature | |
| Date | 3/12/15 |

| Name of Co-Author | A. Aggarwal |
|---|---|
| Signature | |
| Date | |

| Name of Co-Author | S.G. Turville |
|---|---|
| Signature | |
| Date | 2/3/2015 |

| Name of Co-Author | M.R. Beard |
|---|---|
| Signature | |
| Date | 12/3/15 |

Publication included immediately after identically to its publication in Journal of Virology:

JVI Journals.ASM.org

# Dynamic Imaging of the Hepatitis C Virus NS5A Protein during a Productive Infection

**Nicholas S. Eyre,[a,b] Guillaume N. Fiches,[a,b] Amanda L. Aloia,[a,b] Karla J. Helbig,[a,b] Erin M. McCartney,[a,b] Christopher S. P. McErlean,[c] Kui Li,[d] Anupriya Aggarwal,[e] Stuart G. Turville,[e] Michael R. Beard[a,b]**

School of Molecular and Biomedical Science and Centre for Molecular Pathology, University of Adelaide, Adelaide, South Australia, Australia[a]; Centre for Cancer Biology, SA Pathology, Adelaide, South Australia, Australia[b]; School of Chemistry, The University of Sydney, Sydney, New South Wales, Australia[c]; Department of Microbiology, Immunology and Biochemistry, University of Tennessee Health Science Center, Memphis, Tennessee, USA[d]; Kirby Institute UNSW, Immunovirology and Pathogenesis Program, Darlinghurst, New South Wales, Australia[e]

**ABSTRACT**

**Hepatitis C virus (HCV) NS5A is essential for viral genome replication within cytoplasmic replication complexes and virus assembly at the lipid droplet (LD) surface, although its definitive functions are poorly understood. We developed approaches to investigate NS5A dynamics during a productive infection. We report here that NS5A motility and efficient HCV RNA replication require the microtubule network and the cytoplasmic motor dynein and demonstrate that both motile and relatively static NS5A-positive foci are enriched with host factors VAP-A and Rab5A. Pulse-chase imaging revealed that newly synthesized NS5A foci are small and distinct from aged foci, while further studies using a unique dual fluorescently tagged infectious HCV chimera showed a relatively stable association of NS5A foci with core-capped LDs. These results reveal new details about the dynamics and maturation of NS5A and the nature of potential sites of convergence of HCV replication and assembly pathways.**

**IMPORTANCE**

**Hepatitis C virus (HCV) is a major cause of serious liver disease worldwide. An improved understanding of the HCV replication cycle will enable development of novel and improved antiviral strategies. Here we have developed complementary fluorescent labeling and imaging approaches to investigate the localization, traffic and interactions of the HCV NS5A protein in living, virus-producing cells. These studies reveal new details as to the traffic, composition and biogenesis of NS5A foci and the nature of their association with putative sites of virus assembly.**

Hepatitis C virus (HCV) is a major cause of serious liver disease worldwide and is the founding member of the *Hepacivirus* genus within the *Flaviviridae* family of positive sense RNA viruses. Following entry and uncoating, the ~9.6-kb HCV genome is directly translated at the rough endoplasmic reticulum (ER) and the encoded polyprotein is co- and posttranslationally cleaved by host and viral proteases to liberate the structural proteins (core, E1, and E2), the hydrophobic peptide p7 and the nonstructural (NS) proteins (NS2, NS3, NS4A, NS4B, NS5A, and NS5B) (reviewed in reference 1). Together with a growing list of essential host factors, the viral NS3-5B proteins are each essential components of cytoplasmic replication complexes (RCs) that are responsible for replication of the viral genome (2). In contrast, the remaining HCV proteins are dispensable for genome replication, but all play critical roles in the assembly of infectious virus particles (reviewed in reference 3). Interestingly, most if not all of the NS proteins also play essential roles in virus particle assembly. Although NS5A is considered to be a critical regulator of both viral RNA replication in RCs and infectious virion assembly, little is known about the dynamics of RCs and their NS5A-dependent association with sites of virus assembly.

Like all positive-strand RNA viruses, HCV induces cytoplasmic membrane alterations that support and compartmentalize the replication of its genome (4). In this context the NS4B protein has been shown to induce the formation of a convoluted multivesiculated cytoplasmic structure known as the "membranous web" that is at least partly derived from the ER (5, 6). These structures are enriched with other NS proteins and HCV RNA and, at the ultrastructural level, contain numerous heterogeneous single-membrane vesicles, double-membrane vesicles, and multimembrane vesicles (7–9). Recent studies have indicated that double-membrane vesicles are the likely sites of efficient HCV RNA replication and that NS5A is essential for their formation (7, 9). This function of NS5A may be at least partially attributable to its ability to recruit and activate the lipid kinase phosphatidylinositol-kinase III alpha (PI4KIIIα) to stimulate the local production of phosphatidylinositol 4-phosphate and induce morphologically normal membranous webs (10, 11). Among a growing list of other host factors that have been described as important cofactors for HCV RNA replication are proteins involved in lipid transport (VAP-A and ANXA2) and early endosome regulation and traffic (Rab5 and EEA1) (12–14).

Another essential property of RCs is their association with sites of virus particle assembly (4). In this context a function(s) of NS5A that maps to its C terminus (domain III) is thought to dictate the transfer of HCV RNA between RCs and core-coated LDs for encapsidation, potentially via a direct core-NS5A interac-

**Received** 11 September 2013 **Accepted** 24 December 2013
**Published ahead of print** 15 January 2014
**Editor:** M. S. Diamond
Address correspondence to Michael R. Beard, michael.beard@adelaide.edu.au.
Supplemental material for this article may be found at http://dx.doi.org/10.1128/JVI.02490-13.

doi:10.1128/JVI.02490-13

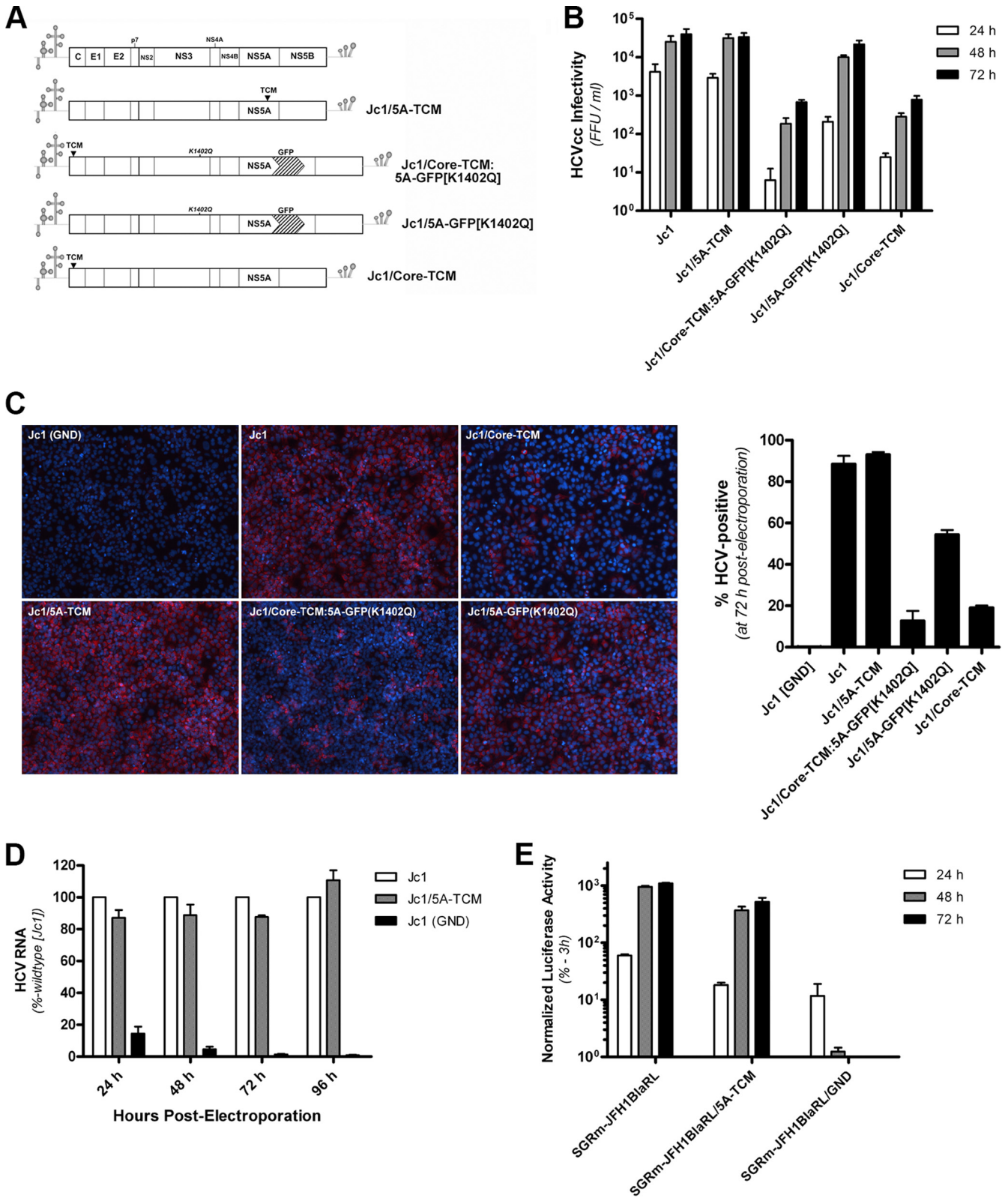


**FIG 1** Development and characterization of Jc1 derivatives for live cell imaging. (A) Schematic diagrams of virus constructs (see the supplemental material for details). (B) Infectious virus particle production was determined at 24 to 72 h postelectroporation with the indicated HCV RNA transcripts. The data are means + the SEM for at least three separate electroporations. (C) Immunofluorescent labeling of HCV proteins (patient HCV antisera; red) at 72 h postelectroporation. Nuclei were counterstained with DAPI (blue). The graph inset depicts the percentage of HCV-positive cells (means + the SEM, $n = 3$). (D) Intracellular HCV RNA levels (normalized to *RPLPO* mRNA) were quantified by qRT-PCR (data are expressed as % Jc1 HCV RNA levels; means + the SEM [$n = 3$]). (E) Huh-7.5+FLuc cells were electroporated with the indicated RLuc-encoding subgenomic replicon transcripts before determination of normalized luciferase activity (RLuc/FLuc) at the indicated time points, expressed as % 3 h (input). The data are means ± the SEM ($n = 4$). Normalized RLuc activity was significantly lower for SGRm-JFH1BlaRL/5A-TCM compared to SGRm-JFH1BlaRL at each time point ($P < 0.05$).

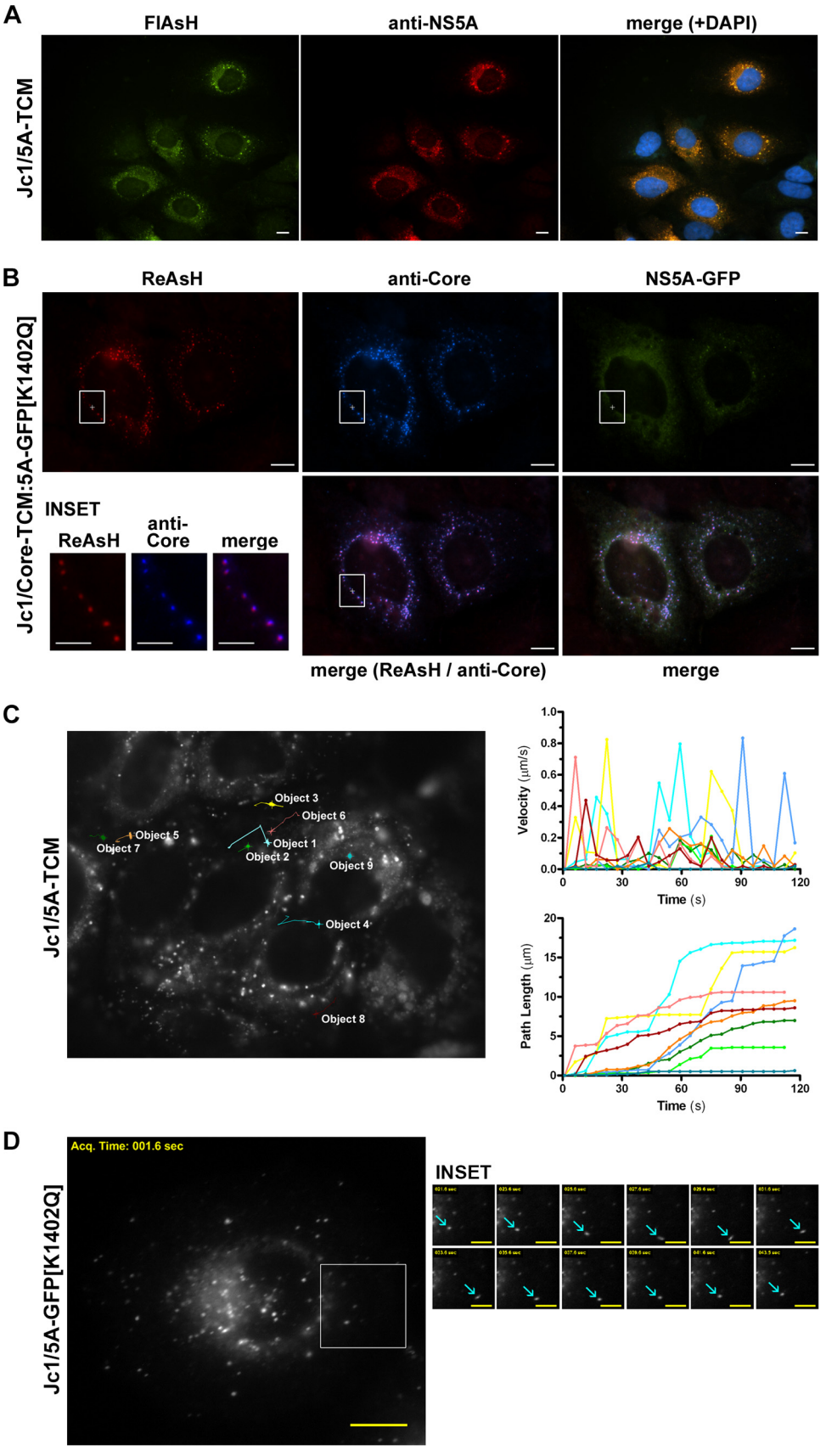
A
FlAsH
anti-NS5A
merge (+DAPI)
Jc1/5A-TCM
B
ReAsH
anti-Core
NS5A-GFP
Jc1/Core-TCM:5A-GFP[K1402Q]
INSET
ReAsH
anti-Core
merge
merge (ReAsH / anti-Core)
merge
C
Jc1/5A-TCM
Object 3
Object 6
Object 5
Object 7
Object 1
Object 2
Object 9
Object 4
Object 8
Velocity (μm/s)
Time (s)
Path Length (μm)
Time (s)
D
Jc1/5A-GFP[K1402Q]
Acq. Time: 001.6 sec
INSET

tion (15–17). Although new details about the biogenesis of HCV RCs and their association with potential sites of virus assembly are emerging, there is a paucity of information regarding the dynamics of these events. In the present study we have developed approaches to visualize the localization and traffic of fluorescently tagged NS5A during a productive HCV replication cycle. We show that long-range motility of NS5A-positive structures (putative RCs) is dependent on host microtubules and cytoplasmic dynein and that both relatively static and motile NS5A-positive structures are enriched with previously identified co-opted host factors. Using pulse-chase imaging, we show that newly synthesized NS5A is localized to foci that are smaller than and distinct from those of aged NS5A, although both classes display characteristics of microtubule-dependent transport. Finally, for the first time, we have visualized the association of putative RCs with sites of virus assembly in living cells and suggest that weak and/or transient interactions of HCV core and NS5A proteins may link HCV replication and assembly pathways. Collectively, these studies provide new details as to the dynamics, components, and biogenesis of NS5A foci and their association with sites of virion assembly.

## MATERIALS AND METHODS

**Viruses, plasmids, siRNAs, and cells.** Plasmids pJc1/GFP (18) and pJFH1 (19) were generously provided by Ralf Bartenschlager (University of Heidelberg, Heidelberg, Germany) and Takaji Wakita (National Institute of Infectious Diseases, Tokyo, Japan), respectively. Subgenomic replicon SGRm-JFH1BlaRL and replication-defective derivative SGRm-JFH1BlaRL/GND have been described previously (20). Detailed descriptions of all tagged Jc1- and SGRm-JFH1BlaRL derivatives and lentiviral expression/shRNA vectors are provided in the supplemental material, as are details regarding *in vitro* HCV RNA transcription, electroporation/transfection, infections, and determination of HCV infectivity. CellLight Tubulin-RFP (Life Technologies) was used to visualize microtubules according to manufacturer's instructions. Nontargeting and DYNC1H1-specific small interfering RNAs (siRNAs) were purchased from Life Technologies (Silencer Select; catalogue numbers s4202 and 4390846, respectively).

Huh-7.5 cells (21) were generously provided by Charles Rice (Rockefeller University, New York, NY). Huh-7.5 and 293T cells were cultured in complete Dulbecco modified Eagle medium (i.e., Dulbecco modified Eagle medium [DMEM] supplemented with 100 U of penicillin/ml, 100 mg of streptomycin/ml, and 10% fetal bovine serum [Life Technologies]). Details regarding the generation of stable Huh-7.5-derived cell lines are given in the supplemental material. For live cell imaging studies, cells were cultured in complete DMEM lacking phenol red.

**Antibodies and chemical inhibitors.** Primary antibodies against NS5A (mouse monoclonal antibody [MAb] 9E10) and core (rabbit polyclonal RR8) were generously provided by Charles Rice (Rockefeller University) and Michinori Kohara (Tokyo Metropolitan Institute of Medical Science, Tokyo, Japan), respectively. Mouse MAbs against core (C7-50; Thermo Scientific), FLAG (M2; Sigma), Myc (9E10; Roche Applied Science), and β-actin (AC-15; Sigma) were purchased. Mouse IgG1(κ) and IgG2a(κ) isotype control MAbs (BD Pharmingen) and rabbit polyclonal antibodies against VAP-A (Novus Biologicals), Rab5 (Cell Signaling Technology), DYNC1H1 (Santa Cruz; R-325), and GAPDH (glyceraldehyde-3-phosphate dehydrogenase; Rockland Immunochemicals) were purchased as indicated. Human anti-HCV antiserum was prepared as described previously (22). Alexa Fluor-350-, -488-, -555-, and -594-conjugated secondary antibodies (Life Technologies) and horseradish peroxidase-conjugated secondary antibodies (Thermo Scientific) were purchased as indicated. Chemical inhibitors are detailed in the supplemental material.

**Labeling of TCM-tagged proteins with biarsenical dyes.** The biarsenical dyes FlAsH-$EDT_2$ and ReAsH-$EDT_2$ were synthesized as described previously (23). Labeling of tetracysteine motif (TCM)-tagged HCV proteins was performed as described previously (24), with minor modifications. Briefly, for each 35-mm dish of cells, 1 μl of 1 mM FlAsH (or ReAsH) solution (prepared in dimethyl sulfoxide [DMSO]) was mixed with 1 μl of 25 mM 1,2-ethanedithiol (EDT; Sigma) (diluted in DMSO) and then incubated for 10 min at room temperature. Meanwhile, cells were washed twice with complete Hanks balanced salt solution (Life Technologies) containing 5.6 mM glucose (HBSS/glucose) before the addition of 1 ml of HBSS/glucose. Next, 1 ml of HBSS/glucose was added to a new tube, and a 100-μl aliquot of this was taken and added to the FlAsH/EDT solution and mixed by pipetting. After incubation for 5 min at room temperature, this FlAsH/EDT/HBSS/glucose solution was mixed with the remaining 900 μl of HBSS/glucose and added to the cell culture dish to achieve a final concentration of 500 nM FlAsH-$EDT_2$. The cells were then returned to culture at 37°C for 30 min before being washed twice with HBSS/glucose and three times at 37°C for 15 min with HBSS/glucose containing 2.8 mM 2,3-dimercapto-1-propanol (Sigma). The cells were then washed twice with HBSS/glucose and fixed for immunofluorescent labeling or harvested by trypsinization and reseeded into 0.2% gelatin-coated 35-mm coverslip bottom dishes (MatTek) and returned to culture for 24 h prior to live cell imaging.

**Labeling of SNAP-tagged NS5A with fluorescent SNAP-tag substrates.** Labeling of SNAP-tagged NS5A with fluorescent SNAP-tag substrates, SNAP-Cell 505 and SNAP-Cell TMR-Star, was performed according to the manufacturer's instructions (New England BioLabs).

***In situ* PLAs.** *In situ* proximity ligation assays (PLAs) were performed using a Duolink II In Situ Red Starter Kit (Olink Bioscience) according to the manufacturer's instructions. Briefly, cells were first cultured on 0.2% gelatin-coated coverslips, fixed with ice-cold acetone-methanol (1:1) for 10 min at 4°C, permeabilized, blocked, and incubated with primary antibodies (mouse anti-core [C7-50] + rabbit anti-core [RR8] or mouse anti-NS5A [9E10] + rabbit anti-core [RR8]; each diluted 1:200). Samples were then washed three times with phosphate-buffered saline (PBS)–1% bovine serum albumin (BSA) and incubated with appropriately diluted PLA probes (anti-Mouse MINUS and anti-Rabbit PLUS diluted in PBS–1% BSA [1:1:3]) for 1 h at 37°C in a humidity chamber. The samples were then washed and processed for probe ligation, signal amplification, and mounting according to manufacturer's instructions.

**FIG 2** Specific labeling of TCM-tagged HCV proteins with biarsenical dyes. (A) At 3 days postelectroporation with Jc1/5A-TCM RNA, Huh-7.5 cells were labeled with FlAsH (green; left panel), fixed, and processed for immunofluorescence with anti-NS5A antibody (red; middle panel). Merged images (right panel) show colocalization (yellow) and DAPI-stained nuclei (blue) (Pearson correlation = 0.95). (B) At 3 days postelectroporation with Jc1/Core-TCM:5A-GFP[K1402Q] RNA, Huh-7.5 cells were labeled with ReAsH (red; top left panel), fixed, and processed for immunofluorescent labeling of core (blue; top middle panel). NS5A-GFP epifluorescence was also captured (green; top right panel). Insets and merged images are depicted in the lower panels. Pearson correlations for colocalization of ReAsH-labeling with antibody labeling and NS5A-GFP epifluorescence were 0.84 and 0.65, respectively. (C) Live cell imaging of NS5A-TCM. At 48 h postelectroporation with Jc1/5A-TCM RNA, Huh-7.5 cells were labeled with ReAsH and examined by live cell imaging at 72 h. Images were acquired every 5.3 s for 2 min (see Movie S1 in the supplemental material). The velocities and path lengths of a number of discrete NS5A-positive are depicted in adjacent graphs. (D) Live cell imaging of NS5A-GFP at 4 days postinfection with Jc1/5A-GFP[K1402Q] (multiplicity of infection [MOI] of ~0.05) (see Movie S2 in the supplemental material). Images were acquired every 2 s for 3 min. The insets depict the traffic of a representative motile NS5A-GFP structure (arrows). Image sharpening (using a Gaussian blur filter with a radius of 1.5 pixels), background subtraction, and contrast stretching were then applied (see the supplemental material). For all micrographs, scale bars represent 10 and 5 μm for main and inset images, respectively.

**Fluorescence microscopy.** Laser scanning confocal microscopy was performed using a Bio-Rad Radiance 2100 confocal system linked to an Olympus IX70 inverted microscope or a Zeiss LSM 700 confocal microscope system. For both systems, samples were visualized using a ×60/1.4NA water immersion objective lens (with a ×2 to ×3 zoom), and images were acquired sequentially for each fluorophore. Wide-field fluorescence microscopy was performed using a Nikon TiE inverted fluorescence microscope using a Plan Apochromat ×60 NA 1.4 oil immersion lens or a Super Plan Fluor ×40 NA 0.4 or Plan Fluor ×10 NA 0.3 objective lens (Nikon), as appropriate. Illumination was provide by an Intensilight C-HGFIE precentered fiber illuminator mercury light source (Nikon), while BrightLine single-band filter sets (DAPI-5060C-NTE-ZERO, FITC-3540C-NTE-ZERO, and TxRed-4040C-NTE-ZERO) were from Semrock, and emitted light was collected with a monochrome 12-bit cooled charge-coupled device camera with a maximum resolution of 1,280×1,024 (DS-Qi1; Nikon). For live cell imaging, cells cultured on coverslip bottom 35-mm dishes (MatTek) were maintained at 37°C using a heated microscope stage insert (Okolab) and visualized using the above ×60 NA 1.4 oil immersion objective lens. For some of these experiments, a Nikon perfect focus system was applied. Unless otherwise indicated (see movie legends in the supplemental material), images were acquired (without binning) every 3 s using exposure times of 1 s and a maximum camera gain setting of 2. Image processing and analysis is described in the supplemental material.

**Statistical analysis.** Data are expressed as means ± the standard errors of the mean (SEM). Statistical analysis was performed by using the Student *t* test or the Mann-Whitney U-test using Prism 5 (GraphPad Software), with $P < 0.05$ considered to be statistically significant.

## RESULTS

**Development and characterization of infectious HCV derivatives for live cell imaging of NS5A and core.** To track NS5A localization with minimal disruption of the HCV life cycle, we used complementary fluorescent tagging approaches. First, we inserted an optimized tetracysteine motif (TCM; amino acids FLNCCPG CCMEP) within domain III of NS5A in the infectious HCV chimera Jc1 (25), to generate Jc1/5A-TCM and enable covalent labeling of encoded NS5A-TCM with fluorescent biarsenical dyes (FlAsH/ReAsH) for live cell imaging. Second, to complement our findings with Jc1/5A-TCM, we incorporated the adaptive mutation K1402Q (11) into Jc1/GFP (18), which encodes a GFP insertion in domain III of NS5A in Jc1, to generate Jc1/5A-GFP[K1402Q]. Similarly, to enable simultaneous visualization of the localization and traffic of HCV NS5A and core proteins, we inserted a TCM within the HCV core coding sequence (26, 27) of Jc1/5A-GFP[K1402Q], to generate Jc1/Core-TCM:5A-GFP[K1402Q] (Fig. 1A). Compared to parent Jc1, the incorporation of a TCM within NS5A had no appreciable effect on NS5A processing (not shown) and no significant impact on infectious virus production (Fig. 1B) or the spread of HCV infection through Huh-7.5 cell culture (Fig. 1C) or intracellular HCV RNA levels (Fig. 1D). Accordingly, incorporation of a TCM within NS5A in a *Renilla* luciferase (RLuc)-encoding JFH1-derived subgenomic replicon had minimal impact on its replicative capacity (Fig. 1E). As reported previously (11), we found that the incorporation of the K1402Q adaptive mutation into Jc1/GFP restored infectivity to levels approaching those of untagged Jc1, despite delayed kinetics (Fig. 1B). Jc1/Core-TCM:5A-GFP[K1402Q] displayed an ~1.5-log impairment of infectious virus production compared to untagged Jc1 and delayed spread of infection through Huh-7.5 cell culture (Fig. 1B and C) that could be attributed predominantly to the TCM insertion in core (Fig. 1B). Importantly, neither TCM nor GFP insertions in NS5A nor the TCM insertion in core appreciably altered the localization of these proteins or the degree of core/NS5A colocalization in Huh-7.5 cells (not shown).

We next confirmed specific labeling of TCM-tagged HCV proteins with fluorescent biarsenical dyes. Huh-7.5 cells were electroporated with Jc1/5A-TCM RNA, cultured, and labeled with FlAsH, before fixation and immunofluorescent labeling of NS5A. This revealed near-complete overlap between the signals associated with FlAsH- and antibody-mediated labeling of NS5A-TCM, with minimal labeling of uninfected cells (Pearson correlation = 0.95) (Fig. 2A). The specificity of labeling of core-TCM encoded by Jc1/Core-TCM:5A-GFP[K1402Q] was similarly determined, except that cells were labeled with ReAsH and an anti-core antibody. This revealed a close overlap between ReAsH (red)- and antibody (blue)-mediated labeling of core-TCM (Pearson correlation = 0.84) and a partial overlap of ReAsH signals with NS5A-GFP epifluorescence (Pearson correlation = 0.65) (Fig. 2B). Assessment of the impact of biarsenical dye labeling on infectious virus production revealed a 50.6% ± 3.3% decrease (means ± the SEM; $n = 3$) in infectious virus production over a 24-h period following labeling (not shown).

Next, we examined the localization and traffic of NS5A in living cells during a productive HCV infection. Huh-7.5 cells were electroporated with Jc1/5A-TCM RNA, labeled with ReAsH and analyzed by live cell imaging (Fig. 2C; see Movie S1 in the supplemental material). This labeling strategy, with a 24-h culture period between FlAsH/ReAsH labeling and live cell imaging, was used to minimize background labeling and limit any unanticipated effects of labeling, such as the exposure of cells to reducing agents and serum deprivation. ReAsH-labeled NS5A-TCM was predominantly found in large, relatively static structures and smaller highly motile structures that shuttle throughout the cytoplasm in a sporadic manner (Fig. 2C; see Movie S1 in the supplemental material). Manual tracking analysis demonstrated that these structures traffic at velocities in the order of 1 $\mu m\ s^{-1}$ and frequently pause and change direction, sometimes moving back along what appear to be the same paths (e.g., "Object 3"). Consistent with this, in cells that had been infected with Jc1/5A-GFP[K1402Q], GFP-tagged NS5A displayed similar localization and trafficking patterns (Fig. 2D and see Movie S2 in the supplemental material). Further analysis of NS5A-GFP traffic at high temporal resolution (16 frames $s^{-1}$), which more readily distinguishes velocity changes within bursts, revealed that typical motile NS5A-GFP foci display bidirectional traffic at peak velocities of ~5 $\mu m\ s^{-1}$ for runs of ~2 $\mu m$ (not shown). Collectively, these results show that in a productive infection TCM-tagged NS5A and core proteins can be specifically labeled with fluorescent biarsenical dyes and that NS5A localizes to both relatively static structures and highly motile structures that traffic sporadically throughout the cytoplasm. These results raise questions as to the mechanisms and purpose of NS5A motility and whether both motile and immotile NS5A foci represent RCs.

**NS5A traffic is dependent on the host microtubule network and cytoplasmic dynein.** In the context of a subgenomic HCV replicon it has previously been shown that NS5A traffic is microtubule dependent (28). To confirm and extend this work, we observed the traffic of motile NS5A-positive structures in close association with α-tubulin-RFP-positive microtubules during a productive infection (Fig. 3A and see Movie S3 in the supplemental material) and demonstrated that treatment of parallel cultures with inhibitors of microtubule dynamics, nocodazole and vinblas-

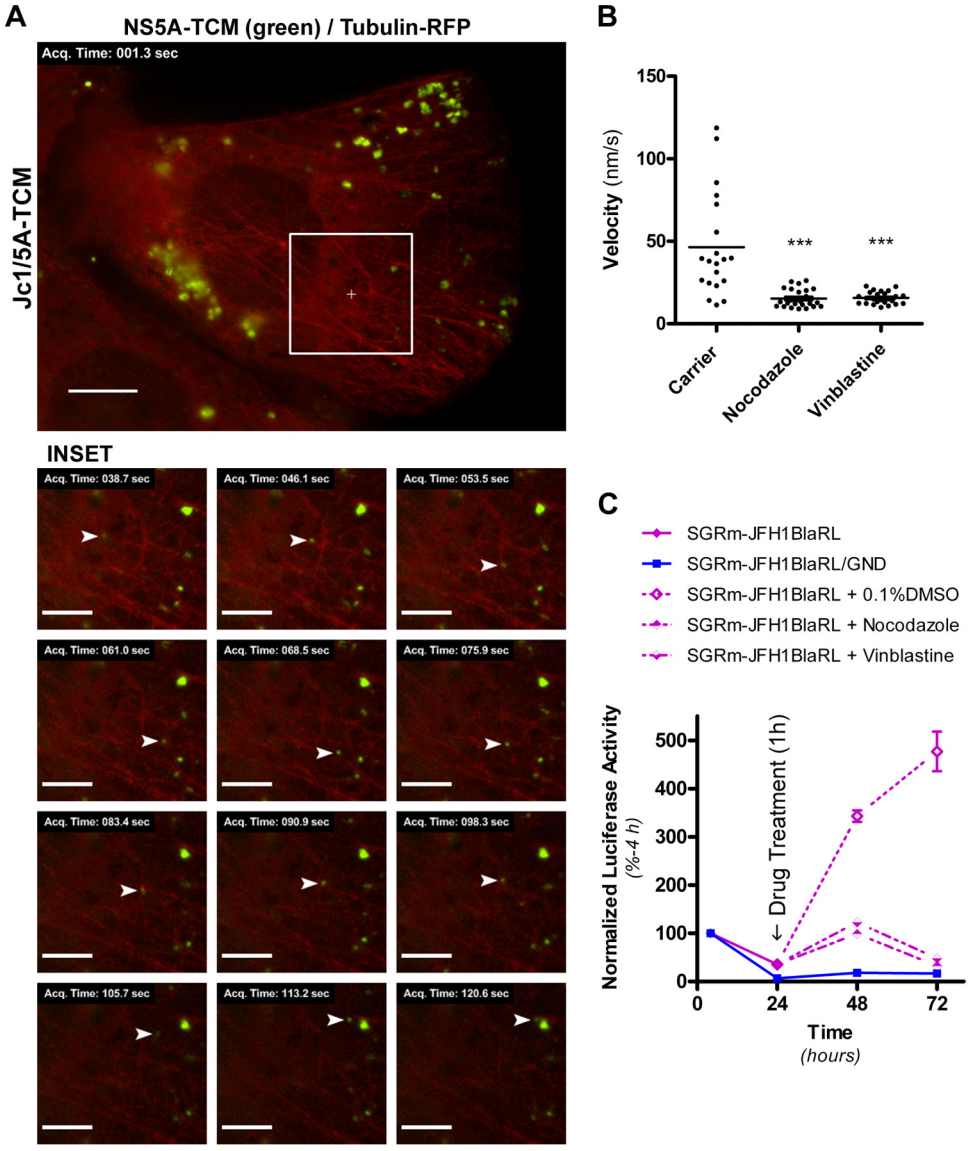


**FIG 3** Involvement of the microtubule network in NS5A-TCM traffic and HCV replication. (A) Huh-7.5 cells were electroporated with Jc1/5A-TCM RNA, labeled with FlAsH (green) at 48 h postelectroporation, transduced with CellLight Tubulin-RFP (red), and analyzed by live cell imaging at 72 h postelectroporation. Images were acquired every 7.5 s for 3 min. Image sharpening (using a Gaussian blur filter with a radius of 1.5 pixels), background subtraction, and contrast stretching were then applied (see Materials and Methods). The traffic of a representative NS5A-TCM-positive structure (arrowhead) in close proximity to RFP-labeled microtubules is depicted in the inset images (see Movie S3 in the supplemental material). Scales bars represent 10 and 5 μm for main and inset images, respectively. (B) Huh-7.5 cells were electroporated, transduced, and labeled, as described above, before exposure to 20 μM nocodazole, 20 μM vinblastine, or carrier alone (0.1% DMSO) for 1 h and live cell imaging. These treatments induced gross disruption of the microtubule network, as judged by diffuse cytoplasmic localization of α-tubulin-RFP (not shown). The graph depicts the mean velocities of arbitrarily selected NS5A-TCM-positive structures over the course of 3 min ($n = 20$ to 25 structures/group). Compared to the controls the mean velocities of NS5A-TCM-positive structures were significantly different for the nocodazole (***, $P < 0.0001$) and vinblastine (***, $P < 0.0001$) treatment groups (unpaired Student $t$ tests). (C) Huh-7.5+FLuc cells were electroporated with SGRm-JFH1BlaRL or SGRm-JFH1BlaRL/GND transcripts and exposed to carrier (0.1% DMSO), 20 μM nocodazole, or 20 μM vinblastine for 1 h at 24 h postelectroporation before being washed and returned to culture. Samples were collected at the indicated time points before determination of the normalized luciferase activity (RLuc:FLuc, to normalize HCV replication levels to cell number/viability), and values are expressed as a percentage of normalized input values at 4 h. The data are means ± the SEM ($n = 4$).

tin, resulted in arrest of these structures and no apparent linear foci movement (Fig. 3B). Furthermore, consistent with earlier studies (29), we found that transient disruption of microtubule dynamics dramatically inhibited HCV RNA replication (Fig. 3C).

We next investigated the involvement of the motor protein dynein in the traffic of NS5A-positive foci, given the central role of this motor in microtubule-dependent vesicular/organellar traffic, including that of early endosomes (see references 30 and 31 and references therein) which are co-opted by HCV (13). First, we investigated the impact of the selective cytoplasmic dynein inhibitor ciliobrevin D (32) on HCV RNA replication. For this, Huh-7.5+FLuc cells were electroporated with mSGR-JFH1BlaRL RNA and treated 48 h later with ciliobrevin D at various concentrations for 24 h. Dual luciferase assays revealed a ca. 40% reduction in

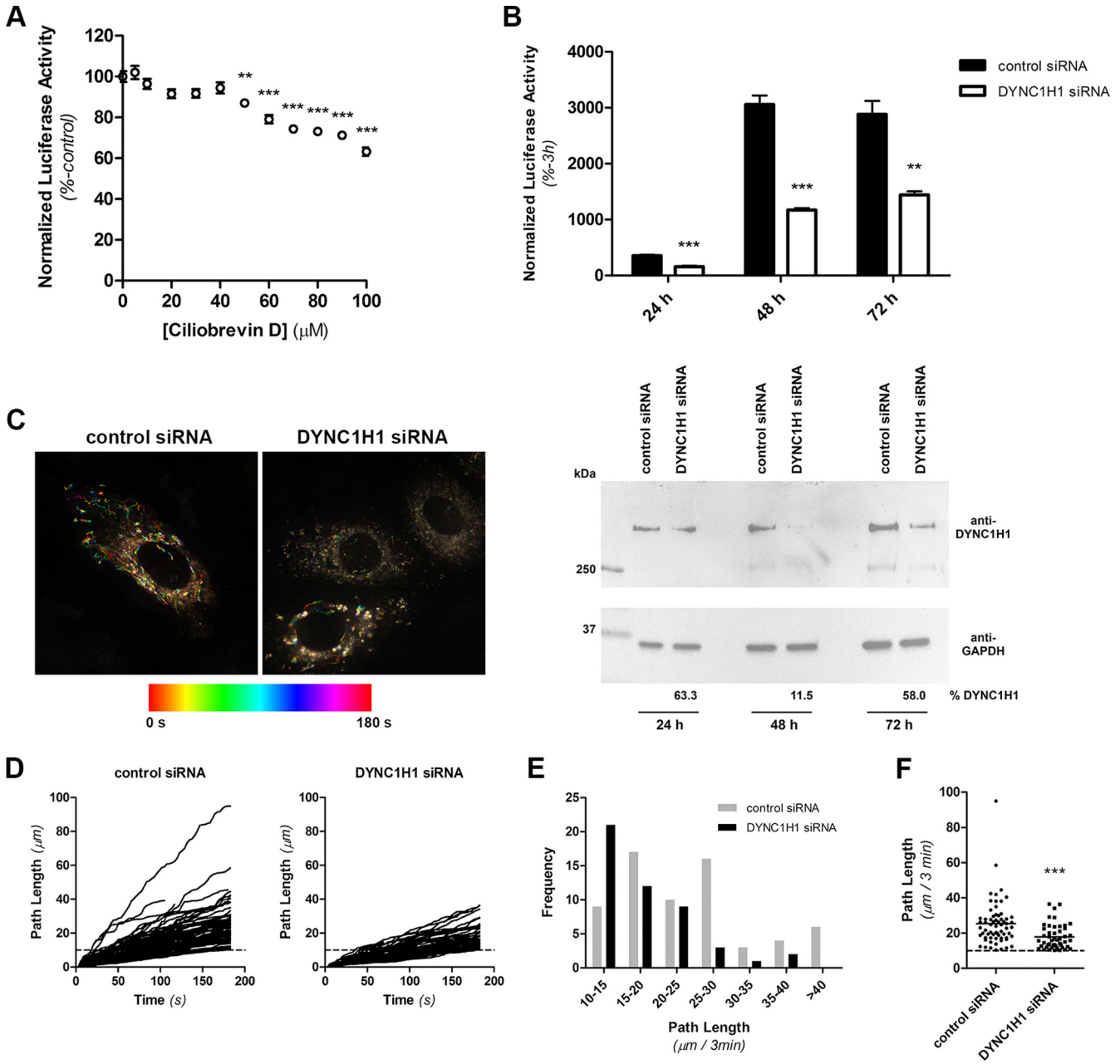


**FIG 4** Involvement of cytoplasmic dynein in HCV RNA replication and NS5A motility. (A) Huh-7.5+FLuc cells were electroporated with SGRm-JFH1BlaRL RNA and cultured for 48 h before exposure to ciliobrevin D (or 1% DMSO) for 24 h and determination of normalized luciferase activity (RLuc/FLuc). The data are expressed as the % control. (B) Huh-7.5+FLuc cells were cotransfected with SGRm-JFH1BlaRL RNA (1 μg) and either nontargeting or DYNC1H1-specific siRNAs (118 pmol) before determination of normalized luciferase activity at the indicated time points. The data are expressed as the % 3 h (input). For panels A and B, data are means + the SEM ($n = 4$). **, $P < 0.01$; ***, $P < 0.001$ (Student $t$ test). (C) Huh-7.5 cells were coelectroporated with Jc1/5A-GFP[K1402Q] RNA (5 μg) and either nontargeting or DYNC1H1-specific siRNAs (1 nmol of each) and cultured for 48 h prior to live cell imaging. Images were acquired every 3 s for 3 min. Images (taken from Movie S4 in the supplemental material) are color-coded projections of entire time-lapse acquisitions. (D) Manual tracking of NS5A-GFP foci in control and DYNC1H1 siRNA-transfected cells. Motile structures (identified as being displaced in the first 6 s of each time-lapse acquisition) were subjected to manual tracking analysis, excluding structures that moved <10 μm in 3 min. Path lengths for control ($n = 92$ foci) and DYNC1H1 siRNA-transfected ($n = 63$ foci) cells are depicted in panel D. (E and F) The frequencies of structures that display the indicated path lengths are depicted in panel E, and total path lengths are depicted in panel F. Horizontal bars represent mean values for control and DYNC1H1 siRNA transfected cells ($n = 65$ and 48 foci, respectively). ***, $P < 0.001$, Mann-Whitney U-test.

normalized replicon-encoded RLuc activity for cells exposed to 100 μM ciliobrevin D (Fig. 4A). Consistent with this, we found that siRNA knockdown of the heavy chain of cytoplasmic dynein 1 (DYNC1H1) significantly inhibited normalized HCV replicon-encoded RLuc activity (Fig. 4B, upper panel) to a degree that was similar to the degree of knockdown of DYNC1H1 protein, determined by Western blotting of lysates from the same experiment (Fig. 4B, lower panel).

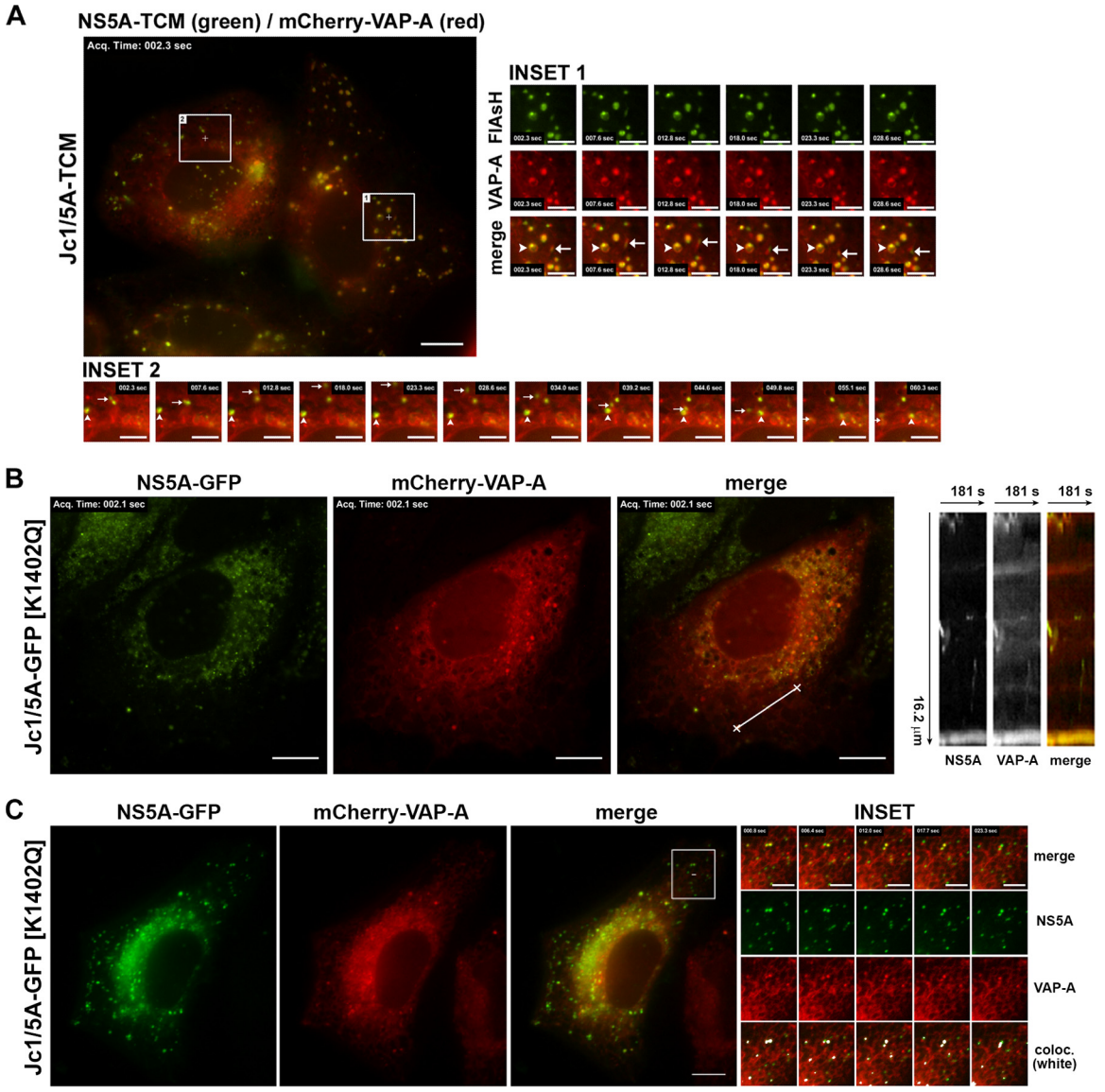


**FIG 5** Colocalization and cotraffic of NS5A with VAP-A. (A) Huh-7.5+mCherry-VAP-A cells were electroporated with Jc1/5A-TCM RNA, labeled with FlAsH (green) at 48 h and analyzed by live cell imaging at 72 h (see Movie S5 in the supplemental material). Inset 1 shows enrichment of mCherry-VAP-A in both relatively static and motile NS5A-TCM-positive structures (arrowheads and arrows, respectively), while inset 2 depicts the additional reticular localization of mCherry-VAP-A and the movements of two representative motile NS5A-TCM foci. (B) Huh-7.5+mCherry-VAP-A cells were electroporated with Jc1/5A-GFP[K1402Q] RNA and analyzed by live cell imaging at 72 h postelectroporation (see Movie S6 in the supplemental material). A 16.2-μm line-scan (3 pixels wide) was used to generate the inset kymograph. (C) Huh-7.5+mCherry-VAP-A cells were infected with Jc1/5A-GFP[K1402Q] (MOI of ~0.05) and analyzed by live cell imaging at 3 days postinfection. Scale bars are 10 and 5 μm for main and inset images, respectively.

To correlate these effects with changes in NS5A traffic, Huh-7.5 cells were coelectroporated with Jc1/5A-GFP[K1402Q] RNA and either control or DYNC1H1 siRNAs before live cell imaging (Fig. 4C; see Movie S4 in the supplemental material). Although motile NS5A-GFP foci were still readily detectable in DYNC1H1 siRNA-transfected cells, the frequency of long-range NS5A-GFP foci movements (>20 μm/3 min) and the average path length of motile NS5A-GFP foci were significantly reduced in DYNC1H1 siRNA-transfected cells compared to controls (Fig. 4D to F). Together, these results show that the microtubule network is essential for NS5A foci motility and efficient HCV RNA replication and that cytoplasmic dynein plays an important role in long-range traffic of NS5A foci and efficient HCV RNA replication.

**NS5A colocalizes and cotraffics with proviral host factors.** The identification of relatively static and motile subclasses of NS5A foci led us to investigate their composition in regard to host factors that are known to be important for HCV RNA replication. One such factor is vesicle-associated membrane protein-associated protein A (VAP-A); a SNARE-like protein that interacts with NS5A and NS5B and may help to anchor these proteins to ER-derived membranes that are sites of HCV replication (14, 33, 34). To examine the localization and traffic of NS5A with respect to VAP-A, Huh-7.5+mCherry-VAP-A cells were electroporated with Jc1/5A-TCM RNA transcripts, labeled with FlAsH, and visualized by live cell imaging (Fig. 5A and see Movie S5 in the supplemental material). Both relatively static and motile NS5A-posi-

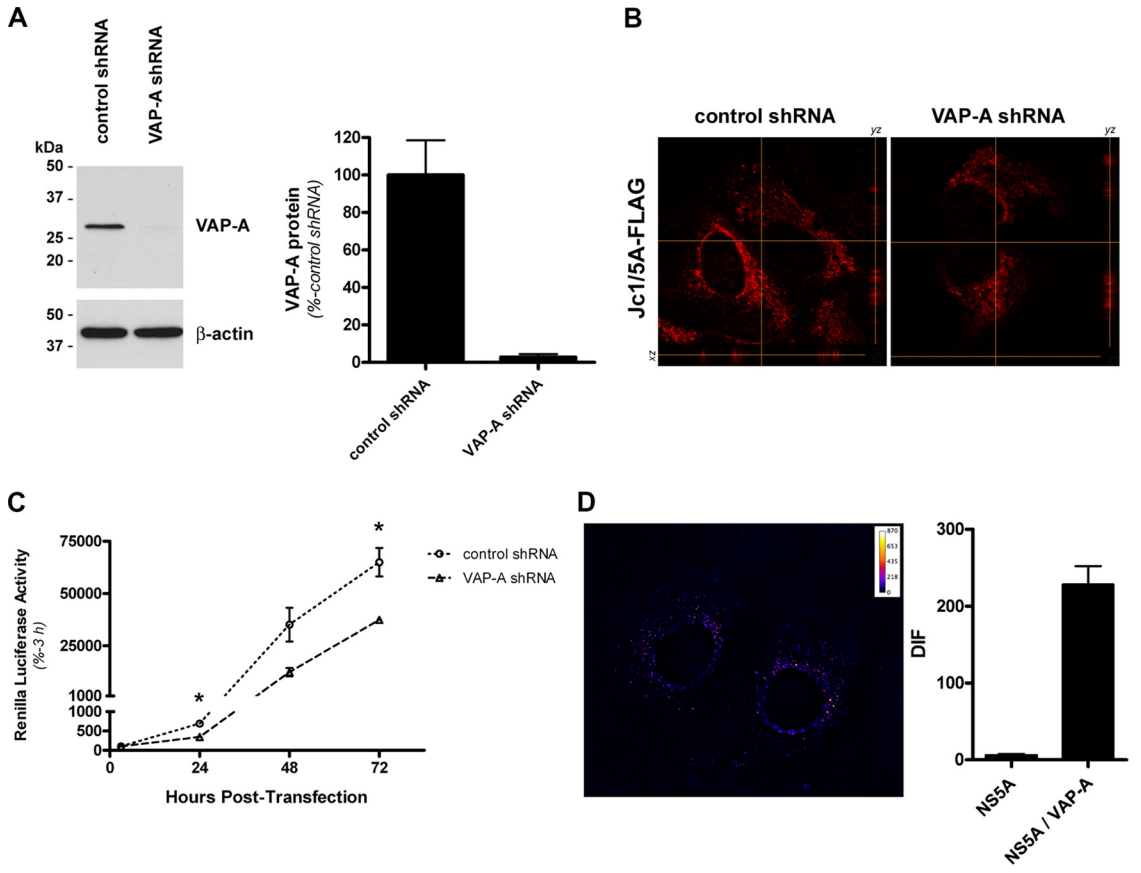
A
control shRNA
VAP-A shRNA
kDa
50
37
25
20
VAP-A
50
37
β-actin
VAP-A protein
(%-control shRNA)
120
100
80
60
40
20
0
control shRNA
VAP-A shRNA
B
control shRNA
VAP-A shRNA
Jc1/5A-FLAG
yz
xz
C
Renilla Luciferase Activity
(%-3 h)
75000
50000
25000
1000
1000
500
0
0
24
48
72
Hours Post-Transfection
control shRNA
VAP-A shRNA
*
D
DIF
300
200
100
0
NS5A
NS5A / VAP-A
E
mCherry-Rab5A
mCherry-Rab5A (S34N)
mCherry-Rab5A (Q79L)
Normalized Luciferase Activity
(%-3h)
1500
1000
500
0
100
500
1000
Doxycycline Concentration
(ng/ml)
F
DOX:
(ng/ml)
0
100
500
1000
kDa
anti-
mCherry
anti-
Rab5A
anti-
β-actin
50
37
25
20

tive structures were enriched with mCherry-VAP-A, indicating that the presence of VAP-A does not distinguish between static and motile putative replication complexes (Fig. 5A, inset 1; see Movie S5 in the supplemental material). Furthermore, motile NS5A-positive structures appeared to traffic along VAP-A-positive ER-like membranes (Fig. 5A, inset 2; see Movie S5 in the supplemental material). Similarly, in Huh-7.5+mCherry-VAP-A cells that were electroporated with Jc1/5A-GFP[K1402Q] transcripts NS5A-GFP and mCherry-VAP-A colocalized (Pearson correlation = 0.83 ± 0.02 [$n = 9$ cells]) and cotrafficked, in close association with mCherry-VAP-A-positive ER tubules (Fig. 5B and see Movie S6 in the supplemental material). This cotrafficking was also observed in an infection scenario, indicating that colocalization was not an artifact of HCV RNA electroporation (Fig. 5C). Although effective shRNA knockdown of VAP-A (Fig. 6A) inhibited HCV RNA replication (Fig. 6C), neither the subcellular localization of NS5A (Fig. 6B) nor NS5A-TCM traffic (not shown) were appreciably altered, suggesting that VAP-A is not a major determinant of NS5A localization and traffic. Furthermore, FRET analysis revealed the interaction of mCherry-VAP-A with NS5A-GFP in cytoplasmic foci of varying size in Jc1/5A-GFP[K1402Q]-infected Huh-7.5+mCherry-VAP-A cells (Fig. 6D), suggesting that the interaction of these proteins is not restricted to a particular subset of NS5A-positive structures.

Another host factor that is reported to be important for HCV RNA replication is the early endosomal protein Rab5A (13, 35). Rab5A regulates tethering and homotypic fusion of early endosomes and has been shown to interact with NS4B and influence the formation of sites of HCV RNA replication (35, 36). First, we investigated the influence of Rab5A overexpression and GTPase activity on HCV RNA replication, given previous reports that siRNA knockdown of Rab5A inhibits HCV RNA replication (13, 36). These experiments revealed minor inhibitory effects of inducible mCherry-Rab5A, mCherry-Rab5A (S34N), and mCherry-Rab5A (Q79L) overexpression on HCV RNA replication (Fig. 6E). Second, we examined the localization and traffic of NS5A with respect to Rab5A by live cell imaging. Infection of Huh-7.5 cells that constitutively express low levels of mCherry-tagged Rab5A with Jc1/5A-GFP[K1402Q] and live cell imaging revealed a close overlap in the localization and traffic of NS5A-GFP and mCherry-Rab5A in both small, motile structures and larger, relatively static structures (Fig. 7A). To complement these findings and investigate the influence of Rab5A GTPase activity, Jc1/5A-GFP[K1402Q]-infected Huh-7.5 cells were transiently transfected with wild-type, GDP-locked (S34N) or GTP-locked (Q79L) mCherry-Rab5A expression constructs, before live cell imaging. While NS5A-GFP extensively colocalized and cotrafficked with wild-type, GDP-locked (S34N), and GTP-locked (Q79L) mCherry-Rab5A proteins in small mCherry-Rab5A-positive structures, it was largely excluded from enlarged mCherry-Rab5A(Q79L)-positive endosomes (Fig. 7B and C), such that colocalization of NS5A-GFP with mCherry-Rab5A (Q79L) was significantly lower than that of mCherry-Rab5A (S34N) (extensive colocalization and cotraffic of NS5A-GFP with mCherry-Rab5A[S34N] is depicted in Movie S7 in the supplemental material). However, manual tracking analysis revealed that, compared to the wild type, neither average nor peak velocities of NS5A-positive structures were significantly altered by the presence of GDP-locked or GTP-locked mCherry-Rab5A (Fig. 7D). Although more complex aspects of NS5A traffic, such as directionality, may be altered by expression of GDP-/GTP-locked Rab5A, these results indicate that the GTPase activity of Rab5A does not alter the velocities at which putative RCs travel. Taken together, these results indicate that Rab5A is enriched in both relatively static and motile NS5A-positive structures and that this colocalization at least is partly dependent on the GTPase activity of Rab5A.

**Imaging the biogenesis of replication complexes using SNAP-tagged NS5A.** Although both TCM- and GFP-tagged NS5A localized to cytoplasmic foci of various sizes and motilities, it was not clear whether NS5A-positive foci interacted and exchanged components with one another and whether time influenced their appearance and motility. To further investigate this, we replaced the GFP-coding sequence of Jc1/5A-GFP[K1402Q] with that of a SNAP tag to generate Jc1/5A-SNAP. This insertion minimally altered infectious HCV production (Fig. 8A), had no unexpected effects on NS5A processing (Fig. 8C), and importantly enabled specific labeling of SNAP-tagged NS5A with fluorescent SNAP ligands (Fig. 8B; Pearson correlation = 0.98). Furthermore, this virus enabled reliable pulse-chase labeling of NS5A-SNAP with spectrally distinct fluorescent SNAP ligands (Fig. 8D). Interestingly, aged NS5A-SNAP foci (synthesized in the period from 0 to 48 h postelectroporation) minimally colocalized with newly synthesized NS5A (synthesized in the period from 48 to 72 h postelectroporation) (Pearson correlation = 0.36 ± 0.04 [$n = 11$ fields]). Furthermore, aged NS5A foci were ~2-fold larger than

**FIG 6** Involvement of VAP-A and Rab5A in HCV replication. (A) Stable knockdown of VAP-A in Huh-7.5 cells. After transduction with lentiviral shRNA vectors, antibiotic selection, and enrichment by FACS, the VAP-A protein levels were assessed by Western blotting. The graph inset depicts densitometric analysis of VAP-A proteins levels, normalized to the loading control β-actin (means + the SEM, $n = 3$). (B) NS5A localization in control shRNA- and VAP-A shRNA-expressing cell lines. Cells were infected with Jc1/5A-FLAG (MOI of ~0.05), fixed at 72 h postinfection, and processed for indirect immunofluorescence labeling using anti-FLAG antibody. Samples were analyzed by confocal microscopy (using identical settings), collecting serial 0.5-μm z-sections. (C) HCV replication is impaired by VAP-A knockdown. Huh-7.5 cells expressing control- or VAP-A-specific shRNAs were transfected with SGRm-JFH1BlaRL transcripts before determination of RLuc activity at the indicated time points, expressed as a percentage of input values at 3 h. The data are means ± the SEM ($n = 4$). *, $P < 0.05$, unpaired Student $t$ test. (D) NS5A-GFP interacts with mCherry-VAP-A as determined by FRET by acceptor photobleaching. Huh-7.5 cells or Huh-7.5 cells stably expressing mCherry-VAP-A were electroporated with Jc1/5A-GFP[K1402Q] transcripts and fixed at 72 h postelectroporation before FRET analysis. NS5A-GFP-positive Huh-7.5 cells serve as "donor only" controls. The difference in fluorescence (DIF) between NS5A-GFP fluorescence pre- and postbleaching of the mCherry channel is depicted. The "Fire" look-up table for ImageJ has been applied to indicate the intensity of DIF signals. The graph inset displays the mean DIF+SEM for individual NS5A-GFP-positive structures from control ($n = 30$) and NS5A/VAP-A ($n = 33$) groups (*, $P < 0.05$ [unpaired Student $t$ test]). (E) Huh-7.5+FLuc cells were transduced with lentiviral vectors enabling tetracycline-inducible expression of mCherry-Rab5A or mutant derivatives (S34N or Q79L). After selection and enriched by FACS, stable cell lines were electroporated with SGRm-JFH1BlaRL transcripts and cultured in the presence of doxycycline at the indicated concentrations before determination of normalized luciferase activity (RLuc/FLuc) at 48 h postelectroporation. The data are expressed as % 3 h (input) (means + the SEM [$n = 3$]). *, $P < 0.05$; **, $P < 0.01$ (Student $t$ test). (F) For each group in panel E, samples were pooled and processed for Western analysis of doxycycline-induced mCherry-Rab5A and mutant derivatives (S34N and Q79L), endogenous Rab5A, and β-actin (loading control).

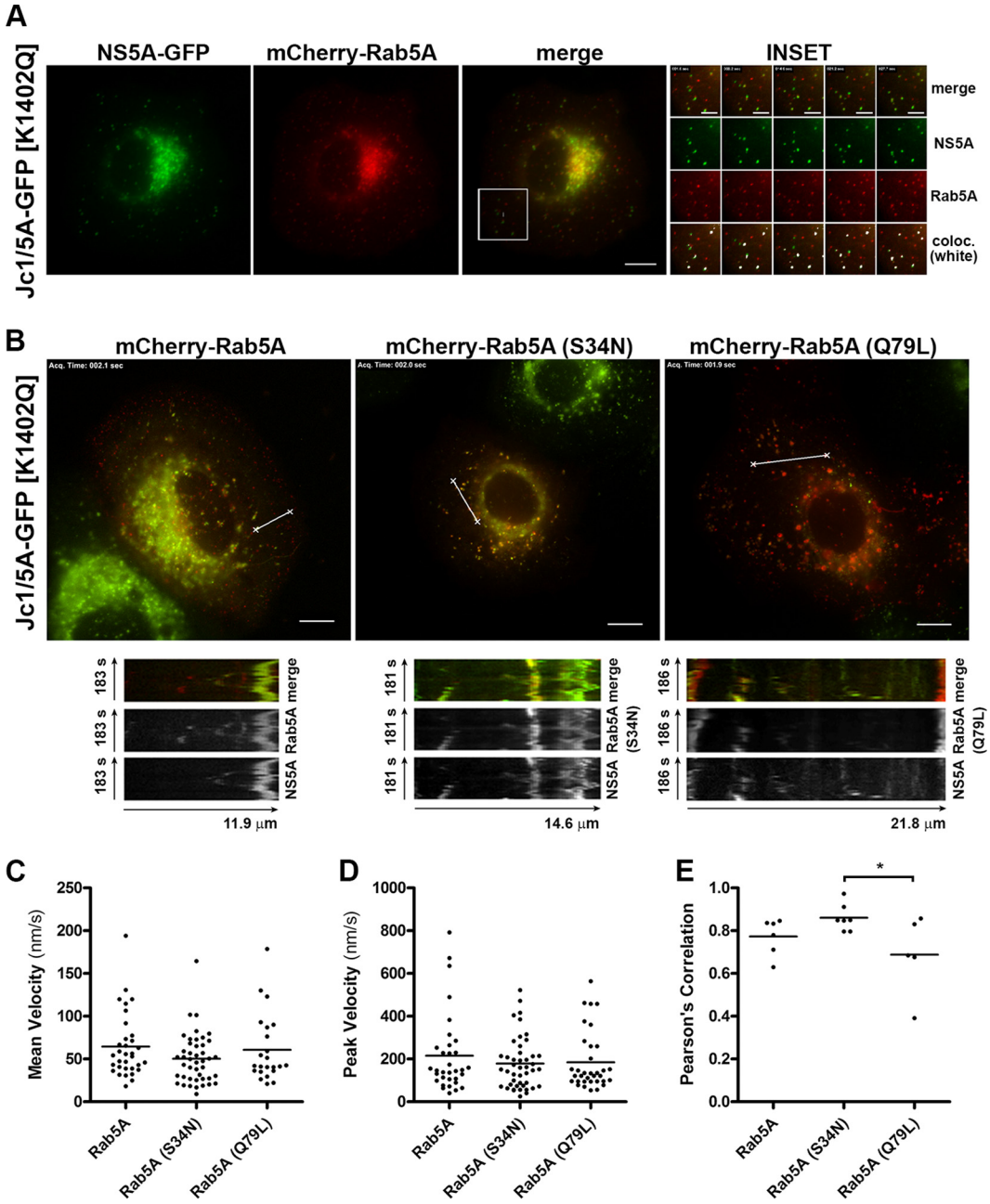


**FIG 7** Colocalization and cotraffic of NS5A with Rab5A. (A) Huh-7.5+mCherry-Rab5A cells were infected with Jc1/5A-GFP (MOI of ~0.05) and analyzed by live cell imaging at 4 days postinfection. The inset depicts examples of colocalization in both relatively static and motile structures (colocalized pixels are highlighted in white using NIS Elements software and a Pearson correlation threshold of 1%). (B) Huh-7.5 cells were electroporated with Jc1/5A-GFP[K1402Q] RNA, transfected with mCherry-Rab5A, mCherry-Rab5A (S34N) (see also Movie S7 in the supplemental material), or mCherry-Rab5A (Q79L) expression vectors (at 48 h) and analyzed by live cell imaging (at 72 h), collecting images every 6 s for 3 min. The indicated line scans were used to generate the inset kymographs. Manual tracking analysis was performed for NS5A/Rab5A double-positive foci in Jc1/5A-GFP[K1402Q]-infected cells expressing mCherry-Rab5A ($n = 35$ foci), mCherry-Rab5A (S34N) ($n = 49$ foci), or mCherry-Rab5A (Q79L) ($n = 24$ foci) and mean velocities (C) and peak velocities (D) are depicted. (E) Colocalization of NS5A-GFP with mCherry-Rab5A was determined for representative Jc1/5A-GFP[K1402Q]-infected cells that expressed mCherry-Rab5A ($n = 6$ cells), mCherry-Rab5A (S34N) ($n = 7$ cells), or mCherry-Rab5A (Q79L) ($n = 5$ cells). Horizontal bars represent the mean values for each group. *, $P < 0.05$ (Student $t$ test). For all micrographs, scale bars represent 10 and 5 μm for main and inset images, respectively.

their younger counterparts (Fig. 8E), although both pools were comprised of both relatively static and highly motile foci (Fig. 8F).

**Visualization of fluorescently labeled core and NS5A proteins in living cells.** Beyond its essential role in HCV RNA replication, NS5A also plays a critical role in virus particle assembly, potentially by delivering associated viral genomes to core-positive sites of assembly at the LD surface (reviewed in reference 3). However, the dynamics of RC association with LDs are completely unknown. Initially, to visualize the association of NS5A with LDs in living cells, Huh-7.5 cells that stably express an mCherry-tagged

derivative of the LD structural protein ADRP were electroporated with Jc1/5A-TCM transcripts before labeling with FlAsH and live cell imaging. Consistent with previous studies in fixed cells (9, 37), we observed only moderate colocalization between NS5A-TCM and ADRP-coated LDs. However, both motile and relatively static NS5A-TCM-positive foci could frequently be observed in close proximity to ADRP-positive LDs, with motile NS5A-TCM-positive foci even observed to traverse the surface of LDs (see Movie S8 in the supplemental material). Given that ADRP is actively displaced from the LD surface by core (27, 38), we next investigated the localization and short-term traffic of core-TCM and NS5A-GFP in living Jc1/Core-TCM:5A-GFP[K1402Q]-infected Huh-7.5 cells (see Movie S9 in the supplemental material). As for singly NS5A-tagged viruses, NS5A-GFP encoded by Jc1/Core-TCM:5A-GFP[K1402Q] localized to bright cytoplasmic foci of various sizes and motilities that did not extensively colocalize with core-TCM (Pearson correlation = 0.31), which was predominantly localized to "caps" on LD-like structures (Fig. 9). Where NS5A-GFP and core-TCM were found in close proximity on core-TCM-capped LD-like structures, NS5A-GFP predominantly remained in distinct foci in contrast to core-TCM, which was more homogenously distributed across the LD surface. Furthermore, at least in the short-term, we found that these core-proximal NS5A-GFP-positive foci were relatively immotile (see Movie S9 in the supplemental material).

It has been previously reported that HCV core interacts with NS5A (16). In contrast, Appel et al. reported a failure to detect core-NS5A interactions in the context of the complete HCV life cycle, suggesting that core-NS5A interactions may be unstable, transient, and/or indirect (15). We therefore investigated the presence and localization of core-NS5A complexes by *in situ* proximity ligation assays (PLAs) that allow for the detection of weak or transient protein-protein interactions. These studies revealed the ready and specific detection of core-NS5A complexes in both Jc1- and Jc1/5A-GFP[K1402Q]-infected cells in cytoplasmic foci (Fig. 10). Surprisingly, core-NS5A complexes minimally colocalized with bright NS5A-positive foci (Pearson correlation = 0.26 ± 0.02 [$n$ = 13 cells]), suggesting that few copies of NS5A are complexed with core at any given time. Taken together, these results confirm the interaction (<40-nm proximity) of NS5A with core in the context of an authentic HCV infection system and reveal new details about the localization of these complexes.

## DISCUSSION

The factors that dictate segregation of NS5A into both relatively static and highly motile cytoplasmic structures and the possible role(s) of NS5A (putative RC) motility in the HCV life cycle are unknown. Consistent with a previous study of NS5A dynamics in the context of a subgenomic replicon (28), we found that the motility of NS5A-positive structures were dramatically impaired by inhibitors of microtubule polymerization, as was HCV RNA replication. It is not clear how microtubule dynamics and/or microtubule-dependent traffic of NS5A foci may contribute to efficient HCV replication. Given that the localization and microtubule-dependent trafficking patterns of NS5A foci bear a striking resemblance to putative RCs of the unrelated plus-strand virus mouse hepatitis coronavirus (39), it is appealing to speculate that common mechanisms in RC traffic and function exist. However, in contrast to our findings with HCV, a functional microtubule network was dispensable for efficient mouse hepatitis coronavirus replication and virus production (39). Interestingly, it has been reported that both HCV NS3 and NS5A proteins directly interact with microtubules and actin filaments (40), and this may contribute to RC architecture, motility and/or functionality.

Although we observed a close overlap of NS5A and VAP-A in motile and relatively static punctae, mCherry-VAP-A also displayed an extensive ER-like localization, suggesting that it may be incorporated into RCs during their biogenesis at the ER membrane. In contrast, NS5A was strongly localized to cytoplasmic foci that were also enriched with the early endosome protein Rab5A. Furthermore, a reliance on endocytic trafficking machinery for NS5A traffic was also suggested by the observation that, expressed alone, fluorescently tagged Rab5A displays localization and trafficking profiles that bear striking similarities to those of NS5A during active HCV replication (31; data not shown). We therefore speculate that the interaction of NS4B with Rab5 (35, 36) strongly influences the localization and motility of RCs.

The complex movements of endosomes along microtubules are dictated by interactions of endosomes with motor proteins, including the minus-end motor dynein, minus-end kinesins (such as KIFC1 and KIFC2), plus-end kinesins (such as kinesin-1), and the kinesin-3 family member KIF16B (reviewed in references 31, 41, and 42). Consistent with this, we found that dynein knockdown significantly inhibited the proportion of NS5A foci that displayed long-range motility and, like the chemical inhibition of dynein, significantly inhibited HCV RNA replication. However, it is not clear whether NS5A motility directly contributes to efficient HCV RNA replication or whether disruption of dynein-dependent organellar/vesicular traffic indirectly limits HCV RNA replication, for example, by depriving RCs of access to essential host factors or lipids. Future endeavors to identify the HCV protein(s) and residues that directly or indirectly couple NS5A foci to motor proteins may enable definitive determination of the contribution of RC motility to HCV replication and accordingly may reveal future targets of antiviral therapy.

Along with playing essential roles in viral RNA replication and translation, viral RCs must also closely associate with sites of virus particle assembly, at least transiently, to enable transfer of progeny viral genomes to virus particle assembly complexes (4). For HCV, newly synthesized viral RNA is thought to be transferred from RCs to LD-associated core for encapsidation in a process that depends on core-NS5A interaction (3). Our studies involving near-simultaneous visualization of core and NS5A localization and traffic in virus-producing cells revealed that the colocalization of these proteins was relatively infrequent and that, where NS5A-GFP was found in close proximity to core-TCM at the surface of LD-like structures, NS5A-GFP remained largely in discrete foci. Our observation that core-NS5A complexes minimally overlap in localization with NS5A-enriched foci suggest that a minor proportion of NS5A interacts with core at any given time and that these interactions may not occur in the context of putative RCs. The localization of NS5A-GFP in LD-proximal foci was in contrast to that of core-TCM, which more uniformly coated the LD surface. This observation is consistent with immunoelectron microscopic analysis of the localization of core and NS5A in JFH-1-infected Huh-7 cells, whereby NS5A was detected in clusters at LD-proximal sites and core was more dispersedly embedded in the LD surface (43). It is interesting that more uniform localization of NS5A to the LD surface is particularly prominent when it is expressed alone or when its localization is altered by exposure of HCV replicon-har-

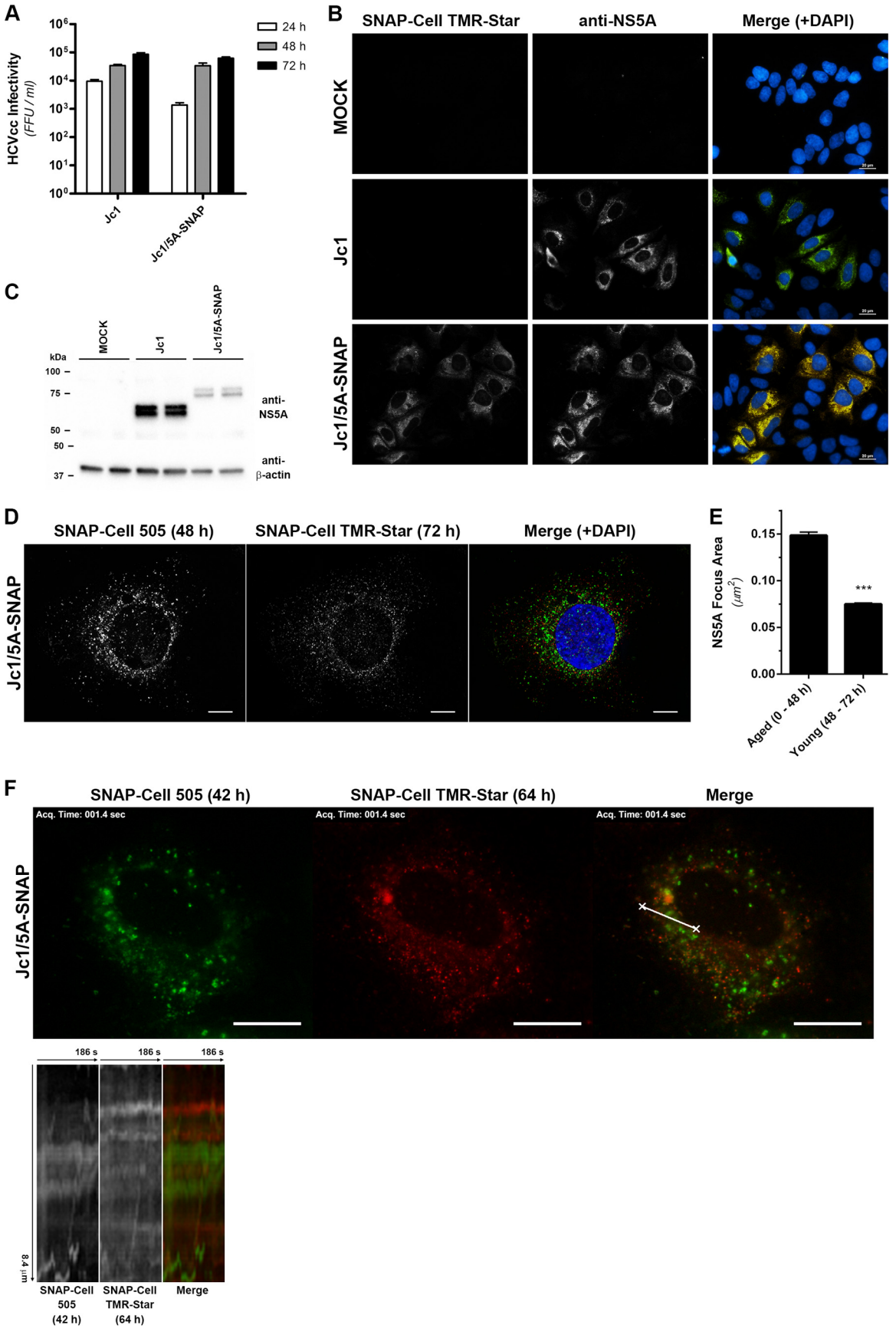
A
HCVcc Infectivity (FFU / ml)
24 h
48 h
72 h
Jc1
Jc1/5A-SNAP
B
SNAP-Cell TMR-Star
anti-NS5A
Merge (+DAPI)
MOCK
Jc1
Jc1/5A-SNAP
C
MOCK
Jc1
Jc1/5A-SNAP
kDa
100
75
50
50
37
anti-NS5A
anti-β-actin
D
SNAP-Cell 505 (48 h)
SNAP-Cell TMR-Star (72 h)
Merge (+DAPI)
Jc1/5A-SNAP
E
NS5A Focus Area (μm²)
0.15
0.10
0.05
0.00
***
Aged (0 - 48 h)
Young (48 - 72 h)
F
SNAP-Cell 505 (42 h)
SNAP-Cell TMR-Star (64 h)
Merge
Jc1/5A-SNAP
Acq. Time: 001.4 sec
186 s
8.4 μm
SNAP-Cell 505 (42 h)
SNAP-Cell TMR-Star (64 h)
Merge

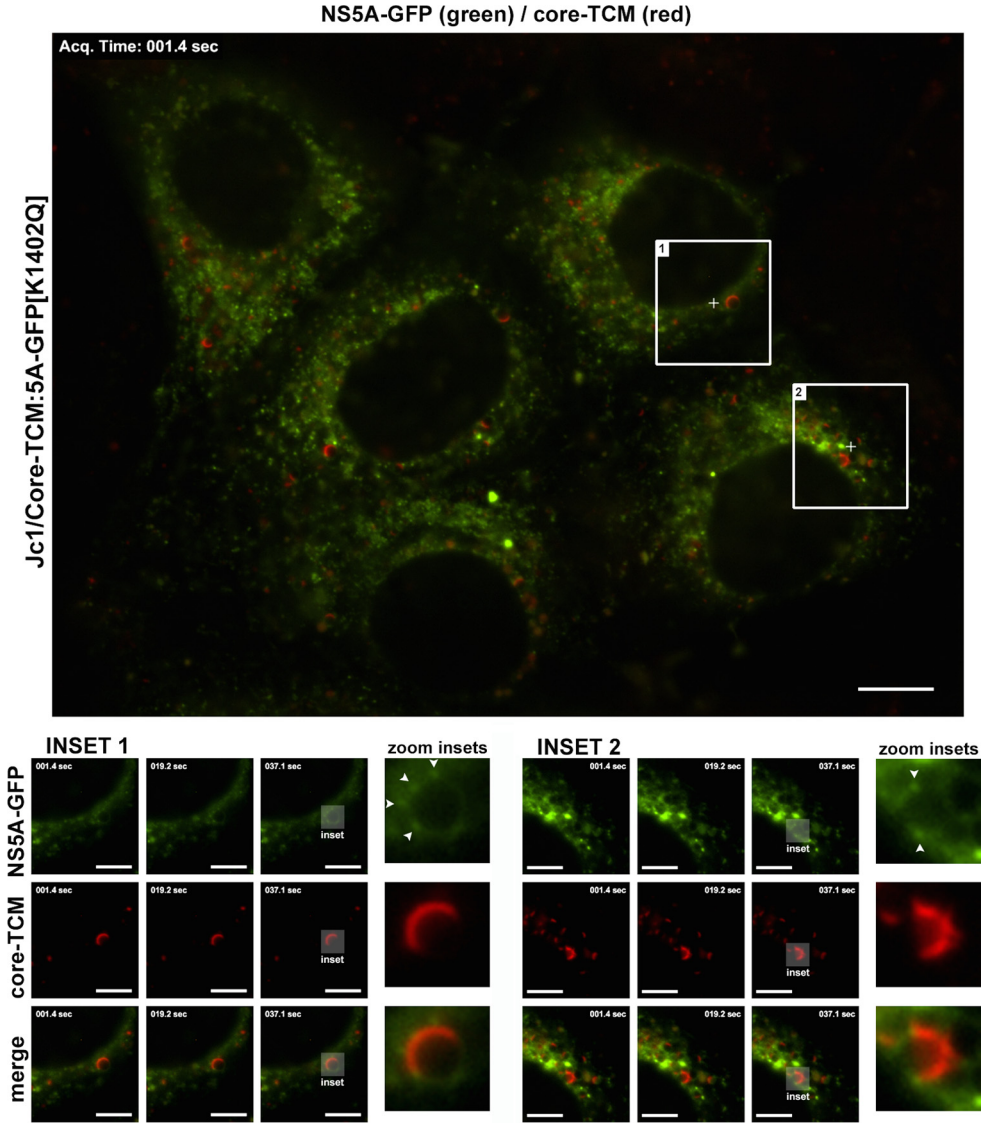


**FIG 9** Live cell imaging of HCV core and NS5A proteins in the context of a productive infection. Huh-7.5 cells were electroporated with Jc1/Core-TCM:5A-GFP[K1402Q] transcripts and labeled with ReAsH at 48 h postelectroporation, before live cell imaging of ReAsH-labeled core-TCM (red) and NS5A-GFP epifluorescence (green) at 72 h postelectroporation. Insets 1 and 2 (see Movie S9 in the supplemental material) highlight the relatively stable association of NS5A-GFP-positive foci with core-TCM-coated LDs (arrowheads). Note that brightness and contrast settings have been linearly increased for the "zoom insets" to enhance the visibility of dim structures. For all micrographs, scale bars represent 10 and 5 μm for main and inset images, respectively.

boring cells to potent NS5A-targeted antiviral drugs (37). We therefore speculate that uniform localization of NS5A to LDs is the result of its dissociation from RCs as a result of changes in its conformation and interaction with viral RC components (such as NS3 and/or NS5B) and/or co-opted host factors (such as VAP-A and/or PI4KIIIα) during virus particle assembly. It will therefore be interesting to examine how NS5A-targeted antiviral drugs alter the localization and traffic of NS5A in the context of a productive

**FIG 8** Pulse-chase imaging of SNAP-tagged NS5A. (A) Infectious virus production by Huh-7.5 cells electroporated with Jc1 or Jc1/5A-SNAP transcripts. (B) Specific labeling of NS5A-SNAP with fluorescent SNAP-tag ligands. Huh-7.5 cells were mock electroporated or electroporated with Jc1 or Jc1/5A-SNAP transcripts and labeled with SNAP-Cell TMR-Star (red) at 3 days, immediately prior to fixation and immunofluorescent labeling of NS5A (green). Merged images (with DAPI-stained nuclei; blue) are depicted in the right panels. Scale bars, 25 μm. (C) Western analysis of NS5A protein encoded by wild-type Jc1 and Jc1/5A-SNAP at 72 h postelectroporation. β-Actin served as a loading control. (D) Huh-7.5 cells were electroporated with Jc1/5A-SNAP transcripts and labeled with SNAP-Cell 505 at 48 h, blocked (with SNAP-Cell Block), and returned to culture before labeling with SNAP-Cell TMR-Star at 72 h. Cells were then fixed, counterstained with DAPI, and analyzed by deconvolution fluorescence microscopy. A maximum intensity projection of a representative z-stack is shown. (E) Quantification of the size of "aged" (24- to 72-h-old) and "young" (0- to 24-h-old) NS5A foci. The areas of SNAP-Cell 505-labeled foci ("aged"; $n = 5998$) and SNAP-Cell TMR-Star-labeled foci ("young"; $n = 7682$) foci were quantified (from 14 representative cells) from middle z-sections of Jc1/5A-SNAP-infected Huh-7.5 cells. ***, $P < 0.0001$ (Student $t$ test). (F) Live cell imaging of Huh-7.5 cells that were electroporated with Jc1/5A-SNAP transcripts and labeled with fluorescent SNAP-tag ligands at the indicated time points. The 8.4-μm line scan was used to generate the inset kymograph. Scale bars, 10 μm.

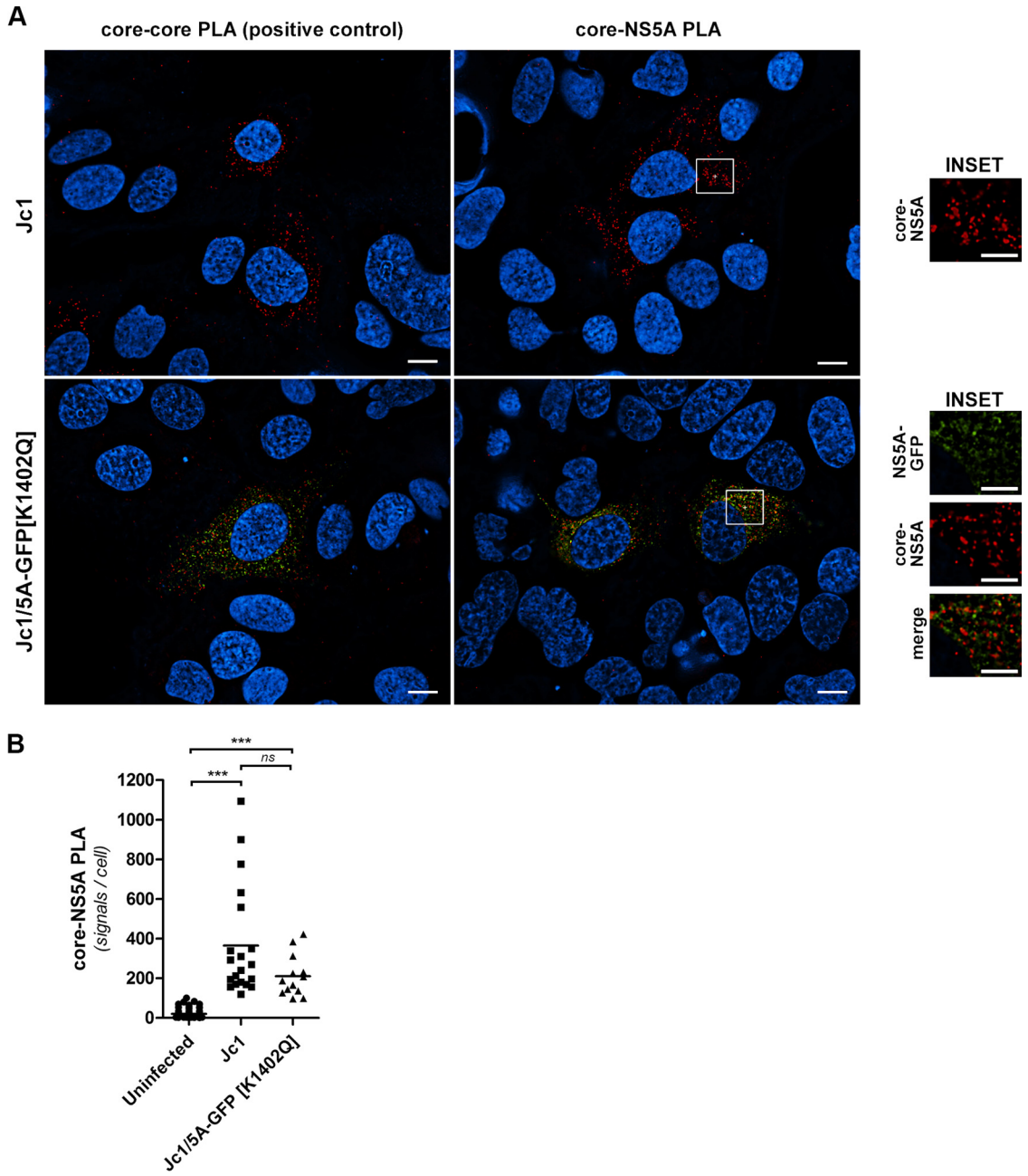


**FIG 10** Localization of core-NS5A complexes as determined by *in situ* PLA. Huh-7.5 cells were electroporated with Jc1 or Jc1/5A-GFP[K1402Q] RNA, fixed at 3 days postelectroporation, and processed for detection of core-NS5A complexes (red; right panels) by *in situ* PLA in Jc1- and Jc1/5A-GFP[K1402Q]-infected cells (top and bottom panels, respectively). Labeling of core with both rabbit and mouse anti-core antibodies served as a positive control for *in situ* PLA (left panels). Nuclei were counterstained with DAPI (blue). For Jc1/5A-GFP[K1402Q]-infected cells NS5A-GFP epifluorescence (green) was also captured. Serial (0.25-μm) z-sections were acquired and deconvoluted using the 3D AutoQuant Blind Deconvolution plug-in of NIS Elements AR v3.22. Images are single representative z-sections. The graph inset depicts an enumeration of core-NS5A PLA signals per cell (in central z-sections) in uninfected ($n = 73$), Jc1-infected ($n = 20$), and Jc1/5A-GFP[K1402Q]-infected ($n = 13$) cells. The frequency of PLA signals were significantly higher for Jc1- and Jc1/5A-GFP[K1402Q]-infected cells compared to uninfected controls ($P < 0.0001$, Student $t$ test). Minimal colocalization was observed between core-NS5A PLA signals and NS5A-GFP in Jc1/5A-GFP[K1402Q]-infected cells (Pearson correlation = 0.26 ± 0.02 [$n = 13$ cells]). For all micrographs, scale bars represent 10 and 5 μm for main and inset images, respectively.

infection and whether the colocalization and cotraffic of NS5A with viral RC components and co-opted host factors is maintained following exposure to these drugs.

In summary, we demonstrated here that NS5A traffic and efficient HCV RNA replication are reliant on cytoplasmic dynein and the host microtubule network and that co-opted host factors, VAP-A and Rab5A, are similarly enriched in both relatively static and motile NS5A foci. Furthermore, we demonstrated that newly synthesized NS5A foci are smaller than and distinct from mature foci and that these foci can be observed to stud core-coated lipid

droplets in living, virus-producing cells. These results uncover previously undescribed dynamics of NS5A in a productive HCV infection and provide a foundation to further dissect the mechanisms involved in RC biogenesis, motility, and association with sites of virus assembly for genome transfer and encapsidation.

## ACKNOWLEDGMENTS

We are grateful to Ralf Bartenschlager, Michinori Kohara, John McLauchlan, Charles Rice, Paul Targett-Adams, and Takaji Wakita for generously providing reagents. Assistance with confocal microscopy and fluorescence-activated cell sorting (FACS) were kindly provided by Ghafar Sarvestani and Katherine Pilkington, respectively (SA Pathology, Adelaide, Australia). We thank all members of our laboratory for helpful discussions.

This study was supported by grants from the NHMRC of Australia (1027641 and 510448), an NHMRC Career Development Award (to S.G.T.), and an NHMRC Senior Research Fellowship (to M.R.B.).

## REFERENCES

1. **Moradpour D, Penin F, Rice CM.** 2007. Replication of hepatitis C virus. Nat. Rev. Microbiol. **5:**453–463. http://dx.doi.org/10.1038/nrmicro1645.
2. **Lohmann V, Korner F, Koch J, Herian U, Theilmann L, Bartenschlager R.** 1999. Replication of subgenomic hepatitis C virus RNAs in a hepatoma cell line. Science **285:**110–113. http://dx.doi.org/10.1126/science.285.5424.110.
3. **Bartenschlager R, Penin F, Lohmann V, Andre P.** 2011. Assembly of infectious hepatitis C virus particles. Trends Microbiol. **19:**95–103. http://dx.doi.org/10.1016/j.tim.2010.11.005.
4. **den Boon JA, Diaz A, Ahlquist P.** 2010. Cytoplasmic viral replication complexes. Cell Host Microbe **8:**77–85. http://dx.doi.org/10.1016/j.chom.2010.06.010.
5. **Egger D, Wolk B, Gosert R, Bianchi L, Blum HE, Moradpour D, Bienz K.** 2002. Expression of hepatitis C virus proteins induces distinct membrane alterations including a candidate viral replication complex. J. Virol. **76:**5974–5984. http://dx.doi.org/10.1128/JVI.76.12.5974-5984.2002.
6. **Gosert R, Egger D, Lohmann V, Bartenschlager R, Blum HE, Bienz K, Moradpour D.** 2003. Identification of the hepatitis C virus RNA replication complex in Huh-7 cells harboring subgenomic replicons. J. Virol. **77:**5487–5492. http://dx.doi.org/10.1128/JVI.77.9.5487-5492.2003.
7. **Ferraris P, Beaumont E, Uzbekov R, Brand D, Gaillard J, Blanchard E, Roingeard P.** 2013. Sequential biogenesis of host cell membrane rearrangements induced by hepatitis C virus infection. Cell. Mol. Life Sci. **70:**1297–1306. http://dx.doi.org/10.1007/s00018-012-1213-0.
8. **Ferraris P, Blanchard E, Roingeard P.** 2010. Ultrastructural and biochemical analyses of hepatitis C virus-associated host cell membranes. J. Gen. Virol. **91:**2230–2237. http://dx.doi.org/10.1099/vir.0.022186-0.
9. **Romero-Brey I, Merz A, Chiramel A, Lee JY, Chlanda P, Haselman U, Santarella-Mellwig R, Habermann A, Hoppe S, Kallis S, Walther P, Antony C, Krijnse-Locker J, Bartenschlager R.** 2012. Three-dimensional architecture and biogenesis of membrane structures associated with hepatitis C virus replication. PLoS Pathog. **8:**e1003056. http://dx.doi.org/10.1371/journal.ppat.1003056.
10. **Berger KL, Kelly SM, Jordan TX, Tartell MA, Randall G.** 2011. Hepatitis C virus stimulates the phosphatidylinositol 4-kinase III alpha-dependent phosphatidylinositol 4-phosphate production that is essential for its replication. J. Virol. **85:**8870–8883. http://dx.doi.org/10.1128/JVI.00059-11.
11. **Reiss S, Rebhan I, Backes P, Romero-Brey I, Erfle H, Matula P, Kaderali L, Poenisch M, Blankenburg H, Hiet MS, Longerich T, Diehl S, Ramirez F, Balla T, Rohr K, Kaul A, Buhler S, Pepperkok R, Lengauer T, Albrecht M, Eils R, Schirmacher P, Lohmann V, Bartenschlager R.** 2011. Recruitment and activation of a lipid kinase by hepatitis C virus NS5A is essential for integrity of the membranous replication compartment. Cell Host Microbe **9:**32–45. http://dx.doi.org/10.1016/j.chom.2010.12.002.
12. **Backes P, Quinkert D, Reiss S, Binder M, Zayas M, Rescher U, Gerke V, Bartenschlager R, Lohmann V.** 2010. Role of annexin A2 in the production of infectious hepatitis C virus particles. J. Virol. **84:**5775–5789. http://dx.doi.org/10.1128/JVI.02343-09.
13. **Berger KL, Cooper JD, Heaton NS, Yoon R, Oakland TE, Jordan TX, Mateu G, Grakoui A, Randall G.** 2009. Roles for endocytic trafficking and phosphatidylinositol 4-kinase III alpha in hepatitis C virus replication. Proc. Natl. Acad. Sci. U. S. A. **106:**7577–7582. http://dx.doi.org/10.1073/pnas.0902693106.
14. **Gao L, Aizaki H, He JW, Lai MM.** 2004. Interactions between viral nonstructural proteins and host protein hVAP-33 mediate the formation of hepatitis C virus RNA replication complex on lipid raft. J. Virol. **78:**3480–3488. http://dx.doi.org/10.1128/JVI.78.7.3480-3488.2004.
15. **Appel N, Zayas M, Miller S, Krijnse-Locker J, Schaller T, Friebe P, Kallis S, Engel U, Bartenschlager R.** 2008. Essential role of domain III of nonstructural protein 5A for hepatitis C virus infectious particle assembly. PLoS Pathog. **4:**e1000035. http://dx.doi.org/10.1371/journal.ppat.1000035.
16. **Masaki T, Suzuki R, Murakami K, Aizaki H, Ishii K, Murayama A, Date T, Matsuura Y, Miyamura T, Wakita T, Suzuki T.** 2008. Interaction of hepatitis C virus nonstructural protein 5A with core protein is critical for the production of infectious virus particles. J. Virol. **82:**7964–7976. http://dx.doi.org/10.1128/JVI.00826-08.
17. **Tellinghuisen TL, Foss KL, Treadaway J.** 2008. Regulation of hepatitis C virion production via phosphorylation of the NS5A protein. PLoS Pathog. **4:**e1000032. http://dx.doi.org/10.1371/journal.ppat.1000032.
18. **Schaller T, Appel N, Koutsoudakis G, Kallis S, Lohmann V, Pietschmann T, Bartenschlager R.** 2007. Analysis of hepatitis C virus superinfection exclusion by using novel fluorochrome gene-tagged viral genomes. J. Virol. **81:**4591–4603. http://dx.doi.org/10.1128/JVI.02144-06.
19. **Wakita T, Pietschmann T, Kato T, Date T, Miyamoto M, Zhao Z, Murthy K, Habermann A, Krausslich HG, Mizokami M, Bartenschlager R, Liang TJ.** 2005. Production of infectious hepatitis C virus in tissue culture from a cloned viral genome. Nat. Med. **11:**791–796. http://dx.doi.org/10.1038/nm1268.
20. **Zhou Z, Wang N, Woodson SE, Dong Q, Wang J, Liang Y, Rijnbrand R, Wei L, Nichols JE, Guo JT, Holbrook MR, Lemon SM, Li K.** 2011. Antiviral activities of ISG20 in positive-strand RNA virus infections. Virology **409:**175–188. http://dx.doi.org/10.1016/j.virol.2010.10.008.
21. **Blight KJ, McKeating JA, Rice CM.** 2002. Highly permissive cell lines for subgenomic and genomic hepatitis C virus RNA replication. J. Virol. **76:**13001–13014. http://dx.doi.org/10.1128/JVI.76.24.13001-13014.2002.
22. **Eyre NS, Phillips RJ, Bowden S, Yip E, Dewar B, Locarnini SA, Beard MR.** 2009. Hepatitis B virus and hepatitis C virus interaction in Huh-7 cells. J. Hepatol. **51:**446–457. http://dx.doi.org/10.1016/j.jhep.2009.04.025.
23. **Adams SR, Tsien RY.** 2008. Preparation of the membrane-permeant biarsenicals FlAsH-EDT2 and ReAsH-EDT2 for fluorescent labeling of tetracysteine-tagged proteins. Nat. Protoc. **3:**1527–1534. http://dx.doi.org/10.1038/nprot.2008.144.
24. **Hoffmann C, Gaietta G, Zurn A, Adams SR, Terrillon S, Ellisman MH, Tsien RY, Lohse MJ.** 2010. Fluorescent labeling of tetracysteine-tagged proteins in intact cells. Nat. Protoc. **5:**1666–1677. http://dx.doi.org/10.1038/nprot.2010.129.
25. **Pietschmann T, Kaul A, Koutsoudakis G, Shavinskaya A, Kallis S, Steinmann E, Abid K, Negro F, Dreux M, Cosset FL, Bartenschlager R.** 2006. Construction and characterization of infectious intragenotypic and intergenotypic hepatitis C virus chimeras. Proc. Natl. Acad. Sci. U. S. A. **103:**7408–7413. http://dx.doi.org/10.1073/pnas.0504877103.
26. **Coller KE, Heaton NS, Berger KL, Cooper JD, Saunders JL, Randall G.** 2012. Molecular determinants and dynamics of hepatitis C virus secretion. PLoS Pathog. **8:**e1002466. http://dx.doi.org/10.1371/journal.ppat.1002466.
27. **Counihan NA, Rawlinson SM, Lindenbach BD.** 2011. Trafficking of hepatitis C virus core protein during virus particle assembly. PLoS Pathog. **7:**e1002302. http://dx.doi.org/10.1371/journal.ppat.1002302.
28. **Wolk B, Buchele B, Moradpour D, Rice CM.** 2008. A dynamic view of hepatitis C virus replication complexes. J. Virol. **82:**10519–10531. http://dx.doi.org/10.1128/JVI.00640-08.
29. **Bost AG, Venable D, Liu L, Heinz BA.** 2003. Cytoskeletal requirements for hepatitis C virus (HCV) RNA synthesis in the HCV replicon cell culture system. J. Virol. **77:**4401–4408. http://dx.doi.org/10.1128/JVI.77.7.4401-4408.2003.
30. **Driskell OJ, Mironov A, Allan VJ, Woodman PG.** 2007. Dynein is required for receptor sorting and the morphogenesis of early endosomes. Nat. Cell Biol. **9:**113–120. http://dx.doi.org/10.1038/ncb1525.
31. **Flores-Rodriguez N, Rogers SS, Kenwright DA, Waigh TA, Woodman PG, Allan VJ.** 2011. Roles of dynein and dynactin in early endosome dynamics revealed using automated tracking and global analysis. PLoS One **6:**e24479. http://dx.doi.org/10.1371/journal.pone.0024479.

32. **Firestone AJ, Weinger JS, Maldonado M, Barlan K, Langston LD, O'Donnell M, Gelfand VI, Kapoor TM, Chen JK.** 2012. Small-molecule inhibitors of the AAA+ ATPase motor cytoplasmic dynein. Nature **484:** 125–129. http://dx.doi.org/10.1038/nature10936.
33. **Evans MJ, Rice CM, Goff SP.** 2004. Phosphorylation of hepatitis C virus nonstructural protein 5A modulates its protein interactions and viral RNA replication. Proc. Natl. Acad. Sci. U. S. A. **101:**13038–13043. http://dx.doi.org/10.1073/pnas.0405152101.
34. **Tu H, Gao L, Shi ST, Taylor DR, Yang T, Mircheff AK, Wen Y, Gorbalenya AE, Hwang SB, Lai MM.** 1999. Hepatitis C virus RNA polymerase and NS5A complex with a SNARE-like protein. Virology **263:** 30–41. http://dx.doi.org/10.1006/viro.1999.9893.
35. **Stone M, Jia S, Heo WD, Meyer T, Konan KV.** 2007. Participation of rab5, an early endosome protein, in hepatitis C virus RNA replication machinery. J. Virol. **81:**4551–4563. http://dx.doi.org/10.1128/JVI.01366-06.
36. **Manna D, Aligo J, Xu C, Park WS, Koc H, Heo WD, Konan KV.** 2010. Endocytic Rab proteins are required for hepatitis C virus replication complex formation. Virology **398:**21–37. http://dx.doi.org/10.1016/j.virol.2009.11.034.
37. **Targett-Adams P, Graham EJ, Middleton J, Palmer A, Shaw SM, Lavender H, Brain P, Tran TD, Jones LH, Wakenhut F, Stammen B, Pryde D, Pickford C, Westby M.** 2011. Small molecules targeting hepatitis C virus-encoded NS5A cause subcellular redistribution of their target: insights into compound modes of action. J. Virol. **85:**6353–6368. http://dx.doi.org/10.1128/JVI.00215-11.
38. **Boulant S, Douglas MW, Moody L, Budkowska A, Targett-Adams P, McLauchlan J.** 2008. Hepatitis C virus core protein induces lipid droplet redistribution in a microtubule- and dynein-dependent manner. Traffic **9:**1268–1282. http://dx.doi.org/10.1111/j.1600-0854.2008.00767.x.
39. **Hagemeijer MC, Verheije MH, Ulasli M, Shaltiel IA, de Vries LA, Reggiori F, Rottier PJ, de Haan CA.** 2010. Dynamics of coronavirus replication-transcription complexes. J. Virol. **84:**2134–2149. http://dx.doi.org/10.1128/JVI.01716-09.
40. **Lai CK, Jeng KS, Machida K, Lai MM.** 2008. Association of hepatitis C virus replication complexes with microtubules and actin filaments is dependent on the interaction of NS3 and NS5A. J. Virol. **82:**8838–8848. http://dx.doi.org/10.1128/JVI.00398-08.
41. **Hunt SD, Stephens DJ.** 2011. The role of motor proteins in endosomal sorting. Biochem. Soc. Trans. **39:**1179–1184. http://dx.doi.org/10.1042/BST0391179.
42. **Soldati T, Schliwa M.** 2006. Powering membrane traffic in endocytosis and recycling. Nat. Rev. Mol. Cell. Biol. **7:**897–908. http://dx.doi.org/10.1038/nrm2060.
43. **Miyanari Y, Atsuzawa K, Usuda N, Watashi K, Hishiki T, Zayas M, Bartenschlager R, Wakita T, Hijikata M, Shimotohno K.** 2007. The lipid droplet is an important organelle for hepatitis C virus production. Nat. Cell Biol. **9:**1089–1097. http://dx.doi.org/10.1038/ncb1631.

# References


Agnello, V., Abel, G., Elfahal, M., Knight, G.B., Zhang, Q.X., 1999. Hepatitis C virus and other flaviviridae viruses enter cells via low density lipoprotein receptor. Proceedings of the National Academy of Sciences of the United States of America 96, 12766-12771.

Albornoz, A., Carletti, T., Corazza, G., Marcello, A., 2014. The Stress Granule Component TIA-1 Binds Tick-Borne Encephalitis Virus RNA and Is Recruited to Perinuclear Sites of Viral Replication To Inhibit Viral Translation. Journal of virology 88, 6611-6622.

Ali, N., Pruijn, G.J., Kenan, D.J., Keene, J.D., Siddiqui, A., 2000. Human La antigen is required for the hepatitis C virus internal ribosome entry site-mediated translation. The Journal of biological chemistry 275, 27531-27540.

Ali, N., Siddiqui, A., 1997. The La antigen binds 5' noncoding region of the hepatitis C virus RNA in the context of the initiator AUG codon and stimulates internal ribosome entry site-mediated translation. Proceedings of the National Academy of Sciences of the United States of America 94, 2249-2254.

Aloia, A.L., Eyre, N.S., Black, S., Bent, S.J., Gaeguta, A., Guo, Z., Narayana, S.K., Chase, R., Locarnini, S., Carr, J.M., Howe, J.A., Beard, M.R., 2014. Generation of a chimeric hepatitis C replicon encoding a genotype-6a NS3 protease and assessment of boceprevir (SCH503034) sensitivity and drug-associated mutations. Antiviral therapy.

Appel, N., Pietschmann, T., Bartenschlager, R., 2005. Mutational analysis of hepatitis C virus nonstructural protein 5A: potential role of differential phosphorylation in RNA replication and identification of a genetically flexible domain. Journal of virology 79, 3187-3194.

Appel, N., Zayas, M., Miller, S., Krijnse-Locker, J., Schaller, T., Friebe, P., Kallis, S., Engel, U., Bartenschlager, R., 2008. Essential role of domain III of nonstructural protein 5A for hepatitis C virus infectious particle assembly. PLoS pathogens 4, e1000035.

Ariumi, Y., Kuroki, M., Maki, M., Ikeda, M., Dansako, H., Wakita, T., Kato, N., 2011. The ESCRT system is required for hepatitis C virus production. PloS one 6, e14517.

Baek, J., Kang, S., Min, H., 2014. MicroRNA-targeting therapeutics for hepatitis C. Archives of pharmacal research 37, 299-305.

Bankwitz, D., Steinmann, E., Bitzegeio, J., Ciesek, S., Friesland, M., Herrmann, E., Zeisel, M.B., Baumert, T.F., Keck, Z.Y., Foung, S.K., Pecheur, E.I., Pietschmann, T., 2010. Hepatitis C virus hypervariable region 1 modulates receptor interactions, conceals the CD81 binding site, and protects conserved neutralizing epitopes. Journal of virology 84, 5751-5763.

Barba, G., Harper, F., Harada, T., Kohara, M., Goulinet, S., Matsuura, Y., Eder, G., Schaff, Z., Chapman, M.J., Miyamura, T., Brechot, C., 1997. Hepatitis C virus core protein shows a cytoplasmic localization and associates to cellular lipid storage droplets. Proceedings of the National Academy of Sciences of the United States of America 94, 1200-1205.

Bartosch, B., Dubuisson, J., Cosset, F.L., 2003. Infectious hepatitis C virus pseudo-particles containing functional E1-E2 envelope protein complexes. The Journal of experimental medicine 197, 633-642.

Basyuk, E., Galli, T., Mougel, M., Blanchard, J.M., Sitbon, M., Bertrand, E., 2003. Retroviral genomic RNAs are transported to the plasma membrane by endosomal vesicles. Developmental cell 5, 161-174.

Behrens, S.E., Tomei, L., De Francesco, R., 1996. Identification and properties of the RNA-dependent RNA polymerase of hepatitis C virus. The EMBO journal 15, 12-22.

Benga, W.J., Krieger, S.E., Dimitrova, M., Zeisel, M.B., Parnot, M., Lupberger, J., Hildt, E., Luo, G., McLauchlan, J., Baumert, T.F., Schuster, C., 2010. Apolipoprotein E interacts with hepatitis C virus nonstructural protein 5A and determines assembly of infectious particles. Hepatology 51, 43-53.

Berger, K.L., Cooper, J.D., Heaton, N.S., Yoon, R., Oakland, T.E., Jordan, T.X., Mateu, G., Grakoui, A., Randall, G., 2009. Roles for endocytic trafficking and phosphatidylinositol 4-kinase III alpha in hepatitis C virus replication. Proceedings of the National Academy of Sciences of the United States of America 106, 7577-7582.

Berger, K.L., Kelly, S.M., Jordan, T.X., Tartell, M.A., Randall, G., 2011. Hepatitis C virus stimulates the phosphatidylinositol 4-kinase III alpha-dependent phosphatidylinositol 4-phosphate production that is essential for its replication. Journal of virology 85, 8870-8883.

Bernardi, A., Spahr, P.F., 1972. Nucleotide sequence at the binding site for coat protein on RNA of bacteriophage R17. Proceedings of the National Academy of Sciences of the United States of America 69, 3033-3037.

Bertrand, E., Chartrand, P., Schaefer, M., Shenoy, S.M., Singer, R.H., Long, R.M., 1998. Localization of ASH1 mRNA particles in living yeast. Molecular cell 2, 437-445.

Binder, M., Quinkert, D., Bochkarova, O., Klein, R., Kezmic, N., Bartenschlager, R., Lohmann, V., 2007. Identification of determinants involved in initiation of hepatitis C virus RNA synthesis by using intergenotypic replicase chimeras. Journal of virology 81, 5270-5283.

Blight, K.J., Kolykhalov, A.A., Rice, C.M., 2000. Efficient initiation of HCV RNA replication in cell culture. Science 290, 1972-1974.

Blight, K.J., McKeating, J.A., Rice, C.M., 2002. Highly permissive cell lines for subgenomic and genomic hepatitis C virus RNA replication. Journal of virology 76, 13001-13014.

Blight, K.J., Rice, C.M., 1997. Secondary structure determination of the conserved 98-base sequence at the 3' terminus of hepatitis C virus genome RNA. Journal of virology 71, 7345-7352.

Boireau, S., Maiuri, P., Basyuk, E., de la Mata, M., Knezevich, A., Pradet-Balade, B., Backer, V., Kornblihtt, A., Marcello, A., Bertrand, E., 2007. The transcriptional cycle of HIV-1 in real-time and live cells. The Journal of cell biology 179, 291-304.

Bostrom, P., Rutberg, M., Ericsson, J., Holmdahl, P., Andersson, L., Frohman, M.A., Boren, J., Olofsson, S.O., 2005. Cytosolic lipid droplets increase in size by microtubule-dependent complex formation. Arteriosclerosis, thrombosis, and vascular biology 25, 1945-1951.

Boulant, S., Douglas, M.W., Moody, L., Budkowska, A., Targett-Adams, P., McLauchlan, J., 2008. Hepatitis C virus core protein induces lipid droplet redistribution in a microtubule- and dynein-dependent manner. Traffic 9, 1268-1282.

Boulant, S., Vanbelle, C., Ebel, C., Penin, F., Lavergne, J.P., 2005. Hepatitis C virus core protein is a dimeric alpha-helical protein exhibiting membrane protein features. Journal of virology 79, 11353-11365.

Bradley, D.W., 1985. The agents of non-A, non-B viral hepatitis. Journal of virological methods 10, 307-319.

Bradley, D.W., Maynard, J.E., Popper, H., Cook, E.H., Ebert, J.W., McCaustland, K.A., Schable, C.A., Fields, H.A., 1983. Posttransfusion non-A, non-B hepatitis: physicochemical properties of two distinct agents. The Journal of infectious diseases 148, 254-265.

Brandenburg, B., Zhuang, X., 2007. Virus trafficking - learning from single-virus tracking. Nature reviews. Microbiology 5, 197-208.

Brazzoli, M., Bianchi, A., Filippini, S., Weiner, A., Zhu, Q., Pizza, M., Crotta, S., 2008. CD81 is a central regulator of cellular events required for hepatitis C virus infection of human hepatocytes. Journal of virology 82, 8316-8329.

Brazzoli, M., Helenius, A., Foung, S.K., Houghton, M., Abrignani, S., Merola, M., 2005. Folding and dimerization of hepatitis C virus E1 and E2 glycoproteins in stably transfected CHO cells. Virology 332, 438-453.

Brown, E.A., Zhang, H., Ping, L.H., Lemon, S.M., 1992. Secondary structure of the 5' nontranslated regions of hepatitis C virus and pestivirus genomic RNAs. Nucleic acids research 20, 5041-5045.

Camus, G., Herker, E., Modi, A.A., Haas, J.T., Ramage, H.R., Farese, R.V., Jr., Ott, M., 2013. Diacylglycerol acyltransferase-1 localizes hepatitis C virus NS5A protein to lipid droplets and enhances NS5A interaction with the viral capsid core. The Journal of biological chemistry 288, 9915-9923.

Chang, J., Nicolas, E., Marks, D., Sander, C., Lerro, A., Buendia, M.A., Xu, C., Mason, W.S., Moloshok, T., Bort, R., Zaret, K.S., Taylor, J.M., 2004. miR-122, a mammalian liver-specific microRNA, is processed from hcr mRNA and may downregulate the high affinity cationic amino acid transporter CAT-1. RNA biology 1, 106-113.

Chang, K.S., Jiang, J., Cai, Z., Luo, G., 2007. Human apolipoprotein e is required for infectivity and production of hepatitis C virus in cell culture. Journal of virology 81, 13783-13793.

Choo, Q.L., Kuo, G., Weiner, A.J., Overby, L.R., Bradley, D.W., Houghton, M., 1989. Isolation of a cDNA clone derived from a blood-borne non-A, non-B viral hepatitis genome. Science 244, 359-362.

Chu, P.W., Westaway, E.G., 1985. Replication strategy of Kunjin virus: evidence for recycling role of replicative form RNA as template in semiconservative and asymmetric replication. Virology 140, 68-79.

Chukkapalli, V., Randall, G., 2014. Hepatitis C virus replication compartment formation: mechanism and drug target. Gastroenterology 146, 1164-1167.

Clarke, D., Griffin, S., Beales, L., Gelais, C.S., Burgess, S., Harris, M., Rowlands, D., 2006. Evidence for the formation of a heptameric ion channel complex by the hepatitis C virus p7 protein in vitro. The Journal of biological chemistry 281, 37057-37068.

Coller, K.E., Berger, K.L., Heaton, N.S., Cooper, J.D., Yoon, R., Randall, G., 2009. RNA interference and single particle tracking analysis of hepatitis C virus endocytosis. PLoS pathogens 5, e1000702.

Coller, K.E., Heaton, N.S., Berger, K.L., Cooper, J.D., Saunders, J.L., Randall, G., 2012. Molecular determinants and dynamics of hepatitis C virus secretion. PLoS pathogens 8, e1002466.

Corless, L., Crump, C.M., Griffin, S.D., Harris, M., 2010. Vps4 and the ESCRT-III complex are required for the release of infectious hepatitis C virus particles. The Journal of general virology 91, 362-372.

Counihan, N.A., Rawlinson, S.M., Lindenbach, B.D., 2011. Trafficking of hepatitis C virus core protein during virus particle assembly. PLoS pathogens 7, e1002302.

Dansako, H., Hiramoto, H., Ikeda, M., Wakita, T., Kato, N., 2014. Rab18 is required for viral assembly of hepatitis C virus through trafficking of the core protein to lipid droplets. Virology 462-463, 166-174.

Dao Thi, V.L., Granier, C., Zeisel, M.B., Guerin, M., Mancip, J., Granio, O., Penin, F., Lavillette, D., Bartenschlager, R., Baumert, T.F., Cosset, F.L., Dreux, M., 2012. Characterization of hepatitis C virus particle subpopulations reveals multiple usage of the scavenger receptor BI for entry steps. The Journal of biological chemistry 287, 31242-31257.

Diaz-Toledano, R., Ariza-Mateos, A., Birk, A., Martinez-Garcia, B., Gomez, J., 2009. In vitro characterization of a miR-122-sensitive double-helical switch element in the 5' region of hepatitis C virus RNA. Nucleic acids research 37, 5498-5510.

DiDonato, D., Brasaemle, D.L., 2003. Fixation methods for the study of lipid droplets by immunofluorescence microscopy. The journal of histochemistry and cytochemistry : official journal of the Histochemistry Society 51, 773-780.

Dohner, K., Sodeik, B., 2005. The role of the cytoskeleton during viral infection. Current topics in microbiology and immunology 285, 67-108.

Dubuisson, J., Hsu, H.H., Cheung, R.C., Greenberg, H.B., Russell, D.G., Rice, C.M., 1994. Formation and intracellular localization of hepatitis C virus envelope glycoprotein complexes expressed by recombinant vaccinia and Sindbis viruses. Journal of virology 68, 6147-6160.

Duvet, S., Cocquerel, L., Pillez, A., Cacan, R., Verbert, A., Moradpour, D., Wychowski, C., Dubuisson, J., 1998. Hepatitis C virus glycoprotein complex localization in the endoplasmic reticulum involves a determinant for retention and not retrieval. The Journal of biological chemistry 273, 32088-32095.

Egger, D., Wolk, B., Gosert, R., Bianchi, L., Blum, H.E., Moradpour, D., Bienz, K., 2002. Expression of hepatitis C virus proteins induces distinct membrane alterations including a candidate viral replication complex. Journal of virology 76, 5974-5984.

El-Hage, N., Luo, G., 2003. Replication of hepatitis C virus RNA occurs in a membrane-bound replication complex containing nonstructural viral proteins and RNA. The Journal of general virology 84, 2761-2769.

Evans, M.J., Rice, C.M., Goff, S.P., 2004. Phosphorylation of hepatitis C virus nonstructural protein 5A modulates its protein interactions and viral RNA replication. Proceedings of the National Academy of Sciences of the United States of America 101, 13038-13043.

Eyre, N.S., Fiches, G.N., Aloia, A.L., Helbig, K.J., McCartney, E.M., McErlean, C.S., Li, K., Aggarwal, A., Turville, S.G., Beard, M.R., 2014a. Dynamic imaging of the hepatitis C virus NS5A protein during a productive infection. Journal of virology 88, 3636-3652.

Eyre, N.S., Helbig, K.J., Beard, M.R., 2014b. Current and future targets of antiviral therapy in the hepatitis C virus life cycle. Future Virology 9, 947-965.

Eyre, N.S., Phillips, R.J., Bowden, S., Yip, E., Dewar, B., Locarnini, S.A., Beard, M.R., 2009. Hepatitis B virus and hepatitis C virus interaction in Huh-7 cells. Journal of hepatology 51, 446-457.

Farese, R.V., Jr., Walther, T.C., 2009. Lipid droplets finally get a little R-E-S-P-E-C-T. Cell 139, 855-860.

Farquhar, M.J., Hu, K., Harris, H.J., Davis, C., Brimacombe, C.L., Fletcher, S.J., Baumert, T.F., Rappoport, J.Z., Balfe, P., McKeating, J.A., 2012. Hepatitis C virus induces CD81 and claudin-1 endocytosis. Journal of virology 86, 4305-4316.

Feinstone, S.M., Kapikian, A.Z., Purcell, R.H., Alter, H.J., Holland, P.V., 1975. Transfusion-associated hepatitis not due to viral hepatitis type A or B. The New England journal of medicine 292, 767-770.

Feinstone, S.M., Mihalik, K.B., Kamimura, T., Alter, H.J., London, W.T., Purcell, R.H., 1983. Inactivation of hepatitis B virus and non-A, non-B hepatitis by chloroform. Infection and immunity 41, 816-821.

Ferraris, P., Beaumont, E., Uzbekov, R., Brand, D., Gaillard, J., Blanchard, E., Roingeard, P., 2013. Sequential biogenesis of host cell membrane rearrangements induced by hepatitis C virus infection. Cellular and molecular life sciences : CMLS 70, 1297-1306.

Ferraris, P., Blanchard, E., Roingeard, P., 2010. Ultrastructural and biochemical analyses of hepatitis C virus-associated host cell membranes. The Journal of general virology 91, 2230-2237.

Foster, T.L., Belyaeva, T., Stonehouse, N.J., Pearson, A.R., Harris, M., 2010. All three domains of the hepatitis C virus nonstructural NS5A protein contribute to RNA binding. Journal of virology 84, 9267-9277.

Fouts, D.E., True, H.L., Celander, D.W., 1997. Functional recognition of fragmented operator sites by R17/MS2 coat protein, a translational repressor. Nucleic acids research 25, 4464-4473.

Friebe, P., Bartenschlager, R., 2002. Genetic analysis of sequences in the 3' nontranslated region of hepatitis C virus that are important for RNA replication. Journal of virology 76, 5326-5338.

Friebe, P., Boudet, J., Simorre, J.P., Bartenschlager, R., 2005. Kissing-loop interaction in the 3' end of the hepatitis C virus genome essential for RNA replication. Journal of virology 79, 380-392.

Fusco, D., Accornero, N., Lavoie, B., Shenoy, S.M., Blanchard, J.M., Singer, R.H., Bertrand, E., 2003. Single mRNA molecules demonstrate probabilistic movement in living mammalian cells. Current biology : CB 13, 161-167.

Gao, L., Aizaki, H., He, J.W., Lai, M.M., 2004. Interactions between viral nonstructural proteins and host protein hVAP-33 mediate the formation of hepatitis C virus RNA replication complex on lipid raft. Journal of virology 78, 3480-3488.

Gao, M., Nettles, R.E., Belema, M., Snyder, L.B., Nguyen, V.N., Fridell, R.A., Serrano-Wu, M.H., Langley, D.R., Sun, J.H., O'Boyle, D.R., 2nd, Lemm, J.A., Wang, C., Knipe, J.O., Chien, C., Colonno, R.J., Grasela, D.M., Meanwell, N.A., Hamann, L.G., 2010. Chemical genetics strategy identifies an HCV NS5A inhibitor with a potent clinical effect. Nature 465, 96-100.

Gastaminza, P., Cheng, G., Wieland, S., Zhong, J., Liao, W., Chisari, F.V., 2008. Cellular determinants of hepatitis C virus assembly, maturation, degradation, and secretion. Journal of virology 82, 2120-2129.

Gastaminza, P., Kapadia, S.B., Chisari, F.V., 2006. Differential biophysical properties of infectious intracellular and secreted hepatitis C virus particles. Journal of virology 80, 11074-11081.

Germi, R., Crance, J.M., Garin, D., Guimet, J., Lortat-Jacob, H., Ruigrok, R.W., Zarski, J.P., Drouet, E., 2002. Cellular glycosaminoglycans and low density lipoprotein receptor are involved in hepatitis C virus adsorption. Journal of medical virology 68, 206-215.

Gosert, R., Egger, D., Lohmann, V., Bartenschlager, R., Blum, H.E., Bienz, K., Moradpour, D., 2003. Identification of the hepatitis C virus RNA replication complex in Huh-7 cells harboring subgenomic replicons. Journal of virology 77, 5487-5492.

Gosert, R., Kanjanahaluethai, A., Egger, D., Bienz, K., Baker, S.C., 2002. RNA replication of mouse hepatitis virus takes place at double-membrane vesicles. Journal of virology 76, 3697-3708.

Gouttenoire, J., Roingeard, P., Penin, F., Moradpour, D., 2010. Amphipathic alpha-helix AH2 is a major determinant for the oligomerization of hepatitis C virus nonstructural protein 4B. Journal of virology 84, 12529-12537.

Gower, E., Estes, C., Blach, S., Razavi-Shearer, K., Razavi, H., 2014. Global epidemiology and genotype distribution of the hepatitis C virus infection. Journal of hepatology 61, S45-57.

Griffin, S.D., Beales, L.P., Clarke, D.S., Worsfold, O., Evans, S.D., Jaeger, J., Harris, M.P., Rowlands, D.J., 2003. The p7 protein of hepatitis C virus forms an ion channel that is blocked by the antiviral drug, Amantadine. FEBS letters 535, 34-38.

Gross, D.A., Silver, D.L., 2014. Cytosolic lipid droplets: from mechanisms of fat storage to disease. Critical reviews in biochemistry and molecular biology 49, 304-326.

Gross, S.P., Vershinin, M., Shubeita, G.T., 2007. Cargo transport: two motors are sometimes better than one. Current biology : CB 17, R478-486.

Gross, S.P., Welte, M.A., Block, S.M., Wieschaus, E.F., 2000. Dynein-mediated cargo transport in vivo. A switch controls travel distance. The Journal of cell biology 148, 945-956.

Guidotti, L.G., Chisari, F.V., 2006. Immunobiology and pathogenesis of viral hepatitis. Annual review of pathology 1, 23-61.

Hagemeijer, M.C., Verheije, M.H., Ulasli, M., Shaltiel, I.A., de Vries, L.A., Reggiori, F., Rottier, P.J., de Haan, C.A., 2010. Dynamics of coronavirus replication-transcription complexes. Journal of virology 84, 2134-2149.

Hagemeijer, M.C., Vonk, A.M., Monastyrska, I., Rottier, P.J., de Haan, C.A., 2012. Visualizing coronavirus RNA synthesis in time by using click chemistry. Journal of virology 86, 5808-5816.

Halfon, P., Locarnini, S., 2011. Hepatitis C virus resistance to protease inhibitors. Journal of hepatology 55, 192-206.

Hamamoto, I., Nishimura, Y., Okamoto, T., Aizaki, H., Liu, M., Mori, Y., Abe, T., Suzuki, T., Lai, M.M., Miyamura, T., Moriishi, K., Matsuura, Y., 2005. Human VAP-B is involved in hepatitis C virus replication through interaction with NS5A and NS5B. Journal of virology 79, 13473-13482.

He, L.F., Alling, D., Popkin, T., Shapiro, M., Alter, H.J., Purcell, R.H., 1987. Determining the size of non-A, non-B hepatitis virus by filtration. The Journal of infectious diseases 156, 636-640.

Henke, J.I., Goergen, D., Zheng, J., Song, Y., Schuttler, C.G., Fehr, C., Junemann, C., Niepmann, M., 2008. microRNA-122 stimulates translation of hepatitis C virus RNA. The EMBO journal 27, 3300-3310.

Herker, E., Harris, C., Hernandez, C., Carpentier, A., Kaehlcke, K., Rosenberg, A.R., Farese, R.V., Jr., Ott, M., 2010. Efficient hepatitis C virus particle formation requires diacylglycerol acyltransferase-1. Nature medicine 16, 1295-1298.

Herrmann, E., Neumann, A.U., Schmidt, J.M., Zeuzem, S., 2000. Hepatitis C virus kinetics. Antiviral therapy 5, 85-90.

Hinson, E.R., Cresswell, P., 2009. The antiviral protein, viperin, localizes to lipid droplets via its N-terminal amphipathic alpha-helix. Proceedings of the National Academy of Sciences of the United States of America 106, 20452-20457.

Hoffmann, C., Gaietta, G., Zurn, A., Adams, S.R., Terrillon, S., Ellisman, M.H., Tsien, R.Y., Lohse, M.J., 2010. Fluorescent labeling of tetracysteine-tagged proteins in intact cells. Nature protocols 5, 1666-1677.

Honda, M., Rijnbrand, R., Abell, G., Kim, D., Lemon, S.M., 1999. Natural variation in translational activities of the 5' nontranslated RNAs of hepatitis C virus genotypes 1a and 1b:

evidence for a long-range RNA-RNA interaction outside of the internal ribosomal entry site. Journal of virology 73, 4941-4951.

Hsu, M., Zhang, J., Flint, M., Logvinoff, C., Cheng-Mayer, C., Rice, C.M., McKeating, J.A., 2003. Hepatitis C virus glycoproteins mediate pH-dependent cell entry of pseudotyped retroviral particles. Proceedings of the National Academy of Sciences of the United States of America 100, 7271-7276.

Huang, L., Hwang, J., Sharma, S.D., Hargittai, M.R., Chen, Y., Arnold, J.J., Raney, K.D., Cameron, C.E., 2005. Hepatitis C virus nonstructural protein 5A (NS5A) is an RNA-binding protein. The Journal of biological chemistry 280, 36417-36428.

Jensen, D.M., 2011. A new era of hepatitis C therapy begins. The New England journal of medicine 364, 1272-1274.

Jirasko, V., Montserret, R., Lee, J.Y., Gouttenoire, J., Moradpour, D., Penin, F., Bartenschlager, R., 2010. Structural and functional studies of nonstructural protein 2 of the hepatitis C virus reveal its key role as organizer of virion assembly. PLoS pathogens 6, e1001233.

Jones, D.M., Atoom, A.M., Zhang, X., Kottilil, S., Russell, R.S., 2011. A genetic interaction between the core and NS3 proteins of hepatitis C virus is essential for production of infectious virus. Journal of virology 85, 12351-12361.

Jopling, C.L., Yi, M., Lancaster, A.M., Lemon, S.M., Sarnow, P., 2005. Modulation of hepatitis C virus RNA abundance by a liver-specific MicroRNA. Science 309, 1577-1581.

Jouvenet, N., Bieniasz, P.D., Simon, S.M., 2008. Imaging the biogenesis of individual HIV-1 virions in live cells. Nature 454, 236-240.

Jouvenet, N., Simon, S.M., Bieniasz, P.D., 2009. Imaging the interaction of HIV-1 genomes and Gag during assembly of individual viral particles. Proceedings of the National Academy of Sciences of the United States of America 106, 19114-19119.

Kato, T., Date, T., Miyamoto, M., Furusaka, A., Tokushige, K., Mizokami, M., Wakita, T., 2003. Efficient replication of the genotype 2a hepatitis C virus subgenomic replicon. Gastroenterology 125, 1808-1817.

Kato, T., Furusaka, A., Miyamoto, M., Date, T., Yasui, K., Hiramoto, J., Nagayama, K., Tanaka, T., Wakita, T., 2001. Sequence analysis of hepatitis C virus isolated from a fulminant hepatitis patient. Journal of medical virology 64, 334-339.

Khromykh, A.A., Westaway, E.G., 1997. Subgenomic replicons of the flavivirus Kunjin: construction and applications. Journal of virology 71, 1497-1505.

Kim, J.H., Paek, K.Y., Ha, S.H., Cho, S., Choi, K., Kim, C.S., Ryu, S.H., Jang, S.K., 2004. A cellular RNA-binding protein enhances internal ribosomal entry site-dependent translation through an interaction downstream of the hepatitis C virus polyprotein initiation codon. Molecular and cellular biology 24, 7878-7890.

Kim, S., Welsch, C., Yi, M., Lemon, S.M., 2011. Regulation of the production of infectious genotype 1a hepatitis C virus by NS5A domain III. Journal of virology 85, 6645-6656.

Kim, Y.K., Lee, S.H., Kim, C.S., Seol, S.K., Jang, S.K., 2003. Long-range RNA-RNA interaction between the 5' nontranslated region and the core-coding sequences of hepatitis C virus modulates the IRES-dependent translation. Rna 9, 599-606.

Krieger, N., Lohmann, V., Bartenschlager, R., 2001. Enhancement of hepatitis C virus RNA replication by cell culture-adaptive mutations. Journal of virology 75, 4614-4624.

Kulic, I.M., Brown, A.E., Kim, H., Kural, C., Blehm, B., Selvin, P.R., Nelson, P.C., Gelfand, V.I., 2008. The role of microtubule movement in bidirectional organelle transport. Proceedings of the National Academy of Sciences of the United States of America 105, 10011-10016.

Kunwar, A., Tripathy, S.K., Xu, J., Mattson, M.K., Anand, P., Sigua, R., Vershinin, M., McKenney, R.J., Yu, C.C., Mogilner, A., Gross, S.P., 2011. Mechanical stochastic tug-of-war models cannot

explain bidirectional lipid-droplet transport. Proceedings of the National Academy of Sciences of the United States of America 108, 18960-18965.

Lai, C.K., Jeng, K.S., Machida, K., Lai, M.M., 2008. Association of hepatitis C virus replication complexes with microtubules and actin filaments is dependent on the interaction of NS3 and NS5A. Journal of virology 82, 8838-8848.

Landgraf, P., Rusu, M., Sheridan, R., Sewer, A., Iovino, N., Aravin, A., Pfeffer, S., Rice, A., Kamphorst, A.O., Landthaler, M., Lin, C., Socci, N.D., Hermida, L., Fulci, V., Chiaretti, S., Foa, R., Schliwka, J., Fuchs, U., Novosel, A., Muller, R.U., Schermer, B., Bissels, U., Inman, J., Phan, Q., Chien, M., Weir, D.B., Choksi, R., De Vita, G., Frezzetti, D., Trompeter, H.I., Hornung, V., Teng, G., Hartmann, G., Palkovits, M., Di Lauro, R., Wernet, P., Macino, G., Rogler, C.E., Nagle, J.W., Ju, J., Papavasiliou, F.N., Benzing, T., Lichter, P., Tam, W., Brownstein, M.J., Bosio, A., Borkhardt, A., Russo, J.J., Sander, C., Zavolan, M., Tuschl, T., 2007. A mammalian microRNA expression atlas based on small RNA library sequencing. Cell 129, 1401-1414.

Lavanchy, D., 2008. Chronic viral hepatitis as a public health issue in the world. Best practice & research. Clinical gastroenterology 22, 991-1008.

Le Guillou-Guillemette, H., Vallet, S., Gaudy-Graffin, C., Payan, C., Pivert, A., Goudeau, A., Lunel-Fabiani, F., 2007. Genetic diversity of the hepatitis C virus: impact and issues in the antiviral therapy. World journal of gastroenterology : WJG 13, 2416-2426.

Lemay, K.L., Treadaway, J., Angulo, I., Tellinghuisen, T.L., 2013. A hepatitis C virus NS5A phosphorylation site that regulates RNA replication. Journal of virology 87, 1255-1260.

Lim, F., Peabody, D.S., 1994. Mutations that increase the affinity of a translational repressor for RNA. Nucleic acids research 22, 3748-3752.

Lindenbach, B.D., Evans, M.J., Syder, A.J., Wolk, B., Tellinghuisen, T.L., Liu, C.C., Maruyama, T., Hynes, R.O., Burton, D.R., McKeating, J.A., Rice, C.M., 2005. Complete replication of hepatitis C virus in cell culture. Science 309, 623-626.

Lindenbach, B.D., Meuleman, P., Ploss, A., Vanwolleghem, T., Syder, A.J., McKeating, J.A., Lanford, R.E., Feinstone, S.M., Major, M.E., Leroux-Roels, G., Rice, C.M., 2006. Cell culture-grown hepatitis C virus is infectious in vivo and can be recultured in vitro. Proceedings of the National Academy of Sciences of the United States of America 103, 3805-3809.

Listenberger, L.L., Brown, D.A., 2007. Fluorescent detection of lipid droplets and associated proteins. Current protocols in cell biology / editorial board, Juan S. Bonifacino ... [et al.] Chapter 24, Unit 24 22.

Lohmann, V., Korner, F., Herian, U., Bartenschlager, R., 1997. Biochemical properties of hepatitis C virus NS5B RNA-dependent RNA polymerase and identification of amino acid sequence motifs essential for enzymatic activity. Journal of virology 71, 8416-8428.

Lohmann, V., Korner, F., Koch, J., Herian, U., Theilmann, L., Bartenschlager, R., 1999. Replication of subgenomic hepatitis C virus RNAs in a hepatoma cell line. Science 285, 110-113.

Luik, P., Chew, C., Aittoniemi, J., Chang, J., Wentworth, P., Jr., Dwek, R.A., Biggin, P.C., Venien-Bryan, C., Zitzmann, N., 2009. The 3-dimensional structure of a hepatitis C virus p7 ion channel by electron microscopy. Proceedings of the National Academy of Sciences of the United States of America 106, 12712-12716.

Ma, Y., Yates, J., Liang, Y., Lemon, S.M., Yi, M., 2008. NS3 helicase domains involved in infectious intracellular hepatitis C virus particle assembly. Journal of virology 82, 7624-7639.

Mackenzie, J., 2005. Wrapping things up about virus RNA replication. Traffic 6, 967-977.

Maiuri, P., Knezevich, A., Bertrand, E., Marcello, A., 2011. Real-time imaging of the HIV-1 transcription cycle in single living cells. Methods 53, 62-67.

Martin, D.N., Uprichard, S.L., 2013. Identification of transferrin receptor 1 as a hepatitis C virus entry factor. Proceedings of the National Academy of Sciences of the United States of America 110, 10777-10782.

Martin, S., Parton, R.G., 2006. Lipid droplets: a unified view of a dynamic organelle. Nature reviews. Molecular cell biology 7, 373-378.

Masaki, T., Suzuki, R., Murakami, K., Aizaki, H., Ishii, K., Murayama, A., Date, T., Matsuura, Y., Miyamura, T., Wakita, T., Suzuki, T., 2008. Interaction of hepatitis C virus nonstructural protein 5A with core protein is critical for the production of infectious virus particles. Journal of virology 82, 7964-7976.

McCartney, E.M., Eyre, N.S., Beard, M.R., 2011. Border patrol intensifies for hepatitis C virus entry. Hepatology 54, 1472-1475.

McLauchlan, J., Lemberg, M.K., Hope, G., Martoglio, B., 2002. Intramembrane proteolysis promotes trafficking of hepatitis C virus core protein to lipid droplets. The EMBO journal 21, 3980-3988.

Menzel, N., Fischl, W., Hueging, K., Bankwitz, D., Frentzen, A., Haid, S., Gentzsch, J., Kaderali, L., Bartenschlager, R., Pietschmann, T., 2012. MAP-kinase regulated cytosolic phospholipase A2 activity is essential for production of infectious hepatitis C virus particles. PLoS pathogens 8, e1002829.

Merz, A., Long, G., Hiet, M.S., Brugger, B., Chlanda, P., Andre, P., Wieland, F., Krijnse-Locker, J., Bartenschlager, R., 2011. Biochemical and morphological properties of hepatitis C virus particles and determination of their lipidome. The Journal of biological chemistry 286, 3018-3032.

Michalak, J.P., Wychowski, C., Choukhi, A., Meunier, J.C., Ung, S., Rice, C.M., Dubuisson, J., 1997. Characterization of truncated forms of hepatitis C virus glycoproteins. The Journal of general virology 78 ( Pt 9), 2299-2306.

Miller, S., Krijnse-Locker, J., 2008. Modification of intracellular membrane structures for virus replication. Nature reviews. Microbiology 6, 363-374.

Miorin, L., Maiuri, P., Hoenninger, V.M., Mandl, C.W., Marcello, A., 2008. Spatial and temporal organization of tick-borne encephalitis flavivirus replicated RNA in living cells. Virology 379, 64-77.

Miorin, L., Romero-Brey, I., Maiuri, P., Hoppe, S., Krijnse-Locker, J., Bartenschlager, R., Marcello, A., 2013. Three-dimensional architecture of tick-borne encephalitis virus replication sites and trafficking of the replicated RNA. Journal of virology 87, 6469-6481.

Mittelholzer, C., Moser, C., Tratschin, J.D., Hofmann, M.A., 1997. Generation of cytopathogenic subgenomic RNA of classical swine fever virus in persistently infected porcine cell lines. Virus research 51, 125-137.

Miyanari, Y., Atsuzawa, K., Usuda, N., Watashi, K., Hishiki, T., Zayas, M., Bartenschlager, R., Wakita, T., Hijikata, M., Shimotohno, K., 2007. The lipid droplet is an important organelle for hepatitis C virus production. Nature cell biology 9, 1089-1097.

Miyanari, Y., Hijikata, M., Yamaji, M., Hosaka, M., Takahashi, H., Shimotohno, K., 2003. Hepatitis C virus non-structural proteins in the probable membranous compartment function in viral genome replication. The Journal of biological chemistry 278, 50301-50308.

Moradpour, D., Englert, C., Wakita, T., Wands, J.R., 1996. Characterization of cell lines allowing tightly regulated expression of hepatitis C virus core protein. Virology 222, 51-63.

Moradpour, D., Evans, M.J., Gosert, R., Yuan, Z., Blum, H.E., Goff, S.P., Lindenbach, B.D., Rice, C.M., 2004. Insertion of green fluorescent protein into nonstructural protein 5A allows direct visualization of functional hepatitis C virus replication complexes. Journal of virology 78, 7400-7409.

Nagai, T., Ibata, K., Park, E.S., Kubota, M., Mikoshiba, K., Miyawaki, A., 2002. A variant of yellow fluorescent protein with fast and efficient maturation for cell-biological applications. Nature biotechnology 20, 87-90.

Nakabayashi, H., Taketa, K., Miyano, K., Yamane, T., Sato, J., 1982. Growth of human hepatoma cells lines with differentiated functions in chemically defined medium. Cancer research 42, 3858-3863.

Nayak, A., Pattabiraman, N., Fadra, N., Goldman, R., Kosakovsky Pond, S.L., Mazumder, R., 2014. Structure-function analysis of hepatitis C virus envelope glycoproteins E1 and E2. Journal of biomolecular structure & dynamics, 1-13.

Neddermann, P., Quintavalle, M., Di Pietro, C., Clementi, A., Cerretani, M., Altamura, S., Bartholomew, L., De Francesco, R., 2004. Reduction of hepatitis C virus NS5A hyperphosphorylation by selective inhibition of cellular kinases activates viral RNA replication in cell culture. Journal of virology 78, 13306-13314.

Neumann, A.U., Lam, N.P., Dahari, H., Gretch, D.R., Wiley, T.E., Layden, T.J., Perelson, A.S., 1998. Hepatitis C viral dynamics in vivo and the antiviral efficacy of interferon-alpha therapy. Science 282, 103-107.

Neveu, G., Barouch-Bentov, R., Ziv-Av, A., Gerber, D., Jacob, Y., Einav, S., 2012. Identification and targeting of an interaction between a tyrosine motif within hepatitis C virus core protein and AP2M1 essential for viral assembly. PLoS pathogens 8, e1002845.

Niepmann, M., 2013. Hepatitis C virus RNA translation. Current topics in microbiology and immunology 369, 143-166.

Op De Beeck, A., Montserret, R., Duvet, S., Cocquerel, L., Cacan, R., Barberot, B., Le Maire, M., Penin, F., Dubuisson, J., 2000. The transmembrane domains of hepatitis C virus envelope glycoproteins E1 and E2 play a major role in heterodimerization. The Journal of biological chemistry 275, 31428-31437.

OuYang, B., Xie, S., Berardi, M.J., Zhao, X., Dev, J., Yu, W., Sun, B., Chou, J.J., 2013. Unusual architecture of the p7 channel from hepatitis C virus. Nature 498, 521-525.

Owen, D.M., Huang, H., Ye, J., Gale, M., Jr., 2009. Apolipoprotein E on hepatitis C virion facilitates infection through interaction with low-density lipoprotein receptor. Virology 394, 99-108.

Ozawa, T., Natori, Y., Sato, M., Umezawa, Y., 2007. Imaging dynamics of endogenous mitochondrial RNA in single living cells. Nature methods 4, 413-419.

Ozeki, S., Cheng, J., Tauchi-Sato, K., Hatano, N., Taniguchi, H., Fujimoto, T., 2005. Rab18 localizes to lipid droplets and induces their close apposition to the endoplasmic reticulum-derived membrane. Journal of cell science 118, 2601-2611.

Park, H.Y., Buxbaum, A.R., Singer, R.H., 2010. Single mRNA tracking in live cells. Methods in enzymology 472, 387-406.

Park, S.M., Paek, K.Y., Hong, K.Y., Jang, C.J., Cho, S., Park, J.H., Kim, J.H., Jan, E., Jang, S.K., 2011. Translation-competent 48S complex formation on HCV IRES requires the RNA-binding protein NSAP1. Nucleic acids research 39, 7791-7802.

Patel, J., Patel, A.H., McLauchlan, J., 2001. The transmembrane domain of the hepatitis C virus E2 glycoprotein is required for correct folding of the E1 glycoprotein and native complex formation. Virology 279, 58-68.

Paul, D., Hoppe, S., Saher, G., Krijnse-Locker, J., Bartenschlager, R., 2013. Morphological and biochemical characterization of the membranous hepatitis C virus replication compartment. Journal of virology 87, 10612-10627.

Paul, D., Madan, V., Bartenschlager, R., 2014. Hepatitis C virus RNA replication and assembly: living on the fat of the land. Cell host & microbe 16, 569-579.

Paul, D., Romero-Brey, I., Gouttenoire, J., Stoitsova, S., Krijnse-Locker, J., Moradpour, D., Bartenschlager, R., 2011. NS4B self-interaction through conserved C-terminal elements is required for the establishment of functional hepatitis C virus replication complexes. Journal of virology 85, 6963-6976.

Pawlotsky, J.M., 2011. Treatment failure and resistance with direct-acting antiviral drugs against hepatitis C virus. Hepatology 53, 1742-1751.

Peritz, T., Zeng, F., Kannanayakal, T.J., Kilk, K., Eiriksdottir, E., Langel, U., Eberwine, J., 2006. Immunoprecipitation of mRNA-protein complexes. Nature protocols 1, 577-580.

Perlman, M., Resh, M.D., 2006. Identification of an intracellular trafficking and assembly pathway for HIV-1 gag. Traffic 7, 731-745.

Petracca, R., Falugi, F., Galli, G., Norais, N., Rosa, D., Campagnoli, S., Burgio, V., Di Stasio, E., Giardina, B., Houghton, M., Abrignani, S., Grandi, G., 2000. Structure-function analysis of hepatitis C virus envelope-CD81 binding. Journal of virology 74, 4824-4830.

Phan, T., Beran, R.K., Peters, C., Lorenz, I.C., Lindenbach, B.D., 2009. Hepatitis C virus NS2 protein contributes to virus particle assembly via opposing epistatic interactions with the E1-E2 glycoprotein and NS3-NS4A enzyme complexes. Journal of virology 83, 8379-8395.

Pietschmann, T., Zayas, M., Meuleman, P., Long, G., Appel, N., Koutsoudakis, G., Kallis, S., Leroux-Roels, G., Lohmann, V., Bartenschlager, R., 2009. Production of infectious genotype 1b virus particles in cell culture and impairment by replication enhancing mutations. PLoS pathogens 5, e1000475.

Ploss, A., Evans, M.J., Gaysinskaya, V.A., Panis, M., You, H., de Jong, Y.P., Rice, C.M., 2009. Human occludin is a hepatitis C virus entry factor required for infection of mouse cells. Nature 457, 882-886.

Pol, A., Gross, S.P., Parton, R.G., 2014. Review: biogenesis of the multifunctional lipid droplet: lipids, proteins, and sites. The Journal of cell biology 204, 635-646.

Popescu, C.I., Callens, N., Trinel, D., Roingeard, P., Moradpour, D., Descamps, V., Duverlie, G., Penin, F., Heliot, L., Rouille, Y., Dubuisson, J., 2011. NS2 protein of hepatitis C virus interacts with structural and non-structural proteins towards virus assembly. PLoS pathogens 7, e1001278.

Poynard, T., Bedossa, P., Opolon, P., 1997. Natural history of liver fibrosis progression in patients with chronic hepatitis C. The OBSVIRC, METAVIR, CLINIVIR, and DOSVIRC groups. Lancet 349, 825-832.

Rackham, O., Brown, C.M., 2004. Visualization of RNA-protein interactions in living cells: FMRP and IMP1 interact on mRNAs. The EMBO journal 23, 3346-3355.

Reiss, S., Rebhan, I., Backes, P., Romero-Brey, I., Erfle, H., Matula, P., Kaderali, L., Poenisch, M., Blankenburg, H., Hiet, M.S., Longerich, T., Diehl, S., Ramirez, F., Balla, T., Rohr, K., Kaul, A., Buhler, S., Pepperkok, R., Lengauer, T., Albrecht, M., Eils, R., Schirmacher, P., Lohmann, V., Bartenschlager, R., 2011. Recruitment and activation of a lipid kinase by hepatitis C virus NS5A is essential for integrity of the membranous replication compartment. Cell host & microbe 9, 32-45.

Remenyi, R., Qi, H., Su, S.Y., Chen, Z., Wu, N.C., Arumugaswami, V., Truong, S., Chu, V., Stokelman, T., Lo, H.H., Olson, C.A., Wu, T.T., Chen, S.H., Lin, C.Y., Sun, R., 2014. A comprehensive functional map of the hepatitis C virus genome provides a resource for probing viral proteins. mBio 5, e01469-01414.

Romero-Brey, I., Merz, A., Chiramel, A., Lee, J.Y., Chlanda, P., Haselman, U., Santarella-Mellwig, R., Habermann, A., Hoppe, S., Kallis, S., Walther, P., Antony, C., Krijnse-Locker, J., Bartenschlager, R., 2012. Three-dimensional architecture and biogenesis of membrane structures associated with hepatitis C virus replication. PLoS pathogens 8, e1003056.

Ronaghi, M., Karamohamed, S., Pettersson, B., Uhlen, M., Nyren, P., 1996. Real-time DNA sequencing using detection of pyrophosphate release. Analytical biochemistry 242, 84-89.

Ross-Thriepland, D., Harris, M., 2014. Insights into the complexity and functionality of hepatitis C virus NS5A phosphorylation. Journal of virology 88, 1421-1432.

Rouille, Y., Helle, F., Delgrange, D., Roingeard, P., Voisset, C., Blanchard, E., Belouzard, S., McKeating, J., Patel, A.H., Maertens, G., Wakita, T., Wychowski, C., Dubuisson, J., 2006.

Subcellular localization of hepatitis C virus structural proteins in a cell culture system that efficiently replicates the virus. Journal of virology 80, 2832-2841.

Sainz, B., Jr., Barretto, N., Martin, D.N., Hiraga, N., Imamura, M., Hussain, S., Marsh, K.A., Yu, X., Chayama, K., Alrefai, W.A., Uprichard, S.L., 2012. Identification of the Niemann-Pick C1-like 1 cholesterol absorption receptor as a new hepatitis C virus entry factor. Nature medicine 18, 281-285.

Salloum, S., Wang, H., Ferguson, C., Parton, R.G., Tai, A.W., 2013. Rab18 binds to hepatitis C virus NS5A and promotes interaction between sites of viral replication and lipid droplets. PLoS pathogens 9, e1003513.

Salonen, A., Ahola, T., Kaariainen, L., 2005. Viral RNA replication in association with cellular membranes. Current topics in microbiology and immunology 285, 139-173.

Scarselli, E., Ansuini, H., Cerino, R., Roccasecca, R.M., Acali, S., Filocamo, G., Traboni, C., Nicosia, A., Cortese, R., Vitelli, A., 2002. The human scavenger receptor class B type I is a novel candidate receptor for the hepatitis C virus. The EMBO journal 21, 5017-5025.

Schaller, T., Appel, N., Koutsoudakis, G., Kallis, S., Lohmann, V., Pietschmann, T., Bartenschlager, R., 2007. Analysis of hepatitis C virus superinfection exclusion by using novel fluorochrome gene-tagged viral genomes. Journal of virology 81, 4591-4603.

Schonborn, J., Oberstrass, J., Breyel, E., Tittgen, J., Schumacher, J., Lukacs, N., 1991. Monoclonal antibodies to double-stranded RNA as probes of RNA structure in crude nucleic acid extracts. Nucleic acids research 19, 2993-3000.

Seeff, L.B., Buskell-Bales, Z., Wright, E.C., Durako, S.J., Alter, H.J., Iber, F.L., Hollinger, F.B., Gitnick, G., Knodell, R.G., Perrillo, R.P., et al., 1992. Long-term mortality after transfusion-associated non-A, non-B hepatitis. The National Heart, Lung, and Blood Institute Study Group. The New England journal of medicine 327, 1906-1911.

Sharma, N.R., Mateu, G., Dreux, M., Grakoui, A., Cosset, F.L., Melikyan, G.B., 2011. Hepatitis C virus is primed by CD81 protein for low pH-dependent fusion. The Journal of biological chemistry 286, 30361-30376.

Shav-Tal, Y., Darzacq, X., Shenoy, S.M., Fusco, D., Janicki, S.M., Spector, D.L., Singer, R.H., 2004a. Dynamics of single mRNPs in nuclei of living cells. Science 304, 1797-1800.

Shav-Tal, Y., Singer, R.H., Darzacq, X., 2004b. Imaging gene expression in single living cells. Nature reviews. Molecular cell biology 5, 855-861.

Shavinskaya, A., Boulant, S., Penin, F., McLauchlan, J., Bartenschlager, R., 2007. The lipid droplet binding domain of hepatitis C virus core protein is a major determinant for efficient virus assembly. The Journal of biological chemistry 282, 37158-37169.

Shendure, J., Ji, H., 2008. Next-generation DNA sequencing. Nature biotechnology 26, 1135-1145.

Shimakami, T., Yamane, D., Jangra, R.K., Kempf, B.J., Spaniel, C., Barton, D.J., Lemon, S.M., 2012a. Stabilization of hepatitis C virus RNA by an Ago2-miR-122 complex. Proceedings of the National Academy of Sciences of the United States of America 109, 941-946.

Shimakami, T., Yamane, D., Welsch, C., Hensley, L., Jangra, R.K., Lemon, S.M., 2012b. Base pairing between hepatitis C virus RNA and microRNA 122 3' of its seed sequence is essential for genome stabilization and production of infectious virus. Journal of virology 86, 7372-7383.

Shimizu, Y.K., 1992. Ultrastructural alterations and expression of cytoplasmic antigen 48-1 in hepatocytes in association with hepatitis C virus infection. Microbiology and immunology 36, 911-922.

Smith, D.B., Bukh, J., Kuiken, C., Muerhoff, A.S., Rice, C.M., Stapleton, J.T., Simmonds, P., 2014. Expanded classification of hepatitis C virus into 7 genotypes and 67 subtypes: updated criteria and genotype assignment web resource. Hepatology 59, 318-327.

Sourisseau, M., Michta, M.L., Zony, C., Israelow, B., Hopcraft, S.E., Narbus, C.M., Parra Martin, A., Evans, M.J., 2013. Temporal analysis of hepatitis C virus cell entry with occludin directed blocking antibodies. PLoS pathogens 9, e1003244.

Spahn, C.M., Kieft, J.S., Grassucci, R.A., Penczek, P.A., Zhou, K., Doudna, J.A., Frank, J., 2001. Hepatitis C virus IRES RNA-induced changes in the conformation of the 40s ribosomal subunit. Science 291, 1959-1962.

Spangenburg, E.E., Pratt, S.J., Wohlers, L.M., Lovering, R.M., 2011. Use of BODIPY (493/503) to visualize intramuscular lipid droplets in skeletal muscle. Journal of biomedicine & biotechnology 2011, 598358.

Sumpter, R., Jr., Loo, Y.M., Foy, E., Li, K., Yoneyama, M., Fujita, T., Lemon, S.M., Gale, M., Jr., 2005. Regulating intracellular antiviral defense and permissiveness to hepatitis C virus RNA replication through a cellular RNA helicase, RIG-I. Journal of virology 79, 2689-2699.

Tamai, K., Shiina, M., Tanaka, N., Nakano, T., Yamamoto, A., Kondo, Y., Kakazu, E., Inoue, J., Fukushima, K., Sano, K., Ueno, Y., Shimosegawa, T., Sugamura, K., 2012. Regulation of hepatitis C virus secretion by the Hrs-dependent exosomal pathway. Virology 422, 377-385.

Tanji, Y., Kaneko, T., Satoh, S., Shimotohno, K., 1995. Phosphorylation of hepatitis C virus-encoded nonstructural protein NS5A. Journal of virology 69, 3980-3986.

Targett-Adams, P., Boulant, S., McLauchlan, J., 2008. Visualization of double-stranded RNA in cells supporting hepatitis C virus RNA replication. Journal of virology 82, 2182-2195.

Targett-Adams, P., Chambers, D., Gledhill, S., Hope, R.G., Coy, J.F., Girod, A., McLauchlan, J., 2003. Live cell analysis and targeting of the lipid droplet-binding adipocyte differentiation-related protein. The Journal of biological chemistry 278, 15998-16007.

Targett-Adams, P., Graham, E.J., Middleton, J., Palmer, A., Shaw, S.M., Lavender, H., Brain, P., Tran, T.D., Jones, L.H., Wakenhut, F., Stammen, B., Pryde, D., Pickford, C., Westby, M., 2011.

Small molecules targeting hepatitis C virus-encoded NS5A cause subcellular redistribution of their target: insights into compound modes of action. Journal of virology 85, 6353-6368.

Tellinghuisen, T.L., Evans, M.J., von Hahn, T., You, S., Rice, C.M., 2007. Studying hepatitis C virus: making the best of a bad virus. Journal of virology 81, 8853-8867.

Tellinghuisen, T.L., Foss, K.L., Treadaway, J., 2008a. Regulation of hepatitis C virion production via phosphorylation of the NS5A protein. PLoS pathogens 4, e1000032.

Tellinghuisen, T.L., Foss, K.L., Treadaway, J.C., Rice, C.M., 2008b. Identification of residues required for RNA replication in domains II and III of the hepatitis C virus NS5A protein. Journal of virology 82, 1073-1083.

Tellinghuisen, T.L., Marcotrigiano, J., Gorbalenya, A.E., Rice, C.M., 2004. The NS5A protein of hepatitis C virus is a zinc metalloprotein. The Journal of biological chemistry 279, 48576-48587.

Tellinghuisen, T.L., Marcotrigiano, J., Rice, C.M., 2005. Structure of the zinc-binding domain of an essential component of the hepatitis C virus replicase. Nature 435, 374-379.

Thomssen, R., Bonk, S., Propfe, C., Heermann, K.H., Kochel, H.G., Uy, A., 1992. Association of hepatitis C virus in human sera with beta-lipoprotein. Medical microbiology and immunology 181, 293-300.

Tsukiyama-Kohara, K., Iizuka, N., Kohara, M., Nomoto, A., 1992. Internal ribosome entry site within hepatitis C virus RNA. Journal of virology 66, 1476-1483.

Tuplin, A., Struthers, M., Simmonds, P., Evans, D.J., 2012. A twist in the tail: SHAPE mapping of long-range interactions and structural rearrangements of RNA elements involved in HCV replication. Nucleic acids research 40, 6908-6921.

Valencia-Burton, M., Broude, N.E., 2007. Visualization of RNA using fluorescence complementation triggered by aptamer-protein interactions (RFAP) in live bacterial cells.

Current protocols in cell biology / editorial board, Juan S. Bonifacino ... [et al.] Chapter 17, Unit 17 11.

Valencia-Burton, M., McCullough, R.M., Cantor, C.R., Broude, N.E., 2007. RNA visualization in live bacterial cells using fluorescent protein complementation. Nature methods 4, 421-427.

Vieyres, G., Thomas, X., Descamps, V., Duverlie, G., Patel, A.H., Dubuisson, J., 2010. Characterization of the envelope glycoproteins associated with infectious hepatitis C virus. Journal of virology 84, 10159-10168.

Wakita, T., Pietschmann, T., Kato, T., Date, T., Miyamoto, M., Zhao, Z., Murthy, K., Habermann, A., Krausslich, H.G., Mizokami, M., Bartenschlager, R., Liang, T.J., 2005. Production of infectious hepatitis C virus in tissue culture from a cloned viral genome. Nature medicine 11, 791-796.

Walther, T.C., Farese, R.V., Jr., 2009. The life of lipid droplets. Biochimica et biophysica acta 1791, 459-466.

Wang, C., Le, S.Y., Ali, N., Siddiqui, A., 1995. An RNA pseudoknot is an essential structural element of the internal ribosome entry site located within the hepatitis C virus 5' noncoding region. Rna 1, 526-537.

Wang, C., Sarnow, P., Siddiqui, A., 1993. Translation of human hepatitis C virus RNA in cultured cells is mediated by an internal ribosome-binding mechanism. Journal of virology 67, 3338-3344.

Welte, M.A., 2004. Bidirectional transport along microtubules. Current biology : CB 14, R525-537.

Westaway, E.G., Khromykh, A.A., Mackenzie, J.M., 1999. Nascent flavivirus RNA colocalized in situ with double-stranded RNA in stable replication complexes. Virology 258, 108-117.

Westaway, E.G., Mackenzie, J.M., Kenney, M.T., Jones, M.K., Khromykh, A.A., 1997. Ultrastructure of Kunjin virus-infected cells: colocalization of NS1 and NS3 with double-stranded RNA, and of NS2B with NS3, in virus-induced membrane structures. Journal of virology 71, 6650-6661.

Wolk, B., Buchele, B., Moradpour, D., Rice, C.M., 2008. A dynamic view of hepatitis C virus replication complexes. Journal of virology 82, 10519-10531.

Wozniak, A.L., Griffin, S., Rowlands, D., Harris, M., Yi, M., Lemon, S.M., Weinman, S.A., 2010. Intracellular proton conductance of the hepatitis C virus p7 protein and its contribution to infectious virus production. PLoS pathogens 6, e1001087.

Yi, M., Lemon, S.M., 2003. 3' nontranslated RNA signals required for replication of hepatitis C virus RNA. Journal of virology 77, 3557-3568.

Yi, M., Nakamoto, Y., Kaneko, S., Yamashita, T., Murakami, S., 1997. Delineation of regions important for heteromeric association of hepatitis C virus E1 and E2. Virology 231, 119-129.

Yu, G.Y., Lee, K.J., Gao, L., Lai, M.M., 2006. Palmitoylation and polymerization of hepatitis C virus NS4B protein. Journal of virology 80, 6013-6023.

Zhong, J., Gastaminza, P., Cheng, G., Kapadia, S., Kato, T., Burton, D.R., Wieland, S.F., Uprichard, S.L., Wakita, T., Chisari, F.V., 2005. Robust hepatitis C virus infection in vitro. Proceedings of the National Academy of Sciences of the United States of America 102, 9294-9299.

Zhou, Z., Wang, N., Woodson, S.E., Dong, Q., Wang, J., Liang, Y., Rijnbrand, R., Wei, L., Nichols, J.E., Guo, J.T., Holbrook, M.R., Lemon, S.M., Li, K., 2011. Antiviral activities of ISG20 in positive-strand RNA virus infections. Virology 409, 175-188.

Zielinski, J., Kilk, K., Peritz, T., Kannanayakal, T., Miyashiro, K.Y., Eiriksdottir, E., Jochems, J., Langel, U., Eberwine, J., 2006. In vivo identification of ribonucleoprotein-RNA interactions.

Proceedings of the National Academy of Sciences of the United States of America 103, 1557-1562.